BMR JOURNAL
OF AUSTRALIAN GEOLOGY & GEOPHYSICS

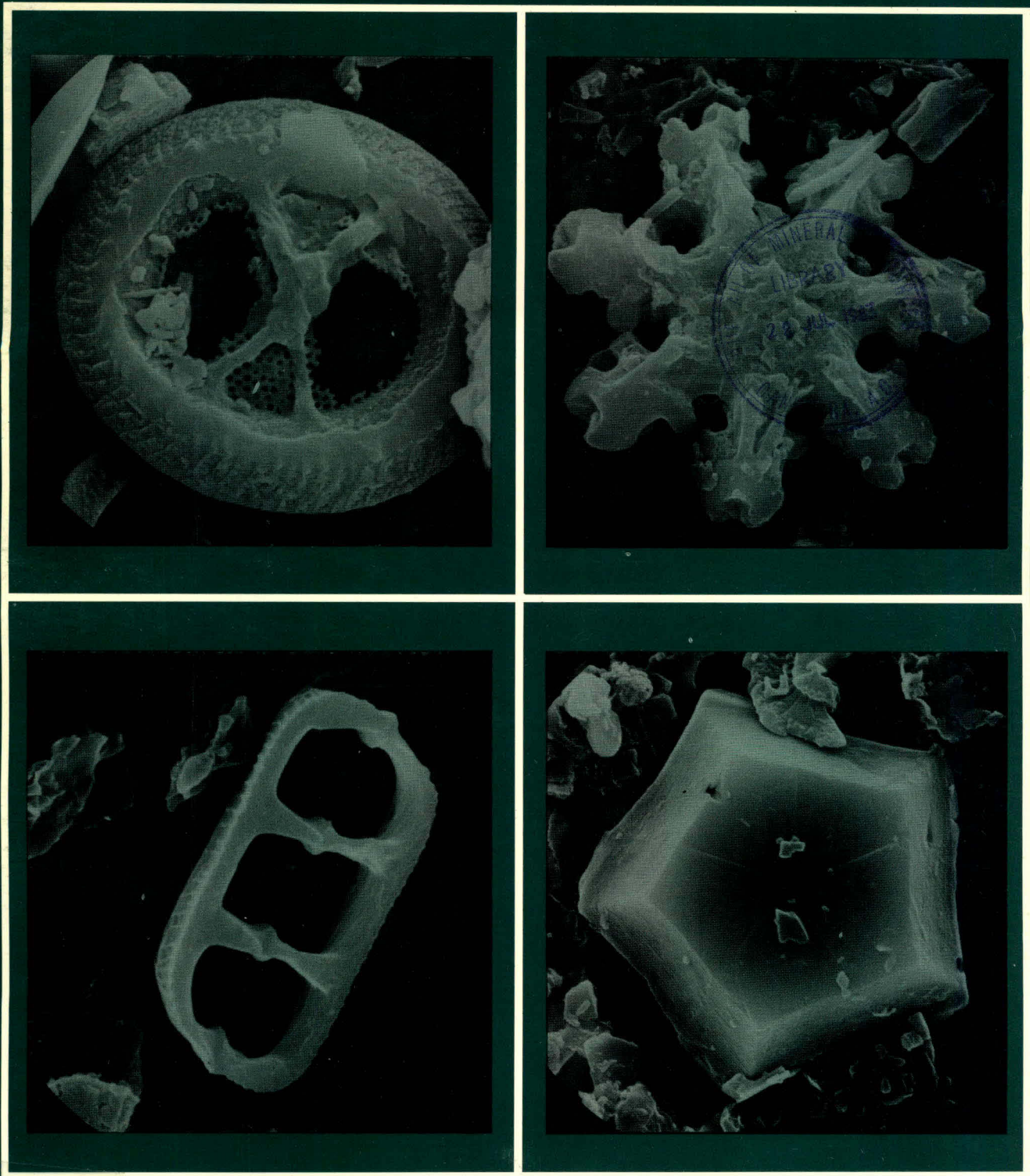

VOLUME 8 NUMBER 1 MARCH 1983

BMR JOURNAL
OF AUSTRALIAN GEOLOGY & GEOPHYSICS

VOLUME 8 NUMBER 1 MARCH 1983

CONTENTS

Front cover: Tertiary coccoliths and discoasters, magnified 6000–8000 times: nannofossils such as these have been used to determine a biostratigraphy for sediments in the Otway Basin of southeastern Australia, described in this issue in a paper by S. Shafik.

AUSTRALIAN GOVERNMENT PUBLISHING SERVICE CANBERRA 1983

Department of Resources and Energy

Minister: Senator the Hon. Peter Walsh

Secretary: A. J. Woods

Bureau of Mineral Resources, Geology and Geophysics

Director: R. W. R. Rutland

Editor, BMR Journal: I. M. Hodgson

The BMR Journal of Australian Geology & Geophysics is a quarterly journal of research and related activities. Contributions are from officers of the BMR, from BMR officers working in collaboration with others, or requested work sponsored by the BMR. In addition to articles the Journal may include shorter notes and discussion of papers published in it. Discussion of papers is invited from anyone.

Annual subscription to the Journal is $25 (Australian). Individual numbers, if available, cost $8.50. Subscriptions, etc., made payable to the Receiver of Public Moneys in Australian dollars should be sent to the Director, Bureau of Mineral Resources, Geology and Geophysics, P.O. Box 378, Canberra, A.C.T. 2601, Australia.

Other matters concerning the Journal should be sent to the Director, marked for the attention of the Editor, BMR Journal.

The text figures in this issue were drafted by P. Jorritsma, P. Griffiths, & B. Pashley.

ISSN 0312-9608

Printed by Graphic Services Pty. Ltd. 516–518 Grand Junction Road, Northfield, S.A. 5085

BMR Journal of Australian Geology & Geophysics, 8, 1-17

CALCAREOUS NANNOFOSSIL BIOSTRATIGRAPHY: AN ASSESSMENT OF FORAMINFERAL AND SEDIMENTATION EVENTS IN THE EOCENE OF THE OTWAY BASIN, SOUTHEASTERN AUSTRALIA

Samir Shafik

From a study of middle to late Eocene calcareous nannofossil assemblages in four sections in the Otway Basin of southeastern Australia, a sequence of biostratigraphic events has been deduced, spanning the interval from the lowest appearance of *Cyclicargolithus reticulatus* (middle Eocene) to the disappearance of *Discoaster saipanensis* (latest Eocene). The sequence is compared with its counterpart in New Zealand, and is placed against the planktic foraminiferal P. zones of the tropics. The previously determined foraminiferal biostratigraphy of the sections studied has been compared with the nannofossil biostratigraphy, and, as a result, the local highest appearance of the foraminiferid *Acarinina primitiva* is now placed in zone P.13 of the tropics, and not P.12 or P.14, as previously. The disappearance up the section of the foraminiferid *Acarinina collactea* is found to be locally inconsistent with other evidence. During the middle Eocene, marine ingressions, represented by isolated nannofossil assemblages, occurred in the Gambier Embayment of the western Otway Basin, but did not reach the Browns Creek area, eastern Otway Basin, attesting to the diachroneity of Eocene marine sedimentation in the basin. The diachroneity is also indicated by transgressive rock units in the Gambier Embayment. The ingressions seem to coincide with a major change in the sea-floor spreading rate south of Australia. During the latest middle to early late Eocene, a major transgression began synchronously in widely separated areas across the basin. The upper Eocene section in the Gambier Embayment represents condensed sedimentation and ends in a sharp disconformity, indicated by the simultaneous disappearance of *Cyclicargolithus reticulatus* and *Discoaster saipanensis*. At Browns Creek, that part of the section between the highest appearances of *C. reticulatus* and *D. saipanensis* is thick, suggesting relatively rapid rates of sedimentation. However, in the expanded part of the section at Browns Creek and also at Castle Cove, there is evidence that extreme shoal conditions existed as a result of imbalance between sedimentation and subsidence. During the middle and late Eocene, conditions along the Australian southern margin were generally temperate, with surface-water temperature decreasing eastward, and the depositional environment was essentially shallow marine — nearshore or shelf.

Introduction

Currently, the Eocene calcareous microfossil biostratigraphy of the Otway Basin and other areas along the Australian southern margin is based essentially on extratropical planktic foraminiferal taxa. In the middle and late Eocene, the events recognised are mainly extinctions (McGowran, 1978a, b), and some problems exist with respect to their chronological order and correlation with counterparts in New Zealand. Also, the absence of those planktic foraminiferal species used to define low-latitude zones (cf. P. zones of Blow, 1969, 1979; and Berggren, 1969) makes it extremely difficult to relate the local foraminiferal biostratigraphy to the tropical zonation. However, attempts have been made to relate the foraminiferal events in the Eocene of the Otway Basin to the P. zones of the tropics (mainly by McGowran, e.g. 1973, 1978a).

Studies of Eocene calcareous nannofossil assemblages from the southern and western margins of Australia (Shafik, 1973, 1978, 1981) suggest a local order of events broadly similar to that recorded in New Zealand by Edwards (1971). The basis for several Eocene 'standard nannoplankton zones' (Martini, 1971) or low- latitude zones (e.g. Bukry, 1973a, b) can be recognised in the Australian Eocene. These, and other related nannofossil zones, have been correlated adequately with the foraminiferal P. zones (e.g. Martini, 1971; Gartner, 1971; Roth & others, 1971; Hardenbol & Berggren, 1978).

In this study the calcareous nannofossil assemblages in Eocene sediments in the Otway Basin have been investigated in order to better understand the local calcareous microfossil biostrati-

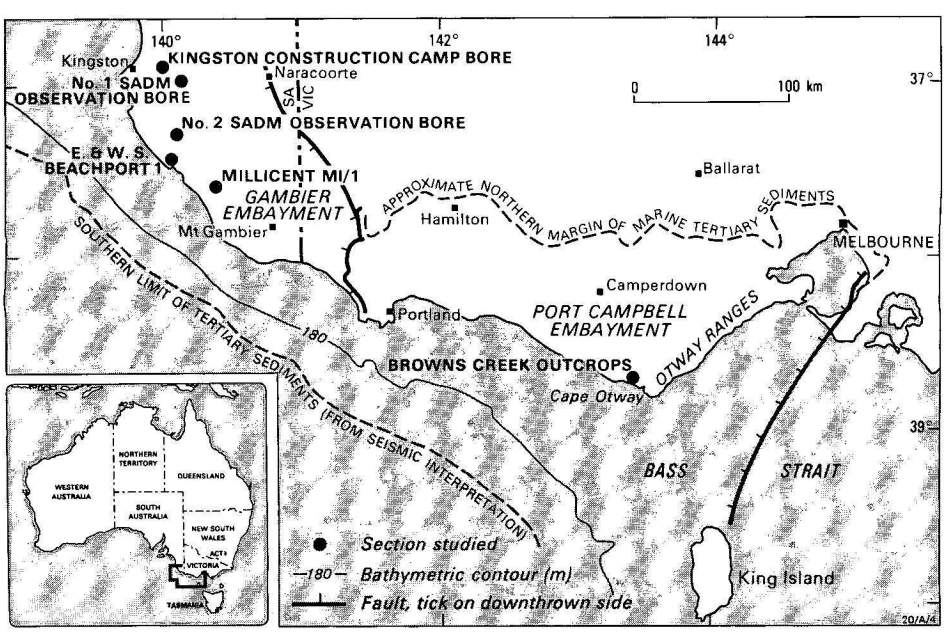

Figure 1. Location of material studied.

Table 1. Main lithologies of the Browns Creek Section.

Formation	*Approximate thickness in metres and lithologic description*
Browns Creek Clays	10 Medium grey biogenic clay becoming quartzose sandy silt near base; 2 thin calcarenite bands about 2 m from top.
	18 Predominantly light grey, coarse to medium biogenic marl; dark grey "mud rolls" occur near the middle.
	1–2 Glauconitic sand ('*Notostrea*' greensand) with *Notostrea lubra* Finlay and *Aturia clarkei* Teichert & Cotton.
	10 Dark grey '*Turritella*' clay with *Spirocolpus aldingae* (Tate) and *Limopsis chapmani* Singleton, becoming glauconitic near top and more silty with quartz sand near base; 2 thin calcarenite bands — separated by 35 cm of clayey quartz sand at about 3 m from base.
Johanna River Sand	10 Dark grey, carbonaceous, pyritic, silty quartz sand. No calcareous microfossil remains, but arenaceous foraminiferids (e.g. *Haplophragmoides* spp.) present.
	? Rest of formation obscured.

Table 2. Lithostratigraphic units of the Lower Tertiary in the Gambier Embayment.
Except for the Gambier Limestone, the units are exclusively subsurface.

Unit name (proposer)	*Lithologic description and type thickness*
Gambier Limestone (Sprigg, 1952)	Bryzoan calcirudite, calcarenite and calcisiltite; some horizons with chert nodules.
Lacepede Formation (Ludbrook, 1969)	Lithology varied. Greensand in one bore; varies from sandy clay to marl and calcareous sandy silt, with abundant quartz and muscovite in other bores. Typically brown carbonaceous silt and dark grey sandy clay rich in glauconite, and shelly marl with glauconite and limonite pellets: 11 m.
Kongorong Sand (Ludbrook, 1969)	Brownish yellow quartz grit with angular to subangular grains stained and coated with limonite; carbonaceous clay matrix, slightly calcareous; common glauconite pellets: 12 m.
Knight Formation and its Burrungule Member (Harris, 1966)	Unconsolidated poorly sorted coarse sand grit and minor conglomerates, with interbeds of lignitic clay (Burrungule Member). Type Burrungule is 13 m of laminated silty clay with some sand intercalations, slightly calcareous and very carbonaceous.

graphy and its relation to its counterparts in New Zealand and the tropics. A pattern has been identified of Eocene marine sedimentation in the Otway Basin, and an attempt made to provide a time framework for it.

Stratigraphic sections

Four sections have been studied (Fig. 1): one at Browns Creek, in the eastern Otway Basin, and three in the Gambier Embayment, in the western Otway Basin. A brief account of the section at Browns Creek is given in Table 1 (for details see Raggatt & Crespin, 1955; Carter, 1958; Abele & others, 1976), and the gross stratigraphy of the Lower Tertiary of the Gambier Embayment is summarised in Table 2 (for details see Ludbrook, 1971). Samples from the Johanna River Sand and the Burrungule Member of the Knight Formation are excluded from this study, because they lack calcareous nannofossils.

Assemblages and events

The distribution of selected calcareous nannofossil taxa recovered from the Gambier Embayment material is shown in Tables 3, 4 and 5. The distribution of those from the lower part of the Browns Creek section was given by Shafik (1981). Identification of all taxa was made mainly by optical microscopy. Illustration of selected taxa (Figs. 2-4) was made by using optical and scanning electron microscopy. Negatives of figured specimens are deposited in the Commonwealth Palaeontological Collection (CPC) in the Bureau of Mineral Resources, Canberra.

Browns Creek section

The Johanna River Sand at the base of the Browns Creek Section is devoid of calcareous nannofossils, and the first appearance up the section of these fossils in the Browns Creek Clays coincides with the first appearance also of planktic foraminiferids.

The Browns Creek section does not contain any nannofossils older than late Eocene: the base of the calcareous planktic/marine section at Browns Creek contains the age-diagnostic species, *Chiasmolithus oamaruensis, Cyclicargolithus reticulatus, Discoaster saipanensis,* and *Neococcolithes*

Figure 2. OM micrographs of some selected nannofossil taxa. All x2000.
A–C, *Chiasmolithus grandis* (Bramlette & Riedel): A — CPC 22355, B — CPC 22356, C — CPC 22357; D — E, *Chiasmolithus expansus* (Bramlette & Sullivan): D — CPC 22358, E — CPC 22359; F, *Chiasmolithus oamaruensis* (Deflandre), CPC 22360; G, *Coccolithus eopelagicus* (Bramlette & Riedel), CPC 22361; H, *Braarudosphaera bigelowi* (Gran & Braarud) CPC 22362; Ia–c, a transitional form between *B. bigelowi* and *Micrantholithus* sp., CPC 22363; Ja–b, *Micrantholithus procerus* Bukry & Percival, CPC 22364; K, *Micrantholithus attenuatus* Bramlette & Sullivan, CPC 22365; L–M, *Pemma basquensis* (Martini): L — CPC 22366, M — CPC 22367; N, *Zygrhablithus bijugatus bijugatus* (Deflandre), CPC 22368; O, *Daktylethra punctulata* Gartner, CPC 22369; P, a form resembling *D. punctulata*, but lacking the thickening of the sides, CPC 22370; Q–R, *Lanternithus minutus* Stradner: Q — CPC 23371, R — CPC 22372; S, *Blackites amplus* Roth, CPC 22373; T, *Markalius inversus* (Deflandre), CPC 22374; Ua–b, *Helicosphaera seminulum* (Bramlette & Sullivan), CPC 22375.

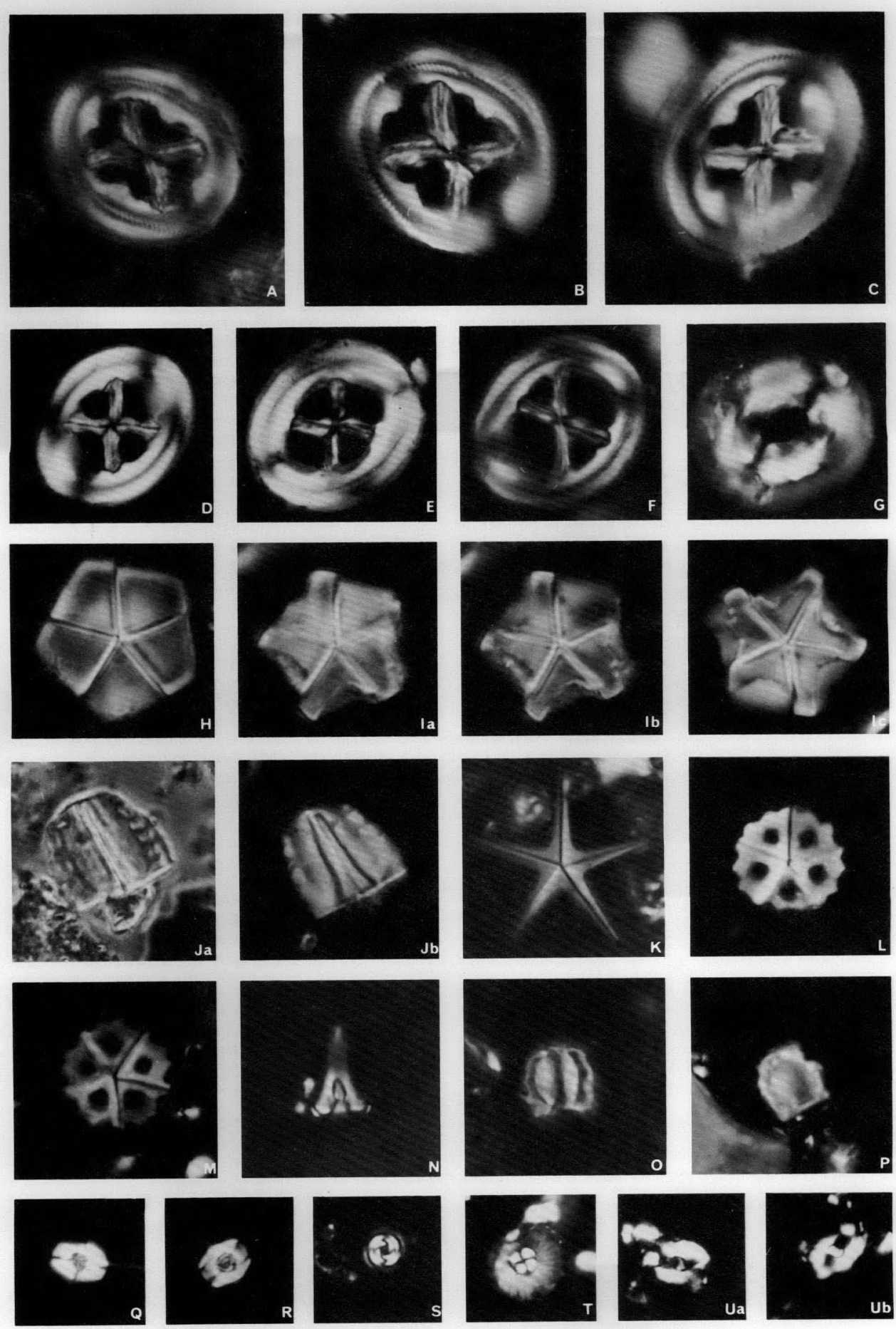
A
B
C
D
E
F
G
H
Ia
Ib
Ic
Ja
Jb
K
L
M
N
O
P
Q
R
S
T
Ua
Ub

dubius. *Chiasmolithus expansus* is rare and *C. grandis* was not encountered. In Figure 5, calcareous microfossil events below this level are inferred.

The age of the lowest appearance of *Chiasmolithus oamaruensis* has not been commonly agreed upon; the differences of interpretation are minimal though. Martini (1971) considered it late Eocene, while Gartner (1971) and Roth & others (1971) placed the event in the latest middle Eocene. Martini (1976) estimated an age of 42.5 m.y. for the event, whereas Hardenbol & Berggren (1978) placed it at 40 m.y., marking the middle/upper Eocene boundary. I consider the age of autochthonous assemblages containing *Chiasmolithus oamaruensis* and *C. grandis* as latest middle Eocene, and conveniently place the middle/upper Eocene boundary immediately above the highest appearance of *C. grandis*. The lowest appearance of *C. oamaruensis* in a sequence of assemblages lacking *C. grandis*, but containing *Cyclicargolithus reticulatus*, *Neococcolithes dubius*, and *Discoaster saipanensis* or its sibling *D. barbadiensis*, is early late Eocene in age. The age of the base of the calcareous planktic/marine section at Browns Creek is, accordingly, early late Eocene (Fig. 5).

The up-section sequence of events of highest appearance of *Neococcolithes dubius*, lowest appearance of *Isthmolithus recurvus*, and highest appearance of *Cyclicargolithus reticulatus* (Fig. 5) is in the lower part of the Browns Creek Clays, i.e. up to and including most of the *'Notostrea'* greensand. This is about 10 m above the base of the calcareous planktic/marine section.

The interval above the highest appearance of *Cyclicargolithus reticulatus* (about 29 m thick) (Fig. 5) contains sporadic *Discoaster saipanensis*, which indicates a late Eocene age. In this interval, taxa such as *Clausicoccus cribellum*, *Coccolithus eopelagicus*, *C. pelagicus*, *Cyclicargolithus floridanus*, *Cyclococcolithus formosus*, *Isthmolithus recurvus*, *Lanternithus minutus*, *Reticulofenestra hampdenensis* 'group', *R. scissura*, *R. scrippsae*, *R. umbilica*, *Sphenolithus moriformis* and *Zygrhablithus bijugatus bijugatus* are abundant and consistently present, whereas other taxa, such as *Blackites amplus*, *B. spinulus*, *B. spinosus*, *B. tenuis*, *B. vitreus*, *Braarudosphaera bigelowi*, *Discoaster tani nodifer*, *Chiasmolithus altus*, *C. oamaruensis*, *Clathrolithus ellipticus*, *Corannulus germanicus*, *Cyclicargolithus luminis*, *Helicosphaera seminulum*, *Holodiscolithus macroporus*, *Markalius inversus*, *Micrantholithus attenuatus*, *Orthozygus aureus*, *Pemma basquensis*, *Polycladolithus opersus*, *Pontosphaera multipora*, *P. plana*, *Transversopontis obliquipons*, *T. pulcher*, and *Trochoaster simplex* occur inconsistently, and range from abundant to rare.

The extinction of *Cyclicargolithus reticulatus* (within the *'Notostrea'* greensand) roughly separates two phases of deposition with contrasting rates of sedimentation. Thus, the lower part of the Browns Creek Clays resulted from much slower rates of sedimentation than those which produced the upper part (Shafik, 1981; Fig. 5).

Gambier Embayment sections

Calcareous nannofossil distribution in the Kongorong Sand and/or the Lacepede Formation in 3 bores in the western part of the Gambier Embayment (Tables 3, 4 & 5) is the basis for the sequence of nannofossil events presented in Figure 6; the relation to the foraminiferal P. zones of the tropics will be discussed below. The foraminiferids of most of the samples, on which this part of the study is based, were investigated by McGowran (1971, 1973), whose results are also included in Figure 6.

In the Gambier Embayment sections (Fig. 1), intervals barren of calcareous nannofossils also lack calcareous foraminiferids, and these two groups of microfossils disappear and reappear at the same levels (Tables 3 & 4).

Middle Eocene. Identification of the middle Eocene in the Gambier Embayment is based on the co-occurrence of the key taxa, *Chiasmolithus grandis*, *Cyclicargolithus reticulatus*, *Discoaster saipanensis*, *Neococcolithes dubius*, and *Reticulofenestra umbilica*, in assemblages recovered from the three sections studied: two assemblages in Kingston Bore (Table 3), the younger of which is also found in Observation Bore No. 1 (Table 4), and two other assemblages in Observation Bore No. 2 (Table 5). *Daktylethra punctulata* is prominent in the assemblages of Kingston Bore and Observation Bore No. 1, but is absent from the younger assemblages of Observation Bore No. 2.

In the Kingston Bore section, the calcareous planktic record is punctuated by intervals devoid of calcareous microfossils, so that the two middle Eocene assemblages are isolated from each other and from the overlying upper Eocene, which contains abundant nannofossils. The older assemblage in the Kingston Bore section may be referred to as the *Chiasmolithus solitus–Cyclicargolithus reticulatus* association, on account of the presence of rare *C. solitus* together with the other species listed above (Table 3). The other middle Eocene assemblage in the same bore section may be referred to as the *Daktylethra punctulata–Reticulofenestra scissura* association: its important species are *Chiasmolithus expansus*, *C. grandis*, *Cyclicargolithus reticulatus*, *Daktylethra punctulata*, *Discoaster saipanensis*, *Neococcolithes dubius*, *Reticulofenestra scissura*, and *R. umbilica; Chiasmolithus solitus* is absent.

Common *Chiasmolithus solitus*, in association with other Eocene taxa (e.g. *Cyclicargolithus reticulatus* and *Chiasmolithus expansus*), occurs in sludge samples from the Lacepede Formation in the (E. & W.S.) Beachport Bore No. 1, suggesting the presence of an assemblage correlatable with that referred to as the *Chiasmolithus solitus–Cyclicargolithus reticulatus* association in Kingston Bore. The Beachport Bore No. 1 assemblage includes, however, much younger taxa (e.g. *Helicosphaera recta*) in addition to extremely rare reworked upper Cretaceous forms. Downhole contamination of the Beachport Bore No. 1 samples hindered reliable reporting on the biostratigraphic details of the Eocene in that bore.

A middle Eocene assemblage, similar to the *Daktylethra punctulata–Reticulofenestra scissura* association in Kingston Bore, occurs in the Kongorong Sand in Observation Bore No. 1 (Table 4). This assemblage is also isolated, being separated from an overlying upper Eocene section with abundant nannofossils by an interval devoid of calcareous microfossils; samples from below this assemblage also lack calcareous microfossils.

Figure 3. OM micrographs of some selected nannofossil taxa. All x2000.
A–B, *Reticulofenestra scissura* Hay, Mohler & Wade: A — CPC 22376, B — CPC 22377; C–F, *Reticulofenestra hampdenensis* Edwards 'group': C — CPC 22378, D — CPC 22379, E — CPC 22380, F — CPC 22381; G, *Pontosphaera multipora* (Kamptner), CPC 22382; Ha–b, *Cyclococcolithus formosus* Kamptner CPC 22383; I–J, *Cyclicargolithus floridanus* (Roth & Hay): I — CPC 22384;, J — CPC 22385; K, *Cyclicargolithus reticulatus* (Gartner & Smith), CPC 22386; L–M, *Neococcolithes dubius* (Deflandre): L — CPC 22387, M — CPC 22388; N, *Isthmolithus recurvus* Deflandre, CPC 22389; O, *Discoaster barbadiensis* Tan Sin Hok, CPC 22390; P, *Discoaster elegans* Bramlette & Sullivan, CPC 22391; Q, *Discoaster saipanensis* Bramlette & Riedel, CPC 22392; R–S, *Discoaster tani nodifer* Bramlette & Riedel: R — CPC 22393, S — CPC 22394; T, distorted *Corannulus germanicus*, CPC 22395; U, *Holodiscolithus macroporus* (Deflandre), CPC 22396; V–W, *Orthozygus aureus* (Stradner): V — CPC 22397, W — CPC 22398; X, *Zygrhablithus bijugatus bijugatus* (Deflandre), CPC 22399; Y, *Clausicoccus cribellum* (Bramlette & Sullivan), CPC 22400.

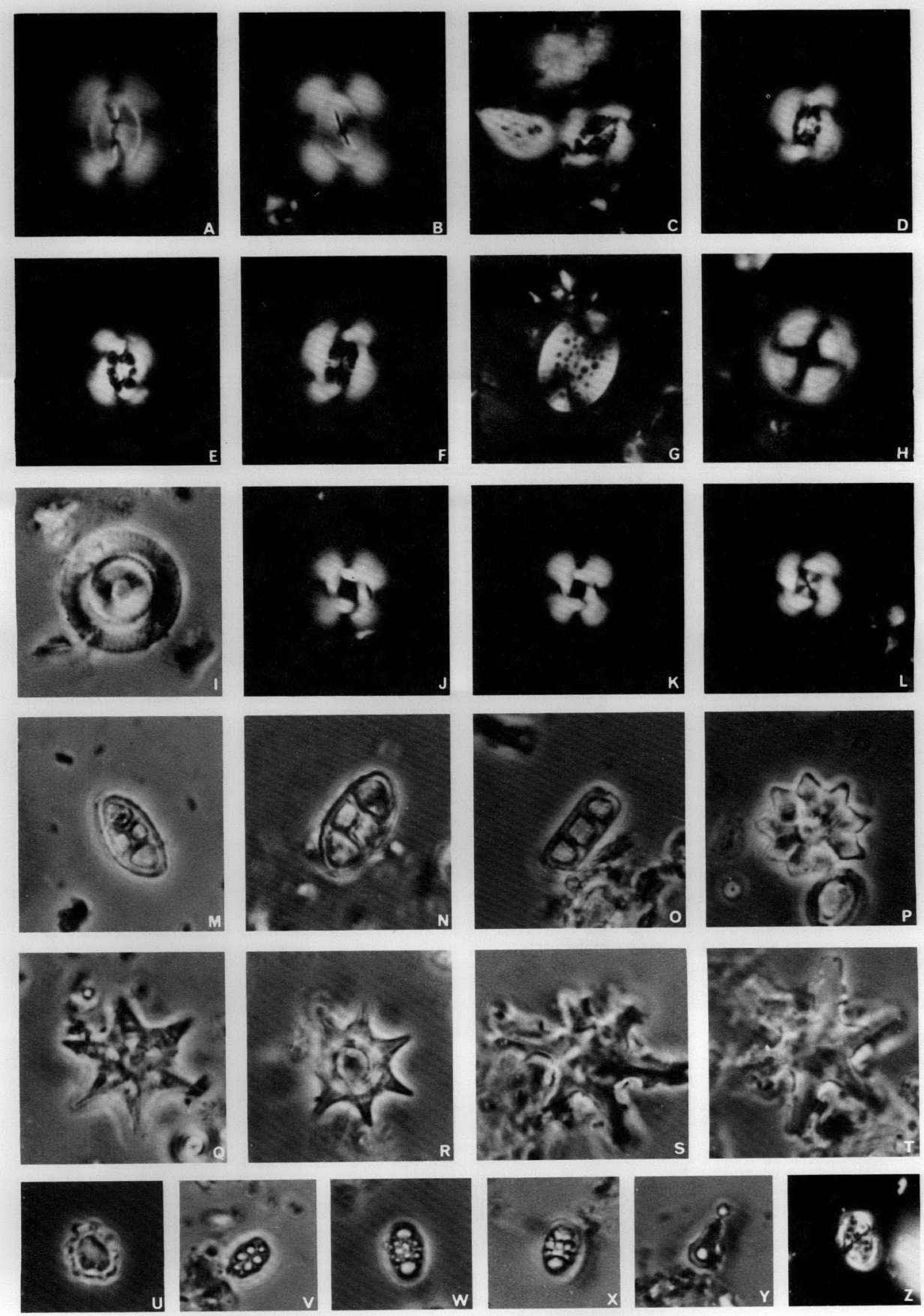
A
B
C
D
E
F
G
H
I
J
K
L
M
N
O
P
Q
R
S
T
U
V
W
X
Y
Z

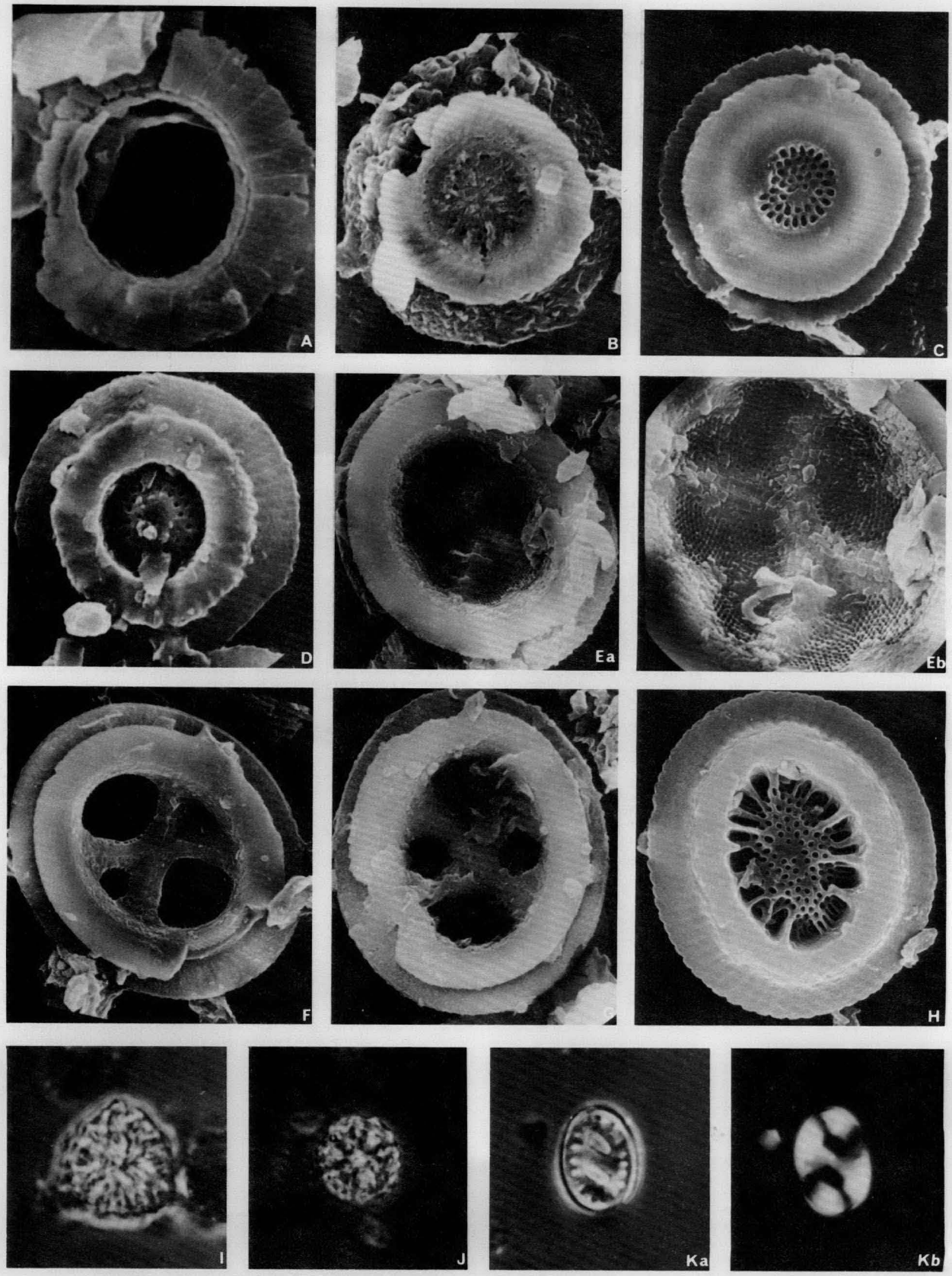

Figure 4. SEM and OM micrographs of some selected nannofossil taxa. OM micrographs (I–K) x2000.
A, *Cyclococcolithus protoannulus* (Gartner), CPC 22401 (distal view) x10380; B, *Markalius inversus* (Deflandre), CPC 22402 (proximal view) x6530; C–D, *Cyclicargolithus reticulatus* (Gartner & Smith): C — CPC 22403 (proximal view) x8250, D — CPC 22404 (distal view) x8300; Ea–b, *Chiasmolithus grandis* (Bramlette & Riedel) CPC 22405 (proximal view) x2540, 4300; F, *Chiasmolithus oamaruensis* (Deflandre), CPC 22406 (proximal view) x3200; G, *Chiasmolithus expansus* (Bramlette & Sullivan), CPC 22407 (proximal view) x3750; H, *Reticulofenestra hampdenensis* Edwards, CPC 22408 (distal view) x10960, I, *Trochoaster simplex* Klumpp, CPC 22409; J, *Polycladolithus opersus* (Bramlette & Sullivan) CPC 22410; Ka–b, *Transversopontis zigzag* Roth & Hay, CPC 22411.

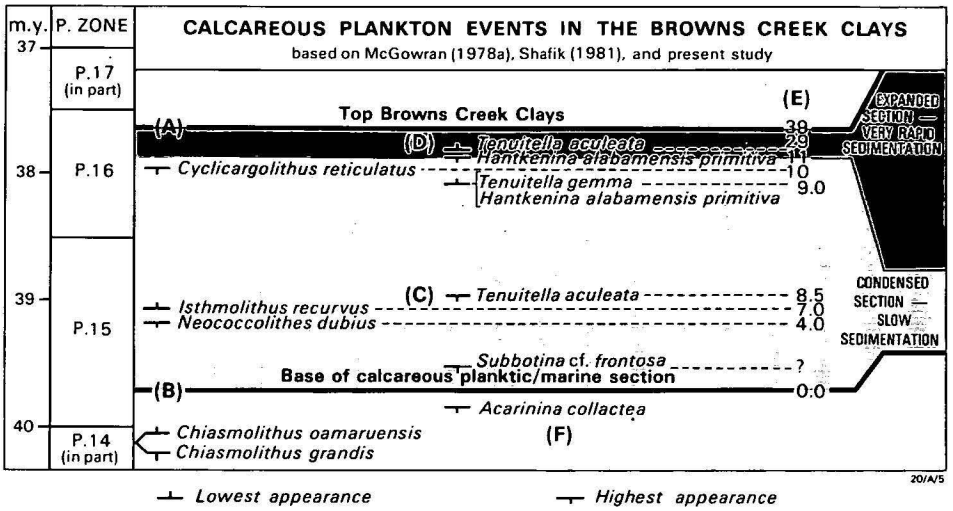

Figure 5. Integration of the nannofossil and foraminiferal events occurring in the Browns Creek Clays, and their correlation with the foraminiferal P. zones of the tropics.

Relative rates of sedimentation above and below the extinction of *Cyclicargolithus reticulatus* (approximately equivalent to the extinction of *Hantkenina*) within the *'Notostrea'* greensand are also shown.

A — top of Browns Creek Clays at Browns Creek section; placement of A against the P. zonation is more tentative than that of B. B — first up-section appearance of calcareous microfossils. C — first up-section disappearance of the foraminiferid *Tenuitella aculeata*; note that the same taxon re-appears higher in the section. D — interval with *Discoaster saipanensis* and *Reticulofenestra hampdenensis*, and the foraminiferids *Globigerinatheka index* and *Tenuitella aculeata*. E — levels in metres of calcareous microfossil events, relative to B. F — Calcareous microfossil events are inferred below B.

The middle Eocene assemblages identified in Observation Bore No. 2 occur in the Lacepede Formation cores F86-70 and F85-70. These lack *Daktylethra punctulata*, despite the presence of other holococcoliths (Table 5), and are considered to be near the middle/upper Eocene limit in the bore, and younger than the *Daktylethra punctulata–Reticulofenestra scissura* association in Kingston Bore and Observation Bore No. 1. Sludge samples from the Lacepede Formation below core F86-70 contain late Eocene nannofossil elements, suggesting downhole contamination. Foraminiferids from the same sludge samples suggest contamination also, but a sample from the contact with the Knight Formation, not available for the present study, contained middle Eocene taxa, including the important foraminiferid *Acarinina primitiva* (McGowran, 1973); the foraminiferal assemblage of the Kongorong Sand in Observation Bore No. 1 also includes *A. primitiva*.

The middle Eocene calcareous planktic record in the Kongorong Sand and/or the lower part of the Lacepede Formation in Kingston Bore and Observation Bore No. 1, being broken, contrasts with the uninterrupted record in the remaining (upper Eocene) part of the Lacepede Formation above. The same situation may also exist in Observation Bore No. 2, with the possible occurrence of a middle Eocene assemblage — older than those in cores F86-70 and F85-70 — at the contact of the Lacepede and Knight Formations. This evidence indicates that the onset of the Eocene transgression in the Gambier Embayment was not abrupt, but rather in pulses. The pattern of ingressions preceding a main transgression, as given by Taylor (1967, 1971), describes the situation adequately.

Isolated middle Eocene assemblages, like those identified in Kingston Bore and Observation Bore No. 1, were not found in the Browns Creek section; the oldest nannofossils encountered there being early late Eocene. This suggests that the middle Eocene ingressions did not reach the Browns Creek area, even though the late Eocene is well represented there. Also, it supports, in a sense, the conclusion advanced by Shafik (1973) that the base of the lower Tertiary marine sediments on the Australian southern margin (as detected by the lowest occurrences of nannofossils) is progressively younger eastward.

The ranges of *Chiasmolithus grandis* and *C. oamaruensis* just overlap in Observation Bore No. 2, Core F85-70, with the latter species being absent below this core. According to Gartner (1971), *Chiasmolithus grandis* disappears from JOIDES Blake Plateau cores in the uppermost middle Eocene, at a level corresponding closely with the lowest appearance of *Chiasmolithus oamaruensis*. These two species are only occasionally reported as occurring together in autochthonous sediments. Bukry (1973a) cautioned against misidentification of *Chiasmolithus oamaruensis*, but reported (Bukry, 1978) this species in association with *C. grandis* at DSDP Site 260 (Atlantic Ocean, south of Cape Town). These species also occur together in the Eocene section of Ninetyeast Ridge (Indian Ocean, DSDP Site 214) (personal observation).

Martini (1976) claimed that the highest appearance of *Chiasmolithus grandis* is consistently above the lowest appearance of *Isthmolithus recurvus* in high-latitude DSDP sections and land-based sections in Germany, Italy, and Russia. This claim is at odds with results from elsewhere, and it is possible that Martini was referring to reworked occurrences of *C. grandis*, which are seemingly difficult to detect. In a study of some Italian sections, Roth & others (1971) commented on the amount of reworking, which included *C. grandis*. Indeed, the distribution of *C. grandis* in sediments from high and low latitudes suggests that this species might have disappeared earlier from higher latitudes. Its earlier disappearance, relative to other biostratigraphic evidence, in high-latitude sections in New Zealand (Edwards, 1971) and in the South Campbell Plateau (Edwards & Perch-Nielsen, 1975) supports this conclusion.

Upwards from immediately above cores F86-70 and F85-70 (uppermost middle Eocene), nannofossils occur seemingly uninterrupted in Observation Bore No. 2. The interval with microfossils interpreted as downhole contamination, between the assemblage in core F86-70 and the older foraminiferal assemblage with *Acarinina primitiva* (at the contact with the Knight Formation), is likely to be barren of in situ calcareous microfossils, judging from the nearby sections (Kingston Bore and Observation Bore No. 1). This means that the base of the 'continuous' calcareous planktic/marine section in Observa-

Table 3. Distribution of selected calcareous nannofossil taxa in the Lacepede Formation of the (Highways Department) Kingston Construction Camp Bore, Hd. Lacepede, Section 512

Top of the Lacepede Formation is at 50.3 m; the bore bottomed in the Lacepede Formation. Nannofossils are scarce in the top two samples, presumably because of leaching at the contact Lacepede Formation/ Gambier Limestone, which coincides with a disconformity (see text).

	Blackites amplus	*Blackites spinosus*	*Blackites spinulus*	*Blackites tenuis*	*Blackites vitreus*	*Braarudosphaera bigelowi*	*Chiasmolithus altus*	*Chiasmolithus expansus*	*Chiasmolithus grandis*	*Chiasmolithus oamaruensis*	*Chiasmolithus solitus*	*Clausicoccus cribellum*	*Coccolithus eopelagicus*	*Coccolithus pelagicus*	*Corannulus germanicus*	*Cyclicargolithus floridanus*	*Cyclicargolithus luminis*	*Cyclicargolithus reticulatus*	*Cyclococcolithus formosus*	*Cyclococcolithus protoannulus*	*Daktylethra punctulata*	*Discoaster barbadiensis*	*Discoaster elegans*	*Discoaster saipanensis*	*Discoaster tani nodifer*	*Helicosphaera compacta*	*Helicosphaera reticulata*	*Helicosphaera seminulum*	*Holococcolithus macroporus*	*Isthmolithus recurvus*	*Lanternithus minutus*	*Markalius inversus*	*Micrantholithus attenuatus*	*Micrantholithus procerus*	*Micrantholithus truncus*	*Neococcolithes dubius*	*Orthozygus aureus*	*Pemma basquensis*	*Pemma papillatum*	*Polycladolithus opersus*	*Pontosphaera multipora*	*Pontosphaera plana*	*Reticulofenestra hampdenensis*	*Reticulofenestra scissura*	*Reticulofenestra scrippsae*	*Reticulofenestra umbilica*	*Sphenolithus moriformis*	*Transversopontis obliquipons*	*Transversopontis pulcher*	*Transversopontis zigzag*	*Trochaster simplex*	*Zygrhablithus bijugatus bijugatus*	*Zygrhablithus bijugatus crassus*
45.7 m (150'–165')												x	x	x		x													x							x													x	
50.3 m (165'–172')						x							x	x		x	x	x						x						x													x	x	x		x			x	
52.4 m (172'–177')	x		x	x	x	x	x			x		x		x		x		x	x	x				x							x	x	x				x			x		x		x	x	x	x	x	x	x	x	x
53.9 m (177'–183')	x		x		x	x							x	x		x	x	x					x	x					x			x	x				x	x			x		x	x	x	x	x	x			x	x
55.8 m (183'–190')	x		x			x						x	x	x				x		x				x	x					x	x	x	x				x			x		x	x	x	x	x	x	x			x	
57.9 m (190'–191')	x		x			x				x			x		x	x		x											x	x		x				x				x	x			x	x	x	x			x	x
58.2 m (191'–192')	x	x				x							x	x		x		x							x		x			x	x					x			x		x	x		x	x	x	x		x		x	
58.5 m (192'–193')		x	x			x				x			x	x	x	x		x	x				x							x			x	x		x			x	x	x	x	x	x			x			x	
58.8 m (193'–194')	x		x			x							x	x	x	x		x	x				x							x	x	x		x		x				x			x	x	x			x			x	
59.1 m (194'–195')	x					x							x	x	x	x		x					x					cf.			x	x			x	x				x	x			x	x	x		x			x	
59.4 m (195'–196')			x			x				x				x	x	x		x					x						x		x			x	x	x							x	x	x			x			x	
59.7 m (196'–197')													x		x	x		x	x												x					x								x	x				x			x	
60.0 m (197'–198')						x				x			x	x	x	x		x	x				x	x	x						x	x			x		x			x	x			x	x	x			x			x	
60.3 m (198'–199')	x	x	x			x				x			x	x	x	x		x		x				x							x	x			x	x	x			x	x			x	x	x		x	x			x	
60.6 m (199'–200')	x		x			x				x			x	x	x	x		x	x	x				x							x	x			x	x	x			x	x			x	x			x	x			x	x
60.9 m (200'–201')	x		x	x	x	x		x				x	x	x	x	x	x	x	x	x				x	x						x	x	x			x	x			x	x			x	x	x		x	x			x	x
61.2 m (201'–202')																																																					
61.6 m (202'–203')																																																					
61.9 m (203'–204')																																																					
62.2 m (204'–205')																																																					
62.5 m (205'–206')																																																					
62.8 m (206'–207')																																																					
63.1 m (207'–208')																																																					
63.4 m (208'–209')																																																					
63.7 m (209'–210')			x			x		x					x		x		x	x		x				x						x					x		x			x		x			x	x	x		x	x			x	x
64.0 m (210'–211')						x							x	x	x	x		x			x			x	x					x		x			x	x				x			x	x			x	x			x	x
64.3 m (211'–212')			x	x		x			x					x		x		x	x		x	x	x						x					x		x		x	x			x	x			x	x			x	
64.6 m (212'–213')																																																					
64.9 m (213'–214')																																																					
65.2 m (214'–215')			x	x		x			x		x		x	x		x		x	x		x	x			x					x					x		x	x			x	x			x	x			x	

tion Bore No. 2 is latest middle Eocene in age. It is worth noting, however, that this section is very condensed and the possibility of a (very thin) barren interval between core F85-70 and the lower upper Eocene core F84-70 cannot be ruled out.

Upper Eocene. In Kingston Bore and Observation Bore No. 1, assemblages representing the lowest appearance of nannofossils above the *Daktylethra punctulata–Reticulofenestra scissura* association lack both *Chiasmolithus grandis* and *Daktylethra punctulata*, but contain *Chiasmolithus oamaruensis*, indicating an early late Eocene age. Forms mimicking either *Daktylethra punctulata* or *Corannulus germanicus* in optical microscopy were encountered, sporadically, in most of the late Eocene assemblages, but they either lack the thickened sides, distinctive in *D. punctulata* between crossed nicols or appear as distorted *C. germanicus* (Figs. 2,3).

In Observation Bore No. 2, the assemblages immediately above the highest appearance of *Chiasmolithus grandis* in core F85-70 include *Chiasmolithus oamaruensis* and are considered earliest late Eocene. The events of highest appearance of *Neococcolithes dubius*, lowest appearance of *Isthmolithus recurvus*, and highest appearances of *Cyclicargolithus reticulatus* and *Discoaster saipanensis* (Fig. 6) are discernible in Kingston Bore and Observation Bores No. 1 and 2. The highest appearances of *C. reticulatus* and *D. saipanensis* could not be separated.

The base of the continuous calcareous planktic/marine section in Kingston Bore and Observation Bore No. 1 seems to correlate with the base of the corresponding section at Browns Creek. The base at Browns Creek is early late Eocene, being later than the extinction of *Chiasmolithus grandis* and earlier

Table 4. Distribution of selected calcareous nannofossil taxa in the Kongorong Sand (42.1 — 45.7 m) and Lacepede Formation (21.3 — 42.1 m) of the (South Australian Department of Mines) Observation Bore No. 1, County Robe, Hd. Townsend, Section 125.

Nannofossils are scarce in the top two samples, presumably because of leaching at the contact Lacepede Formation/Gambier Limestone, which coincides with a disconformity (see text).

	Blackites amplus	*Blackites spinosus*	*Blackites spinulus*	*Blackites tenuis*	*Blackites vitreus*	*Braarudosphaera bigelowi*	*Chiasmolithus altus*	*Chiasmolithus expansus*	*Chiasmolithus grandis*	*Chiasmolithus oamaruensis*	*Clathrolithus ellipticus*	*Clausicoccus cribellum*	*Coccolithus eopelagicus*	*Coccolithus pelagicus*	*Corannulus germanicus*	*Cyclicargolithus floridanus*	*Cyclicargolithus luminis*	*Cyclicargolithus reticulatus*	*Cyclococcolithus formosus*	*Cyclococcolithus protoannulus*	*Daktylethra punctulata*	*Discoaster barbadiensis*	*Discoaster elegans*	*Discoaster saipanensis*	*Discoaster tani*	*Discoaster tani nodifer*	*Discoaster tani ornatus*	*Helicosphaera compacta*	*Helicosphaera reticulata*	*Helicosphaera seminulum*	*Holococcolithus macroporus*	*Isthmolithus recurvus*	*Lanternithus minutus*	*Markalius inversus*	*Micrantholithus attenuatus*	*Micrantholithus procerus*	*Micrantholithus truncus*	*Neococcolithes dubius*	*Orthozygus aureus*	*Pemma basquensis*	*Pemma papillatum*	*Polycladolithus opersus*	*Pontosphaera multipora*	*Pontosphaera plana*	*Reticulofenestra hampdenensis*	*Reticulofenestra scissura*	*Reticulofenestra scrippsae*	*Reticulofenestra umbilica*	*Sphenolithus moriformis*	*Sphenolithus predistentus*	*Transversopontis obliquipons*	*Transversopontis pulcher*	*Transversopontis zigzag*	*Trochaster simplex*	*Zygrhablithus bijugatus bijugatus*	*Zygrhablithus bijugatus crassus*
21.3 m (70'–73'6'')						×							×			×	?	×	×					×									×										×	×									×	
22.4 m (73'6''–77'6'')													×			×		×	×	×				×									×											×									×	
23.6 m (77'6''–81')						×							×	×		×		×												cf.		×		×					×					×	×	×	×							×	
24.7 m (81'–85')		×	×			×	×			×		×				×		×						×								×							×					×		×	×								
25.9 m (85'–88'6'')				×		×	×			×				×				×	×		×											×													×	×								
26.4 m (88'6''–95')				×	×	×							×	×		×		×						×								×	×	×							×						×								×	
28.9 m (95'–101')														×		×																	×													×									
32.0 m (105'–108'6'')		×	×		×							×		×				×						×		×	×						×						×					×	×	×	×							×	
33.0 m (108'6''–112'6'')		×	×		×								×	×		×		×	×		×				×	×	×						×	×									×			×	×							×	×
34.3 m (112'6''–115')		×	×	×	×							×	×			×		×	×					×			×				×	×	×											×			×	×								×
35.0 m (115'–118')		×	×	×	×		×			×	×	×	×	×		×		×	×	×						×	×			cf.	×	×	×				?	×		×			×		×	×								×
36.0 m (118'–124')	×	×		×	×	×				×			×	×	×	×	×	×	×	×	cf.		×	×		×	×						×	×	×			×	×		×			×	×	×	×								×
37.8 m (124'–127')	×		×		×	×				×			×	×	×	×		×	×		cf.			×		×	×						×	×	×	×		×	×			×			×	×	×	×							×	×
38.7 m (127'–130')																																																								
39.6 m (130'–133')																																																							
40.5 m (133'–136')																																																							
41.4 m (136'–140')																																																							
42.7 m (140'–143')			×	×				×	×				×	×		×	×		×	×	×	×			×		×							×	×				×			×			×	×	×								×	×
43.6 m (143'–147'6')	×		×	×				×	×				×	×		×	×		×	×	×	×	×	×	×	×	×						×	×				×			×	×	×	×	×	×	×	×	×	×	×	×	×	×	×
44.9 m (147'6''–152'6'')	×		×	×					×				×	×		×	×		×	×	×	×	×	×	×	×	×			cf.			×	×				×			×	×	×	×	×	×	×	×	×	×		×		×	×
46.5 m (152'6''–155')																																																						

than the extinction of *Neococcolithes dubius*. The base of the corresponding section in Observation Bore No. 2 is only slightly older, being latest middle Eocene, as suggested above. Thus, subsequent to the middle Eocene ingressions in the Gambier Embayment, the transgression began during the latest middle to early late Eocene, almost simultaneously in widely separated areas across the Otway Basin.

The order of recognisable nannofossil events in the upper Eocene section in the Gambier Embayment (Fig. 6) is the same as that in the Browns Creek section (Fig. 5). However, the simultaneous disappearance of both *Cyclicargolithus reticulatus* and *Discoaster saipanensis* at the top of the Eocene section in the Gambier Embayment contrasts with the section at Browns Creek, where *C. reticulatus* disappears much lower than the highest appearance of *D. saipanensis*. This indicates that the upper part of the Eocene, present at Browns Creek above the *Cyclicargolithus reticulatus* extinction, is missing from the Gambier Embayment sections.

The evidence from the highly condensed sections in the Gambier Embayment suggests slow sedimentation and a pronounced disconformity at the top of the Eocene. The average rate of sedimentation for the upper Eocene sections in the Gambier Embayment compares with that for the lower part of the Browns Creek Clays, up to and including the *'Notostrea'* greensand. The Gambier Embayment lithological succession of Kongorong Sand and Lacepede Formation can be traced in the lower part of the Browns Creek Clays up to and including the greensand (McGowran, 1973).

The top of the Eocene in the Gambier Embayment, based on the extinction of *Discoaster saipanensis*, coincides with the top of the Lacepede Formation in Observation Bore No. 1 and Kingston Bore (Tables 3,4), but cuts through this formation in Observation Bore No. 2. Based on the presence of *Cyclococcolithus formosus, Lanternithus minutus, Isthmolithus recurvus*, and *Reticulofenestra umbilica* in assemblages above the extinction of both *Cyclicargolithus reticulatus* and *Discoaster saipanensis* (Table 5), the main part of the Lacepede Formation in the Observation Bore No. 2 is early Oligocene. This suggests that the Lacepede Formation is a transgressive unit. The same conclusion is also valid for the Kongorong Sand; although this unit contains a middle Eocene assemblage in the Observation Bore No. 1, nannofossils recovered from an open tube core from the same unit in the SADM Bore MI/1 (Millicent Test area) include *Chiasmolithus oamaruensis, Cyclicargolithus reticulatus, Cyclococcolithus formosus, Helicosphaera compacta, Pontosphaera multipora, Reticulofenestra hampdenensis* 'group', *R. scissura, R. umbilica, Zygrhablithus bijugatus bijugatus*, and *Z. bijugatus crassus*, suggesting a late Eocene age.

Biostratigraphic correlations

Correlation with the Perth Basin

The sequence of nannofossil events recognised in the middle Eocene of the Gambier Embayment slightly overlaps with another sequence of events compiled by Shafik (1978). The latter, based partly on material from the Perth Basin, Western Australia, comprises the events of highest appearance of

Table 5. Distribution of selected calcareous nannofossil taxa in the Lacepede Formation of the (South Australian Department of Mines) Observation Bore No. 2, County Robe, Hd. Ross, Section D.
The contact Knight Formation/Lacepede Formation is at 137.2 m.
Note that *Reticulofenestra hampdenensis* 'group' ranges higher than *Discoaster saipanensis*.

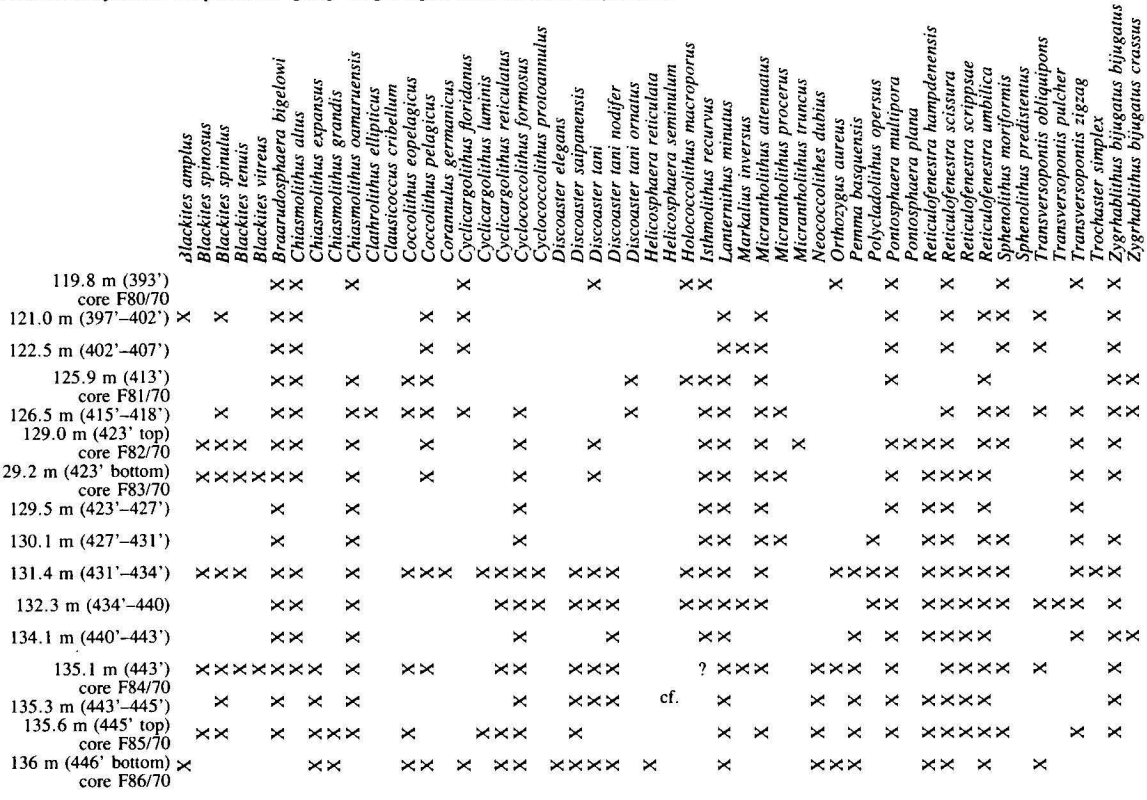

Chiasmolithus solitus (the youngest), lowest appearance of *Helicosphaera reticulata*, lowest appearance of *Cyclicargolithus reticulatus*, and lowest appearances of *Pemma papillatum* and *Reticulofenestra scrippsae* (the oldest).

The middle Eocene Perth Basin material, in the Rottnest Island Bore, can be correlated with the *Chiasmolithus solitus–Cyclicargolithus reticulatus* association in Kingston Bore, on the presence of the nominate species and other taxa, such as *Daktylethra punctulata, Chiasmolithus grandis, Cyclococcolithus formosus, Lanternithus minutus, Neococcolithes dubius* and *Reticulofenestra umbilica* (Shafik, 1978).

Correlation with New Zealand

Middle and late Eocene calcareous nannofossil events recognised in the Otway Basin are broadly similar to those recorded from coeval sediments in New Zealand; differences are minor, and the important events are in the same chronological order. Thus, the set of important events discernible up the section as the highest appearance of *Chiasmolithus solitus*, preceding the sequential appearances of *Reticulofenestra scissura* (reported as *R. bisecta* in New Zealand by Edwards, 1971), *Chiasmolithus oamaruensis* and *Isthmolithus recurvus*, and ending with the highest appearance of *Discoaster saipanensis*, is readily recognisable both in New Zealand (Edwards, 1971) and in the Otway Basin.

Chiasmolithus grandis is absent from the interval in New Zealand, and both *Neococcolithes dubius* (reported as *Zygolithus dubius*) and *Daktylethra punctulata* slightly overlap with *Isthmolithus recurvus* (Edwards, 1971). *Cyclicargolithus reticulatus* was not reported by Edwards (1971) even though it is present in the New Zealand upper Eocene (Shafik, unpublished data).

Reticulofenestra hampdenensis, an important biostratigraphic marker in Eocene sections in New Zealand (Edwards, 1971), is common in the sections studied in the Otway Basin, though it is difficult to discern from other closely related species. Unlike its presently known record in New Zealand (Edwards, 1971), the *R. hampdenensis* 'group' ranges higher than the highest appearance of *Discoaster saipanensis* in the material studied; taxonomic revision of *R. hampdenensis* 'group' in the Australian material may prove biostratigraphically worthwhile.

Integration of nannofossil and foraminiferal results

Middle Eocene. The highest appearance of the nannofossil *Chiasmolithus solitus* has been widely used as a middle Eocene biostratigraphic datum. Roth & others (1971) placed this event high in the equivalent of foraminiferal zone P.12. Bukry (1973b) estimated the age of this datum to be 44 m.y.; according to Hardenbol & Berggren (1978), this corresponds with the date for the P.12/P.13 zonal boundary. I accept the placement of the highest appearance of *Chiasmolithus solitus* in the top part of zone P.12, even though Martini (1971) suggested a younger correlation (early zone P.14).

The lowest appearance of the nannofossil *Cyclicargolithus reticulatus* has been placed tentatively in zone P.12 (Shafik, 1973). This has now been confirmed in the Eocene section of Ninetyeast Ridge (Indian Ocean, DSDP site 214): *C. reticulatus* makes its lowest appearance at site 214 between two foraminiferal events, namely the highest appearance of *Morozovella aragonensis* (below) and the lowest appearance of *Orbulinoides beckmanni* (above), indicating zone P.12 (personal observation).

The middle Eocene nannofossil assemblage in Kingston Bore (and probably also in Beachport Bore No. 1), referred to as the *Chiasmolithus solitus–Cyclicargolithus reticulatus* association,

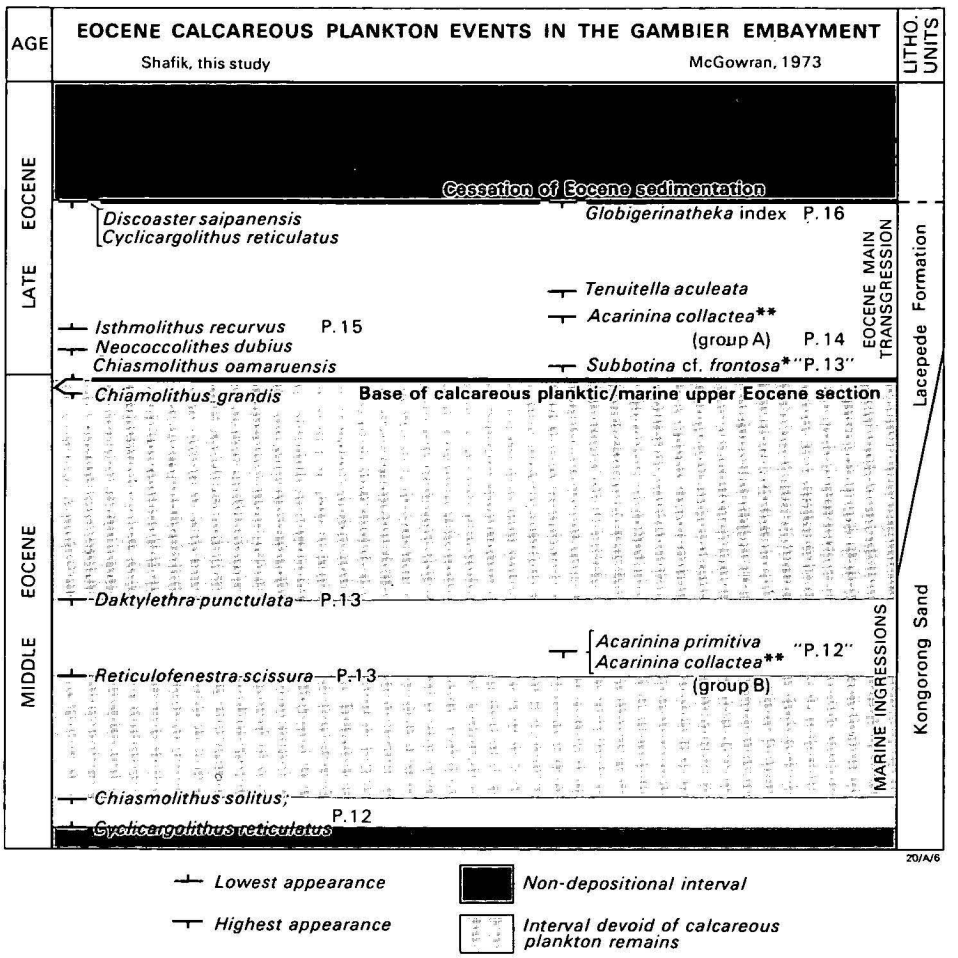

Figure 6. Integration of the nannofossil and foraminiferal events occurring in the middle and upper Eocene of the Gambier Embayment, and their correlation with the P. zones of the tropics.
*mis-identified by McGowran (1973) as *Subbotina frontosa* (McGowran, 1978a).
**McGowran (1973) differentiated *Acarinina collactea* into two groups, but later (McGowran, 1978a) excluded *A. collactea* 'group B' from the biostratigraphic framework, *A. collactea* in Figs. 5 & 7 equals *A. collactea* (group A) here.

therefore correlates with foraminiferal zone P.12. The similar nannofossil assemblage encountered in the Rottnest Island Bore, Perth Basin (Western Australia) has already been correlated with zone P.12 (Shafik, 1978); associated foraminiferids have been correlated with the zonal interval P.11–P.13 (Quilty, 1978).

The lowest appearance of the nannofossil *Reticulofenestra scissura* has been recorded in the range of the foraminiferid *Orbulinoides beckmanni* (= zone P.13), both in the Possagno section, Italy (*R. bisecta* datum in Roth & others, 1971) and at the DSDP site 214 (Gartner, 1974; Shafik, unpublished data). The highest appearance of abundant *Daktylethra punctulata* is placed tentatively near the top of the foraminiferal zone P.13. The middle Eocene *Daktylethra punctulata–Reticulofenestra scissura* association in Kingston Bore and Observation Bore No. 1 is correlated with zone P.13.

The highest appearances of the foraminiferal species *Acarinina collactea* 'group B' of McGowran (1973) and *Acarinina primitiva* in the Gambier Embayment are at the same level (McGowran, 1973). This level, being between the lowest appearance of *Reticulofenestra scissura* (below) and the highest appearance of *Daktylethra punctulata* (above) (Fig. 6), is herein placed in zone P.13. McGowran (1973) tentatively placed the same level in zone P.12. The middle Eocene foraminiferal assemblage in the Rottnest Island material (Quilty, 1978), which is associated with nannofossils coeval with zone P.12, apparently lacks both *Acarinina collactea* 'group B' of McGowran (1973) and *A. primitiva*.

In a review of the foraminiferal biostratigraphy of southern Australia, McGowran (1978a) revised some of his earlier conclusions. He excluded the highest appearance of *Acarinina collactea* 'group B' of McGowran (1973) from the biostratigraphic framework, because the taxon includes several morphotypes, and placed the highest appearance of *A. primitiva* in the younger part of zone P.14.

According to Blow (1979), *Acarinina primitiva* ranges up to zone P.13 and is only questionably present in the earliest part of zone P.14. The highest appearance of the same taxon, as shown by Stainforth & others (1975), is at the top of the *Orbulinoides beckmanni* zone (= zone P.13). The nannofossil evidence from the Gambier Embayment, placing the highest appearance of *A. primitiva* in zone P.13 (Fig. 6), seems to agree with the data given by Blow (1979) and Stainforth & others (1975).

McGowran (1978a) based his correlation of the Kongorong Sand assemblage, which includes *Acarinina primitiva* (seemingly that in the Observation Bore No. 1, McGowran, 1971), with zone P.14 on the absence of the foraminiferids *Planorotalites pseudoscitula* and *Subbotina frontosa*.

Assemblages containing *Acarinina primitiva, Planorotalites pseudoscitula*, and *Subbotina frontosa* occur in southern Australia in the Eucla Basin (McGowran & Lindsay, 1969), where, according to McGowran (1978a), the foraminiferal assemblages are slightly older than in the Gambier Embayment. However, *Planorotalites pseudoscitula* has been shown to range up to the top of the middle Eocene (P.14/P.15 zonal boundary) in several DSDP sections in the Indian Ocean (McGowran, 1978b).

In New Zealand, *Pseudogloboquadrina primitiva* (= *Acarinina primitiva*) disappears at a level slightly below the lowest appearance of *Reticulofenestra bisecta* (= *R. scissura*) (Hornibrook & Edwards, 1971); *Acarinina collactea* 'group B' of McGowran (1973) apparently has not been encountered in the New Zealand Eocene.

The highest appearance of the nannofossil *Chiasmolithus grandis* is slightly below the top of the foraminiferal zone P.14 (Gartner, 1971), notwithstanding Martini's (1976) claim that it overlaps the lowest appearance of *Isthmolithus recurvus* in high-latitude sections. The nannofossil assemblage in core F86-70 (Observation Bore No. 2) includes *Chiasmolithus grandis, C. expansus, Cyclicargolithus reticulatus, Discoaster saipanensis, Reticulofenestra scissura* and some holococcoliths, but lacks *Daktylethra punctulata*. This assemblage is placed against the foraminiferal zone P.14. It is worth noting that core F86-70 is well above the highest appearance of the foraminiferid *Acarinina primitiva* in Observation Bore No. 2 section (McGowran, 1973), especially when the extreme slow rate of sedimentation of the calcareous planktic Eocene section in this bore is considered.

The nannofossil assemblage of core F85-70 (Observation Bore No. 2), characterised by the overlap in the ranges of *Chiasmolithus grandis* and *C. oamaruensis*, is considered coeval with the uppermost part of zone P.14; the lowest appearance of *C. oamaruensis* has been correlated with a level high in zone P.14 (Gartner, 1971; Roth & others, 1971).

Upper Eocene. It is generally agreed that the earliest appearance of *Isthmolithus recurvus* is in the upper part of zone P.15 (Martini, 1971; Roth & others, 1971; Gartner, 1971). The highest appearance of the nannofossil *Neococcolithes dubius*, being between the lowest appearance of *Isthmolithus recurvus* and the highest appearance of *Chiasmolithus grandis*, correlates with a level in zone P.15.

The biostratigraphic summaries presented in Figures 5 and 6 suggest that the highest appearance of *Acarinina collactea* (= *A. collactea* 'group A' of McGowran, 1973) is inconsistent with the nannofossil and other foraminiferal evidence. This foraminiferid is absent from the Browns Creek section, but ranges to above the lowest appearance of the nannofossil *Isthmolithus recurvus* in the Gambier Embayment; the base of the calcareous planktic/marine section at Browns Creek is below the lowest appearance of *I. recurvus*. McGowran (1978a) concluded that the highest appearance of *Acarinina collactea* is very close to the base of the calcareous planktic/marine section at Browns Creek, i.e. below the highest appearance of the foraminiferid *Subbotina* cf. *frontosa*; the order of these foraminiferal events is reversed in the Gambier Embayment.

The highest appearance of *Subbotina* cf. *frontosa* is consistently between the lowest appearances of *Chiasmolithus oamaruensis* and *Isthmolithus recurvus* in the sections studied, and should, therefore, be placed in zone P.15, which is not in agreement with McGowran's (1973) correlation of this foraminiferal event as being within zone P.13 or zone P.14. Subsequently, however, McGowran (1978a, b) combined the highest appearances of *Acarinina collactea* and *Subbotina* cf. *frontosa* into one biostratigraphic horizon, which he placed in zone P.15 of the tropics.

In Figure 7, the highest appearances of *Acarinina collactea* and *Subbotina* cf. *frontosa* are separated; the former is the older, in keeping with the results from the Browns Creek section. The highest appearance of *A. collactea* is considered to be at approximately the level of disappearance of the nannofossil *Chiasmolithus grandis*. The base of the calcareous planktic/marine section at Browns Creek is younger than these two events, but older than the highest appearance of *Subbotina* cf. *frontosa*. In New Zealand, the latter species has not been recorded, and *Chiasmolithus grandis* is absent from the interval. *Acarinina collactea* (reported as *Truncorotaloides*

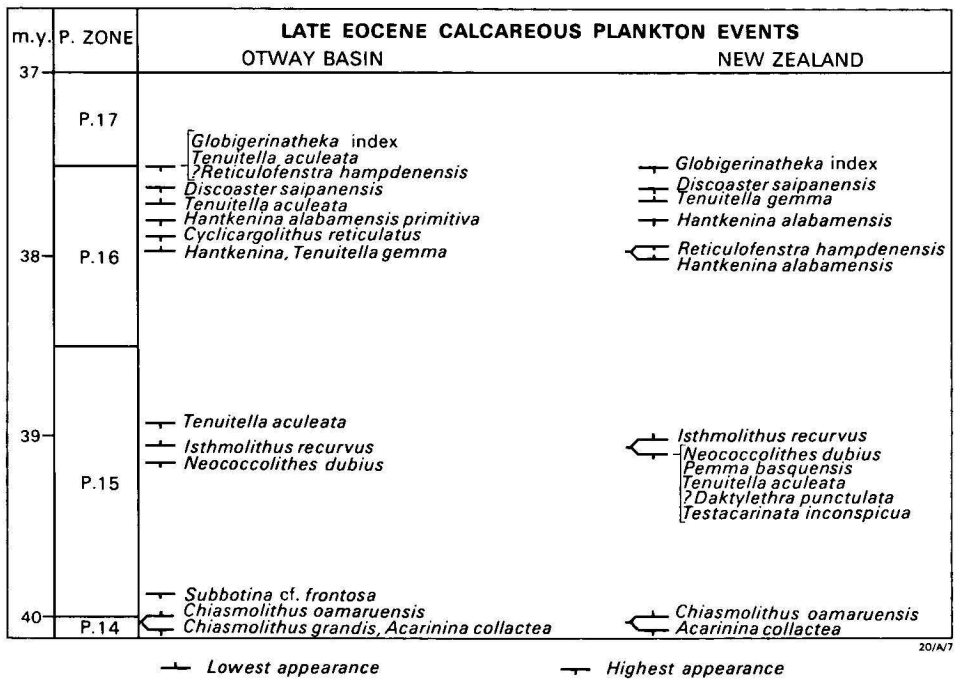

Figure 7. Correlation of upper Eocene calcareous microfossil in the Otway Basin and New Zealand.

collactea) disappears about the level of the lowest appearance of the nannofossil *Chiasmolithus oamaruensis* in the New Zealand upper Eocene (Hornibrook & Edwards, 1971).

The vertical range of the foraminiferid *Tenuitella aculeata* in the Browns Creek section is disjunct (McGowran, 1978a) and, on the available nannofossil evidence, the highest appearance of this species in the Gambier Embayment (as recorded by McGowran, 1973) may be correlated with the first up-section disappearance of the species at the Browns Creek section. In relation to the nannofossil sequence of events, this level is distinctly above the lowest appearance of *Isthmolithus recurvus* but lower than the disappearance of *Cyclicargolithus reticulatus*. *Tenuitellaaculeata* (reported as *Globorotalia aculeata*) disappears about the same level as the lowest appearance of *Isthmolithus recurvus* in New Zealand (Hornibrook & Edwards, 1971). However, McGowran (1978a) presented the first up-section disappearance of *T. aculeata* as an isochronous event across southern Australia, New Zealand, and the South Campbell Plateau. This would require the presence of a hiatus in the upper Eocene sections in New Zealand at about a level where *Tenuitella aculeata, Testacaromata inconspicua, Pemma basquensis* and *Neococcolithes dubius* disappear, and where *Isthmolithus recurvus* first appears (Hornibrook & Edwards, 1971). That this might be the case cannot be judged, but Jenkins (in Kennett, Houtz & others, 1975, p. 51) concluded that the extinction levels of *T. aculeata* in New Zealand, South Australia and Europe ' . . . appear to be diachronous' (see also Jenkins, 1974). In Figure 7, the first up-section disappearance of *T. aculeata* in the Otway Basin and New Zealand is shown at slightly different levels.

Shafik (1981) argued for placing the highest appearance of *Cyclicargolithus reticulatus* in the younger part of zone P.16, and evidence from elsewhere suggests that the highest appearance of *Discoaster saipanensis* is near the P.16/P.17 zonal boundary (e.g. Roth & others, 1971; Bukry, 1973b; Hardenbol & Berggren, 1978). In the Gambier Embayment, *Cyclicargolithus reticulatus* and *Discoaster saipanensis* disappear at the same level, and with current knowledge it is difficult to correlate this level in terms of the foraminiferal P. zonation.

Discussion

Cande & others (1981) have pushed back the age of the break up of Australia and Antarctica by about 30 m.y., to the mid-late Cretaceous, and suggested a very slow sea-floor spreading rate during the interval ending in the mid-middle Eocene (45 m.y.), and a faster rate thereafter. They also suggested that their postulated (mid-middle Eocene) change in spreading rate coincided with global plate reorganisations.

The relationship between changes in the spreading rate or in the volume of mid-ocean ridge and eustacy has been acknowledged (e.g. Pessagno, 1972; Hayes & Pitman, 1973): a major acceleration in the spreading rate is likely to be concomitant with a rise in sea level or a transgression.

A major change in spreading rate south of Australia at 45 m.y. matches well the dates of the middle Eocene marine ingressions detected herein in the Gambier Embayment: nannofossils representing the first ingression in the Kingston Bore section are coeval with foraminiferal zone P.12, and the co-occurrence of *Chiasmolithus solitus* and *Cyclicargolithus reticulatus* suggests an age close to 45 m.y. The nannofossils of the younger and more widespread ingression in the Gambier Embayment suggest a correlation with foraminiferal zone P.13, which spans the interval 42–44 m.y. (Hardenbol & Berggren, 1978). These ingressions also correlate well with the onset of the Eucla Basin transgression.

Palaeoenvironmental considerations

The biostratigraphic usefulness of a nannofossil taxon over a wide area can largely be measured by its sensitivity to such parameters as water depth and temperature. Susceptibility to dissolution in deep water suggests low reliability in deep oceanic sediments, but not necessarily in shallow-water sediments. Low tolerance to temperature variation makes biostratigraphic reliability of a taxon outside its preferred latitudes uncertain. Unfortunately, with the available evidence, determination of these parameters has to be in broad terms.

Water depth

The calcareous nannofossil assemblages recovered include different combinations of species of the genera *Blackites, Braarudosphaera, Corannulus, Daktylethra, Lanternithus, Micrantholithus, Orthozygus, Pemma, Polycladolithus, Pontosphaera, Transversopontis, Trochoaster* and *Zygrhablithus* which indicate deposition in a marginal marine environment (nearshore or shelf conditions). That some of these taxa have been considered as indicative of the middle to inner neritic (e.g. *Blackites amplus* and *Trochoaster simplex*) or the outer neritic (e.g. *Pontosphaera plana* and *Micrantholithus procerus*) environments (Sherwood, 1974) can only affirm the nearshore or shelf conditions, where dissolution of the calcareous plankton remains is usually negligible or absent. This is supported by lithological evidence from the Browns Creek Clays, Kongorong Sand and Lacepede Formation.

Among the biostratigraphically important nannofossil taxa, *Daktylethra punctulata, Neococcolithes dubius* and *Cyclicargolithus reticulatus* are believed to be susceptible to dissolution in deep water, as evidenced by their rarity or total absence from deep oceanic sediments. Biostratigraphic events based on these taxa can only be regarded as reliable in sediments deposited in shallow-water conditions, like those studied here. That other taxa, such as *Chiasmolithus grandis* and *Discoaster saipanensis* seem to have preferred deeper water or were better preserved under deeper-water conditions (Sherwood, 1974) suggests that the exclusion of these taxa from sediments deposited in shallow-water conditions may not be true extinction. This is particularly so in regard to the sporadic record of *Discoaster saipanensis* in the uppermost part of the Browns Creek Clays, where extreme shoal conditions (described as regression by McGowran, 1978a) apparently prevailed.

Discussion. Shafik (1981) concluded that the sedimentation rates were relatively very high for the thick upper Eocene section above the disappearance level of *Cyclicargolithus reticulatus* or the foraminiferid *Hantkenina alabamensis primitiva* at Browns Creek and in the St Vincent Basin. Earlier, McGowran (1978a) noted a regressive phase, in the same expanded section, and suggested that it was due to some eustatic event. The Chinamans Gully beds in the section in the St Vincent Basin were cited as evidence for this 'regressive phase'. These beds are devoid of nannofossils.

The basal part of the section at Castle Cove (near Browns Creek) includes a facies with benthic foraminiferids, but not planktic remains; a similar horizon occurs in the top 10 m of the Browns Creek Clays at Browns Creek (McGowran, 1978a). The nannofossil evidence for a detectable water-depth change in the upper part of the section at Browns Creek is tenuous, but it is not so in the lower part of the section at Castle Cove, where the nannofossil abundance and diversity decline drastically.

An alternative interpretation of the evidence from the Castle Cove–Browns Creek area and the St Vincent Basin is that it is the result of shoaling caused by sedimentation. During most of

the late Eocene, the depositional environment was essentially shallow marine (nearshore or shelf), as evinced by the nannofossils. Rates of sedimentation increased substantially soon after the disappearance of *Cyclicargolithus reticulatus* or *Hantkenina* (Shafik, 1981), but water depth seemingly did not change significantly during most of the ensuing late Eocene interval; the areas of deposition were probably subsiding. Sediments deposited then continued to contain calcareous plankton remains. However, as the rate of sedimentation increased with respect to subsidence, extreme shoal conditions resulted, restricting access of some or all of the calcareous plankton. The sediments that accumulated at that time (Castle Cove–Browns Creek area) contain little or no calcareous planktic remains, though benthic foraminiferids are present. The shoaling culminated in the deposition of the paralic Chinamans Gully beds (and their equivalent) in the St Vincent Basin. Subsequent renewed subsidence caused 'normal' hemipelagic sedimentation (with calcareous planktic remains) to resume.

Water temperature

The isotopic temperature curve for the middle and late Eocene of the South Campbell Plateau (Shackleton & Kennett, 1975) indicates a trend of gradual cooling (in the 15'C to slightly less than 10'C range, culminating in a sharp drop in the early Oligocene) with several reversals. The nannofossil biostratigraphy of the same section (Edwards & Perch-Nielsen, 1975) reveals a late middle and late Eocene sequence of events essentially similar to that in the Otway Basin, though the Campbell Plateau occupied higher latitudes. The exception is a belated appearance of *Reticulofenestra scissura* in the Campbell Plateau section. Combining the results of Shackleton & Kennett (1975) and Edwards & Perch-Nielsen (1975) indicates that *Cyclicargolithus reticulatus, Chiasmolithus oamaruensis* and *Isthmolithus recurvus* appeared during a period of reversal in the trend, i.e. during a warmer pulse, and *Cyclicargolithus reticulatus* and *Discoaster saipanensis* disappeared before the early Oligocene chilling.

Conditions along the Australian southern margin during the middle and late Eocene were generally temperate, with surface-water temperature decreasing eastward. The newly formed wide gulf south of Australia was open to the Indian Ocean (Deighton & others, 1976), where surface-water temperatures were high (Frakes & Kemp, 1972). Marine sedimentation along the Australian southern margin was diachronous, as attested to by the age of the lowest occurrences of nannofossils, being younger eastward (Shafik, 1973). In the same fashion, surface-water temperature decreased eastward.

Dealing with the Paleogene regional plankton biogeography, Sancetta (1979) suggested temperate conditions for the entire Australian southern margin during the Eocene, and distinguished a middle Eocene temperate province, which was confined to the Southern Hemisphere, and a southern late Eocene temperate province. Sancetta based the middle Eocene temperate province on assemblages with numerous *Chiasmolithus grandis, C. expansus, C. solitus* and *Reticulofenestra* species, but also including *Coccolithus pelagicus, Cyclococcolithus formosus* and *Cyclicargolithus reticulatus* and described the southern late Eocene temperate province assemblages as dominated by taxa referable to *Reticulofenestra scissura* and *R. scrippsae* and including *Chiasmolithus* species, *Isthmolithus recurvus, Cyclicargolithus reticulatus* and *Zygrhablithus bijugatus*. Sancetta's (1979) conclusions were based on a synthesis of data from several DSDP sites in the Pacific and Eastern Indian Oceans.

Evidence reviewed by McGowran (1978a) was interpreted as suggesting warm conditions in southern Australia during the late Eocene. I wish to stress that conditions in the Otway Basin during the middle and late Eocene were cooler than those prevailing in the west. Thus, during the middle Eocene (*Chiasmolithus solitus–Cyclicargolithus reticulatus* and *Reticulofenestra scissura–Daktylethra punctulata* associations, i.e. foraminiferal zones P.12 and P.13), conditions were not warm enough to permit an incursion into the Otway Basin of, for example, the larger foraminiferid, *Discocyclina* which is found in Western Australia (Edgell *in* Condon & others, 1956), or the low-latitude planktic foraminifera, *Orbulinoides beckmanni* which occurs in sediments from the Indian Ocean. Likewise, during the late Eocene, conditions in the Otway Basin were generally temperate, except for a brief warmer interval marked by the presence of the foraminiferid, *Hantkenina alabamensis primitiva*. For example, the warm-water foraminiferids, *Asterocyclina, Nummulites* and *Assilina* which are present in the upper Eocene of the Carnarvon Basin, Western Australia (Cockbain, 1978), are absent from the Otway Basin; the geographic range of *Asterocyclina* includes southwestern Australia (Cockbain, 1967). Also, the warm-water foraminiferal genera, *Halkyardia* and *Linderina* occur in the upper Eocene of the St Vincent Basin, South Australia (Lindsay, 1967, 1969), but not eastwards in the Otway Basin.

With temperate conditions prevailing during the middle and late Eocene in the Otway Basin, biostratigraphic events based on the nannofossil taxa, *Chiasmolithus solitus, Cyclicargolithus reticulatus, Daktylethra punctulata, Reticulofenestra scissura, Chiasmolithus grandis, C. oamaruensis, Neococcolithes dubius, Isthmolithus recurvus* and *Discoaster saipanensis* should be considered highly reliable. There is some evidence to suggest that these taxa were successful under temperate conditions. For example, *Cyclicargolithus reticulatus* apparently tolerated a wide range of temperatures: it occurs abundantly in hemipelagic sediments in the Gulf of Mexico (Bukry, 1973b) and the South Campbell Plateau (Edwards & Perch-Nielsen, 1975), but preferred warm-water conditions. The geographic distribution of *Reticulofenestra scissura* (e.g. Italy, Ninetyeast Ridge, New Zealand, and elsewhere) suggests that this species was temperate with a preference for warmer conditions during the middle Eocene. Sancetta (1979) considered this taxon (reported as *Dictyococcites bisecta*) among the cosmopolitan species with tolerance to cool waters.

The geographic distribution of *Chiasmolithus grandis* seems to suggest that the species was cosmopolitan with preference for warm oceanic conditions, whereas *Chiasmolithus oamaruensis* as well as *Isthmolithus recurvus* seem to have preferred cool water, as can be inferred from their apparent bipolar geographic distribution; the last two taxa are usually absent from low-latitude sediments.

Summary and conclusions

Among the patterns of marine transgression described by Taylor (1967, 1971), the pattern of ingressions preceding a main transgression appears to match the middle to late Eocene marine sedimentation in the western part of the Otway Basin. The middle Eocene calcareous planktic/marine record in the Gambier Embayment is broken, so that the nannofossil assemblages are isolated from each other as well as from the overlying abundantly fossiliferous, essentially upper Eocene section by intervals devoid of calcareous microfossils.

During the middle Eocene, marine ingressions, represented by isolated assemblages, occurred in the Gambier Embayment (western Otway Basin), but did not reach the Browns Creek area (eastern Otway Basin), attesting to the diachroneity of Eocene marine sedimentation in the Otway Basin. This is also demonstrated by the rock units being transgressive in the

Gambier Embayment. The Kongorong Sand in Observation Bore No. 1 contains middle Eocene microfossils, whereas in Millicent Bore it contains younger (late Eocene) nannofossils. The Lacepede Formation is entirely Eocene in two sections (Observation Bore No. 1 and Kingston Bore), but in Observation Bore No. 2 it includes the Eocene/Oligocene boundary, marked by a disconformity.

The onset of the main Eocene transgression was apparently synchronous across the Otway Basin. The base of the continuous calcareous planktic/marine Eocene section in Observation No. 1 and Kingston Bore (Gambier Embayment) and at Browns Creek appear to be of the same age, early late Eocene. The base of the corresponding section in Observation Bore No. 2 is only slightly older, latest middle Eocene. The main transgression began across the Otway Basin during the latest middle to early late Eocene.

The middle Eocene ingressions are represented by two assemblages, referred to as the *Chiasmolithus solitus–Cyclicargolithus reticulatus* and *Daktylethra punctulata–Reticulofenestra scissura* associations. These are thought to be coeval with foraminiferal zones P.12 and P.13, respectively. As a consequence of this correlation, the local foraminiferal event of highest appearance of *Acarinina primitiva* is placed in zone P.13 of the tropics.

The middle Eocene assemblages, encountered at the base of the continuous calcareous planktic/marine section in Observation Bore No. 2, are placed immediately below the middle/upper Eocene boundary, and are thought to correlate with the younger part of foraminiferal zone P.14. These assemblages lack *Daktylethra punctulata*, but include *Reticulofenestra scissura*, and the younger of them is characterised by overlap in the ranges of *Chiasmolithus grandis* and *C. oamaruensis*. The middle/upper Eocene boundary is drawn immediately above the highest appearance of *Chiasmolithus grandis*.

The latest middle Eocene nannofossil assemblages in Observation Bore No. 2, coeval with late zone P.14, are well above the highest appearance of the foraminiferid *Acarinina primitiva* in the bore, particularly when the extremely slow rate of sedimentation of the Observation Bore No. 2 Eocene calcareous planktic/marine section is considered.

The upper Eocene sequence of nannofossil events recognised in the Browns Creek section is the same as that in the Gambier Embayment sections. However, in the latter, the events of highest appearances of *Cyclicargolithus reticulatus* and *Discoaster saipanensis* could not be separated, indicating that part of the section at Browns Creek above the extinction of *C. reticulatus* is missing from the upper Eocene of the Gambier Embayment. This same part of the section at Browns Creek was the result of high sedimentation rates, whereas the lower part of the Browns Creek Clays resulted from much slower rates of sedimentation, comparable with the average rate of sedimentation for the upper Eocene of the Gambier Embayment sections.

There is some evidence in the expanded upper Eocene section (above the extinction of *C. reticulatus*) at Browns Creek and Castle Cove, as well as in other sections in the St Vincent Basin, to suggest that extreme shoal conditions existed near the end of the Eocene, as a result of sedimentation exceeding subsidence. Access of the calcareous plankton was severely restricted, but, when the balance was restored, 'normal' hemipelagic sedimentation with calcareous planktic remains resumed.

The sequence of nannofossil biostratigraphic events recognised in the middle and upper Eocene of the Otway Basin is similar to that recognised in New Zealand and can be linked with another compiled by Shafik (1978), based partly on middle Eocene material from the Perth Basin, Western Australia.

The biostratigraphic evidence of disappearance up the section of the foraminiferid *Acarinina collactea* in the Otway Basin is inconsistent with the nannofossil evidence. This, together with its inconsistent relation to the disappearance level of the other foraminiferid *Subbotina* cf. *frontosa*, suggests its unreliability.

Consideration of two parameters, water depth and temperature, important to the biostratigraphic reliability of key nannofossil taxa in the material studied, showed that (1) deposition was in a nearshore or shelf environment, allowing the preservation of several holococcoliths, pentaliths, and other nearshore taxa; and (2) conditions along the Australian southern margin during the middle and late Eocene were generally temperate, with surface-water temperature decreasing eastward.

Acknowledgements

I am grateful to the Director, Geological Survey of South Australia, for permission to use the Survey's samples (all material studied from the Gambier Embayment). I am also grateful to Mr David J. Taylor for the information on the lithology of the Browns Creek section, incorporated in Table 1. The discussions I had with many colleagues, both in the University of Adelaide and the Bureau of Mineral Resources, are greatly appreciated.

References

Abele, C., Gloe, C.S., Hocking, J.B., Holdgate, G., Kenley, P.R., Lawrence, C.R., Ripper, D., & Threlfall, W.F., 1976 — Tertiary. *In* Douglas, J.G., & Ferguson, J.A. (editors), Geology of Victoria. *Geological Society of Australia, Special Publication* 5, 177–273.

Berggren, W.A., 1969 — Cenozoic chronostratigraphy, planktonic foraminiferal zonation and radiometric time scale. *Nature*, 224, 1072–1075.

Blow, W.H., 1969 — Late middle Eocene to Recent planktonic foraminiferal biostratigraphy. *In* Bronnimann, P., & Renz, H.H. (editors), *Proceedings of the First International Conference on Planktonic Microfossils, Geneva*, 1967, 1, 199–422.

Blow, W.H., 1979 — The Cainozoic Globigerinida. *E.J. Brill, Leiden.*

Bukry, D., 1973a — Low-latitude coccolith biostratigraphic zonation. *In* Edgar, N.T., Saunders, J.B., & others, *Initial Reports of the Deep Sea Drilling Project*, 15, 685–703.

Bukry, D., 1973b — Coccolith stratigraphy, Eastern Equatorial Pacific, Leg 16 Deep Sea Drilling Project. *In* Van Andel, T.H., Heath, G.R., & others, *Initial Reports of the Deep Sea Drilling Project*, 16, 653–711.

Bukry, D., 1978 — Cenozoic silicoflagellate and coccolith stratigraphy, Southeastern Atlantic Ocean, Deep Sea Drilling Project Leg 40. *In* Bolli, H.M., Ryan, W.B.F., & others, *Initial Reports of the Deep Sea Drilling Project*, 40, 635–649.

Cande, S.C., Mutter, J., & Weissel, J.F., 1981 — A revised model for the break-up of Australia and Antarctica. *Eos*, 62, 384.

Carter, A.N., 1958 — Tertiary foraminifera from the Aire District, Victoria. *Geological Survey of Victoria, Bulletin* 55, 1–76.

Cockbain, A.E., 1967 — *Asterocyclina* from the Plantagenet Beds near Esperance, W.A. *Australian Journal of Science*, 30, 68–69.

Cockbain, A.E., 1978 — Discocyclinid foraminifers from Western Australia. *Geological Survey of Western Australia, Annual Report*, 1977, 68–70.

Cole, W.S., 1962 — *Asterocyclina* from New Zealand and the Chatham Islands. *American Paleontologist, Bulletin*, 44 (203), 343–357.

Cole, W.S., 1967 — Additional data on New Zealand *Asterocyclina* (Foraminifera). *American Paleontologist, Bulletin*, 52 (233), 5–17.

Condon, M.A., Johnstone, D., Prichard, C.E., & Johnstone, M.H., 1956 — The Giralia and Marrilla Anticlines, Northwest Division, Western Australia. *Bureau of Mineral Resources, Australia, Bulletin* 25, 1–86.

Deighton, I., Falvey, D.A., & Taylor, D.J., 1976 — Depositional environments and geotectonic framework: southern Australian continental margin. *The APEA Journal*, 16, 25–36.

Edwards, A.R., 1971 — A calcareous nannoplankton zonation of the New Zealand Paleogene. *In* Farinacci, A., (editor), *Proceedings of the 2nd Planktonic Conference, Roma 1970*, 1, 318–419.

*Edwards, A.R., 1973 — Key species of New Zealand nannofossils. *New Zealand Journal of Geology and Geophysics*, 18(3), 319–336.

Edwards, A.R., & Perch — Nielsen, K., 1975 — Calcareous nannofossils from the Southwest Pacific, Deep Sea Drilling Project, Leg 29. *In* Kennett, J.P., Houtz, R.E., & others, *Initial Reports of the Deep Sea Drilling Project*, 29, 469–539.

Frakes, L.A., & Kemp, E.M., 1972 — Influence of continental positions on early Tertiary climates. *Nature*, 240, 97–100.

Gartner, S., 1971 — Calcareous nannofossils from the JOIDES Blake Plateau cores, and revision of Paleogene nannofossil zonation. *Tulane Studies in Geology and Paleontology*, 8(3), 101–121.

Gartner, S., 1974 — Nannofossil biostratigraphy, Leg 22, Deep Sea Drilling Project. *In* von der Borch, C.C., Sclater, J.G., & others, *Initial Reports of the Deep Sea Drilling Project*, 22, 577–599.

Hardenbol, J., & Berggren, W.A., 1978 — A new Paleogene numerical time scale. *American Association of Petroleum Geologists, Studies in Geology*, 6, 213–234.

Harris, W.K., 1966 — New and redefined names in South Australian Lower Tertiary stratigraphy. *Quarterly Geological Notes, Geological Survey of South Australia*, 20, 1–3.

Hays, J.D., Pitman, W.C. III, 1973 — Lithospheric plate motion, sea level changes and climatic and ecological consequences. *Nature*, 246, 18–22.

Hornibrook, N. de B., & Edwards, A.R., 1971 — Integrated planktonic foraminiferal and calcareous nannoplankton datum levels in the New Zealand Cenozoic. *In* Farinacci, A. (editor), *Proceedings of the 2nd Planktonic Conference, Roma 1970*, 1, 649–57.

Jenkins, D.G., 1974 — Paleogene planktonic foraminifera of New Zealand and the Austral region. *Journal of Foraminiferal Research*, 4(4), 155–169.

Kennett, J.P., Houtz, R.E., & others, 1975 — Site 277. *In* Kennett, J.P., Houtz, R.E., & others, *Initial Reports of the Deep Sea Drilling Project*, 29, 45–120.

Lindsay, J.M., 1967 — Foraminifera and stratigraphy of the type section of Port Willunga Beds, Aldinga Bay, South Australia. *Royal Society of South Australia, Transactions*, 91, 93–110.

Lindsay, J.M., 1969 — Cainozoic foraminifera and stratigraphy of the Adelaide Plains Sub-basin, South Australia. *Geological Survey of South Australia, Bulletin*, 42, 7–60.

Loeblich, A.R., Jr., & Tappan, H., 1966 — Annotated index and bibliography of the calcareous nannoplankton. *Phycologia*, 5(2 — 3), 81–216.

Loeblich, A.R., Jr., & Tappan, H., 1968 — Annotated index and bibliography of the calcareous nannoplankton II. *Journal of Paleontology*, 42(2), 584–598.

Loeblich, A.R., Jr., & Tappan, H., 1969 — Annotated index and bibliography of the calcareous nannoplankton III. *Journal of Paleontology*, 43(2), 568–588.

Loeblich, A.R., Jr., & Tappan, H., 1970a — Annotated index and bibliography of the calcareous nannoplankton IV. *Journal of Paleontology*, 44(3), 558–574.

Loeblich, A.R., Jr., & Tappan, H., 1970b — Annotated index and bibliography of the calcareous nannoplankton V. *Phycologia*, 9(2), 157–174.

Loeblich, A.R., Jr., & Tappan, H., 1971 — Annotated index and bibliography of the calcareous nannoplankton VI. *Phycologia*, 10(4), 315–339.

Loeblich, A.R., Jr., & Tappan, H., 1973 — Annotated index and bibliography of the calcareous nannoplankton. *Journal of Paleontology*, 47(4), 715–759.

Ludbrook, N.H., 1969 — The Tertiary Period. *In* Parkin, L.W. (editor), Handbook of South Australian Geology. *Geological Survey of South Australia*, 172–203.

Ludbrook, N.H., 1971 — Stratigraphy and correlation of marine sediments in the western part of the Gambier Embayment. *In* Wopfner, H., & Douglas, J.G. (editors), The Otway Basin of southeastern Australia. *Geological Survey of South Australia and Victoria, Special Bulletin*, 47–66.

McGowran, B., 1971 — Observation Bore No. 1, Hundred Townsend, section 125: micropalaeontology and stratigraphy. *South Australian Department of Mines, Unpublished Report*, R.B. 71/77.

McGowran, B., 1973 — Observation Bore No. 2, Gambier Embayment of the Otway Basin: Tertiary micropalaeontology, and stratigraphy. *South Australia Department of Mines, Mineral Resources Review*, 135, 43–55.

McGowran, B., 1978a — Early Tertiary foraminiferal biostratigraphy in southern Australia: a progress report. *Bureau of Mineral Resources, Australia, Bulletin*, 192, 83–95.

McGowran, B., 1978b — Maastrichtian to Eocene foraminiferal assemblages in the northern and eastern Indian Ocean region: correlations and historical patterns. *In* Heirtzler, J.R., & others (editors), Indian Ocean geology and biostratigraphy. *American Geophysical Union, Washington, D.C.*, 417–458.

McGowran, B., & Lindsay, J.M., 1969 — A middle Eocene planktonic foraminiferal assemblage from the Eucla Basin. *Geological Survey of South Australia, Quarterly Geological Notes*, 30, 2–10.

Martini, E., 1971 — Standard Tertiary and Quaternary calcareous nannoplankton zonation. *In* Farinacci, A. (editor), *Proceedings of the 2nd Planktonic Conference, Roma 1970*, 739–785.

Martini, E., 1976 — Cretaceous to Recent calcareous nannoplankton from the Central Pacific Ocean (DSDP Leg 33). *In* Schlanger, S.O., Jackson, E.D., & others, *Initial Reports of the Deep Sea Drilling Project*, 33, 383–423.

Pessagno, E.A. Jr., 1972 — Pulsations, interpulsations, and sea-floor spreading. *In* Shagam, R., & others (editors), Studies in earth and space sciences. *Geological Society of America, Memoir* 132, 67–73.

*Prins, B., 1979 — Notes on nannology — 1. *Clausicoecus*, a new genus of fossil coccolithophorids. *INA (Newsletter, Proceedings of the International Nannoplankton Association)*, 1(1), N2–N4.

Quilty, P.G., 1978 — The late Cretaceous — Tertiary section in Challenger No. 1 (Perth Basin): details and implications. *Bureau of Mineral Resources, Australia, Bulletin*, 192, 109–134.

Raggatt, H.G., & Crespin, I., 1955 — Stratigraphy of the Tertiary rocks between Torquay and Eastern View, Victoria. *Royal Society of Victoria, Proceedings*, 67, 75–142.

*Roth, P.H., 1970 — Oligocene calcareous nannoplankton biostratigraphy. *Eclogae Geologicae Helvetiae*, 63(3), 799–881.

Roth, P.H., Baumann, P., & Bertolino, V., 1971 — Late Eocene — Oligocene calcareous nannoplankton from central and northern Italy. *In* Farinacci, A. (editor), *Proceedings of the 2nd Planktonic Conference, Roma 1970*, 2, 1069–1097.

Sancetta, C., 1979 — Paleogene Pacific microfossils and paleoceanography. *Marine Micropaleontology*, 4, 363–398.

Shackleton, N.J., & Kennett, J.P., 1975 — Paleotemperature history of the Cenozoic and the initiation of Antarctic glaciation: oxygen and carbon isotope analyses in DSDP Sites 277, 279, and 281. *In* Kennett, J.P., Houtz, R.E., & others, *Initial Reports of the Deep Sea Drilling Project*, 29, 743–755.

Shafik, S., 1973 — Eocene — Oligocene biostratigraphy in the western and southern margins of Australia. *Abstracts, 45th Congress, Australia and New Zealand Association for Advancement of Science*, Section 3, 101–103.

Shafik, S., 1978 — Paleocene and Eocene nannofossils from the Kings Park Formation, Perth Basin, Western Australia. *Bureau of Mineral Resources, Australia, Bulletin*, 192, 165–172.

*Shafik, S., 1981 — Nannofossil biostratigraphy of the *Hantkenina* (foraminiferid) interval in the upper Eocene of southern Australia. *BMR Journal of Australian Geology & Geophysics*, 6, 108–116.

*Sherwood, R.W., 1974 — Calcareous nannofossil systematics, paleontology, and biostratigraphy of the middle Eocene Weches Formation of Texas. *Tulane Studies in Geology and Paleontology*, 11(1), 1–79.

Sprigg, R.C., 1952 — The geology of southeast Province, South Australia, with special reference to Quaternary coastline migrations and modern beach developments. *Geological Survey of South Australia, Bulletin* 29, 1–120.

Stainforth, R.M., Lamb, J.L., Luterbacher, H., Beard, J.H., & Jeffords, R.M., 1975 — Cenozoic planktonic foraminiferal zonation and characteristics of index forms. *University of Kansas Paleontological Contributions*, 62, 1–425.

Taylor, D.J., 1967 — Marine transgressive patterns in Victoria. *Abstracts, 39th Congress, Australia and New Zealand Association for Advancement of Science*, Section C, A3–A4.

Taylor, D.J., 1971 — Foraminifera and the Cretaceous and Tertiary depositional history in the Otway Basin in Victoria. *In* Wopfner, H., & Douglas, J.G. (editors), The Otway Basin of Southeastern Australia. *Geological Surveys of South Australia and Victoria, Special Bulletin*, 217–233.

Appendix. Note on systematic palaeontology

Nannofossil taxa considered in this study are listed below. Bibliographic references of most of these taxa are provided by Loeblich & Tappan (1966, 1968, 1970a, 1970b, 1971, 1973); any not included in these publications are given in the references herein and identified by an asterisk.

Blackites amplus Roth & Hay *in* Hay, Mohler, Roth, Schmidt & Boudreau, 1967
Blackites spinosus (Deflandre) Hay & Towe, 1962
Blackites spinulus (Levin) Roth, 1970*
Blackites tenuis (Bramlette & Sullivan) Sherwood, 1974*
Blackites vitreus (Deflandre) Shafik, 1981*
Braarudosphaera bigelowi (Gran & Braarud) Deflandre, 1947
Chiasmolithus altus Bukry & Percival, 1971
Chiasmolithus expansus (Bramlette & Sullivan) Hay, Mohler & Wade, 1966
Chiasmolithus grandis (Bramlette & Riedel) Hay, Mohler & Wade, 1966
Chiasmolithus oamaruensis (Deflandre) Hay, Mohler & Wade, 1966
Chiasmolithus solitus (Bramlette & Sullivan) Perch-Nielsen, 1971
Clathrolithus ellipticus Deflandre in Deflandre & Fert, 1954
Clausicoccus cribellum (Bramlette & Sullivan) Prins, 1979*
Coccolithus eopelagicus (Bramlette & Riedel) Bramlette & Sullivan, 1961
Coccolithus pelagicus (Wallich) Schiller, 1930
Corannulus germanicus Stradner, 1962
Cyclicargolithus floridanus (Roth & Hay) Bukry, 1971
Cyclicargolithus luminis (Sullivan) Bukry, 1971
Cyclicargolithus reticulatus (Gartner & Smith) Bukry, 1971
Cyclococcolithus formosus Kamptner, 1963
Cyclococcolithus protoannulus (Gartner)
Daktylethra punctulata Gartner *in* Gartner & Bukry, 1969
Discoaster barbadiensis Tan Sin Hok, 1927
Discoaster elegans Bramlette & Sullivan, 1961
Discoaster saipanensis Bramlette & Riedel, 1954
Discoaster tani Bramlette & Riedel, 1954
Discoaster tani nodifer Bramlette & Riedel, 1954
Discoaster tani ornatus Bramlette & Wilcoxon, 1967
Helicosphaera bramlettei Muller, 1970
Helicosphaera compacta Bramlette & Wilcoxon, 1967
Helicosphaera recta (Haq) Martini, 1969
Helicosphaera reticulata Bramlette & Wilcoxon, 1967
Helicosphaera seminulum (Bramlette & Sullivan) Stradner, 1969
Holococcolithus macroporus (Deflandre) Roth, 1970*
Isthmolithus recurvus Deflandre *in* Deflandre & Fert, 1954
Lanternithus minutus Stradner, 1961
Markalius inversus (Deflandre) Bramlette & Martini, 1964
Micrantholithus attenuatus Bramlette & Sullivan, 1961
Micrantholithus procerus Bukry & Percival, 1971
Micrantholithus truncus Bramlette & Sullivan, 1961
Neococcolithes dubius (Deflandre) Black, 1967
Orthozygus aureus (Stradner) Bramlette & Wilcoxon, 1967
Pemma basquensis (Martini) Baldi-Beke, 1971
Pemma papillatum Martini, 1959
Polycladolithus opersus Deflandre *in* Deflandre & Fert, 1954
Pontosphaera multipora (Kamptner) Roth, 1970
Pontosphaera plana (Bramlette & Sullivan) Haq, 1971
Reticulofenestra hampdenensis Edwards, 1973*
Reticulofenestra scissura Hay, Mohler & Wade, 1966
Reticulofenestra scrippsae (Bukry & Percival) Shafik, 1981*
Reticulofenestra umbilica (Levin) Martini & Ritzkowski, 1968
Sphenolithus moriformis (Bronnimann & Stradner) Bramlette & Wilcoxon, 1967
Sphenolithus predistentus Bramlette & Wilcoxon, 1967
Transversopontis obliquipons (Deflandre) Hay, Mohler & Wade, 1966
Transversopontis pulcher (Deflandre) Perch-Nielsen, 1967
Transversopontis zigzag Roth & Hay *in* Hay, Mohler, Roth, Schmidt & Boudreau, 1967
Trochaster simplex Klumpp, 1953
Zygrhablithus bijugatus bijugatus (Deflandre) Deflandre, 1959
Zygrhablithus bijugatus crassus Locker, 1967

BMR Journal of Australian Geology & Geophysics, 8, 19-34

CRUSTAL STRUCTURE OF THE SOUTHERN McARTHUR BASIN, NORTHERN AUSTRALIA, FROM DEEP SEISMIC SOUNDING

C.D.N. Collins

Deep seismic refraction and vertical reflection recordings have been made in the southern McArthur Basin, over the Bauhinia Shelf and Batten Trough between Daly Waters and the H.Y.C. mineral deposit, and over the Wearyan Shelf between Borroloola and Westmoreland. In the Batten Trough, McArthur Group rocks have a velocity of 5.81 km/s; no velocity contrast was detected between them and basement. Over the Bauhinia Shelf, 100–200 m of Cainozoic, Mesozoic, and perhaps Cambrian sediments, overlie ?Roper Group sediments (P-wave velocity, V = 4.6 km/s). Below these are probable Tawallah Group rocks (V = 5.8–5.9 km/s). Magnetotelluric measurements define a resistivity contrast, possibly basement, at 6–9 km depth.

On the Wearyan Shelf at Borroloola, 370 m of Roper Group (V = 3.58 km/s) overlies 2.9 km of Tawallah Group (V = 5.55 km/s). At Robinson River, 650 m of Cainozoic, thin McArthur Group, and, perhaps, upper units of Tawallah Group (V = 4.81 km/s) were detected. Tawallah Group rocks (V = 5.44 km/s) crop out northwest of Robinson River and are about 2.8 km thick. Basement velocity is 6.04 km/s. Between Robinson River and Westmoreland, basement is 3.5–2.7 km deep. At Westmoreland the McArthur Basin sequence thins against the Murphy Ridge. A layer 260 m thick (V = 3.50 km/s) lies on top of a 2.4 km thick layer (V = 5.44 km/s), and the basement velocity of 5.99 km/s increases to 6.06 km/s towards Robinson River. At mid-crustal depths velocities are 5.9–6.9 km/s, and in the lower crust, to depths of 43 km in the west and 40 km in the east, 6.8–7.5 km/s. Below this, a velocity gradient is interpreted until upper mantle velocities are reached at 43–53 km depth in the west (V = 7.5–8.4 km/s) and 44 km in the east (V = 7.9 km/s). Generally, the crustal structure of the North Australian Craton is characterised by high lower-crustal velocities, broad velocity gradients, and thick crust, which probably evolved from an Archaean continental crust during Proterozoic tectonism.

Introduction

The Proterozoic McArthur Basin covers 170 000 km^2 in the Northern Territory (Fig. 1). It contains a number of important mineral deposits and has potential for further discoveries. Its geology has been described by Plumb & Derrick (1975), Plumb (1977), and Plumb & others (1980).

The structure of the southern McArthur Basin has been investigated by several geophysical methods, namely, detailed gravity, magnetotellurics, aeromagnetics, and deep seismic reflection and refraction techniques (Plumb, 1977). This paper reports, principally, the structure interpreted from the seismic methods.

The main features of the southern McArthur Basin in the survey area (Fig. 1) are the Batten Trough, about 60 km wide, and its flanking Bauhinia Shelf on the west and Wearyan Shelf on the east. The Emu Fault is considered to define the eastern boundary of the Batten Trough. One objective of the seismic investigation was to define any major velocity differences between the Batten Trough and the Bauhinia and Wearyan

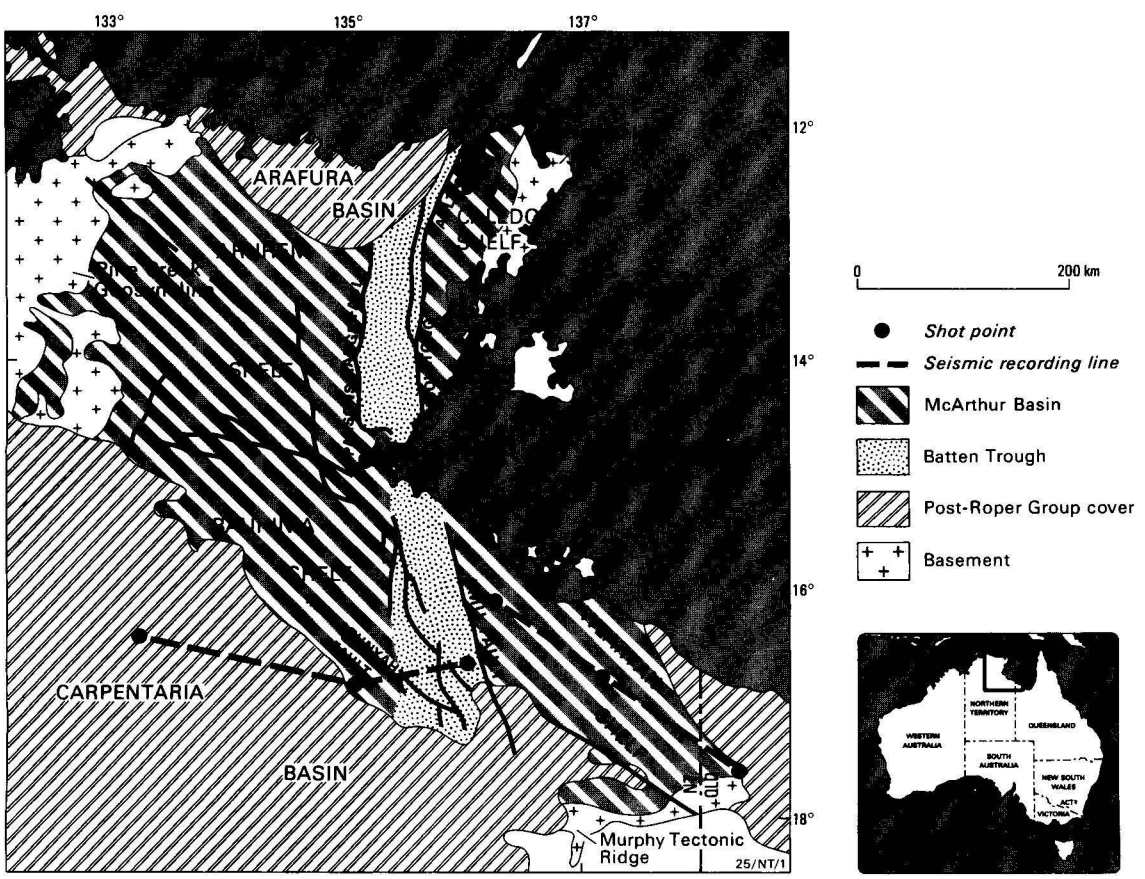

Figure 1. Major tectonic elements of the McArthur Basin (after Plumb & Derrick, 1975).

Shelves. A possible difference in crustal structure is suggested by the distribution of flood basalts, which are abundant on the shelves and very restricted in the trough.

The major faults that bound the Batten Trough may have acted as channels for ore solutions, and important geological questions that need to be answered in relation to these faults are whether they predate the McArthur Basin succession and whether the thickness of rock units changes abruptly at the faults or gradually over tens of kilometres. In particular, the Emu Fault was investigated because of its probable relation to the H.Y.C. lead-zinc deposit (Fig. 2). Other objectives of the seismic investigations were to delineate the basement of the McArthur Basin, to derive velocities and structures beneath extensive Mesozoic–Cainozoic cover above the Bauhinia Shelf, and to identify any marker horizons.

The McArthur Basin succession was deposited about 1700–1400 m.y. ago, is up to 12 km thick, and comprises the Carpentarian Tawallah, McArthur, and Roper Groups. The Tawallah Group is up to 6 km thick, and consists of sandstones and carbonates; the McArthur Group, up to 5.5 km thick, comprises predominantly carbonate rocks; and the Roper Group comprises mainly sandstones and lutites up to 5 km thick. The sediments are predominantly shallow water and often remarkably uniform over large areas.

The north-trending Batten Fault Zone, 50–60 km wide, runs down the axis of the basin and contains a very much thicker succession than those of the mildly deformed Arnhem, Caledon, Bauhinia, and Wearyan Shelves on either side (Fig.1). It has been postulated that the fault zone corresponds to a syndepositional graben, the Batten Trough, within which the thick sequences were confined. In the survey area, the Emu Fault marks the boundary between intense faulting to the west and flat-lying sequences to the east. Since the fault was demonstrably active during at least part of McArthur Group deposition, it has been defined as the eastern boundary of the Batten Trough. The western boundary is gradational (Plumb & Derrick, 1975; Plumb & others, 1980). Later, during the deposition of the Roper Group, the site of maximum sedimentation rate shifted westwards onto the Bauhinia Shelf.

During post-depositional deformation the sense of the faulting has been reversed and the Batten Trough has become a horst. Deformation was more intense in the Batten Fault Zone than on the surrounding shelves, and was related to block faulting along pre-existing basement faults. Although vertical stratigraphic displacements of up to 7.5 km may be seen along the major faults, it has been interpreted that the overall structural development of the basin was controlled by right-lateral horizontal displacements along the north-trending Batten Fault Zone and left-lateral displacements along the northwest-trending faults (Plumb & others, 1980). Deformation of the McArthur Basin ceased before the Cambrian.

Previous geophysical work

Most geophysical surveys carried out in the area have been in the vicinity of individual mineral deposits, particularly the H.Y.C. (Plumb, 1977). Previous deep seismic surveys have been conducted west and south of the area (Hales & Rynn, 1978; Hales & others, 1980; Underwood, 1967; Finlayson, 1981, in press; Cleary, 1973; Denham & others, 1972). Regional gravity coverage extends across the McArthur Basin, and has been supplemented by detailed traverses in the survey area. Heat-flow measurements in the region have been summarised by Cull (1982b).

Field operations

The field procedures used in this study have been reported by Collins (1981), and only a brief description is given here. The crustal investigations involved recording at 71 sites along two 300-km seismic refraction traverses, one west and the other

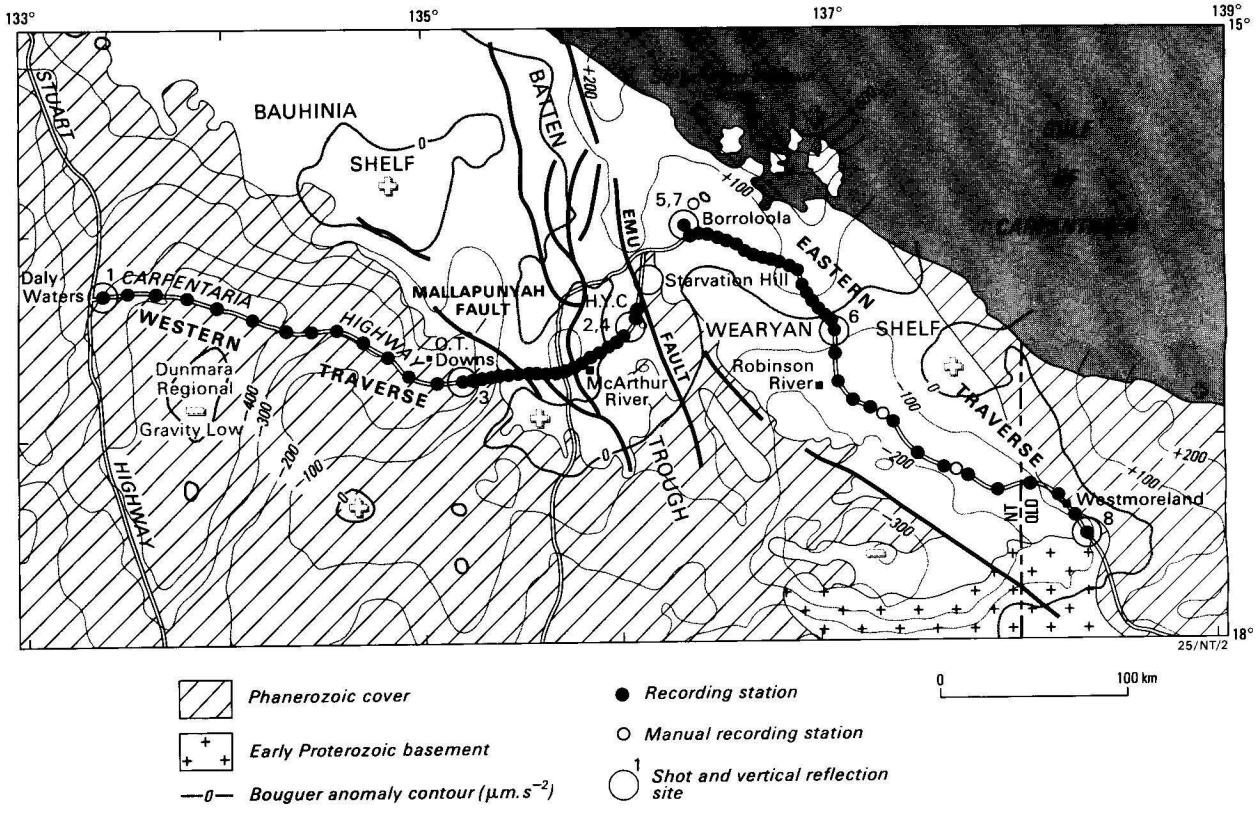

Figure 2. Location of shots and recording stations, simplified geology, and Bouguer gravity.

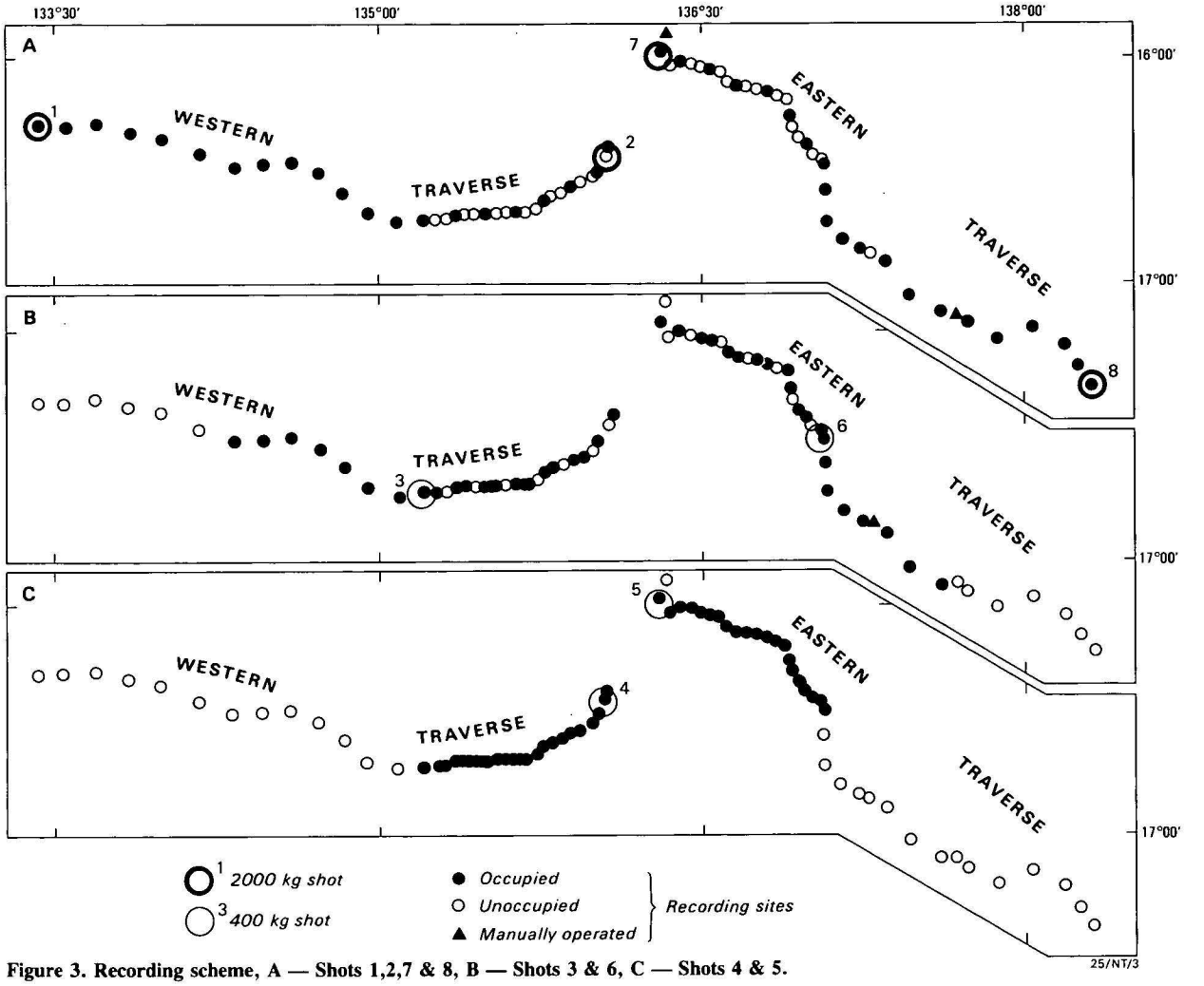

Figure 3. Recording scheme, A — Shots 1,2,7 & 8, B — Shots 3 & 6, C — Shots 4 & 5.

east of the Emu Fault, during June–July, 1979 (Fig. 2). Two large shots of 2000 kg were detonated at Daly Waters and the H.Y.C. deposit, and two smaller shots of 400 kg were detonated at H.Y.C. and 100 km west of H.Y.C., near O.T. Downs. For the larger shots, the station spacing was about 15 km, while for the small shots it was 5–10 km (Fig. 3). A similar pattern was recorded along the second traverse, east of the Emu Fault, with large shots at Borroloola and Westmoreland, and small shots at Borroloola and Robinson River. Deep reflection recordings were made at these six shot points. Figure 3 shows the recording scheme for each shot.

Recordings were made on 21 BMR automatic FM tape recording systems (Finlayson & Collins, 1980) and two manually operated recorders. Each system used a single vertical Willmore seismometer, and the amplifier gain levels, filter settings, and polarity were the same at all sites. The shots consisted of a pattern of drill holes 27 m deep, with 100kg of explosive in each hole. Small (25 kg) weathering shots were fired at each shot site, but these were recorded only to distances of about 14 km from the shot point. All shots were timed on site relative to VNG radio time signals to an accuracy of 0.02 s.

The latitudes and longitudes of the shots and stations were scaled off 1:100 000 topographic maps to within 0.05 minute of arc (approximately 100 m). Elevations ranged between 40 and 310 m on the western traverse, and 20 and 220 m on the eastern traverse. Wherever possible, the seismometer was placed on rock outcrop, but at the majority of sites this was not possible and the seismometer was buried.

Data processing and interpretation methods

The field tapes were played back and digitised at BMR, Canberra. The first-arrival times were read from the original analogue records. In most cases, the record was analogue filtered during playback, with several different passbands to enhance the arrivals against the background noise. Arrivals with impulsive onsets were read to 0.02 s. Emergent arrivals or records with low signal-to-noise ratio were read to 0.1 s or, in some cases, a greater uncertainty. The travel-times (reduced by 6.0 km/s) of all first arrivals recorded from the ends of both long traverses are plotted against distance in Figure 4.

The digitised recordings at each site were compiled into record sections. These have been digitally filtered and reduced by 6.0 km/s before plotting, and each trace has been normalised to a maximum amplitude. The long sections (0–300 km) have been filtered using a passband of 2–12 Hz, and the short sections (0–100 km), 2–15 Hz. These filter limits were chosen because they provide the best improvement in signal-to-noise ratio on most records. Individual records can often be improved further by applying different filter limits. In some cases, the first arrivals cannot be clearly seen unless a narrow passband filter is applied, and they may not be obvious on the illustrated record-sections.

The apparent velocities of arrivals from each shot were derived by linear regression, with the assumption that the travel-time curves are made up of linear segments. This may not be true for all parts of the curves, but it gives a first approximation to the velocity structure.

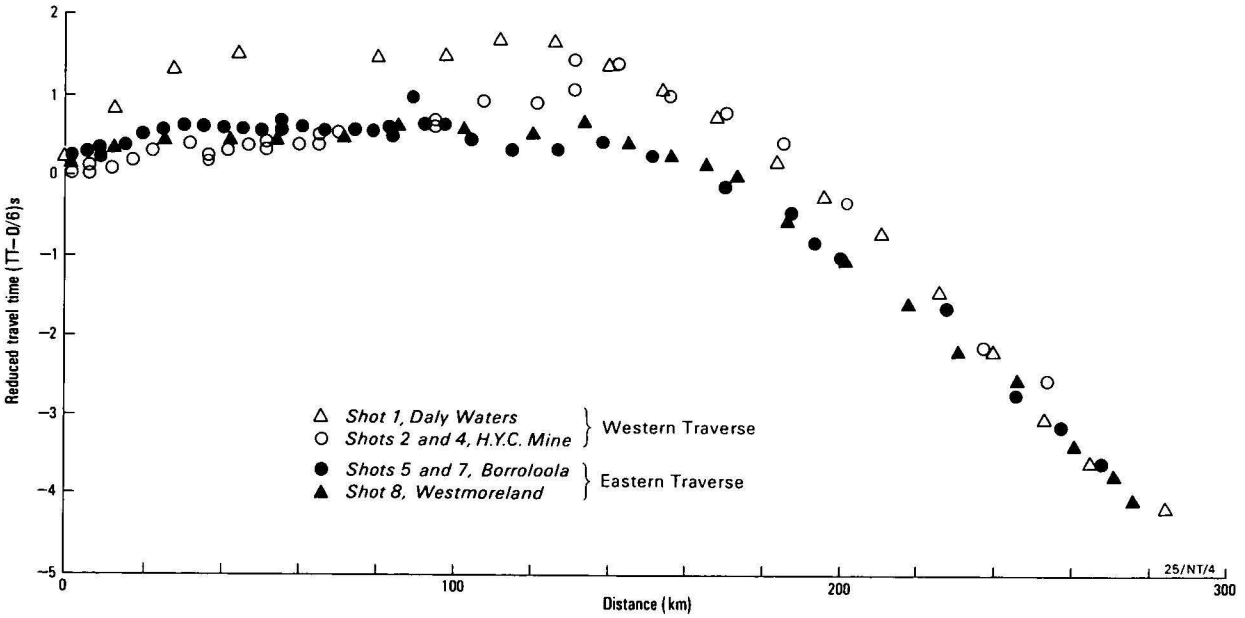

Figure 4. Reduced first-arrival travel-times.

Initial interpretation was made assuming horizontal, homogeneous, plane layering at each shot point. The models derived in this way were then tested by ray-tracing methods, and modified so that the calculated and observed travel-times agreed. They were further modified after comparison of amplitude characteristics of the record sections with synthetic seismograms calculated by the reflectivity method (Fuchs, 1968).

Where the shallow layers showed a marked variation in structure, a two-dimensional gravity modelling program was used to calculate the gravity field. This was compared with the observed Bouguer gravity data, and minor variations consistent with both the seismic and gravity were made, mainly for those parts of the section for which no seismic data exist. Detailed gravity observations were made along the traverses during 1978–1980 and these have been interpreted by Anfiloff (BMR, personal communication, 1982). A ray-tracing program, capable of handling irregular structures, was used to test travel-times calculated from the model against observed arrivals where there were marked structural changes along the traverse. The synthetic seismogram program used in this interpretation can compute seismograms only for planar horizontally layered models, and therefore could not be properly used in these cases. Where possible, the model was averaged to fulfil the requirements of the synthetic seismogram program, and thus provide some information on expected amplitudes. Velocities have been corrected for Earth curvature (Mereu, 1967), but this is only significant for the lower crust and upper mantle (about 0.8 per cent at 50 km depth).

Results

Some of the major features of the seismic data can be seen in the plot of first-arrival travel-times (Fig. 4). Considering, firstly, only the data from the western traverse between Daly Waters and the H.Y.C. deposit, it can be seen that there are marked differences in the travel-times at distances less than 100 km. Shot 1 arrivals are about 1 s later than arrivals from Shots 2 and 4. Beyond 100 km, the arrivals from Shot 2 become increasingly delayed, and, from 140 km to the ends of the traverse, the travel-times from Shots 1 and 2 are substantially the same, with apparent velocity increasing with distance.

In the range 40–110 km, the arrivals from Shots 1 and 2 have similar apparent velocities. The true velocities may differ slightly at either end, but the difference between the travel-times is largely due to the presence of a near-surface low-velocity layer, indicated by the arrivals in the range 0–30 km. The travel-times from Shot 2 between 0 and 80 km exhibit local irregularities, possibly owing to structure, but, otherwise, only one phase velocity is recorded. Thus, there is, at most, only a very thin low-velocity surface layer near Shot 2.

On the eastern traverse, between Borroloola and Westmoreland, very little difference can be seen between the travel-times from Shots 5 and 7 and Shot 8 (Fig. 4). The only clear differences are slightly earlier arrivals from Shot 8 in the range 20–70 km; this trend is reversed between 100 and 140 km. The differences amount to, at most, 0.2 s. Data from both shots exhibit abrupt changes in apparent velocity at about 25 km and 140 km from the shots. From 0 to 140 km, the travel-time plots consist of approximate linear segments; beyond 140 km, the arrivals show a progressive increase in apparent velocity.

Shallow structure

In this paper, the shallow structure is considered to comprise the formations above the basement refractor, which has a velocity of about 5.8–6.0 km/s. This basement refractor is at less than 5 km depth and is evident beneath both traverses. A thin surface layer, of variable thickness and with a velocity of about 1.7 km/s, was found beneath all shot points and, presumably, occurs along the whole length of the traverses. Shallow refracted arrivals, recorded by the 3-km reflection spreads at each shot point, were used to derive an average thickness for this layer, which varied between 35 m at Westmoreland to 120 m at Daly Waters.

Western traverse

Geological constraints. Shots 2 and 4 (H.Y.C.) were situated in a thick faulted sequence of Carpentarian McArthur Group rocks, which crop out for about 80 km westwards along the traverse and are up to 5 km thick (Plumb, 1977; BMR, 1966). These are underlain by sandstone and volcanics of the Tawallah Group, which in turn overlie basement.

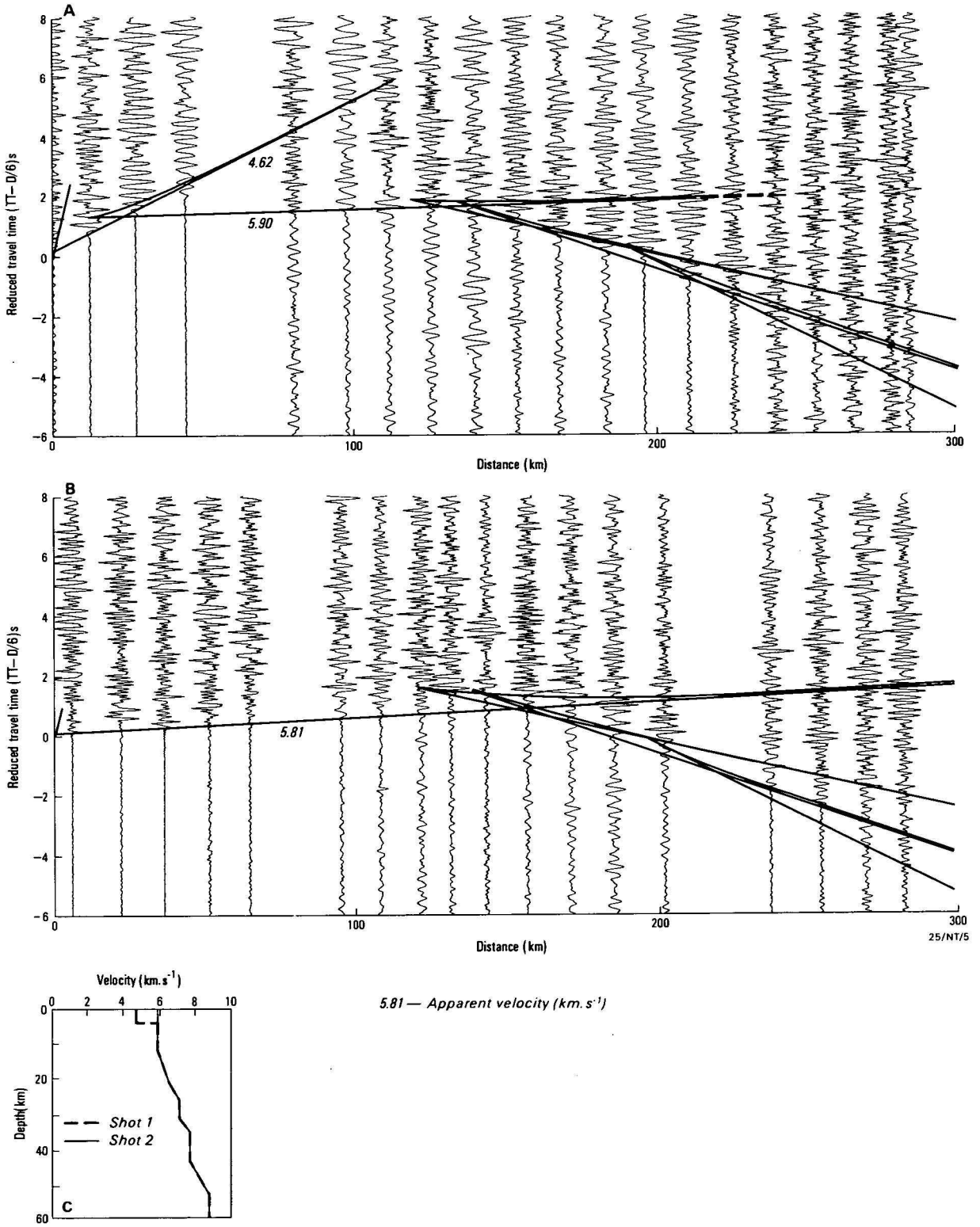

Figure 5. Record sections, western traverse.
Traces normalised and filtered 2–12 Hz. A — Shot 1, Daly Waters, B — Shot 2, H.Y.C. mine, C — velocity/depth functions.

Shots 1 (Daly Waters) and 3 (O.T. Downs) were on deeply weathered Mesozoic sediments, probably less than 100 m thick. At O.T. Downs, the sediments overlie Carpentarian sandstones and siltstones of the Roper Group, which are probably somewhat less than 2 km thick and stop about 23 km east, where their contact with the underlying McArthur Group is exposed. Westwards from Shot 3, the Mesozoic sediments completely cover the underlying rocks, but an inlier about 50 km north suggests that the Roper Group thickens westwards, perhaps to as much as 5 km, and directly overlies the Tawallah Group, owing to wedging out of the McArthur Group.

Cambrian sediments of the Daly River Basin are interpreted to underlie Daly Waters, where the total thickness of Cainozoic, Mesozoic, and Cambrian sediments has been estimated at 300 m (Brown, 1969). Elsewhere, the Cambrian Tindall Limestone alone has been shown to reach 910 m (Randal, 1973).

Seismic interpretation: The seismic record sections from all shots on the western traverse are shown in Figures 5 and 6. Below the surface layer at Daly Waters an apparent velocity of 4.62 km/s was measured. This was recorded at only two stations, so an estimate of the error cannot be made. However, it represents the average velocity of the layer, and is supported by ray tracing and gravity modelling. The estimated error limits of the other shallow velocities are shown in Figure 7. The 4.62 km/s layer is 4.1 km thick at a location 20 km east of Daly Waters; it is not directly evident at O.T. Downs (Shot 3) nor at H.Y.C. (Shots 2,4). Apart from the thin surface layer, the apparent velocity of the shallowest layer at H.Y.C. is 5.81 km/s (Fig. 6A), that of the McArthur Group carbonate rocks.

If a surface velocity of 1.70 km/s is assumed, an unusually thick surface layer of 560 m may be inferred at Shot 3.

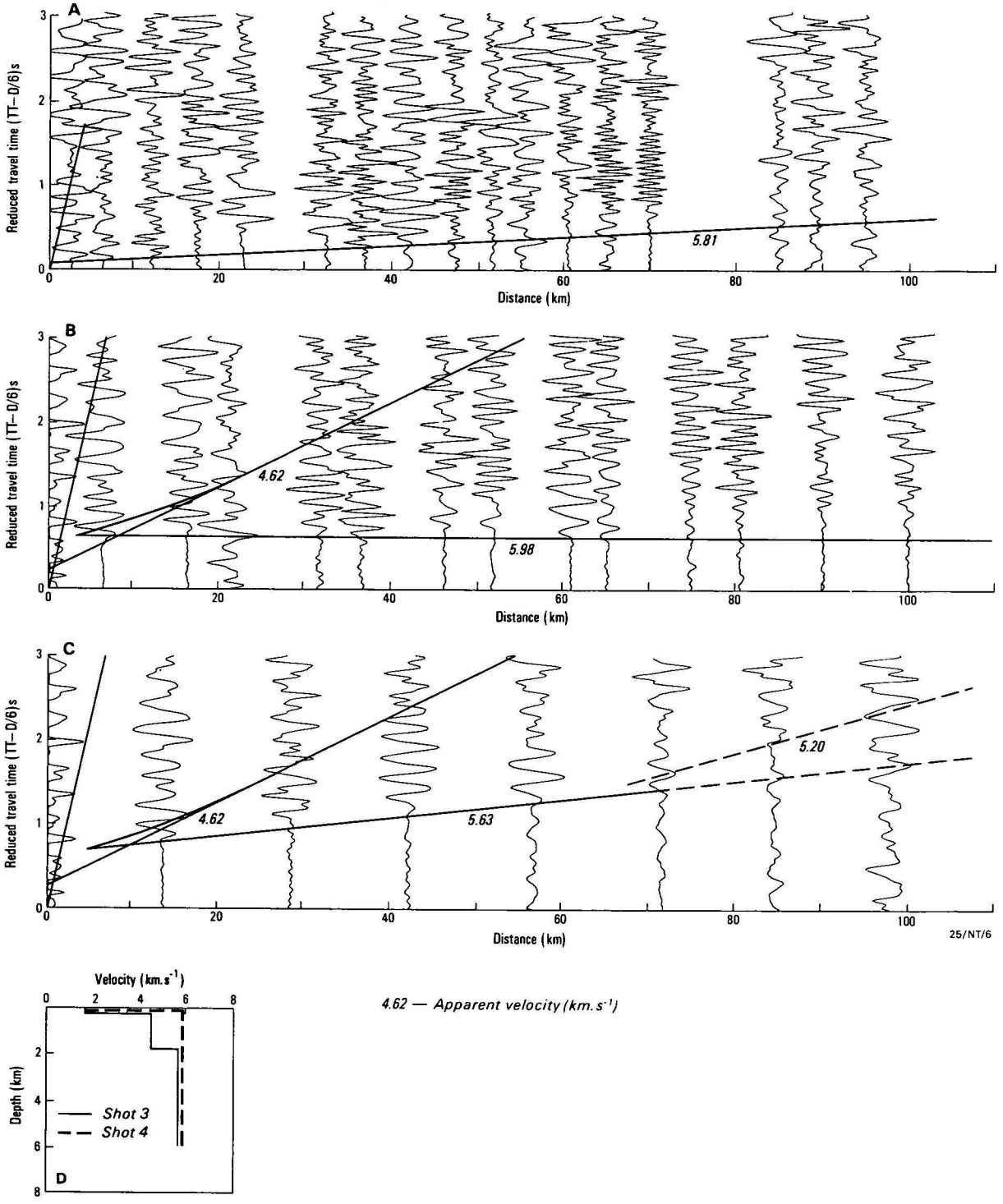

Figure 6. Record sections, western traverse.
Traces normalised and filtered 2–15 Hz. A — Shot 4, H.Y.C. mine, B — Shot 3, O.T. Downs, recorded eastwards, C — Shot 3 O.T. Downs, recorded westwards, D — velocity/depth functions; includes 4.62 km/s layer derived from other data.

However, the 4.62 km/s layer may be present under Shot 3 and may have contributed to the travel-times, because the arrivals from Shot 2 become increasingly delayed from about 23 km east of Shot 3, about the point at which outcrops of Roper Group overlying McArthur Group rocks first appear. Minimum thicknesses of the surface (1.70 km/s) layer and the 4.62 km/s layer can be calculated within the constraints of the travel-times to the nearest stations, and are 210 m and 1.4 km respectively. A vertical reflection at a depth of 1.6 km supports this interpretation. The 4.62 km/s layer is interpreted as wedging out completely 23 km east of O.T. Downs, and so correlates with the Roper Group, both in outcrop and depth below O.T. Downs.

Only the 1.70 km/s surface layer is present further east, and it thins towards H.Y.C. (Fig. 7A). Below it, the apparent refractor velocity is 5.81 km/s from Shot 4 and 5.98 km/s from Shot 3, giving a true velocity of 5.89 km/s, if a constant dip is assumed between the two shots. However, the high apparent velocity towards the east may, in part, be due to the greater thickness of low-velocity material below Shot 3, which would locally cause an increase in dip on the lower refractor; the true velocity could thus be lower. Residuals in the travel-times and the variable character of the wave-train from Shot 4 at H.Y.C. and Shot 3 at O.T. Downs (Fig. 6) are due to local structures in the McArthur Group, including a small syncline of Roper Group sediments. The data are not sufficiently detailed to map these small-scale structures, and the assumption of a homogeneous layer gives a good fit to the first-arrival travel-time data (Fig. 6).

The apparent velocity westwards from Shot 3 is 5.63 km/s, which, with the eastward apparent velocity of 5.98 km/s, gives a true velocity of 5.80 km/s. At Daly Waters (Fig. 7A) the corresponding apparent velocity is 5.90 km/s, giving a true velocity of 5.82 km/s. The data quality is poor to the west of Shot 3, probably owing to the thickening surface layers. West of Shot 3, an average dip of about 0.5° increases beyond about 60 km, where the depth to basement is 2.1 km. From extrapolation of the dips from both Shot 1 and Shot 2, the basement apparently steps downwards to the west at a point about 80 km west of Shot 3 (Fig. 7A).

The interpretation of the basement topography is supported by the gravity data along the traverse (Fig. 2). The main features in the gravity data correlate with the topography of the top of

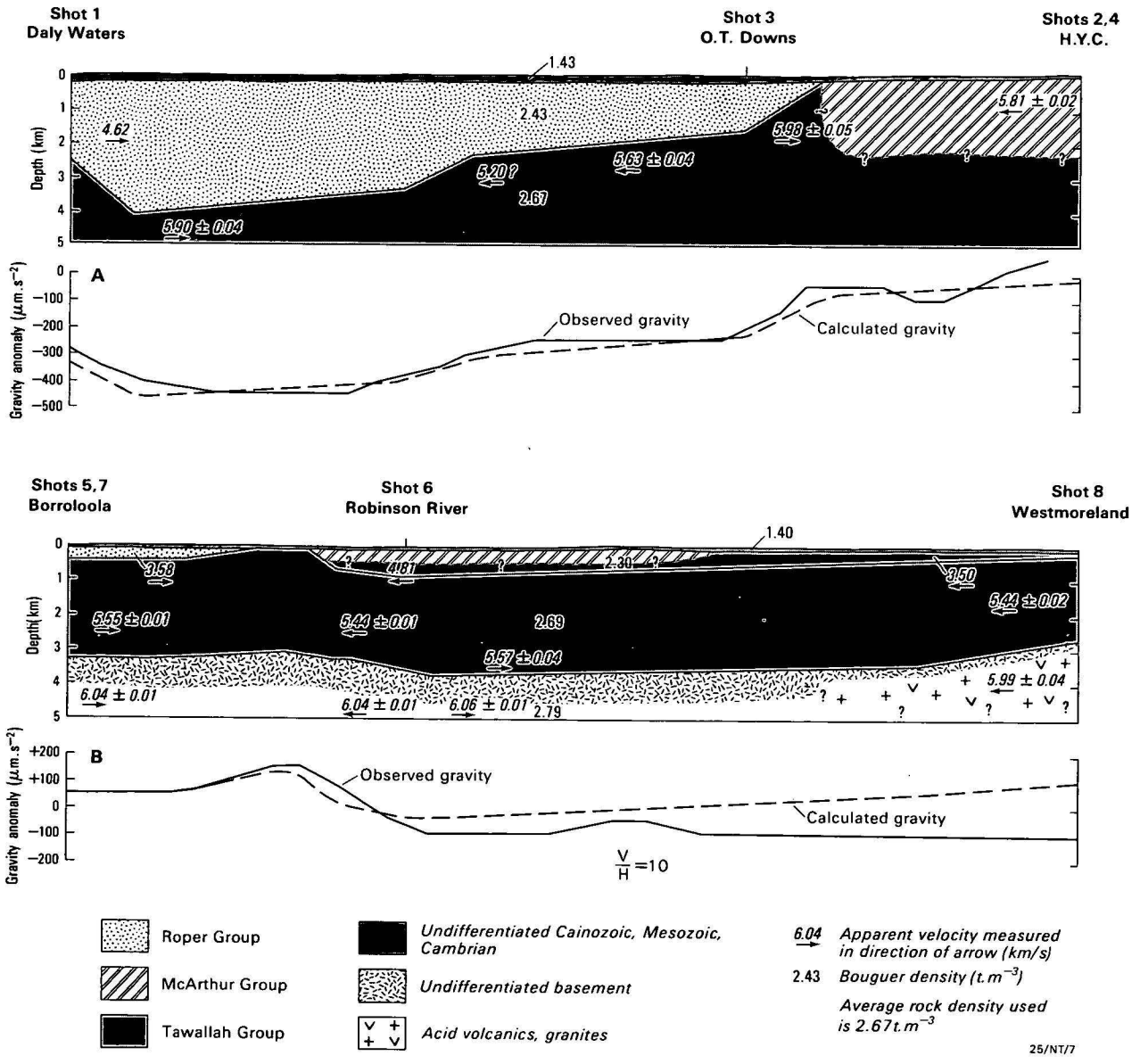

Figure 7. Seismic models and geological interpretation of the shallow structure, with observed and calculated Bouguer gravity, A — Daly Waters to H.Y.C. mine, B — Borroloola to Westmoreland.

the 5.82 km/s layer (Fig. 7A). Near Daly Waters, the gravity increases by 100 μm/s^2 over a distance of about 20 km, which could indicate basement rising to within 2.5 km of the surface at Daly Waters. This does not conflict with the seismic data, which can be interpreted only for distances greater than 20 km east of Daly Waters, owing to the offset distance. The geological data previously discussed indicate that the 4.3 km of sediments above the 5.82 km/s basement, represented by the 4.62 km/s wedge, must be a combination of about 300 m of Cainozoic, Mesozoic, and Cambrian sediments plus about 4 km of Roper Group. The Roper Group sediments, which are responsible for the Dunmara Regional Gravity Low (Fraser, 1976) (Fig. 2), must therefore extend for a considerable distance to the south.

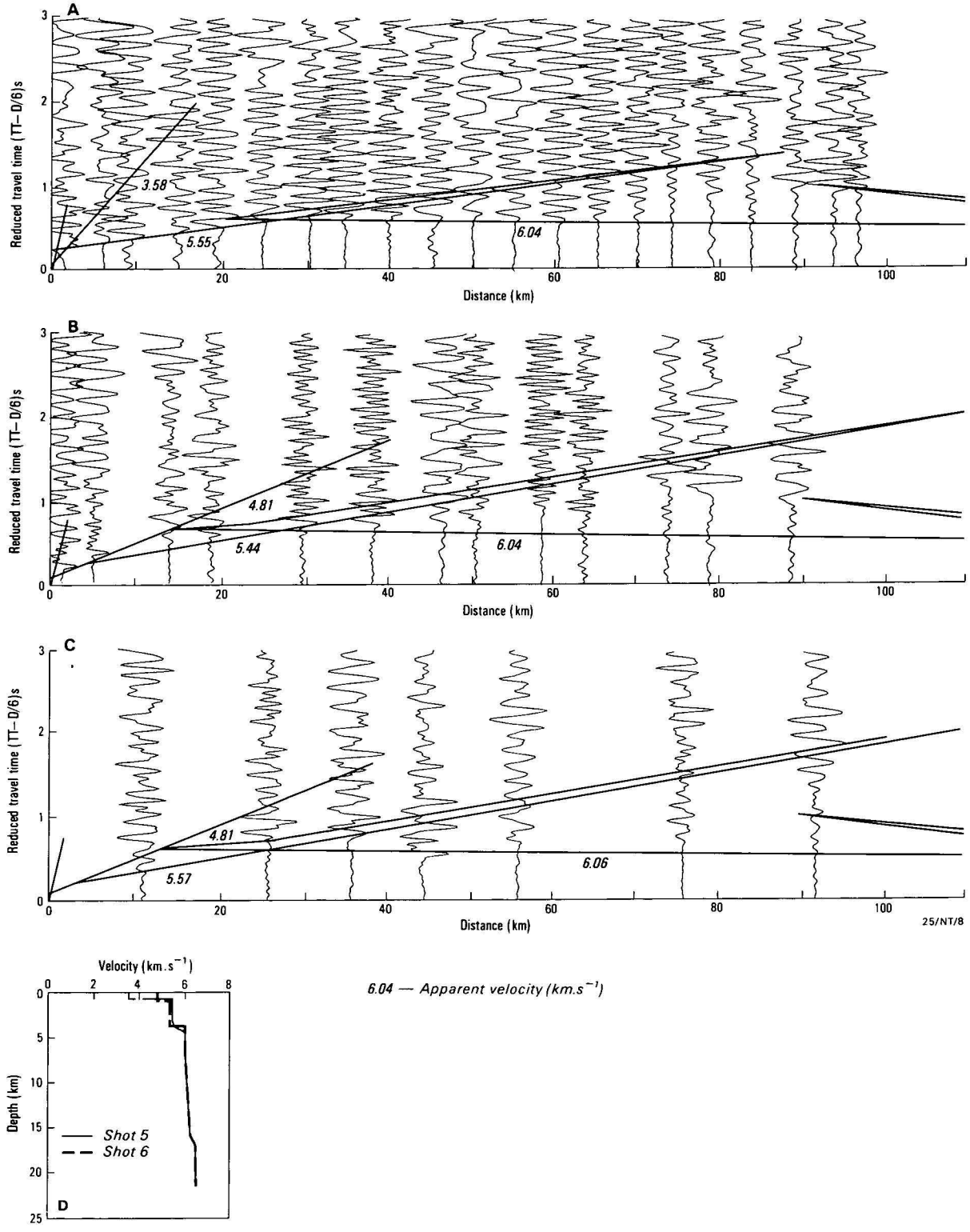

Figure 8. Record sections, eastern traverse.
Traces normalised and filtered 2–15 Hz. A — Shot 5, Borroloola, B — Shot 6, Robinson River, recorded northwards, C — Shot 6, recorded southwards, D — velocity/depth functions.

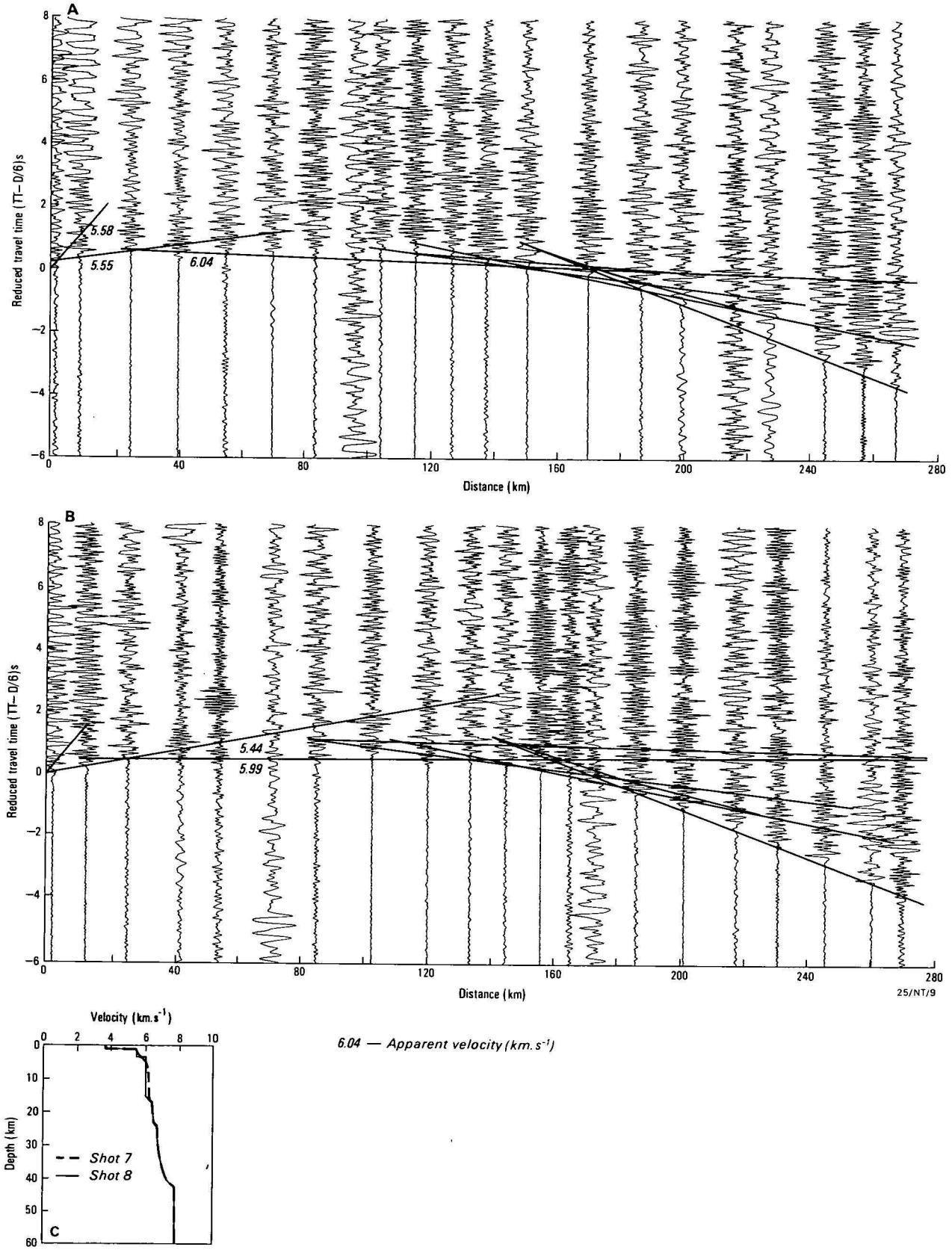

Figure 9. Record sections, eastern traverse.
Traces normalised and filtered 2–12 Hz. A — Shot 7, Borroloola, B — Shot 8, Westmoreland, C — velocity/depth functions.

Eastern traverse

Geological constraints. Shots 5 and 7 (Borroloola) were situated on Roper Group sediments east of the Emu Fault, which crop out along the traverse up to about 50 km southeast of Borroloola (Plumb, 1977; BMR, 1966). The maximum thickness of Roper Group in the area is about 500 m (Smith, 1964), and it is underlain by an unknown thickness of McArthur Group and Tawallah Group. Shot 6 (Robinson River) was situated on thin (< 100 m) McArthur Group rocks overlying Tawallah Group sediments (Yates, 1963). A basement ridge runs northwards from Robinson River homestead and probably crosses the traverse about 60 km southeast of Borroloola.

Shot 8 (Westmoreland) was situated on 200–400m of Westmoreland Conglomerate of the Tawallah Group, which overlies Cliffdale Volcanics (Grimes & Sweet, 1979). Approximately 50 km northwest of Shot 8, 3.5 km of Tawallah Group sandstones, conglomerates, and basalts of the Seigal Volcanics overlie an unknown thickness of Cliffdale Volcanics. The traverse within 50 km of Shot 8 lies over a complex area of faulting and shallowing of basement as the McArthur Basin sequence thins against the Murphy Tectonic Ridge to the south. Granites probably underlie the Cliffdale Volcanics and form part of the basement of the McArthur Basin sequence.

Seismic interpretation. Figures 8 and 9 show the seismic record sections and velocity/depth functions for the eastern traverse; the model shown in Figure 7B was interpreted. The basement arrivals from Shot 5 were slightly earlier in the range 20–50 km northwest of Shot 6, indicating a basement rise there, which coincides with the ridge indicated by the geology.

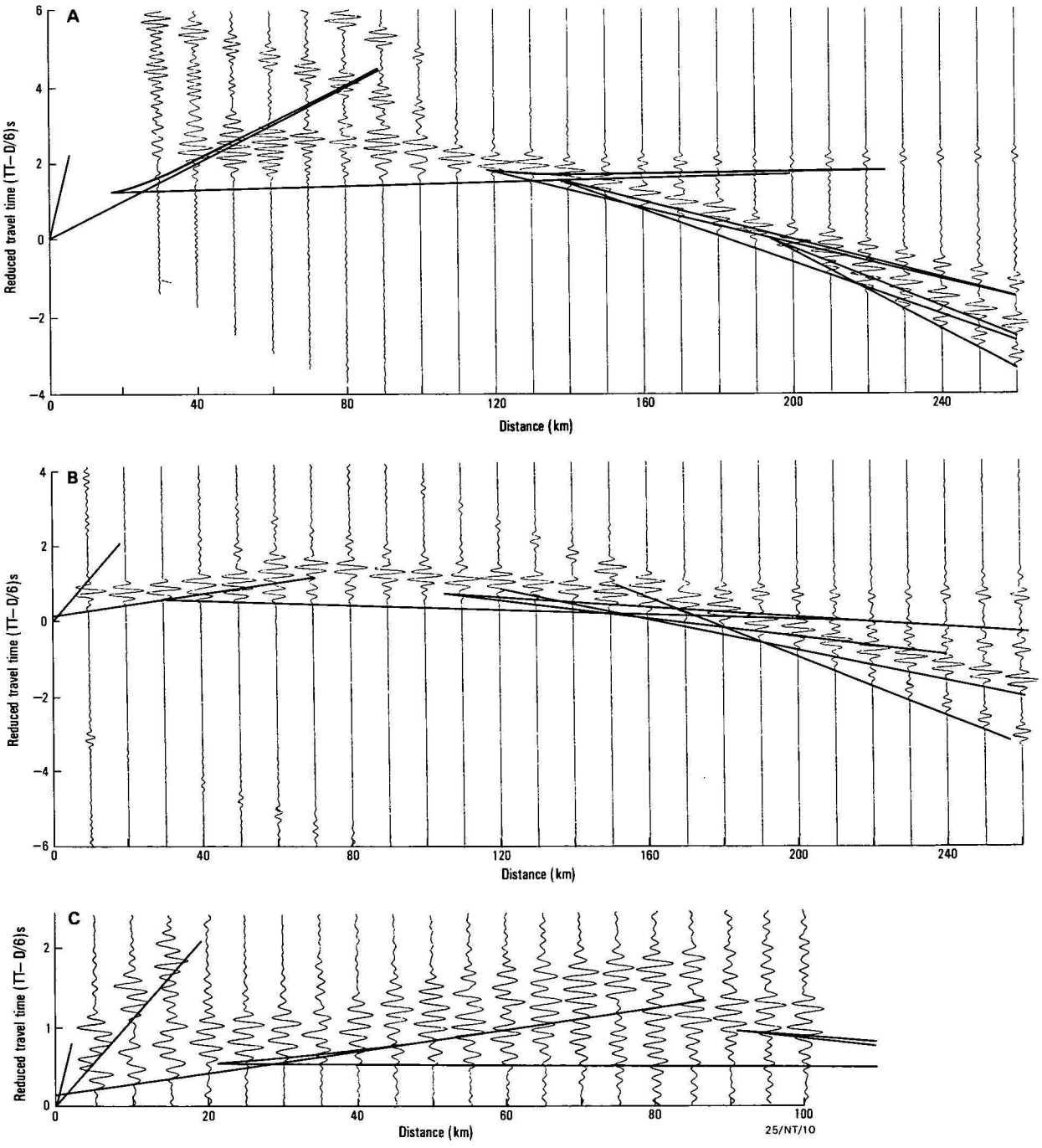

Figure 10. Synthetic seismograms, traces normalised.
A — western traverse, Shot 1 (velocity/depth function in Fig. 5C), B — eastern traverse, Shot 7 (velocity/depth function in Fig. 9C), C — eastern traverse shallow structure, Shot 5 (velocity/depth function in Fig. 8D).

Synthetic seismograms were computed for this model, using the velocity/depth function for Shot 5 (Fig. 8D); the synthetic record section is shown in Figure 10C. If the persistent wave-trains in the observed record section (Fig. 8A) are ignored, many of the details seen in the synthetics become apparent; for example the wide-angle reflection arrival at 1.4 s at 70 km. The termination of the reflection phase at about 85 km is more abrupt on the observed record section (Fig. 8A); the decrease in observed first-arrival amplitudes is also greater. This may suggest a low-velocity layer below the basement; however, modelling gave no more satisfactory results than the synthetic section shown here (Fig. 10C). The detailed shape of the velocity gradient has a marked effect on the synthetics; the shape of the gradient may even change along the traverse, but this cannot be modelled, because the structure is assumed to be laterally homogeneous. The surface layers may also vary along the traverse, and, as Khoketsu (1981) has shown, they can change the relative amplitudes of the synthetic seismograms from deeper layers.

The 3.58 km/s layer at Borroloola correlates with the thin Roper Group sediments. It was not recorded beyond the nearest station, and was interpreted from refracted arrivals recorded on the reflection spread. The 4.81 km/s layer (Fig. 7B) at Robinson River correlates with upper units of the Tawallah Group as well as a thin discontinuous veneer of McArthur Group and Cainozoic sediments. Below this, the Tawallah Group, which crops out along the basement ridge north of Robinson River homestead, correlates with the velocity of 5.44 km/s. The higher velocity of the equivalent layer at Borroloola may indicate the presence of McArthur Group carbonates, but these cannot be resolved from the data.

Pinchin (1979) measured velocities in McArthur Group rocks, using shallow seismic refraction near Mallapunyah. The velocity in the Emerugga Dolomite was 5.30–5.80 km/s, in the Tooganine Formation, 5.50 km/s, and in the Leila Sandstone Member, 6.00 km/s. The basement refractor may comprise pre-McArthur Basin metamorphics or acid volcanics and granites, as is believed to be the case towards the Westmoreland end of the traverse. Finlayson (1981) reported velocities in granites of about 5.69 km/s and a basement velocity of 6.06 km/s, within the Tennant Creek inlier, which are consistent with the present results.

The gravitational effect of the seismic model was calculated assuming two-dimensionality (Fig. 7). This is only approximately true, but the calculated and observed values agree fairly well between Borroloola and Robinson River. Between Robinson River and Westmoreland, the calculated gravity is higher than the observed gravity by up to 200 $\mu m/s^2$. This is because the traverse lies along the northeastern flank of a large gravity low (Fig. 2), which coincides with a basement granite body (Zadoroznyj & Plumb, BMR, personal communication, 1982). The basement velocity is slightly lower at the Westmoreland end of the traverse compared with Borroloola and Robinson River, and may reflect the presence of granites. The assumption of two-dimensionality of the structure used in the gravity modelling is probably not valid at this end of the traverse.

Deep structure

The record sections for Shots 1, 2, 7 and 8 are shown in Figures 5 and 9. The data quality is poor on the western traverse, particularly from Daly Waters and O.T. Downs, and this is believed to be due to near-surface effects at the shot sites attenuating the down-going energy (Pinchin, 1979). These effects have filtered out much of the high-frequency content of the signal from Shot 1 at Daly Waters (compare Figs. 5A and 5B).

A feature of all the 300-km long record sections is the lack of obvious wide-angle reflection branches, particularly from the Moho discontinuity. Later arrivals may be seen on some traces, but few can be correlated with any arrivals on adjacent traces, except at the farthest stations, beyond 250 km on the eastern traverse (Fig. 9). The reflections may be masked to some extent by the prominent wave-trains of the earlier phases, but they are not seen even where the amplitudes should increase, near the travel-time curve cusp points.

Moreover, the amplitudes of the first arrivals are large, which indicates they are diving waves rather than head waves generated at an abrupt velocity discontinuity. These two features indicate that the velocity increases gradually with depth rather than in discrete layers.

Western traverse

The velocity/depth model interpreted for the western traverse is listed in Table 1, and plotted in Figure 5C. The high velocity at the deepest part of the velocity gradient is not well defined, but the average gradient in the lower 20 km of the crust is well defined by the first-arrival data, i.e. an increase of about 0.06 km/s per km depth. The synthetic record section for this model is shown in Figure 10A.

Table 1. Velocity/depth models

The velocity/depth functions listed define the models used in the interpretation programs. Individual velocity/depth values include interpolated values which are necessary to define the gradient zones, and do not imply that the models are known to this accuracy.

Daly Waters (Shot 1)

Z (km)	V (km/s)
0.00	1.73
0.17	1.74
0.18	4.62
4.29	4.63
4.30	5.90
12.00	5.91
21.00	6.42
26.00	6.94
31.00	6.95
35.00	7.52
43.00	7.53
53.00	8.47
60.00	8.48

O.T. Downs (Shot 3)

Z (km)	V (km/s)
0.00	1.68
0.20	1.69
0.21	4.62
1.59	4.63
1.60	6.00
6.00	6.01

H.Y.C. (Shots 2, 4)

Z (km)	V (km/s)
0.00	1.68
0.07	1.69
0.07	5.81
12.00	5.82
21.00	6.42
26.00	6.94
31.00	6.95
35.00	7.52
43.00	7.53
53.00	8.47
60.00	8.48

Borroloola (Shot 7)

Z (km)	V (km/s)
0.00	1.71
0.05	1.72
0.06	3.58
0.42	3.59
0.43	5.55
1.80	5.56
2.20	5.57
2.60	5.60
2.80	5.65
2.90	5.70
2.96	5.75
3.04	5.80
3.14	5.85
3.40	5.93
4.01	6.04
8.00	6.05
15.10	6.15
15.25	6.24
15.35	6.30
15.55	6.38
15.85	6.42
16.15	6.46
16.50	6.47
21.00	6.50
22.00	6.52
22.50	6.55
23.00	6.60
23.50	6.81
26.00	6.82
28.00	6.84
30.00	6.88
32.00	6.94
34.00	7.02
38.00	7.40
40.00	7.80
60.00	7.91

Robinson River (Shot 6)

Z (km/s)	V (km/s)
0.00	1.71
0.05	1.72
0.06	4.81
0.70	4.82
0.71	5.44
3.54	5.45
3.55	6.04
8.00	6.05
12.00	6.17
15.00	6.20
16.00	6.25
16.50	6.47
21.00	6.48

Westmoreland (Shot 8)

Z (km)	V (km/s)
0.00	3.50
0.26	3.51
0.27	5.44
2.69	5.45
2.70	5.99
15.00	6.00
15.25	6.24
15.35	6.30
15.55	6.38
15.85	6.42
16.15	6.46
16.50	6.47
21.00	6.50
22.00	6.52
22.50	6.55
23.00	6.60
23.50	6.81
26.00	6.82
28.00	6.84
30.00	6.88
32.00	6.94
34.00	7.02
38.00	7.40
40.00	7.80
60.00	7.91

A model in which the velocity increases linearly with depth satisfies the travel-time data for depths below 15 km, and also the amplitude data in so far as there are no large later phases. This model does not show the prolonged, large amplitude, wave-trains visible in the observed records (Fig. 5), which are probably due to multiple reflections and scattering in the crust. However, the model in Figure 5C is preferred, because some later arrivals recorded could possibly be wide-angle reflections from the velocity gradients between 31 and 35 km, and 43 and 53 km depth.

At H.Y.C. (Fig. 5C), the 5.81 km/s layer is interpreted at 70 m below the surface; the next feature interpreted is the gradual velocity increase commencing at about 12 km depth. Any arrivals from intermediate depths are masked by these strong surface-layer arrivals (Figs. 5B & 6A). The deeper crustal section is assumed to be the same as the model derived from Daly Waters. The calculated travel-times are early by up to 0.4 s at distances beyond about 100 km from the shot. A correction has been applied to take account of the low-velocity surface layer on the western part of the traverse; however, it does not remove the total effect in the middle part of the traverse.

Eastern traverse

Some later arrivals are evident in the seismic recordings along the eastern traverse, e.g. between 90 and 125 km, Figure 9. The preferred velocity/depth model is listed in Table 1, and plotted in Figure 9C. The velocity increases gradually at depths greater than 44 km, because first-arrival amplitudes are large, but the gradient cannot be derived from the data.

The shapes of the gradient zones were constrained by the synthetic seismograms (Fig. 10B) generated from the model (Fig. 9C), and from the shallow model between Borroloola and Robinson River (Fig. 8D). Linear gradient zones were not adequate to account for the amplitudes of the observed arrivals. However, the average gradient in the lower 20 km of the crust is the same as for the western traverse, i.e., an increase of about 0.06 km/s per km depth.

At distances greater than 250 km, prominent arrivals can be seen about 1.2 s after the first arrivals from both forward and reverse shots (Shots 7 and 8) on the eastern traverse (Figs. 9A,B). Such events are not present on the western traverse record sections. The first arrivals are assumed to be Pn, i.e. arrivals refracted along the crust–mantle boundary. The amplitudes of the later arrivals are at least four times the Pn amplitudes. These arrivals may be reflections from a sub-Moho reflector. They are not simple wide-angle reflections from a sharply defined Moho, because their maximum amplitude occurs at too great a distance. They may represent a forward cusp on the Pn branch, owing to a zone of increasing velocity gradient at the base of the crust (Bullen, 1960); this has been observed in the West Australian Shield (B.J. Drummond, BMR, personal communication, 1981). Various velocity gradients were modelled, but, in all cases, the amplitude at the cusp relative to the first arrival was smaller than in the observed data.

Sub-Moho discontinuities that are shallow enough to produce strong wide-angle reflections in the observed time–distance range have been reported by Simpson (1973), Finlayson & others (1974), Hales & Rynn (1978), and Finlayson & McCracken (1981). They range in depth between 50 and 85 km. Travel-time curves were calculated for models that included sub-Moho discontinuities; none gave a satisfactory fit to the observed travel-times. The arrivals were either too early relative to the first arrivals, or were too far from the shot. To identify these arrivals properly, recordings beyond the maximum range of this survey (276 km) are required.

Vertical reflection recording

Vertical reflection recordings were made at the six refraction shot-points, and at a site near Starvation Hill between Borroloola and H.Y.C. (Fig. 2). A preliminary interpretation of these data was made by Pinchin (1980a).

At each site a 3-km recording spread was laid along the road, i.e. along the same azimuth as the long-range refraction lines, centred on the refraction shot. A short cross-spread, 1 km long, was laid at one end of the long spread, making either a 'T' or an 'L' shape with it, depending on access. The main spread had 36 recording stations at intervals of 83.33 m; the short spread had 12 stations with the same interval. Each recording station had 8 geophones per trace, in line, 5 m apart. Reflections were recorded at each site, from the large refraction shots as well as the small weathering shots. The large shots were offset laterally 15–30 m from the centres of the main spreads; the weathering shots were fired at each end of the main spreads. Digital recordings on magnetic tape were made on a DFS IV recording system; analogue records were produced in the field for monitoring purposes. Recordings were made at a sampling interval of 4 ms and the records were run for a total of 16 s.

The tapes were processed by Geophysical Services International, Sydney. This processing included true-amplitude recovery, time-variant scaling, correction for datum statics, normal move-out corrections, muting, and whitening deconvolution. At H.Y.C. and Borroloola, the two small weathering shots produced excellent reflections, so a 4-fold stack could be performed on the data. A time-varying filter was applied, with a 20–50 Hz passband at 0 s varying to an 8–30 Hz passband at 16 s. The processed section was produced as a variable area display (Fig. 11). Most records show several strong reflections and many weaker line-ups may be seen down to the bottom of the records at 16 s two-way time (about 50 km depth). Many more events were recorded on the eastern traverse than on the western traverse. At Daly Waters, and to a lesser extent at O.T. Downs, the energy was attenuated by near-surface effects (Pinchin, 1979).

Few reflectors can be traced from one shot site to the next, and these line-ups may be fortuitous, as there are numerous reflectors in each section. The most obvious arrivals that appear to be continuous are the reflection bands at about 6 and 6.5 s at Westmoreland, and 5.6 and 6.5 s at Robinson River. These reflection bands may continue to Borroloola, but they are not well defined. Many other strong reflection bands with distinctive characteristics occur both earlier and later in the sections. Some reflections have similar two-way times on two or more sections, but none can be followed from one section to the next on the basis of similar character. The lack of continuity of reflections is evidence of lateral variation of structure. Apart from record quality, there are no obvious features that distinguish the eastern traverse from the western traverse. However, none of the reflectors can be confidently traced from the eastern to the western traverse, which supports the interpretation of different velocity/depth functions from the refraction data for each traverse.

Two-way times to the major velocity changes, such as the tops of the gradient zones, were calculated from the refraction models and compared with the reflection times (Fig. 11). Velocity-gradient zones may be associated with bands of reflections, but, in general, broad gradient zones would be transparent to vertical energy. When reconciliation of refraction models and reflection data is being attempted, the differences between the methods must be considered. The vertical reflections are single probes recorded on 3-km spreads, each separated by 100–200 km. The refraction data are recorded

over large distances with the result that the crustal properties are averaged along the whole ray path. Moreover, for the deeper layers, the velocity boundaries interpreted from the data apply only beyond about 50 km from each shot. If there is lateral structure, the refraction models will not apply at the shot points where the vertical reflection arrivals are recorded.

The characteristic features of the vertical reflection records, i.e. numerous reflectors, some with large dips, have been widely observed (eg. Smithson & others, 1977). Berry & Mair (1980) attempted to reconcile these results with the often different picture presented by the refraction data. They pointed out that the crustal velocity/depth distribution is determined by the

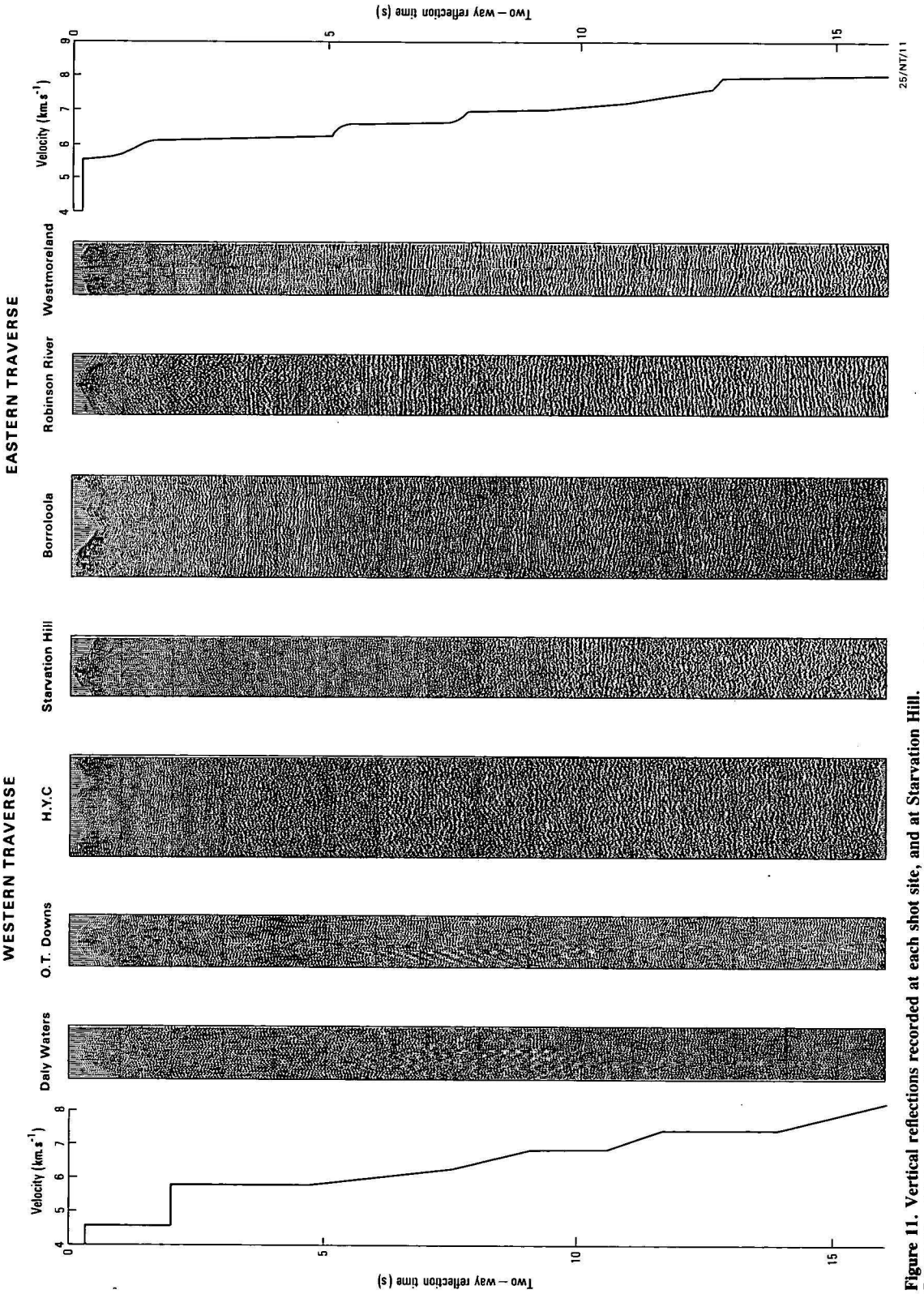

Figure 11. Vertical reflections recorded at each shot site, and at Starvation Hill.
For recording details see Pinchin (1979). The velocity/two-way-time diagrams computed from the velocity/depth function for each traverse (Figures 5(C) and 9(C)) are shown at the same two-way time scale.

following factors: the geochemistry and orogenic history, the distribution of water, and the past and present stress and temperature regimes. In general, vertical reflections are able to resolve the smaller-scale petrological features, while refraction tends to map large-scale variations, such as metamorphic grade, because velocities and depths are averaged along the traverse.

Reflection profiling over at least several tens of kilometres is essential if the true nature and extent of the reflections is to be resolved. Dipping events and diffractions cannot be interpreted from the single probes recorded here. This is obvious from the long profiles recorded by BMR in the Bowen and Eromanga basins (S.P. Mathur, BMR, personal communication), where large-scale continuity of events becomes apparent only when the profile is viewed as a whole. Randomly chosen 'probes' on the profile could give a misleading picture.

One apparent difference between recordings in the McArthur Basin and recordings in the Palaeozoic of eastern Australia is the lack of prominent wide bands of reflectors, which mark the middle to lower crust and the crust–upper mantle boundary. These can be seen even in the short (2–6 km) traverses recorded in the Lachlan Fold Belt (Pinchin, 1980b), but are not visible on the McArthur Basin records.

Discussion

The velocity/depth functions interpreted east and west of the Emu Fault have a similar overall velocity gradient with depth. However, the velocities and velocity gradients at any particular depth are different. Whether these differences occur abruptly at the fault or whether they occur gradually is not resolved except for the velocity structure within the top few kilometres. The shallow structure under the H.Y.C. deposit on the western side of the Emu Fault is markedly different from the nearby structure under Borroloola to the east, supporting geological and MT evidence for marked differences across the fault.

Both east and west of the Emu Fault, velocity gradually increases with depth. The gradients appear to be broader in the west, but this may in part be due to poorer data quality, which makes the interpretation of smaller-scale features difficult. In the lower 20 km of the crust, both traverses have the same overall increase in velocity of about 0.06 km/s per km depth.

Characteristic features of the seismic recordings are a lack of strong reflection branches, erratic large-amplitude later arrivals, strong first arrivals, long wave trains, and vertical reflections that appear to be discontinuous. Mereu & Ojo (1981) have shown that these features can be generated by small random inhomogeneities in an otherwise simple crust, in which the velocity increases linearly with depth, much as in the smooth gradient model, which satisfies the travel-time data and much of the amplitude data, for the western traverse. Moreover, they show that travel-times from this random model, plotted against distance, may form linear segments from which major horizontal velocity discontinuities may be interpreted. The size of the velocity inhomogeneities determines the depths and apparent velocities of the interpreted discontinuities. Uncertainties, such as lateral inhomogeneity in the crust, must be borne in mind when comparing the differences in detail between the eastern and western traverses. However, the major features of the velocity/depth distribution derived for each traverse are necessary to satisfy the travel-time data.

The vertical reflection records show numerous reflections, but they cannot be interpreted geologically without continuous profiling. The character of the records is different from recordings made over the Palaeozoic of eastern Australia, prominent wide bands of reflectors in the lower crust being absent. They are, however, similar to deep reflection recordings made in the southern Yilgarn Block of the Archaean Shield of Western Australia (Mathur & others, 1977); numerous reflectors throughout the records were observed, but no obvious bands of reflectors could be seen.

The basement of the McArthur Basin was identified under the Wearyan Shelf, but was not recorded in the Batten Trough, and probably not under the Bauhinia Shelf. The velocity of the layer below the ?Roper Group on the Bauhinia Shelf closely matches the velocity of the McArthur Group in the Batten Trough. Geological and MT evidence (BMR, 1966; Cull, 1982a) suggests the layer is Tawallah Group sediments. This may, therefore, explain why no velocity contrasts were detected within the Batten Trough. Apart from the relatively high surface velocities due to thick McArthur Group carbonates, which mask later arrivals, there may be little or no velocity contrast between the McArthur Group and Tawallah Group, and probably the same applies to the basement. The velocity of the Wearyan Shelf basement (6.0–6.1 km/s) is close to the velocity of the ?Tawallah Group in the Bauhinia Shelf (5.8–5.9 km/s); the Tawallah Group has a lower velocity on the Wearyan Shelf (5.4–5.5 km/s). Assuming that the basement velocity is similar on both traverses, the Tawallah Group would thus be detected, as has been observed, in the east, but not in the west.

Magnetotelluric (MT) results show a high resistivity basement beneath the Tawallah Group, or its equivalent, about 6 km deep at Daly Waters, increasing to 9.5 km below the thickest section of Roper Group further east (Cull,1982a). Seismic arrivals from any velocity contrast associated with the resistivity boundary may be masked by arrivals from the deeper velocity gradient, which begins at about 12 km depth, or else little or no velocity contrast exists, for the reasons outlined above. The latter case is supported by a lack of vertical reflections associated with the boundary.

MT results in the area are generally consistent with the seismic models (Cull,1982a). On the Bauhinia Shelf, between Daly Waters and O.T.Downs, thicknesses derived for the Roper Group from MT and seismic data are similar and show the same trends. Both MT and seismic data give a depth of about 2 km to the base of the Roper Group sediments near Daly Waters. However, from MT, the maximum depth is 5.5 km, 70 km east of Daly Waters, whereas the seismic data give a maximum depth of 4.1 km, 20 km east of Daly Waters. Both show the Roper Group gradually thinning eastward towards O.T. Downs, in agreement with surface geology.

On the Wearyan Shelf, near Borroloola, the MT results agree fairly well with the seismic model. A major resistivity boundary, believed to be basement, was interpreted at about 3.5 km depth, which correlates with the seismic basement at 3.3 km. However, south of Robinson River, MT defines the basement at 5.4 km, while the seismic basement occurs at 3.5–2.7 km. The seismic data are not sufficiently detailed towards the south to resolve the complex structures around Westmoreland, but they show that between Robinson River and Westmoreland the basement is flat-lying, in agreement with the MT data. Unknown thicknesses of Seigal Volcanics in the Tawallah Group, and the underlying Cliffdale Volcanics, may affect both the seismic and the MT data. Since there is no evidence in the seismic data for significant McArthur Group carbonates between Borroloola and Robinson River, there seems little potential for H.Y.C. type deposits east of the Emu Fault.

Small velocity inversions in the shallow layers of both traverses may exist, and indeed are likely because of the presence of high velocity carbonates and volcanics in the sediments, but there is

no evidence of significant low-velocity zones in the crust. This is consistent with results from other Precambrian areas (eg. Meissner, 1976; Drummond,1979), but differs from the Tennant Creek and Mount Isa areas, where Finlayson (in press) interpreted three low-velocity zones in the upper crust. However, care is needed when generalising crustal structures to fit particular tectonic regimes. For example, the velocity/ depth function of such a vastly different area as south-western Honshu, Japan (Kohketsu,1981), bears a striking resemblance to the velocity/ depth function interpreted here. On the other hand, it is very different from the Proterozoic Cuddapah Basin, India, which otherwise has many similarities to the McArthur Basin (Plumb,1981); very strong wide-angle reflections are observed, which clearly represent abrupt velocity discontinuities (Kaila & others, 1979), particularly at the crust-mantle boundary. Similar wide-angle reflections are observed in the Archaean Pilbara Block of Western Australia (Drummond, 1979, 1981).

By comparing crustal models of the Tennant Creek Inlier, Mount Isa Block, Arafura Sea, and McArthur Basin, Finlayson (in press) interpreted a progressive increase in crustal velocities from south to north in the North Australian Craton. Also, deep crustal velocities appear to be higher under the central part of the craton than under the eastern part. Whether this is a general rule for the whole craton cannot be established until more data are available.

Inliers of Archaean basement underlie the North Australian Orogenic Province in the north (Plumb, 1979), but the extent of this Archaean basement is unknown. Plumb (1979) raised the possibility that an Archaean continental crust might underlie the whole region, because the major fracture pattern in the region is geometrically regular and has existed since at least the Early Proterozoic. The same conclusion was reached by Rutland (1981) on the grounds that the active continental margin during the Proterozoic was likely to be in the east, in the region now occupied by the younger Tasman Province; the Proterozoic crust is postulated to be the result of vertical accretion on and within an Archaean proto-continental crust. The crust in the Archaean Pilbara Block is much thinner (28–33 km) than the north Australian crust, and has relatively low velocities within the lower crust (6.4–6.55 km/s) and a well-defined crust–mantle boundary. The crust of the northern Yilgarn Block is at least 50 km thick; the form of the crust–mantle boundary is undefined, but the lowest layer interpreted has a velocity of 6.9–7.0 km/s compared with 6.4–6.55 km/s in the Pilbara (Drummond, 1981), and the boundary may be gradational. The Proterozoic Capricorn Orogenic Belt between these blocks is distinguished by intermediate crustal thickness and high velocities and velocity gradients at the base of the crust. Drummond (1981) has suggested that the Capricorn Orogenic Belt was derived from the northern Yilgarn Block, which was modified during Proterozoic tectonism; the (assumed) Archaean 'proto-continental' crust of north Australia may, therefore, have been similar in certain respects to the Yilgarn crust.

Acknowledgements

I wish to acknowledge the contributions of D.M. Finlayson, K.A. Plumb and J. Pinchin during the planning of this survey, and their assistance during the field work and interpretation. J.W. Williams and D. Pownall were involved in the refraction recording, and J. Pinchin was responsible for the shooting and vertical reflection recording; their contributions are gratefully acknowledged. Thanks are also due to the owners and managers of the following properties on which the shots were detonated: Kalala, Balbirini, McArthur River, Robinson River, and Westmoreland, and to the Aboriginal Council, Borroloola.

References

Berry, M.J., & Mair, J.A., 1980 — Structure of the continental crust: A reconciliation of seismic reflection and refraction studies. *In* Strangway, D.W., (editor), The continental crust and its mineral deposits. *Geological Association of Canada, Special Paper* 20, 195–213.

BMR, 1966 — McArthur River Area, Northern Territory, Australia, 1:500,000 Geological Map. *Bureau of Mineral Resources, Australia, Canberra.*

Brown, M.C., 1969 — Daly Waters, N.T., 1:250,000 Geological Series. *Bureau of Mineral Resources, Australia, Explanatory Notes,* SE/53-1.

Bullen, K.E., 1960 — Note on cusps in seismic travel-times. *Geophysical Journal of the Royal Astronomical Society*, 3, 354–359.

Cleary, J., 1973 — Australian crustal structure. *Tectonophysics*, 20, 241–248.

Collins, C.D.N., 1981 — Crustal seismic investigations in Northern Australia, 1979: operational report. *Bureau of Mineral Resources, Australia, Record* 1981/2 (unpublished).

Cull, J.P., 1982a — Magnetotelluric profiles in the McArthur Basin of northern Australia. *BMR Journal of Australian Geology & Geophysics*, 7, 275–286.

Cull, J.P., 1982b — An appraisal of Australian heat-flow data. *BMR Journal of Australian Geology & Geophysics*, 7, 11–21.

Denham,D., Simpson, D.W., Gregson, P.J., & Sutton, D.J., 1972 — Travel-times and amplitudes from explosions in Northern Australia. *Geophysical Journal of the Royal Astronomical Society*, 28, 225–235.

Drummond, B.J., 1979 — A crustal profile across the Archaean Pilbara and northern Yilgarn cratons, northwest Australia. *BMR Journal of Australian Geology & Geophysics*, 4, 171–180.

Drummond, B.J., 1981 — Crustal structure of the Precambrian terrains of northwest Australia, from seismic refraction data, *BMR Journal of Australian Geology & Geophysics*, 6, 123–135.

Finlayson, D.M., 1981 — Reconnaissance of upper crustal seismic velocities in the Tennant Creek Block, Northern Territory. *BMR Journal of Australian Geology & Geophysics*, 6, 245–252.

Finlayson, D.M., in press — Seismic crustal structure of the Proterozoic North Australian Craton between Tennant Creek and Mount Isa. *Journal of Geophysical Research.*

Finlayson, D.M., & Collins, C.D.N., 1980 — A brief description of BMR portable seismic tape recording systems. *Australian Society of Exploration Geophysicists, Bulletin*, 11, 75–77.

Finlayson, D.M., Cull, J.P., & Drummond, B.J., 1974 — Upper mantle structure from the Trans-Australia seismic survey (TASS) and other seismic refraction data. *Journal of the Geological Society of Australia*, 21, 447–458.

Finlayson, D.M., & McCracken, H.M., 1981 — Crustal structure under the Sydney Basin and Lachlan Fold Belt determined from explosion seismic studies. *Journal of the Geological Society of Australia*, 28, 177–190.

Fraser, A., 1976 — Gravity provinces and their nomenclature. *BMR Journal of Australian Geology & Geophysics*, 1, 350–352.

Fuchs, K., 1968 — Das Reflexions und Transmissionsvermogen eines geschichteten Mediums mit beliebiger Tiefen — Verteilung der elastichen Moduln unde der Dichte fur schragen Einfall ebener wellen. *Zeitschrift fur Geophysik*, 34, 389–413.

Grimes, K.G., & Sweet, I.P., 1979 — Westmoreland, Queensland, 1:250,000 Geological Series. *Bureau of Mineral Resources, Australia, Explanatory Notes*, SE/54–5.

Hales, A.L., & Rynn, J.M.W., 1978 — A long-range controlled source seismic profile in Northern Australia. *Geophysical Journal of the Royal Astronomical Society*, 55, 633–644.

Hales, A.L., Muirhead, K.J., & Rynn, J.M.W., 1980 — Crust and upper mantle shear velocities from controlled sources. *Geophysical Journal of the Royal Astronomical Society*, 63, 659–670.

Kaila, K.L., Chowdhury, K.R., Reddy, P.R., Krishna, V.G., Narain, H., Subbotin, S.I., Sollogub, V.B., Chekunov, A.V., Kharetchko, G.E., Lazarenko, M.A., & Ilchenko, T.V., 1979 — Crustal structure along Kavali-Udipi profile in the Indian Peninsula Shield from deep seismic sounding. *Journal of the Geological Society of India*, 20, 307–333.

Khoketsu, K., 1981 — Reinterpretation of seismograms obtained by the Kurayosi explosions with the reflectivity method. *Journal of Physics of the Earth*, 29, 255–265.

Mathur, S.P., Moss, F.J., & Branson, J.C., 1977 — Seismic and gravity investigations along the geotraverse, Western Australia, 1969. *Bureau of Mineral Resources Australia, Bulletin*, 191.

Meissner, R., 1976 — Comparison of wide-angle measurements in the U.S.S.R. and the Federal Republic of Germany. *In* Giese, P., Prodehl, C., & Stein, A. (editors) Explosion seismology in central Europe. *Springer, Berlin*, 380–384.

Mereu, R.F., 1967 — Curvature corrections to upper mantle seismic refraction surveys. *Earth and Planetary Science Letters*, 3, 469–475.

Mereu, R.F., & Ojo, S.B., 1981 — The scattering of seismic waves through a crust and upper mantle with random lateral and vertical inhomogeneities. *Physics of the Earth and Planetary Interiors*, 26, 233–240.

Pinchin, J., 1979 — Reflection results. *In* Plumb, K.A., McArthur Basin research, June quarter, 1979. *Bureau of Mineral Resources, Australia, Record* 1979/57 (unpublished).

Pinchin, J., 1980a — Reflection results. *In* Plumb, K.A., McArthur Basin research, March quarter, 1980. *Bureau of Mineral Resources, Australia, Record* 1980/38 (unpublished).

Pinchin, J., 1980b — Intracrustal seismic reflections from the Lachlan Fold Belt near Canberra. *BMR Journal of Australian Geology & Geophysics*, 5, 305–309.

Plumb, K.A., 1977 — McArthur Basin project. *Bureau of Mineral Resources Australia, Record* 1977/33 (unpublished).

Plumb, K.A., 1981 — Workshop: Comparison of the Cuddapah Basin, India, and the Adelaide Geosyncline, Australia. Report of overseas visit — January, 1981. *Bureau of Mineral Resources, Australia Record* 1981/24 (unpublished).

Plumb, K.A., & Derrick, G.M., 1975 — Geology of the Proterozoic rocks of the Kimberly to Mount Isa Region. *In* Knight, C.L. (editor), Economic geology of Australia and Papua New Guinea. 1 — Metals. *Australasian Institute of Mining and Metallurgy, Monograph* 5, 217–252.

Plumb, K.A., Derrick, G.M., & Wilson, I.H., 1980 — Precambrian geology of the McArthur River–Mount Isa region, northern Australia. *In* Henderson, R.A., & Stephenson, P.J. (editors), Geology and geophysics of northeastern Australia. *Geological Society of Australia, Queensland Division, Brisbane*, 71–83.

Randal, M.A., 1973 — Groundwater in the northern Wiso Basin and environs, Northern Territory. *Bureau of Mineral Resources, Australia, Bulletin* 123.

Rutland, R.W.R., 1981 — Structural framework of the Australian Precambrian. *In* Hunter, D.R., (editor) Precambrian of the southern hemisphere, *Developments in Precambrian Geology*, 2, 1–32, *Elsevier, Amsterdam*.

Simpson, D.W., 1973 — P wave velocity structure of the upper mantle in the Australian region. *Ph.D. Thesis, Australian National University, Canberra*.

Smith, J.W., 1964 — Bauhinia Downs, N.T., 1:250,000 Geological Series. *Bureau of Mineral Resources, Australia, Explanatory Notes*, SE/53–3.

Smithson, S.B., Shive, P.N., & Brown, S.K., 1977 — Seismic reflections from Precambrian crust. *Earth and Planetary Science Letters, 37, 333–338*.

Underwood, R., 1967 — The seismic network and its applications. *Ph.D. Thesis, Australian National University, Canberra*.

Yates, K.R., 1963 — Robinson River, N.T., 1:250,000 Geological Series. *Bureau of Mineral Resources, Australia, Explanatory Notes*, SE/53–4.

BMR Journal of Australian Geology & Geophysics, 8, 35-51

DETAILED SEISMIC VELOCITY/DEPTH MODELS OF THE UPPER LITHOSPHERE OF THE PILBARA CRATON, NORTHWEST AUSTRALIA

B.J. Drummond

Detailed velocity/depth models of the crust of the Pilbara Craton have been produced from amplitude studies of refracted and reflected seismic waves and their travel-times. On three profiles, a near-surface high-velocity layer, in which the velocity sometimes reaches 6.65 km s^{-1}, is interpreted as Hamersley Basin strata overlying the crystalline basement. The seismic velocity in the near-surface crystalline basement is about 6.0 km s^{-1}, and increases with depth through the crust, reaching 6.1–6.2 km s^{-1} at 11–14 km depth. Below this, at about 15 km depth, a steeper gradient to 6.35–6.45 km s^{-1} defines an intracrustal seismic boundary. In the lower part of the crust, velocity gradients increase the velocity to 6.6–7.2 km s^{-1}. In some models, second-order velocity increases with depth are used to explain bright cusps in the data, although these could also be caused by topography on the crust/mantle boundary. The crust/mantle boundary is transitional over 4-5 km, and upper mantle (Pn) velocities range from 7.5 to 8.5 km s^{-1}. On one profile, a sub-Moho boundary at which the velocity increases from 8.2 to 8.35 km s^{-1} was recognised 14 km below the crust/mantle boundary.

Previously published seismic models of the region show lateral inhomogeneity in the crust of the Capricorn Orogenic Belt, and this complicates a quantitative analysis of the amplitudes of seismic signals recorded in the orogen. However, a qualitative analysis based on the observed amplitudes, the positions of the ray-critical cusps of the previously published models, and the gravity field suggests that, while the intracrustal boundary at about 15 km depth may be sharp, the lower crust in the orogen must have high seismic velocities (and densities) and the crustal thickness in the previous models is probably not an overestimate. Increasing metamorphic grade with depth in the Yilgarn Craton probably ensures positive velocity gradients in the crust in the craton, so that the crustal thickness in the previously published models is considered reasonable. Thus, the interpreted large difference in crustal thickness between the Pilbara Craton (approximately 30 km) and the Yilgarn Craton (50 km) is substantiated.

Introduction

Seismic velocity models of the crust of the Precambrian shield in north-west Australia published to date (Drummond, 1979a; 1981; Drummond & others, 1981) were all based on the travel times of refracted waves, and, for simplicity, were based on the assumption that discrete layers with uniform velocity exist in the crust. Such models are useful for studies of lateral structures within the crust, and can provide valuable control in studies of the tectonic processes likely to have been active during the evolution of the crust. However, the depths of the boundaries in such models may be in error if velocity gradients exist within the layers (Berry, 1971). This was recognised in the earlier studies, but the effects of velocity gradients on the depths of the seismic boundaries in the models were assumed to apply to the entire region. Thus, the relative crustal thicknesses throughout the region would not change and the assumptions made about crustal evolution based on crustal thicknesses were presumed to be correct.

Drummond (1979a, 1981) used the observed seismic velocities to suggest that the crust of the Pilbara and Yilgarn Cratons was probably of acid to intermediate chemical composition, but, in the absence of detailed velocity/depth information, was not able to fully explore the likely composition of the crust. As positive velocity gradients were likely in the lower crust (Drummond, 1979a, 1981), the density of the lower crust is probably higher than might be presumed from the existing seismic models. Drummond & Shelley (1981) suggested density layering within the crust of the Yilgarn Craton as a possible explanation for differences between the theoretical gravity effect of the existing seismic models and the observed gravity field, although not all the inconsistencies can be explained in this way.

The purpose of this paper is to examine in detail the variation of seismic velocity with depth in northwest Australia. The resulting seismic velocity/depth models are significantly different in many ways from the velocity/depth models of other regions of Australia, and therefore warrant a detailed analysis of the likely chemical composition of the crust, comparisons with younger regions of Australia, and a study of the implications for crustal evolutionary models. The results of these studies will be published separately.

The area of interest

In 1977, the Bureau of Mineral Resources, and the Research School of Earth Sciences of the Australian National University conducted a seismic refraction survey of the crust and upper mantle in the northern part of the Western Australian Precambrian Shield (Fig. 1). As the purpose of this paper is to present the results of an interpretation of seismic data, the following geological description is very brief. More detailed descriptions of the geology are given by Drummond (1979a, 1981) and Drummond & others (1981), and the references cited therein.

The Pilbara Block is the exposed part of the Pilbara Craton, which is shown by seismic modelling (Drummond, 1981), gravity patterns (Wellman, 1978; Drummond & Shelley, 1981), and inliers of Archaean basement outcrop, to extend southwards under the younger Archaean and lower Proterozoic Hamersley Basin cover. The Yilgarn Craton in the south of the survey area forms the basement of the Nabberu Basin.

The Ashburton Trough, Gascoyne Province, and Bangemall Basin lie in the Capricorn Orogenic Belt (Gee, 1979), and the predominantly sedimentary rocks of the belt mask the structural relations between the two Archaean cratons.

Quarry blasts at open-cut iron ore mines in the Pilbara Craton were used as seismic sources. They were located at Shay Gap and Sunrise Hill (A in Figure 1), Goldsworthy (G), Newman (B), Tom Price and Paraburdoo (D) and Pannawonica (F). A specially prepared blast was fired at Meekatharra (C). Portable seismic recorders were deployed along lines between the blasting centres to record the seismic energy. Their positions are shown in Figure 1, and full details of the survey were described by Drummond (1979b).

In the seismic models from the previous studies (Drummond, 1979a, 1981; Drummond & others, 1981), the crust of the Pilbara Craton is 28 km thick in the north and 33 km thick in the south, with little evidence for east/west dip on the crust/mantle boundary. The northern part of the Yilgarn Craton was interpreted as more than 50 km thick. The crust in the Capricorn Orogenic Belt is intermediate in thickness. Thus, the

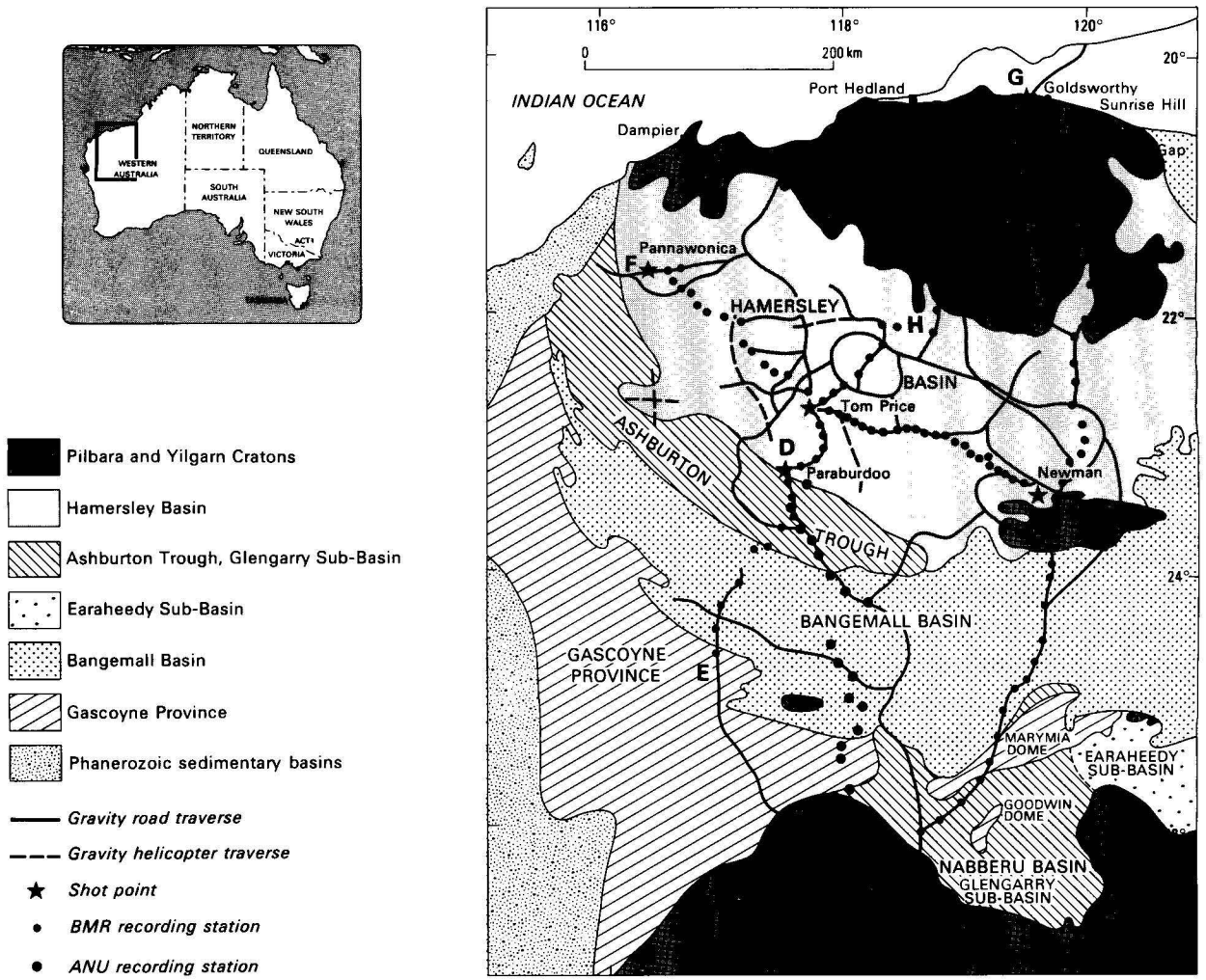

Figure 1. Geology of the survey region, and survey design.

crust in the northern part of the survey area, covering the Pilbara Craton, has little lateral structure, but across the southern part of the survey area, the depth of the crust/mantle boundary doubles, and lateral structures are significant.

Seismic modelling method

Berry (1971) emphasised the importance of recognising, and correlating between seismic traces, later arrivals that can be used to define in more detail the velocity structure with depth. He also stressed the importance of recognising and matching the position of the critical cusps. Mueller & Landisman (1971) suggested that the dynamic properties of seismic arrivals, that is, their amplitudes, phases, and frequencies, and not just their travel times, should be considered in the interpretation.

A study of the dynamic properties of seismic arrivals is inextricably linked to a study of secondary arrivals, because the secondary, wide-angle and near-critical reflections off seismic discontinuities are nearly always of higher amplitude, and therefore more easily identified, than the refracted head waves from the layers above and below the interface (Braile & Smith, 1975). However, although generally small, the amplitudes of head waves are greatly affected by velocity gradients in the refracting medium.

Amplitudes of seismic waves can be studied with the aid of synthetic seismograms. The computer program used to generate the synthetic seismograms in this study was based on the reflectivity method (Fuchs & Muller, 1971) with a modification suggested by Kind (1976) incorporated to increase the efficiency of the program. The program calculates synthetic seismograms for horizontally layered models in a flat Earth, but the models presented below (Tables 1–8; Figures 2–9) have been corrected to allow for the spherical Earth.

This synthetic seismogram technique has some limitations. Firstly, in order that phases be correctly correlated from trace to trace, Mueller & Landisman (1971) suggested that a station spacing of 3 km or less is required or phases will be missed or incorrectly correlated, a conclusion echoed by Berry & Fuchs (1973). In this study, station spacing was between 5 km near shotpoints and 25 to 30 km in the middle of some of the profiles. It is therefore possible that some travel-time branches were not recognised, or incorrect correlations made. However, within the data currently available, most of the recognised phases have been interpreted, and it seems unlikely that any major wave groups were missed.

Secondly, the computer program assumes that the Earth is composed of flat-lying, homogeneous, isotropic layers; zones of vertical velocity gradients may be represented by thin laminae of such layers (Fuchs, 1968). This is usually an over-simplification, as any geological, gravity or magnetic map will reveal. For example, in the survey area, the geological map shows several Archaean cratons, each with large, low density granitoids intruding denser greenstone belts, and separated by Proterozoic mobile belts. The first impression is, therefore, of lateral and not vertical structure. The seismic signature of flat-

lying, vertically stratified structure must, therefore, overprint that of the lateral structure before it can be accurately interpreted. As well, the effects of refractor topography can often appear to come from vertical structure (Mereu, 1969).

The use of synthetic seismograms should, therefore, be limited to regions of limited lateral structure, where a network of traverses can be used to distinguish lateral structure from vertical structure. Within the survey area, this criterion is met only within the confines of the Pilbara Craton (lines AB, FDB and GHD). Furthermore, the velocity/depth models derived below for all the seismic profiles over the Pilbara Craton by synthetic seismogram modelling are similar, and this also justifies using the technique to interpret vertical structure in the craton.

Data processing

To facilitate discussion of the velocity/depth models, their p (ray parameter) versus distance plots, and the observed and synthetic seismogram record sections, the travel-time cusps in the following discussion are annotated by the letters a, b, c, etc. The branches are:

Branch	Phase	Description of the ray path.
ab	Pg	Travels through the near-surface crystalline rocks. Along some profiles in the Hamersley Basin, some phases labelled P_1 and P_2 which travel through the basin strata are also labelled ab. The distinction is made in the text.
bc	P^I	Reflections from an intracrustal boundary.
cd	P*	Refracted below the intracrustal boundary.
de	P^M	Reflections off the crust/mantle boundary.
ef	Pn	Refractions from the uppermost mantle.
fg		Reflections off a sub-Moho boundary about 14 km below the crust/mantle boundary.
gh		Waves refracted below the sub-Moho boundary.

All data are presented in the form of record sections with a reduction velocity of 8 km s^{-1}, and were digitally bandpass filtered in the range 0.5 to 8.0 Hz. This passband removed much of the long period background noise, as well as high frequency local wind noise, while leaving the character of the principal seismic signal inviolate. When plotting the data, corrections were made for recorder gain, so that all traces in each record section are as if recorded at the same gain level.

At large distances, the geometrical spreading of head waves is proportional to distance squared, while, to a first approximation, that of reflected waves is proportional to distance (Aki & Richards, 1980). Consequently, commensurate with the expectation that the reflected waves would have the greatest amplitudes and therefore play the major role in the interpretation of amplitudes, a correction proportional to epicentral distance was applied to all data beyond the interpreted P^M/Pn cusp to account for the geometrical spreading of the wavefronts. Between the shot and about 100 km, which is about the position of the P^M/Pn critical cusp, the seismic traces were often distorted by overmodulation of the seismic channels, because of the large shot sizes. Correction of these amplitudes for geometrical spreading would have been meaningless, and, at worst, misleading. The P^M/Pn cusp was usually, though not always, characterised by large, clear and, therefore, easily recognised arrivals and was a useful datum to which the arrivals on the other traces could be related.

Braile & Smith (1975) and Berry & Fuchs (1973) also used a correction factor for geometrical spreading proportional to epicentral distance, but other workers, for example Mereu & others (1977), prefer the square of the distance. When a factor proportional to the square of the distance was used on these data, the amplitudes of the recorded signal and, especially, those of the reflected phases increased interminably with distance, which cannot happen in real data, because of natural attenuation processes and because it would imply that seismic waves could gain energy with distance from the blast.

In a few cases, additional adjustments were made to the trace amplitudes. These were generally in the form of a reduction of anomalously large amplitude arrivals, which obscured arrivals on adjacent traces and are clearly marked on the record sections by an 'X' and the reduction factor.

No amplitude corrections were made for shot weight. Many of the blasts have individual source characteristics, the differences in the waveforms being in the frequency and time duration of the signals, and not in their amplitude. No simple relationship links the observed amplitudes to the amounts of explosives used in the blasts (see also Berry & Fuchs, 1973, for similar observations of blasts specially prepared for seismic surveys). This probably stems from the practice of firing the quarrying blasts one mining bench at a time, with delays between the benches. The consequence of delays is that the amplitude of the seismic energy is related more to the quantity of explosives in each bench than the total quantity of explosives in the blast.

Synthetic seismogram modelling

Shotpoint A (Sunrise Hill & Shay Gap), along line AB

Because of the overmodulation of the near-source recordings, owing to the large quarrying blasts used for the seismic survey, very little is known about the amplitudes of the Pg phase (ab), and the P^I/P* cusp (c). Some of the smaller blasts at Shay Gap, Sunrise Hill, and Goldsworthy, however, did not overmodulate the traces, and the record section of one such blast is shown in Figure 2b. The location of the profile is shown in Figure 2a.

The Pg phase (ab) decays proportionally to a value between distance and distance squared. This implies that there is very little attenuation of the seismic energy. No upper crustal low-velocity channel similar to that found in both young and old regions elsewhere in the world (eg. Mueller & Landisman, 1966; Berry & Fuchs, 1973; Finlayson & others, 1980) can be implied. Rather, positive velocity gradients can be inferred to limit the amplitude decay to between distance and distance squared.

The amplitude of the P^I/P* cusp (c) is also further evidence that no upper crustal low-velocity channel is present in the region. Mueller & Landisman (1966) suggested that the large amplitudes of the P^I phase (bc) relative to the Pg phase (ab) in the data that they studied were evidence for a low-velocity zone; this zone brought the intracrustal boundary in their model closer to the surface, and moved the P^I/P* cusp closer to the blast. In the record section in Figure 2b, the arrowed P^I arrivals in each trace have about twice the amplitude of the Pg phase in that trace. However, the full interpretation of the P^I/P* cusp (c) cannot be made without comparing it to the P^M/Pn cusp (e). Between about 80 and 120 km, the arrivals of the P^I/P* cusp have about one-third to one-quarter the amplitude of those near the P^M/Pn cusp (e).

The P^M/Pn cusp is shown again in the record section of a different blast in Figure 2e, the location of which is shown in Figure 2d. Figure 2e also shows seismic traces beyond 200 km.

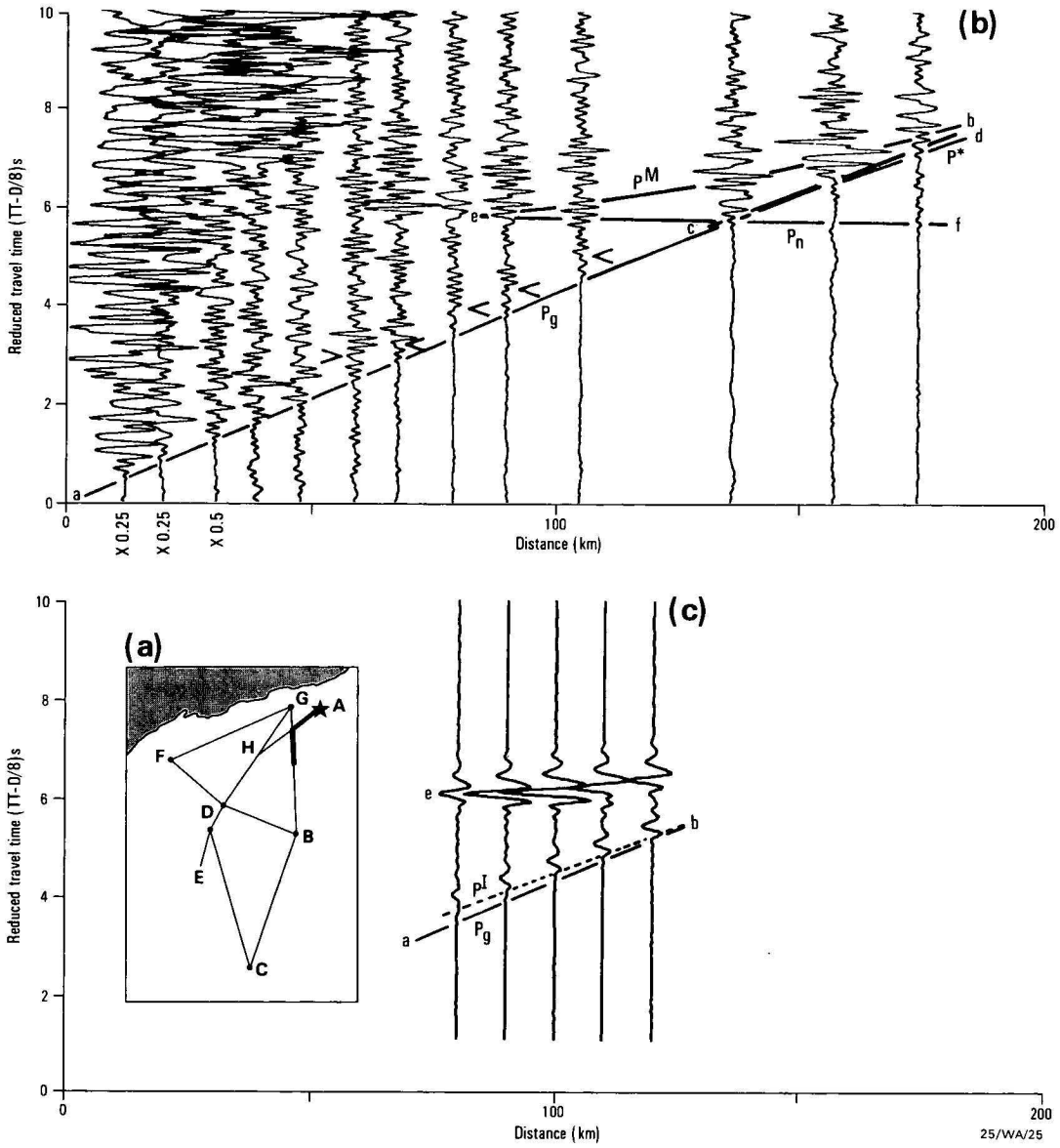

Figure 2. Model for shotpoint A (Sunrise Hill and Shay Gap), along line AB.
(a) location diagram for the record section in Figure 2b; (b) record section southwards from A. The superimposed travel-time curves are for the model in Figure 2f; (c) synthetic seismogram record section and travel-time plot for the model in Figure 2f, but with the Pg phase omitted; (d) location diagram for the record section in Figure 2e; (e) record section southwards from A. The superimposed travel-time curves are for the model in Figure 2f; (f) velocity/depth model for the profile AB; (g) p-versus-distance plot for the model in Figure 2f; (h) synthetic seismogram record section and travel-time plot for the model in Figure 2(f).

In this figure, the P^I cusp (c) is difficult to define, because the arrivals have a much lower frequency than those in Figure 2b, and are difficult to distinguish from the weak Pg phase (ab). The amplitudes of the interpreted P^I phase (arrowed) are very small compared to the amplitudes of the P^M/Pn cusp (e). The velocity/depth function derived from these record sections therefore had to model the amplitudes of the P^I/P* cusp (c) relative to the Pg phase, as well as its amplitudes relative to the P^M/Pn cusp (e). The amplitudes of the cusp at e are more easily defined than those of the Pg phase (ab). Therefore, most emphasis was placed on the comparison of the P^I/P* cusp (c) with the P^M/Pn cusp (e). The resulting model does, however, give a fair match of the amplitudes of the Pg phase and the P^I phase.

The proposed model for profile AB is shown in Figure 2f and listed in Table 1; the ray parameter (p) versus distance plot is shown in Figure 2g. The travel time curves for the model, derived by ray tracing through the model, are superimposed on the record sections in Figures 2b and 2e. The synthetic seismogram record sections, with superimposed travel-time curves, are illustrated in Figures 2c and 2h. In the synthetic seismograms of Figure 2c, the Pg phase was omitted because, as can be seen in the synthetic seismograms of Figure 2h, which contains the Pg phase, the Pg and P^I phases constructively interfere at the frequencies of the wavelet used in the synthetic seismogram modelling, and no meaningful comparison of the P^I and P^M phases can be made. The

Table 1. Velocity/depth model for the profile shotpoint A (Sunrise Hill and Shay Gap), along line AB

Velocity (km s^{-1})	*Depth (km)*	*Travel-time curve cusps*
5.95	0.0	a
6.15	11.0	b
6.25	13.0	c
6.60	28.0	d
8.20	31.0	e
8.25	42.0	f

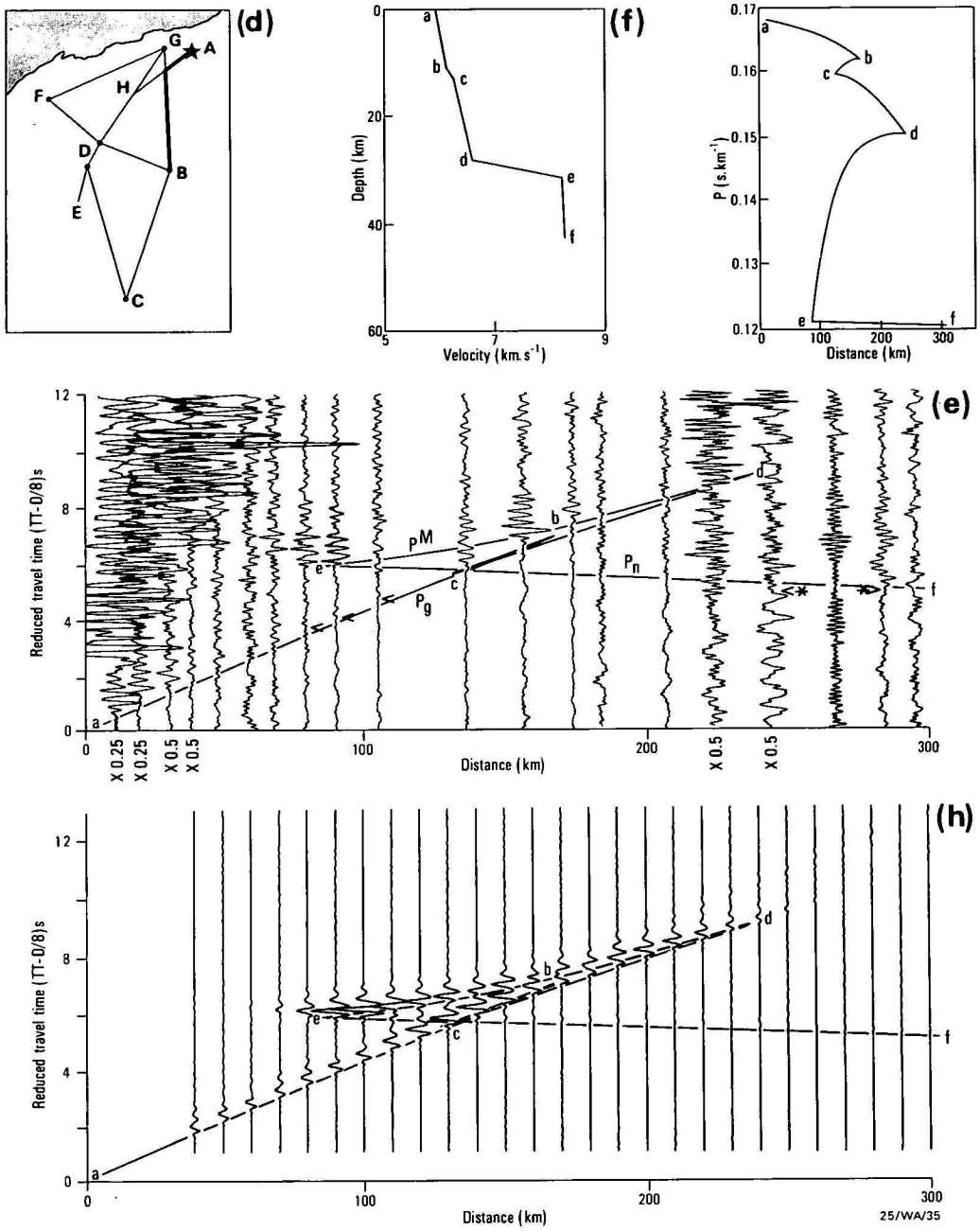

comparison can be made in Figure 2c, where the ratio of the phases' amplitudes is about one-third to one-quarter, as noted previously in the recorded data in Figure 2b.

The amplitudes of the P^I/P^* cusp (c) were reduced relative to those of the P^M/Pn cusp (e) by (1) including velocity gradients above and below the intracrustal boundary, thus forcing energy that would otherwise fall on the reflection branch onto the forward (refraction) branches either side of the reflection branch, and (2) making the boundary gradational, thereby forcing the ray-theoretical cusp further from the blast. Without the gradients above and below the boundary, and with a sharper boundary, the amplitudes of the P^I/P^* cusp (c) were too large compared to the P^M/Pn cusp (e). The intracrustal boundary creates a small triplication in the travel-time curve, and the arrowed P^I phases in Figures 2b and 2e are assumed to be subcritical reflections.

Several arrivals that could be part of the forward Pg/P^I cusp (b) can be interpreted in Figure 2e, but no convincing correlations can be made. The arrivals are generally small. The model gives a correspondingly small cusp at b (Fig. 2h).

The P^M phase weakens beyond about 180 km in the data and beyond about 200 km in the synthetic record section. Note that the Pn phase is weak in the data, although some arrivals (arrowed, with an asterisk in Figure 2e) can be interpreted. This is an important factor in the interpretation of the data from shotpoint G at Goldsworthy along line GBC.

Shotpoint G (Goldsworthy), along line GBC
(Fig. 3, Table 2)

The Pg phase (ab) has large, often overmodulated arrivals out to the crossover distance with Pn, and the arrivals at cusp e in the distance range 90 to 100 km are overmodulated. Conse-

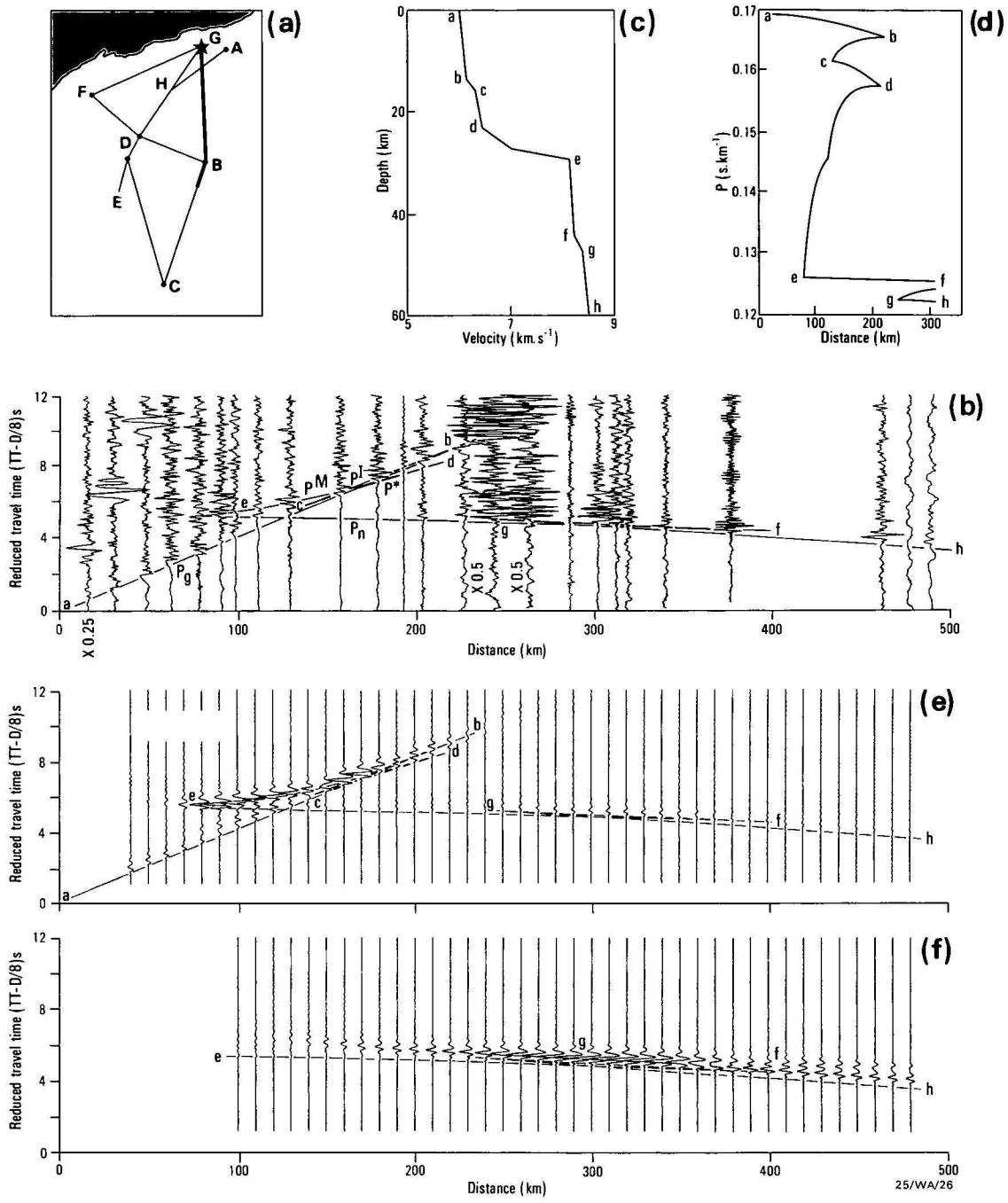

Figure 3. Model for shotpoint G (Goldsworthy), along line GBC.
(a) location diagram for the record section in Figure 3b; (b) record section southwards from G. The superimposed travel time curves are for the model in Figure 3c; (c) velocity/depth model for profile GBC; (d) p-versus-distance plot for the model in Figure 3c; (e) synthetic seismogram record section and travel-time curves for the model in Figure 3c; (f) synthetic seismogram record section for the sub-Moho phases.

quently, the interpretation of the near-surface phases is difficult, so an upper crustal model similar to that in Figure 2f was adopted for this profile.

The P^M reflection branch (de) maintains fairly large amplitudes to about 250 km. Note that the Pn arrivals (ef) are fairly small between 130 and 200 km, but beyond 200 km very large sub-Moho phases are evident. The sub-Moho arrivals have amplitudes comparable to those of the P^M phases in the same traces.

Except for the stations in about the first 100 km of the profile, the stations used in Figure 3b are the same as those used in Figure 2e for the record section of blasts at shotpoint A, in

Table 2. Velocity/depth model for the profile shotpoint G (Goldsworthy), along line GBC

Velocity (km s⁻¹)	*Depth (km)*	*Travel-time curve cusps*
6.01	0.0	a
6.15	13.0	b
6.30	15.0	c
6.45	22.0	
7.00	26.0	d
8.10	28.0	e
8.20	42.0	f
8.35	44.5	g
8.50	57.0	h

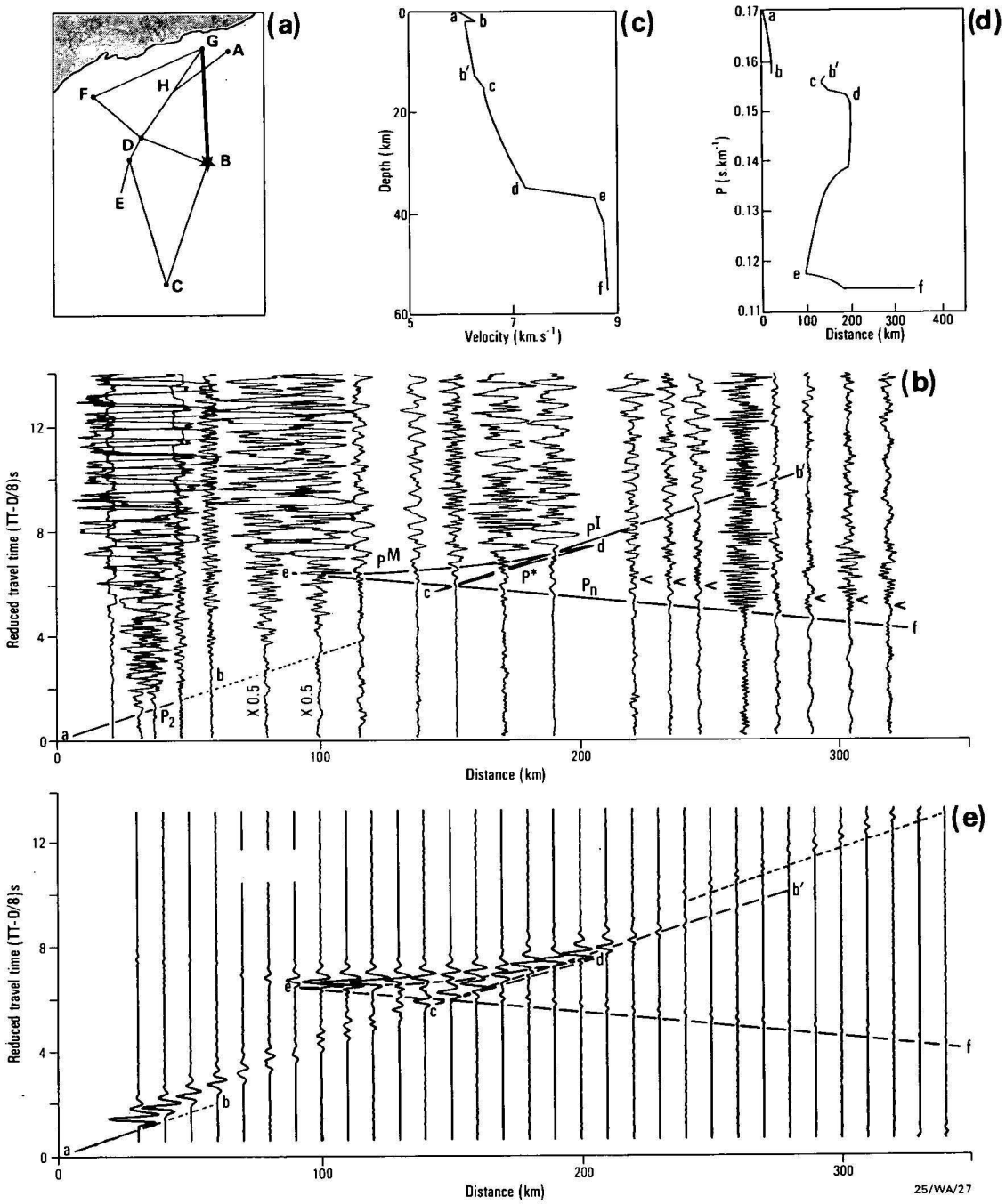

Figure 4. Model for shotpoint B (Newman), along line BG.
(a) location diagram for the record section in Figure 4b; (b) record section northwards from B. The superimposed travel-time curves are for the model in Figure 4d; (c) velocity/depth model for profile GB; (d) p-versus-distance plot for the model in Figure 4c; (e) synthetic seismogram record section and travel-time curves for the model in Figure 4c.

which only small sub-Moho phases are evident. It is, therefore, likely that source effects contributed to the large sub-Moho amplitudes in Figure 3b.

A triplication (fgh) can be interpreted in the travel-time curves at about 300 km in Figure 3b, and defines a boundary in the upper mantle about 14 km below the Moho (Fig. 3c). The triplication is probably present in Figure 2e, corresponding to the arrivals arrowed with an asterisk, but it is not clear because of small amplitudes. Figure 3f shows the amplitudes of the curves efgh in more detail than Figure 3e, in which the absolute amplitudes around the triplication fgh are similar to those of the P^M phase, as in Figure 3b.

Shotpoint B (Newman), along line BG (Fig. 4, Table 3)

The record section of blasts at shotpoint B northwards along line BG reverses the profile on Figure 3b, and differs from it in several ways.

The first arrivals along curve ab, ie. the Pg phase, are weak and emergent, probably owing to the masking effects of the near-surface, high-velocity Hamersley Basin strata. The P^M branch is very clear, with the amplitudes decaying abruptly at 200 km, forming a bright cusp. Thus, in the model (Figure 4c), the lower crust has a second-order increase of velocity with depth. This causes all the rays with ray parameters between about 0.153 and 0.138 s km^{-1}. and which bottom between 15 and

Table 3. Velocity/depth model for the profile shotpoint B (Newman), along line BG.
Note: Velocities are quoted to three decimal places only so that the second-order increase of velocity with depth between C and D is accurately defined.

MODEL 1		
Velocity (km s^{-1})	*Depth (km)*	*Travel-time curve cusps*
5.860	0.0	a
6.350	2.0	b
6.050	2.0	
6.250	13.0	b'
6.400	15.0	c
6.475	17.0	
6.500	18.5	
6.531	20.0	
6.583	22.0	
6.645	24.0	
6.718	26.0	
6.801	28.0	
6.847	29.0	
6.895	30.0	
6.946	31.0	
7.000	32.0	
7.057	33.0	
7.116	34.0	
7.178	35.0	d
8.500	37.0	e
8.700	42.0	
8.750	55.0	

35 km to emerge between 190 and 205 km; note the broad cusp at d in the p versus distance plot in Figure 4d, and compare it with the sharp cusps at d in Figures 2g and 3d. The model gives large amplitudes at cusp d to about 200 to 210 km, after which they decay rapidly (Fig. 4e).

The Pn phase (ef) is clear, with large amplitudes. A zone of high velocity gradient (ef) below the Moho, which is transitional over 2 km, maintains the amplitudes of the Pn phase; the gradient may extend to greater depths, but the profile is too short to provide the relevant information. No triplication similar to fgh in Figure 3b can be interpreted. However, Drummond (1979a) noted that on most traces beyond 150 km a phase (arrowed) could be picked 0.6 s after the Pn arrival. The five traces beyond 250 km, are from a different blast from those between 150 and 250 km and were plotted to show that the effect is independent of the blast used. Linear regression analyses of the travel times of the two phases yielded statistically identical apparent velocities for the phases. It is possible that the second phase forms part of the triplication fgh, and its apparent velocity is rendered the same as Pn by the effects of refractor topography. Alternatively, the second arrival may be a multiple from a structure unique to the crust near shotpoint B.

The dotted travel-time curve later than and beyond b' in Figure 4e represents underside multiples from the high-velocity, near-surface layer. The data are too noisy to verify if they are observed or not.

Table 4. Velocity/depth model for the profile shotpoint G (Goldsworthy), along line GHD.
Note: Velocities are quoted to three decimal places only so that the second- order increases of velocity with depth above B and between C and D are accurately defined.

MODEL 1		
Velocity (km s^{-1})	*Depth (km)*	*Travel-time curve cusps*
6.130	0.0	a
6.130	2.0	
6.131	3.0	
6.137	5.0	
6.142	6.0	
6.156	8.0	
6.164	9.0	
6.174	10.0	
6.185	11.0	
6.200	12.0	b
6.350	14.0	c
6.377	16.0	
6.420	18.0	
6.480	20.0	
6.515	21.0	
6.555	22.0	
6.600	23.0	
6.648	24.0	
6.700	25.0	d
8.150	29.0	e
8.250	45.0	f

Shotpoint G (Goldsworthy), along line GHD
(Fig. 5, Table 4)

The Pg phase has large, overmodulated arrivals on most traces out to the crossover distance with Pn at about 130 km. The trace at about 95 km is not overmodulated and has a clear second arrival (arrowed), interpreted as a sub-critical P^I reflection. The forward cusp d does not have any convincing arrivals beyond 180 km, where it blends with the large-amplitude P^I arrivals of the branch bc, which maintain large amplitudes to about 230 km.

The P^M phase between the forward cusp d and retrograde cusp e is clear with large amplitudes. Pn is generally weak, but is observed (arrowed, with an asterisk) on some traces between 150 and 240 km. Note that there are no large amplitudes which identify an upper mantle triplication similar to fgh observed from this shotpoint southwards along line GB in Figure 3b.

Shotpoint D (Tom Price), along line DHG (Fig. 6, Table 5)

The record section of Tom Price blasts northeast along line DHG reverses the profile of Goldsworthy blasts in Figure 5b. The record section has a gap between 100 and 180 km, across which the correlation of phases is tentative, but the correlations made seem realistic.

This record section has some of the clearest evidence of subcritical P^I reflections from the intracrustal boundary. They appear as high frequency arrivals (arrowed) up to a second after Pg in the four traces between 60 and about 100 km.

The P^M phase must be correlated across the gap in the recordings. Strong arrivals are observed at cusp d, at about 240 km, beyond which they decay rapidly. The Pn phase is weak, although some arrivals (arrowed, with an asterisk) may be identified.

Table 5. Velocity/depth model for the profile shotpoint D (Tom Price), along line DHG.
Note: Velocities are quoted to three decimal places only so that the second- order increase of velocity with depth between C and D is accurately defined.

Velocity (km s^{-1})	*Depth (km)*	*Travel-time curve cusps*
6.100	0.0	a
6.250	11.5	b
6.400	14.5	c
6.500	18.0	
6.520	20.0	
6.550	22.0	
6.589	24.0	
6.638	26.0	
6.696	28.0	
6.728	29.0	d
8.150	34.0	e
8.250	50.0	f

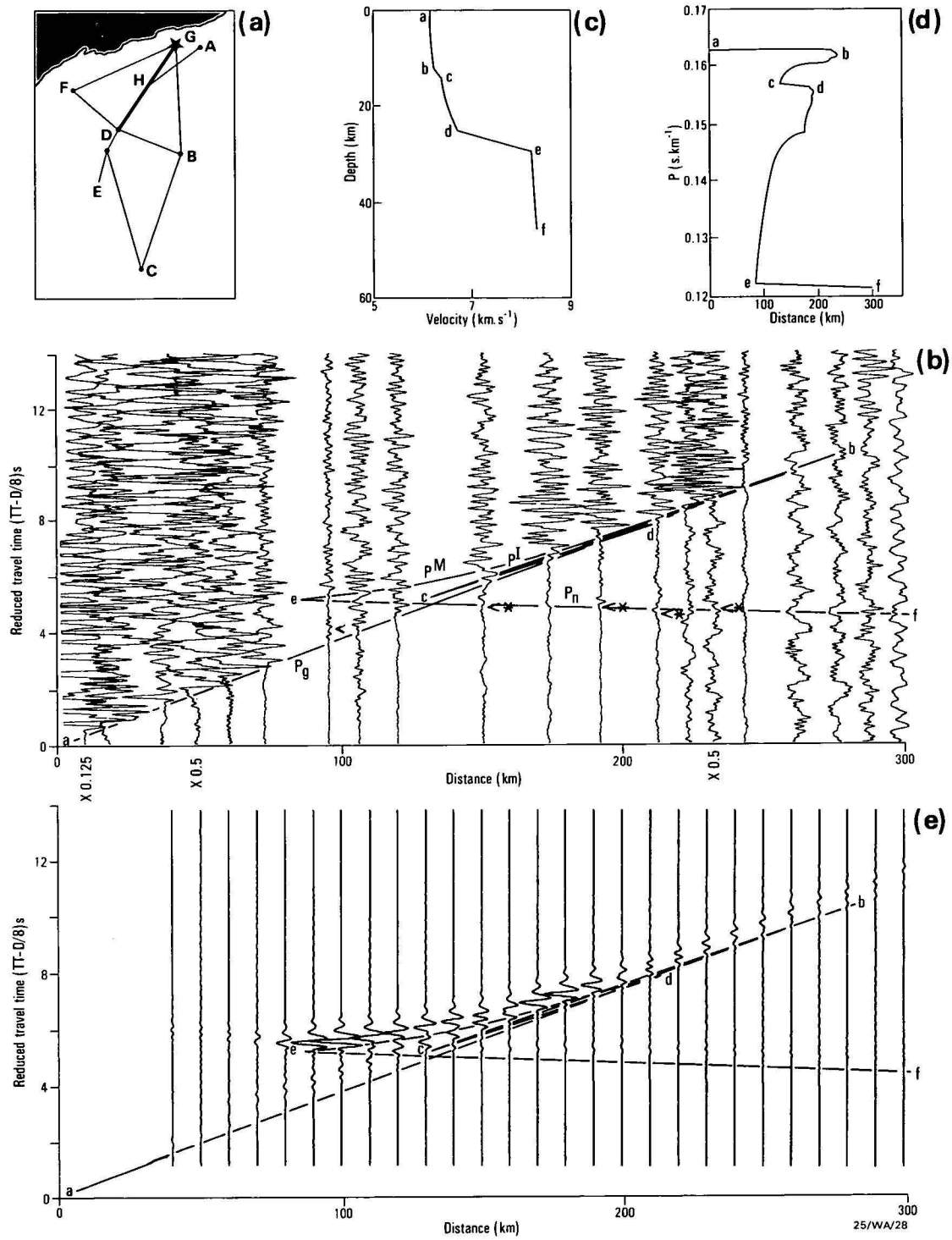

Figure 5. Model for shotpoint G (Goldsworthy), along line GHD.
(a) location diagram for the record section in Figure 5b; (b) record section southwards from G. The superimposed travel-time curves are for the model in Figure 5c; (c) velocity/depth model for profile GHD. (d) p versus distance plot for the model in Figure 5c; (e) synthetic seismogram record section and travel-time curves for the model in Figure 5c.

Shotpoint D (Paraburdoo), along line DHG (Fig. 7, Table 6)

The Pg phase, where observed, decays rapidly near the blast, probably because of the near-surface high-velocity Hamersley Basin rocks at the southern end of the profile (Drummond, 1981). The high-velocity layer extends about 60 km north of Paraburdoo and does not affect the up-going rays for most of this profile.

The intracrustal boundary must be included in the model, because this profile duplicates much of that included in Figure 6b, where very clear subcritical reflections off the boundary were noted, but there is very little evidence for the boundary in this record section at this scale. The boundary is modelled (Fig. 7c, Table 6) as very gradational, with velocity gradients above and below to cause only a small triplication cd.

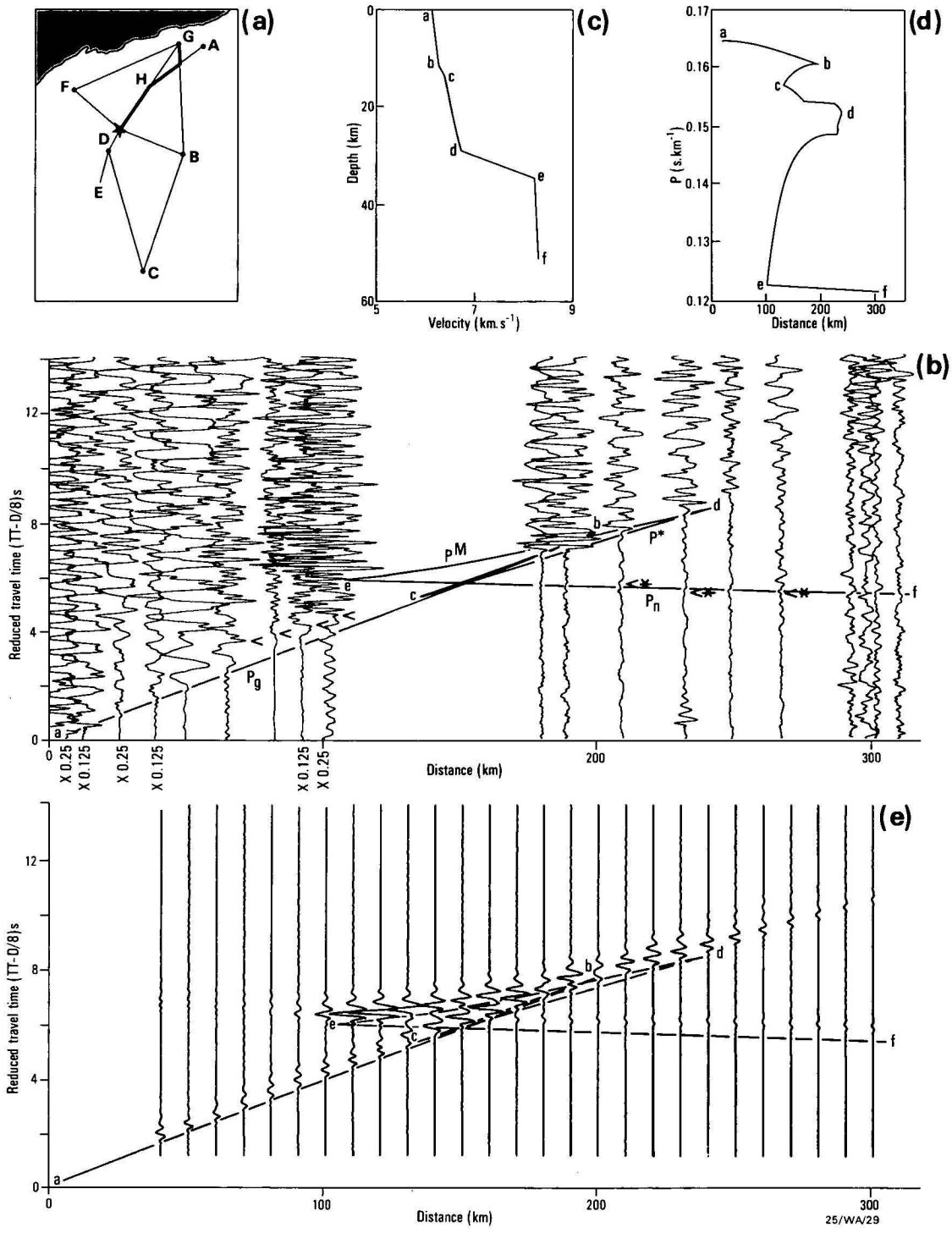

Figure 6. Model for shotpoint D (Tom Price), along line DHG.
(a) location diagram for the record section in Figure 6b; (b) record section northwards from Tom Price, at D. The superimposed travel time curves are for the model in Figure 6c; (c) velocity/depth model for profile DHG, from blasts at Tom Price; (d) p-versus-distance plot for the model in Figure 6c; (e) synthetic seismogram record section and travel-time curves for the model in Figure 6c.

Shotpoint F (Pannawonica), along line FDB (Fig. 8, Table 7)

The blast used to construct the record section from 190 to 370 km was large, dispersed over several kilometres, and had a burning time of 2.17 s. Consequently, the seismic energy from the blast is not a clear, sharp pulse, but an oscillating, high frequency wavelet of over one second duration, and secondary arrivals buried in the coda of previous phases are not easy to distinguish on all traces beyond 190 km. The forward cusps b and d are difficult to identify, but they are interpreted at about 220 and 250 km, respectively. The Pn phase ef has a low apparent velocity (7.6 km s^{-1}), but high amplitude arrivals, compared to Pn on other profiles.

The model for the profile is shown in Figure 8c and Table 7; the synthetic seismogram record section for the model is illustrated in Figure 8e.

Several large amplitude phases are observed as later arrivals beyond 190 km in Figure 8b. They have apparent velocities

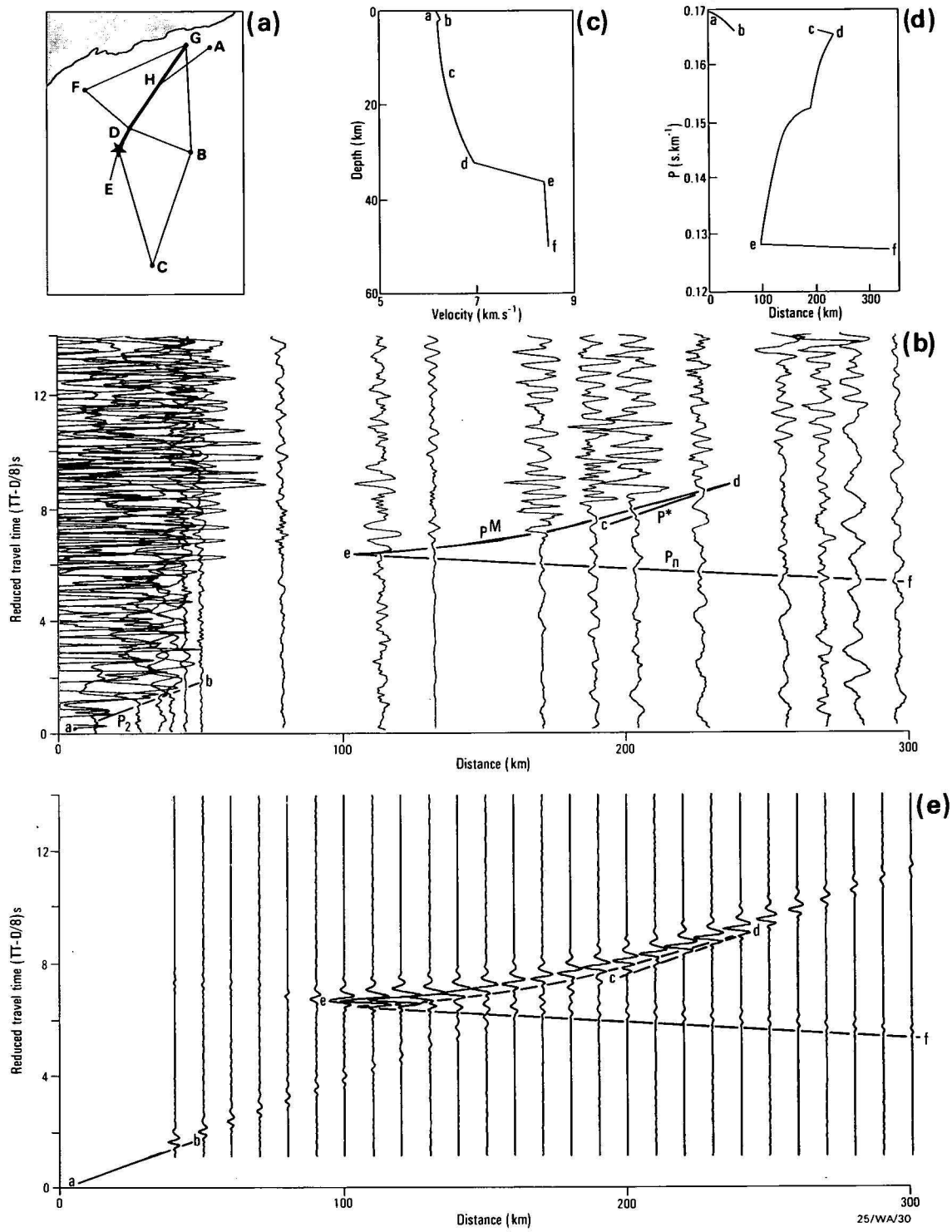

Figure 7. Model for shotpoint D (Paraburdoo), along line DHG.
(a) location diagram for the record section in Figure 7b; (b) record section northwards from Paraburdoo, at D. The superimposed travel-time curves are for the model in Figure 7c; (c) velocity/depth model for profile DHG, from blasts at Paraburdoo; (d) p-versus-distance plot for the model in Figure 7c; (e) synthetic seismogram record section and travel time curves for the model in Figure 7c.

similar to that of the Pg phase, and are similar to multiples from the lower crust recorded in Canada by Mereu & others (1977).

Mereu & others (1977) interpreted their multiples as phases focussed at the surface by strong gradients in the lower crust and then internally reflected at the free surface. However, rays will be internally reflected at the free surface only if the angle of incidence is small, and in Mereu & others' (1977) model this was achieved by including low-velocity sediments in the model. However, the Hamersley Basin strata have higher velocities than the basement, and rays internally reflected to emerge as multiples within 200 to 400 km of the blast would have to have angles of incidence at the free surface greater than 50 degrees. These would not be internally reflected at the free surface. However, energy incident at the base of the Hamersley Basin strata would be partitioned into both transmitted and reflected energy. The transmitted energy would reach the surface as primary waves, and the reflected energy would

Table 6. Velocity/depth model for the profile shotpoint D (Paraburdoo), along line DHG.

Note: Velocities are quoted to three decimal places only, so that the second- order increases of velocity with depth above C and between C and D are accurately defined.

Velocity (km s^{-1})	*Depth (km)*	*Travel-time curve cusps*
6.190	0.0	a
6.300	2.0	b
6.190	2.0	
6.200	8.0	
6.209	9.0	
6.219	10.0	
6.230	11.0	
6.300	14.0	c
6.325	16.0	
6.360	18.0	
6.406	20.0	
6.462	22.0	
6.529	24.0	
6.606	26.0	
6.648	27.0	
6.693	28.0	
6.741	29.0	
6.791	30.0	
6.844	31.0	
6.900	32.0	d
8.350	36.0	e
8.450	50.0	f

return to the surface as multiples at greater distances. The amplitudes of the multiples will be dependent on the degree of partitioning, which, in turn, depends on the angle of incidence, the velocity in the basement, and the velocity in the basin strata. The angle of incidence will in turn be affected by topography of the interface between the basin strata and the basement; the velocity in the basement has to be assumed for part of this profile; and the velocity in the basin strata changes along the profile (Drummond & others, 1981). Thus, to try to model the amplitudes of the multiples with a program that allows only laterally homogeneous models would be fruitless.

The travel-time curves with the crosses and the dots are the times of the multiples off the intracrustal boundary and the Moho, respectively, reflected off the underside of the high-velocity layer, assuming that the velocity in the high-velocity layer at the point of reflection approximately half-way along the profile is 6.3 km s^{-1} (Drummond & others, 1981), and that the layer is 2 km thick, and are in reasonable agreement with the observed times.

Shotpoint B (Newman), along line BDF (Fig. 9)

The record section (Fig. 9b) has a very high (6.65 km s^{-1}) velocity branch (ab) near the source. The large amplitudes of branch ab, which is the P_2 phase of Drummond & others (1981)

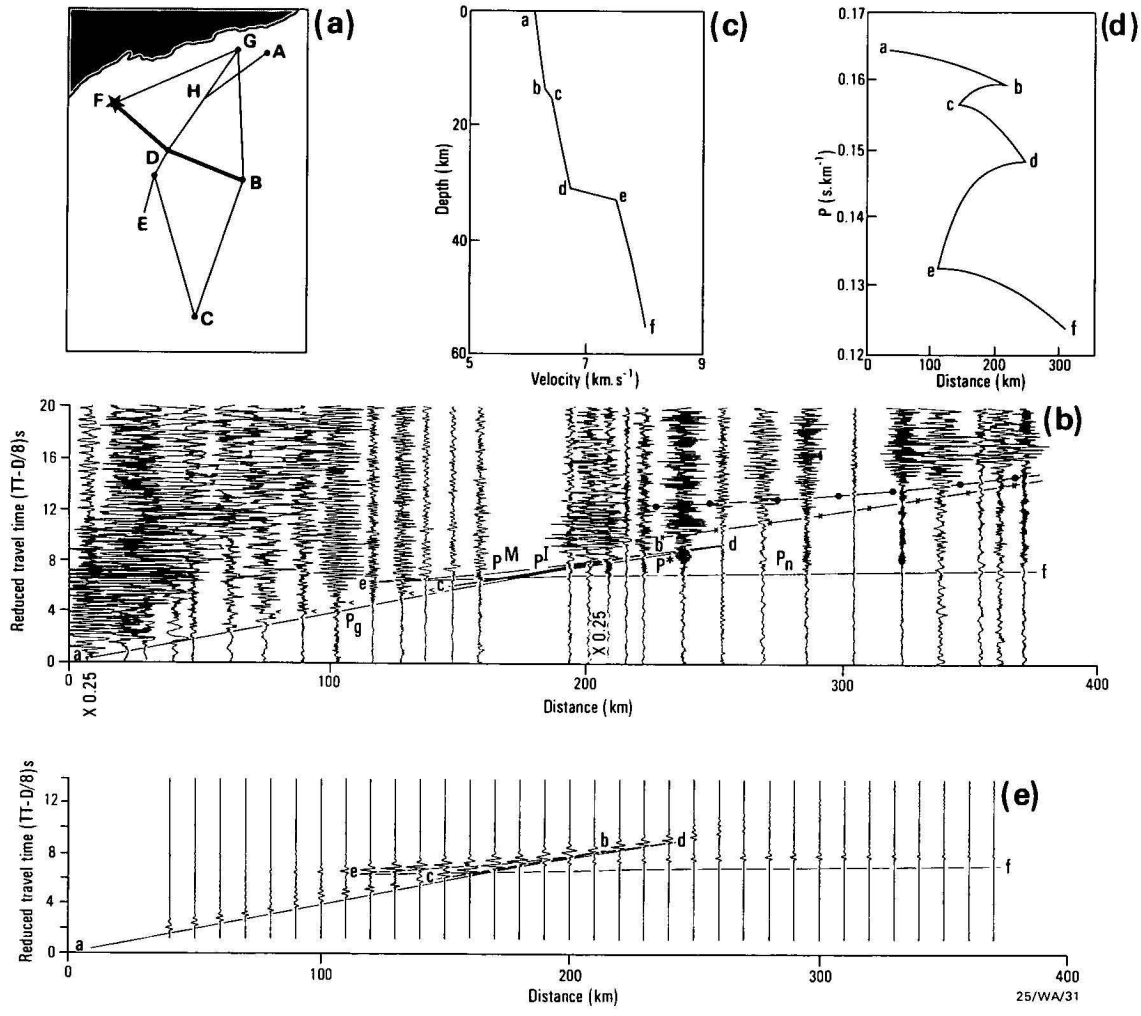

Figure 8. Model for shotpoint F (Pannawonica), along line FDB.

(a) location diagram for the record section in Figure 8b; (b) record section southeastwards from F. The superimposed travel-time curves are for the model in Figure 8c; (c) velocity/depth model for profile FDB. (d) p-versus-distance plot for the model in Figure 8c; (e) synthetic seismogram record section and travel-time curves for the model in Figure 4c.

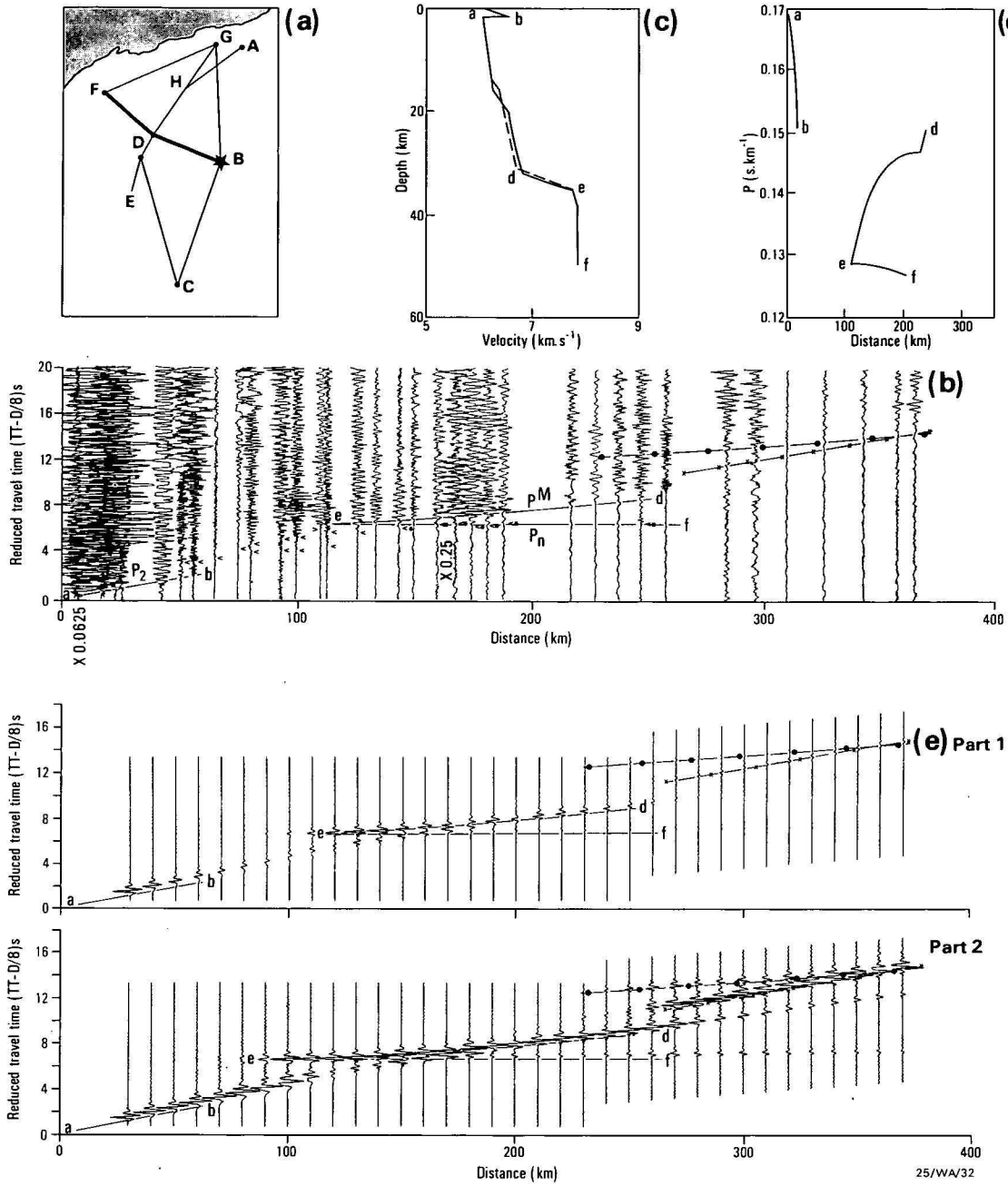

Figure 9. Models for shotpoint B (Newman), along line BDF.
(a) location diagram for the record section in Figure 9b; (b) record section northwestwards from B. The superimposed travel-time curves are for the model drawn with the solid line in Figure 9c. Those marked with dots indicate the first multiple from the Moho, and those marked with crosses, the first multiple from the intracrustal boundary, reflected as underside reflections from the near-surface, high-velocity layer; (c) Model 1 (solid curve) and Model 2 (dotted curve) for profile BDF; (d) p versus distance plot for Model 1 in Figure 9c; (e) synthetic seismogram record section and travel-time curves for Model 1 in Figure 9c. The multiples are as for Figure 9b. Part 1: amplitudes relative to the largest overall peak to trough amplitude, Part 2: trace normalised, so that the maximum peak to trough amplitude is the same for all traces.

Table 7. Velocity/depth model for the profile shotpoint F (Pannawonica), along line FDB.

Velocity (km s^{-1})	*Depth (km)*	*Travel-time curve cusps*
6.07	0.0	a
6.25	14.0	b
6.37	16.0	c
6.70	31.0	d
7.50	33.0	e
8.00	55.0	f

and Drummond (1981), decay rapidly beyond 50 km, and imply a near-surface high-velocity layer overlying a basement with a lower velocity.

The Pg, P^I and P* phases are difficult to identify in the record section. While the near-surface, high-velocity layer might be expected to mask out all of the effects of the upper crust, the P_2 phase velocity decreases to the northwest, and the high-velocity layer pinches out in places against basement domes, so that there are windows in the high-velocity layer through which the crustal phases can reach the surface. Such arrivals can be

Table 8. Velocity/depth models for the profile shotpoint B (Newman), along line BDF.
Note: In Model 1, velocities are quoted to three decimal places only so that the second-order increase of velocity with depth above D is accurately defined.

MODEL 1			*MODEL 2*		
Velocity (km s^{-1})	*Depth (km)*	*Travel-time curve cusps*	*Velocity (km s^{-1})*	*Depth (km)*	*Travel-time curve cusps*
5.950	0.0	a	5.90	0.0	a
6.650	2.0	b	6.65	2.0	b
6.050	2.0		6.10	2.0	
6.250	16.0		6.25	14.0	
6.550	20.0		6.37	16.0	
6.565	22.0		6.70	31.0	d
6.591	24.0		7.75	35.0	e
6.627	26.0		7.85	39.0	f
6.674	28.0	d	7.85	50.0	
6.732	30.0				
6.800	32.0	e			
7.750	35.0				
7.850	39.0	f			
7.850	50.0				

seen (arrowed) between 60 and 140 km in Figure 9b, although correlation between them is difficult.

The P^M phase (de) has large amplitudes which decay abruptly beyond cusp D at 260 km. The Pn phase is observed on some traces (arrowed, with an asterisk, in Fig. 9b) to 250 km, beyond which it is not observed.

Because of the screening effect of the near-surface, high-velocity layer, it is not possible to derive a unique model of the crust from this record section, so two models are presented. Many others would fit the data equally as well.

Model 1 is presented as a solid curve in Figure 9c and listed in Table 8, and is based on the model in Figure 4c for the record section for the same shotpoint to the north along line BG, although some changes were necessary to account for different apparent velocities of the phases ab, de, and ef, and their intercept times.

The synthetic seismogram record section in Figure 9e has multiples from the intracrustal boundary and the Moho. They are especially evident on the trace-normalised synthetic seismogram record section (Figure 9e, part 2) and correlate with a band of recorded arrivals which have considerable energy (Figure 9b). They are similar to those noted in Figure 8b for the reversed profile from shotpoint F.

Model 2 for this profile, presented in Figure 9c as a dotted curve and listed in Table 8, is based on the model for the reversed profile from shotpoint B (Fig. 8). The high-velocity, near-surface layer has been included, and the structure at and below the Moho changed to suit the apparent velocity and amplitudes of the Pn phase. It is not possible on the basis of the present data to give preference to either Model 1 or Model 2 for this profile. Both are based on models from other profiles in the region, and both fit the data for this profile equally well.

Bright cusps caused by lateral structure

Mereu (1969) showed that topography on a boundary can cause amplitude changes, and even triplications, along travel-time branches. Caution was expressed above that the velocity/depth models derived by synthetic seismogram modelling would be valid only if the effects of vertical structure overprinted the effects of lateral structure. The purpose of this section is to examine briefly whether the bright cusps interpreted in Figures 4, 5, 6, and 7 could be caused by the effects of lateral structure.

In all profiles, the bright cusps occur at about 200 km. If the energy which is focussed at these bright cusps is assumed to bottom halfway between the shotpoints and the recorded distances of the bright cusps, the bottoming points must be about 100 km from the shotpoints. In all but Figure 5, this would mean that the bottoming point of the rays was near the axis of the Hamersley Basin. This corresponds to a basin-shaped depression in the intracrustal boundary (Drummond, 1981). While no comparable basin-shaped depression has been interpreted at the crust/mantle boundary, a topography of 1 or 2 km would be within the error limits of the intercept method interpretation.

Figure 10 explores empirically the effects of refractor topography on the concentration of seismic rays at the surface. It must be stressed that while the model in Figure 10 is based loosely on the model of Drummond (1981) for line DHG, no attempt was made to accurately model the travel-times. The topography on the intracrustal boundary is that interpreted by Drummond (1981). The Moho dips from 28 km in the north (right hand end) to 32 km in the south (left hand end), and has superimposed on it a sinusoidal-type topography with an amplitude of less than 2 km and a wavelength of 70 km. It is represented by straight line segments 10 km long. The upper and lower crusts have velocity gradients from 6.0 to 6.15 km s^{-1} and 6.35 to 6.65 km s^{-1}, respectively; these are typical of the gradients of the velocity/depth models above (without the second order increase of velocity with depth required to cause the bright cusps). First order discontinuities were used between the layers.

Only the ray paths for mantle reflections are shown. Those which bottom between A and B, where there is no reflector topography, emerge at the surface between A' and B'. Note that the distance between A' and B' is greater than that between A and B. Rays which bottom between C and D, where the reflecting surface is concave upwards, emerge between C' and D', and because the distance from C' to D' is less than that between C and D, there is some focussing of the seismic energy. This can be seen in some cases where rays which impinge on different straight line segments of the interface emerge at almost the same point at the surface. Rays which strike the reflector between E and F, where the surface is concave downwards, are scattered and emerge between E' and F', and because E'F' is very much greater than EF, there will be a sudden diminution of amplitudes of the reflected waves beyond D'.

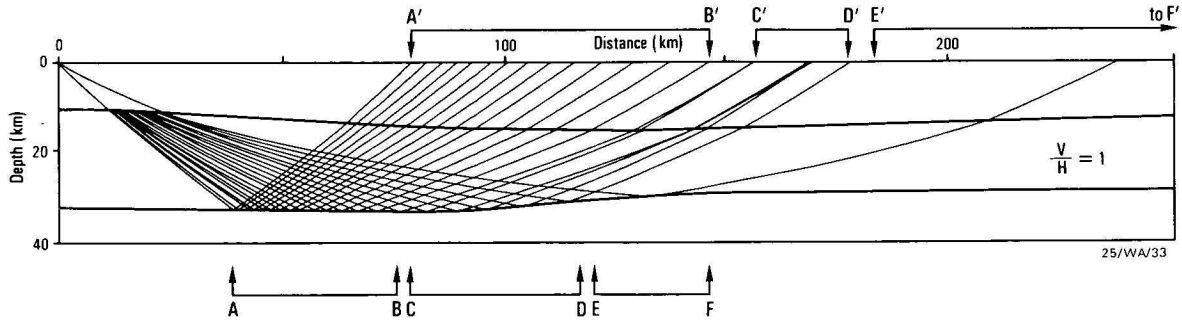

Figure 10. An example of how reflector topography can produce bright cusps.
The model is based loosely on the model for line GHD (Drummond, 1981).

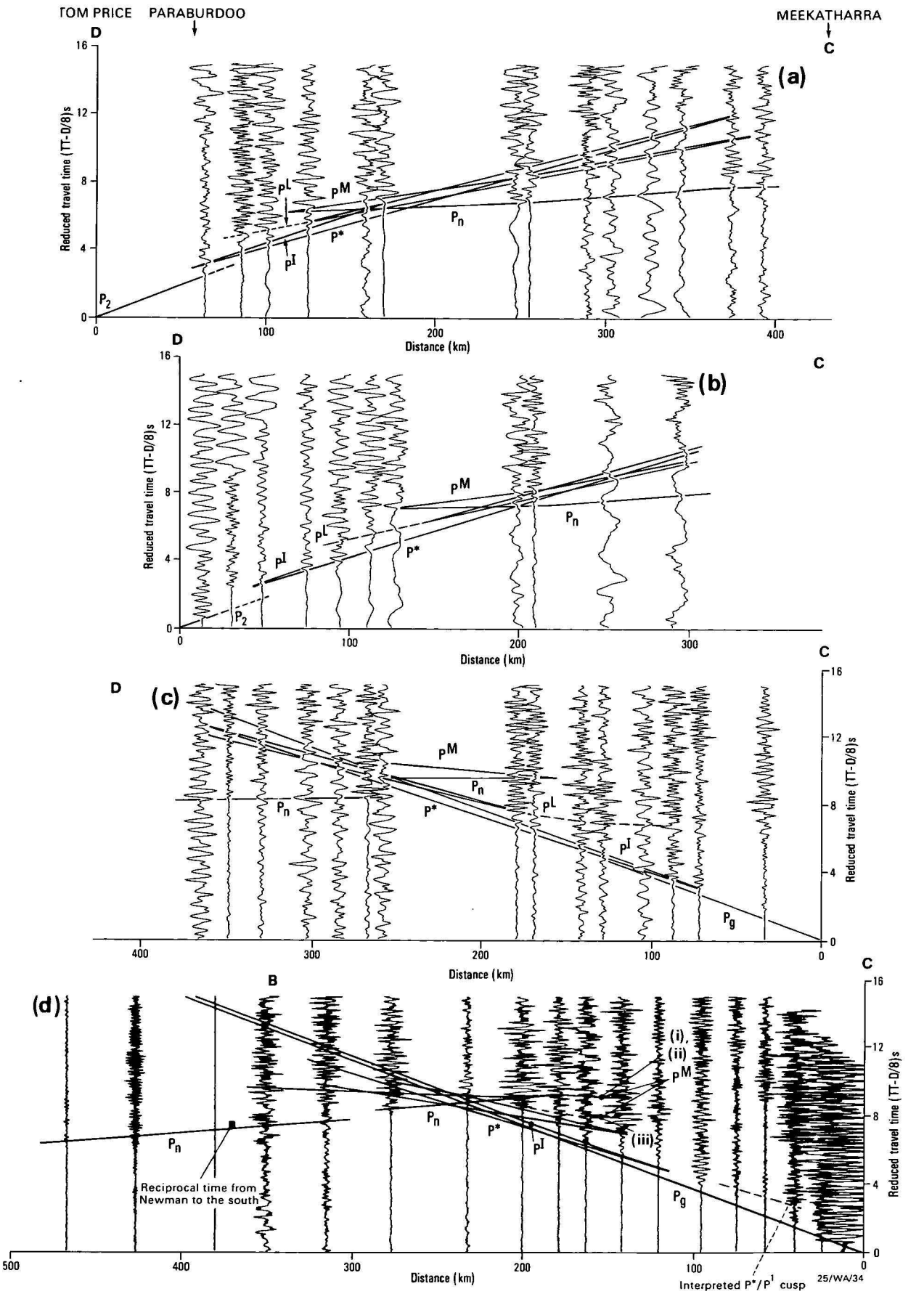

Figure 11. Record sections across the Capricorn Orogen, comparing the positions of the observed P^L and P^I/P^* cusps with the positions of those from the models of the intercept method interpretation.

Parts a, b & c are from Drummond (1981); part d is from Drummond (1979a).

Other models could be found to demonstrate the focussing effects of the reflector between C and D. Figure 10 illustrates that focussing can be caused by structures which are concave towards the energy source, and scattering of the energy will be caused by structures which are convex towards the energy source.

No preference can be given to models with either vertical or lateral structure. In the velocity/depth models from the amplitude studies, the second-order increases of velocity with depth used to produce the bright cusps have little effect on the depths of the seismic boundaries, and the refractor topography required to produce bright cusps in the regions where there are no such second-order increases is very small. Thus the velocity/depth models from the amplitude studies are likely to be good approximations of the velocity/depth functions in the Earth, regardless of whether the bright cusps are caused by lateral or vertical structure (or both).

Observed amplitudes in the Capricorn Orogen.

Current synthetic seismogram techniques are not applicable in the Capricorn Orogen (lines BC and DC), because the crust in the orogen is not laterally homogeneous (Drummond, 1981). However, some observations can be made about the nature of the boundaries, based on the fit to the observed data of the ray-theoretical cusps derived using models from the intercept method of interpretation (Drummond, 1979a; 1981).

Drummond (1981) noted that the P^L phase, assumed to be reflections from a lower crustal layer in the Capricorn Orogen and the northern Yilgarn Craton, occurred much closer to the blast than expected from ray theory (Fig. 11a, 11b and 11c). Similarly, Drummond (1979b) noted that the sub-critical reflections at the P^*/P^I cusp on line CB (dashed in Fig. 4d) were quite large. They are observed within 40 km of the blast, whereas the ray-theoretical cusp falls at about 120 km.

The large amplitudes of the sub-critical phases mean that either the boundaries are sharp, and/or low-velocity zones exist within the crust and the boundaries are, therefore, much shallower than interpreted. With the current data, it is not possible to distinguish between these alternatives, although low-velocity channels extensive enough to halve the critical distance would seem unlikely to be caused by thermal effects in such a geothermally cold region (Cull & Denham, 1979), and changes of lithology are more likely causes. However,the travel times of P^M phases (Drummond, 1979a), and the gravity field (Wellman, 1978; Drummond & Shelley, 1981) both suggest that, in the Capricorn Orogen, the lower crust must have steep velocity (and density?) gradients, and not low velocity (and density) channels. Thus, the crust in the Capricorn Orogen is unlikely to be any thinner than modelled by Drummond (1979b; 1981).

Discussion

The seismic velocity/depth models for the Pilbara Craton (Fig. 2–9, Tables 1–8) all have a two-layered crust (excluding the near-surface high-velocity Hamersley Basin strata in some of the models). Within the crustal layers, the velocity varies from about 6.0 km s^{-1} at the surface to about 6.2 km s^{-1} just above the intracrustal boundary, and from about 6.4 km s^{-1}. just below the intracrustal boundary to between 6.6 and 7.2 km s^{-1} at the base of the crust, which is from 28 to 37 km thick. The intracrustal boundary is transitional over 2–3 km depth, and the Moho is transitional over 2–5 km. Apparent velocities in the uppermost mantle vary from 7.5 to 8.5 km s^{-1}. On one profile, a sub-Moho discontinuity was noted 14 km below the Moho. The crust/mantle boundary dips southwards across the Pilbara Craton (Drummond, 1979a). The highest apparent Pn velocities, the highest apparent velocities in the lowermost crust, and the thickest crust were all interpreted on northerly trending up-dip profiles. The models with the thinnest crust were interpreted on the profiles that trended southwards from the northern shotpoints under which the Moho is shallowest. Thus many of the variations in apparent Pn velocity, crustal velocities, and crustal thickness are caused by the effects of dip on the crust/mantle boundary. However, not all of the differences in apparent Pn velocity can be explained by the effects of refractor dip. The lowest apparent Pn velocities were not observed in the direction of down-dip on the crust/mantle boundary, but along the axis of the Hamersley Basin, which parallels the strike of the crust/mantle boundary. This was noted before by Drummond & others (1981), who suggested that the seismic velocities in the upper mantle were lower along the axis of the basin either because of the effects of metamorphism or partial melting (removal of iron), or because they were exhibiting anisotropy.

The velocity/depth models in Figures 2 to 9 all have slightly thicker crusts than those in the models of Drummond (1979a; 1981) and Drummond & others (1981), but the differences are less than about 10 percent. In the new models, the crust in the Pilbara Craton is still thinner, especially when the effects of refractor dip are considered, than in the previous models for the Capricorn Orogen, where positive velocity gradients are still preferred. The crust in the original models of the Yilgarn Craton was more than 50 km thick. No evidence is available to suggest that massive low-velocity channels exist within the crust of the Yilgarn Craton, and it is reasonable to suggest that increasing metamorphic grade with depth will increase the velocity with depth through the crustal layers. This will have the effect of increasing the crustal thickness in the models. Thus, Drummond's (1981) assumptions about the relative thicknesses of the crust from the Pilbara Craton southwards across the Capricorn Orogen to the Yilgarn Craton are justified, and the implications that the changes in crustal thickness have for tectonic evolutionary models of the region still hold.

Acknowledgements

The work described in this paper forms part of a study of northwest Australia undertaken while I was a research scholar at the Research School of Earth Sciences, Australian National University, under the auspices of an Australian Public Service Postgraduate Scholarship. K.J. Muirhead and C. Wright of RSES made useful comments and read an early draft of the manuscript. D.M. Finlayson and D. Denham also provided advice. The computer program REFLEXION was made available by Prof. K. Fuchs, and J. Leven and G. Bock modified it and converted it to the RSES computer. C.D.N. Collins also provided computing advice.

References

Aki, K., & Richards, P.G., 1980 — Quantitative seismology, Volume 1. *W.H. Freeman & Company.*

Berry, M.J., 1971 — Depth uncertainties from seismic first-arrival refraction studies. *Journal of Geophysical Research*, 76, 6464–6468.

Berry, M.J., & Fuchs, K., 1973 — Crustal structure of the Superior and Grenville Provinces of the northeastern Canadian shield. *Seismological Society of America, Bulletin*, 63, 1393–1432.

Braile, L.W., & Smith, R.B., 1975 — Guide to the interpretation of crustal refraction profiles. *Geophysical Journal of the Royal Astronomical Society*, 40, 145–176.

Bullen, K.E., 1960 — Note on cusps in seismic travel times. *Geophysical Journal of the Royal Astronomical Society*, 3, 354–359.

Cull, J.P., & Denham, D., 1979 — Regional variations in Australian heat flow. *BMR Journal of Australian Geology & Geophysics*, 4, 1–13.

Drummond, B.J., 1979a — A crustal profile across the Archaean Pilbara and northern Yilgarn Cratons, northwest Australia. *BMR Journal of Australian Geology & Geophysics*, 4, 171–180.

Drummond, B.J., 1979b — Pilbara crustal survey, 1977: operational report. *Bureau of Mineral Resources, Australia, Record*, 1979/54 (unpublished).

Drummond, B.J., 1981 — Crustal structure of the Precambrian terrains of north-west Australia from seismic refraction data. *BMR Journal of Australian Geology & Geophysics*, 6, 123–135.

Drummond, B.J., in preparation — Seismic constraints on the chemical composition of the Pilbara Craton, northwest Australia. *Submitted to the Proceedings of the International Symposium of Archaean and early Proterozoic Geologic Evolution and Metallogenesis, Salvador, Brazil, 1982*.

Drummond, B.J., & Shelley, H.M., 1981 — Isostasy and structure of the lowercrust and upper mantle in the Precambrian terrains of northwest Australia. *BMR Journal of Australian Geology & Geophysics*, 6, 137–143.

Drummond, B.J., Smith, R.E., & Horwitz, R.C., 1981 — Crustal structure in the Pilbara and northern Yilgarn Blocks from deep seismic sounding. *In* Glover, J.E., & Groves, D.I. (editors), Archaean geology. *Second International Archaean Symposium. Geological Society of Australia, Special Publication*, 7, 33–41.

Finlayson, D.M., Collins, C.D.N., & Denham, D., 1980 — Crustal structure under the Lachlan Fold Belt, southeastern Australia. *Physics of the Earth and Planetary Interiors*, 21, 321–342.

Fuchs, K., 1968 — Das Reflexions und Transmissionsvermogen eines geschichteten Mediums mit beliebiger Tiefen–Verteilung der elastischen Moduln und der Dichte fur schragen Einfall ebener Wellen. *Journal of Geophysics*, 34, 389–413. English translation by Feeken, E.H., 1979 — The reflectivity and transmittance of a stratified medium with variable depth distribution of moduli of elasticity and density for inclined incidence of plane waves. *In* Collins, C.D.N., 1979 — Adaption of the synthetic seismogram program 'REFLEX' to the CSIRO CYBER 76 computer. *Bureau of Mineral Resources, Australia, Record*, 1979/7 (unpublished).

Fuchs K., & Muller, G., 1971, — Computation of synthetic seismograms with the reflectivity method and comparison with observations. *Geophysical Journal of the Royal Astronomical Society*, 23, 417–433.

Gee, R.D., 1979 — Tectonics of the Western Australian shield. *Tectonophysics*, 50, 327–369.

Kind, R., 1976 — Computation of reflection coefficients for layered media. *Journal of Geophysics*, 41, 191–200.

Mereu, R.F., 1969 — Effect of Mohorovicic topography on the amplitude of seismic P waves. *Journal of Geophysical Research*, 74, 4371–4376.

Mereu, R.F., Majumdar, S.C., & White, R.E., 1977 — The structure of the crust and upper mantle under the highest ranges of the Canadian Rockies from a seismic refraction survey. *Canadian Journal of Earth Sciences*, 14, 196–208.

Mueller, S., & Landisman, M., 1966 — Seismic studies of the earth's crust in continents. I: Evidence for a low-velocity zone in the upper part of the lithosphere. *Geophysical Journal of the Royal Astronomical Society*, 10, 525–538.

Mueller, S., & Landisman, M., 1971 — An example of the unified method of interpretation for crustal seismic data. *Geophysical Journal of the Royal Astronomical Society*, 23, 365–371.

Wellman, P., 1978 — Gravity evidence for abrupt changes in mean crustal density at the junction of Australian crustal blocks. *BMR Journal of Australian Geology & Geophysics*, 3, 153–162.

BMR Journal of Australian Geology & Geophysics, 8, 53-69

THE PROTEROZOIC KALKADOON AND EWEN BATHOLITHS, MOUNT ISA INLIER, QUEENSLAND: SOURCE, CHEMISTRY, AGE, AND METAMORPHISM

Lesley A.I. Wyborn & R.W. Page

The Proterozoic I-type Kalkadoon and Ewen Batholiths and their comagmatic extrusive equivalents, the Leichhardt suite, form an association covering at least 5000 km^2 in the central part of the Mount Isa Inlier. U-Pb zircon data and some Rb-Sr total rock data show that these rocks crystallised from melts emplaced between 1840 and 1870 m.y. ago and are the oldest dated igneous rocks in the Inlier. Chemically and isotopically, these granites are relatively uniform and, compared with most other Mount Isa granites, they have higher Sr and Al_2O_3 contents, and lower TiO_2, Zr, Nb, and Th contents. These chemical characteristics appear to be restricted to felsic igneous rocks known to be older than 1800 m.y. and may be useful in identifying the older felsic melts of the Mount Isa Inlier. The source for the rocks of the Kalkadoon–Ewen–Leichhardt association is estimated to have had an SiO_2 content of 55–60 per cent. Relative to other large Palaeozoic and Mesozoic I-type batholiths elsewhere, this Mount Isa association is enriched in K_2O, Rb, Th, U, La, Ce, Zr, and Nb, and depleted in CaO, MgO, Ni, and Cr. The least isotopically disturbed granites of the association have relatively low initial $^{87}Sr/^{86}Sr$ ratios (about 0.704), which implies that the age of the source for these melts was not much older than the age of their emplacement. As chemically and isotopically similar granites occur in most Proterozoic areas of Northern Australia, it is inferred that during the period 1900–2100 m.y. a significant mantle differentiation event took place, during which large volumes of material were accreted to the base of the crust in these areas.

Post-emplacement metamorphism and deformation, which have a maximum age of 1640 m.y., caused significant textural and mineralogical changes in the Kalkadoon Batholith, but had a lesser effect on the Ewen Batholith. Igneous textures are commonly preserved in the Ewen Batholith, but the Kalkadoon Batholith, which has been metamorphosed from lower greenschist to upper amphibolite grade, shows significant isotopic disturbances.

Introduction

The Proterozoic Mount Isa Inlier of northwestern Queensland (Fig. 1) consists of at least five older basement blocks, termed the Kalkadoon-Leichhardt, Ewen, Blockade, Big Toby-Yaringa, and Malbon blocks (Fig. 2), overlain by younger sedimentary and volcanic sequences (Plumb & Derrick, 1975; Plumb & others, 1980). The Kalkadoon-Leichhardt and Ewen blocks contain abundant felsic volcanics and granites. The volcanics, termed Leichhardt Metamorphics north of latitude 21° (Carter & others, 1961) and Leichhardt Volcanics south of this (Blake & others, 1981), are known to be 1850–1870 m.y. old, and the northern part of the Kalkadoon Batholith (1862 $\pm^{27}_{21}$ m.y.) has been shown to be coeval with its host volcanic pile (Page, 1978; in press).

The aim of this paper is to define the characteristic chemistry and age of some of the granites from the Kalkadoon-Leichhardt and Ewen Blocks. The host volcanics and the granites are compared, chemically, to test for comagmatism. Post-

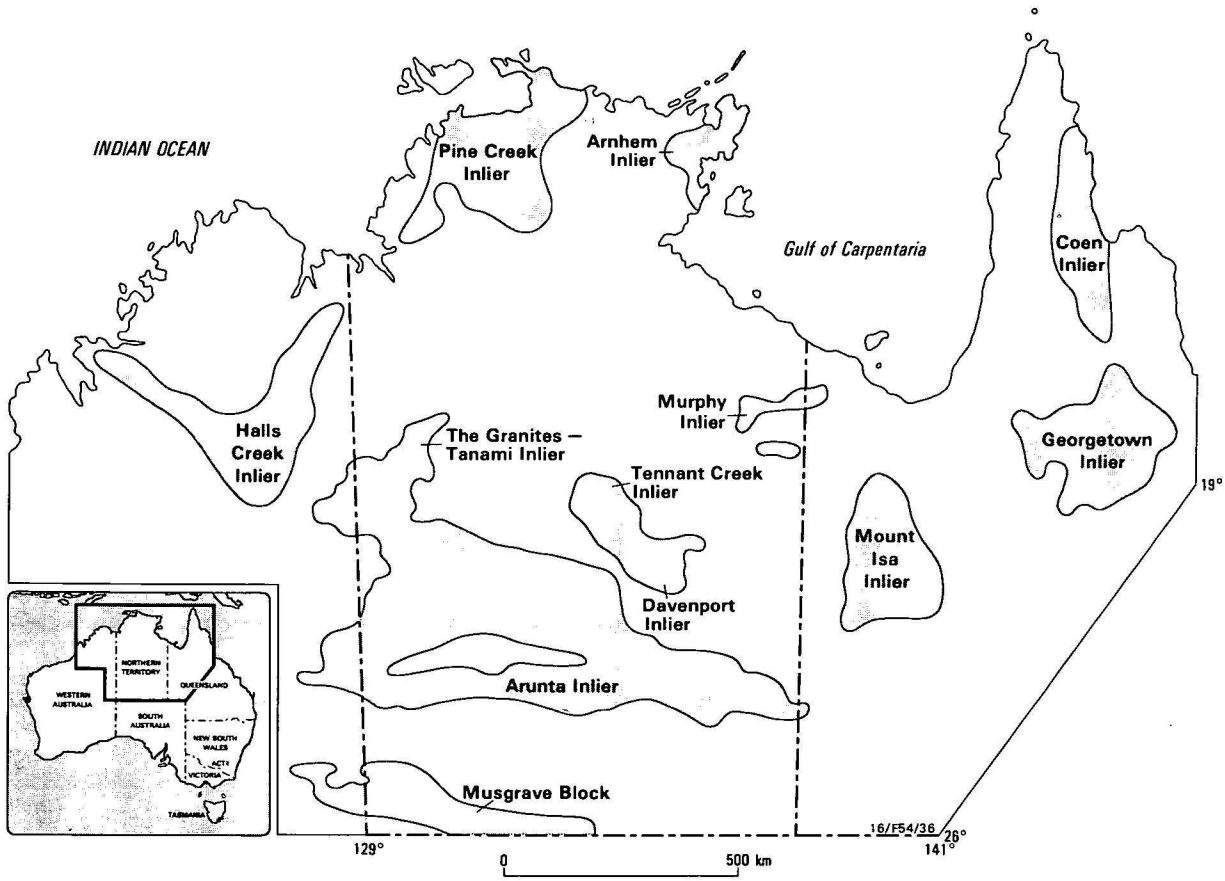

Figure 1. Location of the Mount Isa Inlier and other Proterozoic terrains of northern Australia (based on Plumb & others, 1980).

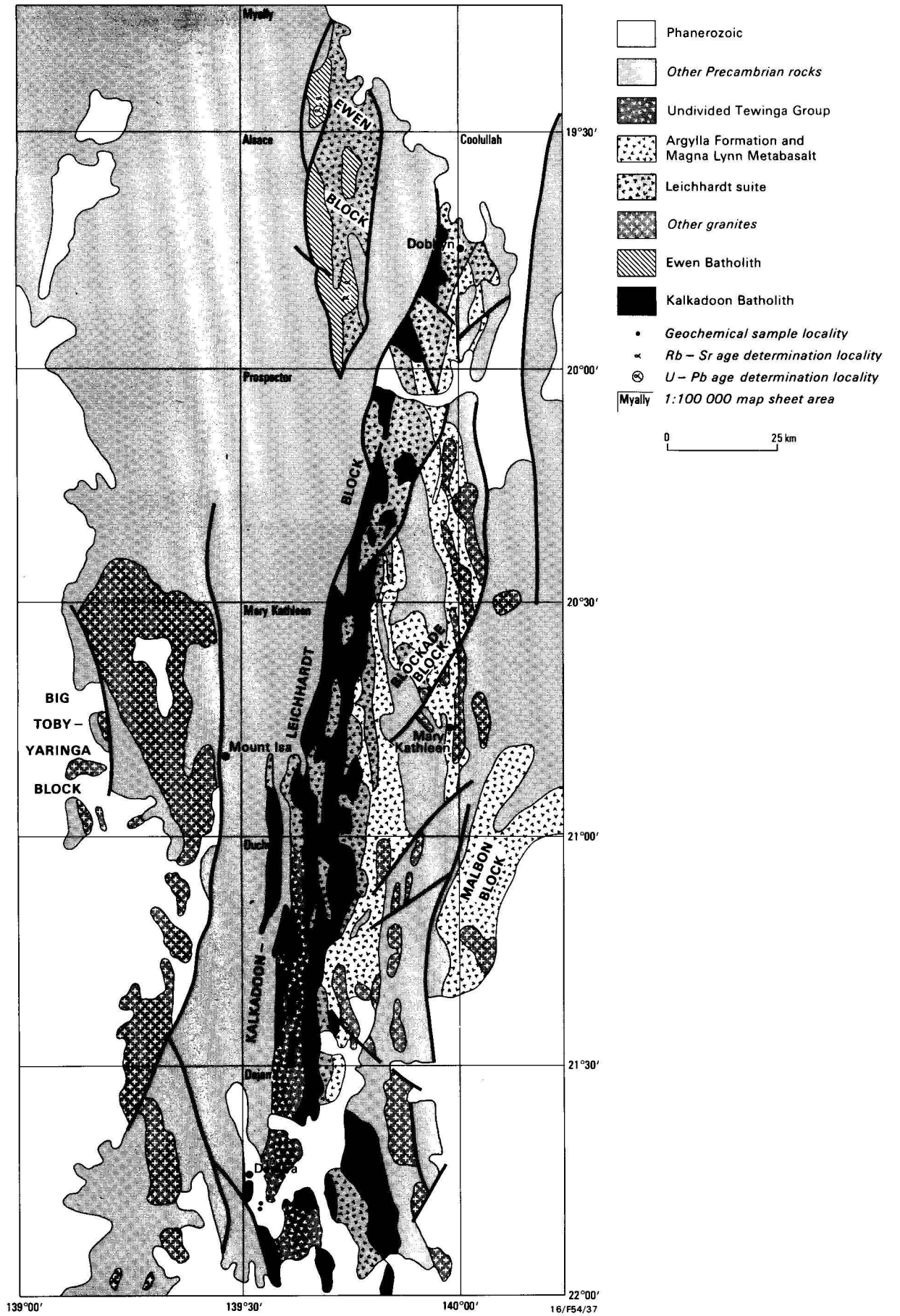

Figure 2. Generalised geology of the Kalkadoon-Leichhardt and Ewen blocks, showing sample localities.

emplacement metamorphism of the igneous bodies has caused significant textural and isotopic changes, which are documented here. The chemical results and the least disturbed isotopic data have been used to delineate the composition and age of the source region from which the melts were derived.

Nomenclature

The terms 'Kalkadoon Batholith' and 'Ewen Batholith' refer to the granite bodies intruding the Kalkadoon-Leichhardt and Ewen blocks, respectively. They imply only geographical areas of granite and do not necessarily refer to granites of a specific age or chemical type. The terms correspond in part to the'Kalkadoon Granite' and 'Ewen Granite' of Carter & others (1961) and Joplin & Walker (1961). Kalkadoon Granodiorite refers to a specific chemical and petrographic type of intrusion within the Kalkadoon Batholith. It is synonymous with the informal term 'Kalkadoon granodiorite' of Joplin & Walker (1961). The One Tree, Woonigan, and Wills Creek Granites (Blake & others, 1982) are specific granite intrusions within the Kalkadoon Batholith. 'Leichhardt suite', as defined by Bultitude & Wyborn (1982), refers to the chemically and isotopically similar Leichhardt Volcanics and Leichhardt Metamorphics. The term 'granite' applies to all rocks of the granite suite, i.e. syenogranite, monzogranite, granodiorite and tonalite.

Field relations

Kalkadoon Batholith

The Kalkadoon Granodiorite crops out over an area of 1280 km^2 between Dobbyn and Dajarra, and intrudes rocks of the Leichhardt suite and, in DUCHESS* and DAJARRA, undivided Tewinga Group (Fig. 1; Derrick & others, 1977; Bultitude & others, 1982; Blake & others, 1982). It is overlain unconformably by rocks of the Bottletree Formation, Haslingden Group, and Quilalar and Surprise Creek Formations in the west (Bultitude & others, 1982; Derrick & others, 1980) and the Magna Lynn Metabasalt, Argylla Formation, and Mary Kathleen Group in the east (Plumb & others, 1980). The Wills Creek Granite, which covers 25 km^2 in DAJARRA, and the Woonigan Granite, covering 36 km^2 in DUCHESS, intrude rocks of the Leichhardt suite and undivided Tewinga Group and have no younger stratigraphic age control. The One Tree Granite, cropping out over 255 km^2, is relatively old, as it is overlain unconformably by, and intruded by dykes comagmatic with, rocks of the Leichhardt suite. At least two generations of dolerite dykes intrude the Kalkadoon Batholith. The older has mostly been metamorphosed to amphibolite grade; the younger is unmetamorphosed.

* 1:100 000 Sheet area names are shown in upper case.

Table 1. Representative modal analyses of the Kalkadoon Granodiorite.
Quartz, K-feldspar and plagioclase based on 2000 points from a 15 x 10 cm stained rock slab; other minerals from 2000 points on a 6 x 2 cm thin section.

Sample No.	*7820 6043*	*7820 6049*	*7820 6045*	*7820 6048*	*7820 6005*	*7820 6004*
Quartz	17.5	17.3	22.4	30.3	27.0	28.7
K-feldspar	5.3	11.5	17.0	19.4	25.0	30.1
Plagioclase	52.9	47.7	44.2	39.4	35.8	34.8
Biotite	12.3	17.8	12.3	8.6	4.8	3.3
Hornblende	1.3	0.8	1.3	0.8	—	0.9
Epidote	4.5	3.9	1.5	0.6	1.6	0.9
Scapolite	—	—	0.3	—	—	—
Muscovite	4.2	0.1	0.1	0.1	3.8	1.2
Chlorite	0.6	0.3	0.2	0.1	0.1	tr
Sphene	0.6	0.2	0.2	0.3	0.4	0.1
Apatite	0.3	0.1	0.2	0.2	0.1	tr
Opaques	—	0.2	—	0.2	—	tr
Allanite	0.4	—	0.3	—	—	tr

Ewen Batholith

Granitic rocks of the Ewen Batholith (345 km^2) mostly intrude volcanic rocks of the Leichhardt suite (Derrick & Wilson, 1982; Wilson & Grimes, in press). One small pluton intrudes the Candover beds, which are thought to be younger than the Leichhardt suite (Derrick & Wilson, 1982). The batholith is overlain unconformably by the Haslingden Group and is itself intruded by numerous, essentially unmetamorphosed, dolerite dykes.

Petrography

Kalkadoon Batholith

All samples in the Kalkadoon Batholith show some degree of recrystallisation and metamorphism, and primary mafic igneous minerals are rarely preserved. Most samples have a foliation, which is parallel to both the axial plane cleavage and the metamorphic foliation in the adjacent country rocks (Derrick & others, 1977). The foliation, formed during a younger deformation event, did not affect the whole batholith, as some areas of massive granite remain.

The Kalkadoon Granodiorite is medium to coarse grained and ranges from a K-feldspar-free tonalite, to granodiorite, and monzogranite, with granodiorite being the most abundant. Representative modal analyses are listed in Table 1 and plotted in Figure 3. Tonalites are even-grained with K-feldspar forming sparse phenocrysts up to 1 cm long in the more felsic varieties. The more mafic granodiorites are strongly porphyritic and contain K-feldspar phenocrysts up to 5 cm long. The phenocrysts decrease in abundance from the granodiorite to the monzogranite, and the rock type becomes more even-grained. Accidental xenoliths of rocks both petrographically and chemically identical to those from the Leichhardt suite are very common, but, in contrast, cognate xenoliths are rare and small, and consist of clots of ferromagnesian minerals rarely more than 5 cm across.

The Kalkadoon Granodiorite has been regionally metamorphosed. Upper amphibolite grade rocks are common in the north of MARY KATHLEEN and the south of

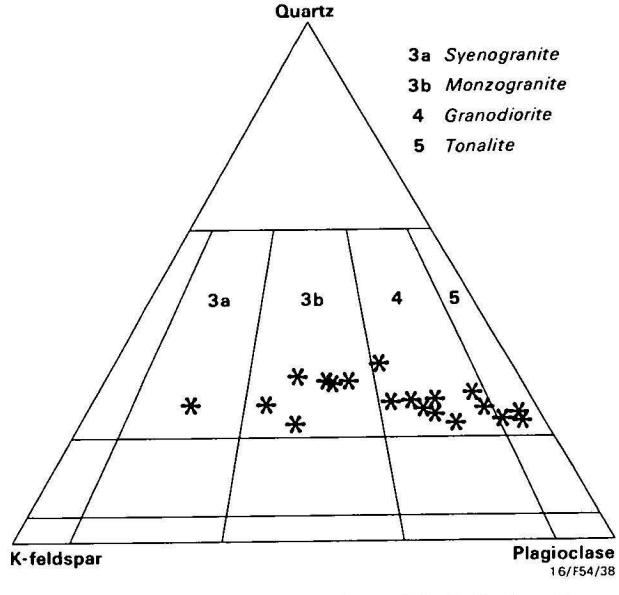

Figure 3. Representative modal analyses of the Kalkadoon Granodiorite (classification after Streckeisen, 1973).

PROSPECTOR, and lower greenschist grade rocks occur in the northwestern part of the granodiorite in DUCHESS. The remaining outcrops are either upper greenschist or lower amphibolite.

The One Tree Granite ranges from tonalite, to granodiorite, and monzogranite. It tends to be more even-textured than the Kalkadoon Granodiorite, and is medium-grained. Most of the pluton has been metamorphosed to amphibolite grade. The Wills Creek and Woonigan Granites are leucocratic syenogranites which are petrographically similar to the most felsic parts of the Kalkadoon Granodiorite.

In the Kalkadoon Batholith, significant textural changes have been recognised with increasing metamorphic grade. Quartz in greenschist grades occurs as large grains (6 mm across), which show strained extinction and, with increasing metamorphic grade, become polygonal aggregates of small grains 0.2 to 0.5 mm across.

Potassium feldspar (microcline) is rarely sericitised, and in greenschist grades usually shows coarse perthite intergrowths (Fig. 4A). With increasing metamorphic grade, the perthite becomes vein-like and patchy (Fig. 4B). It eventually disappears in amphibolite grade as the microcline grains become surrounded with patches of albite (Fig. 4C). In most upper amphibolite grade rocks, microcline is recrystallised to polygonal aggregates (Fig. 4D). Similar changes in K-feldspars with increasing metamorphism have been described by Day & Brown (1980).

Plagioclase is rarely fresh, and, with increasing metamorphism, changes from grains with altered sericite, calcite, and epidote-rich cores and clear albite margins in lower greenschist grades to grains having coarse epidote and muscovite cores surrounded by rims of oligoclase/andesine (An_{17-40}) in upper amphibolite grades. In plane polarised light, the cores are dusty and remnants of broken and fractured grains can be seen.

Biotite in greenschist grade varies from fine (< 0.2 mm), recrystallised, decussate aggregates (α = straw, $\beta = \gamma$ = yellow brown) to coarse (> 1 mm) green brown and green

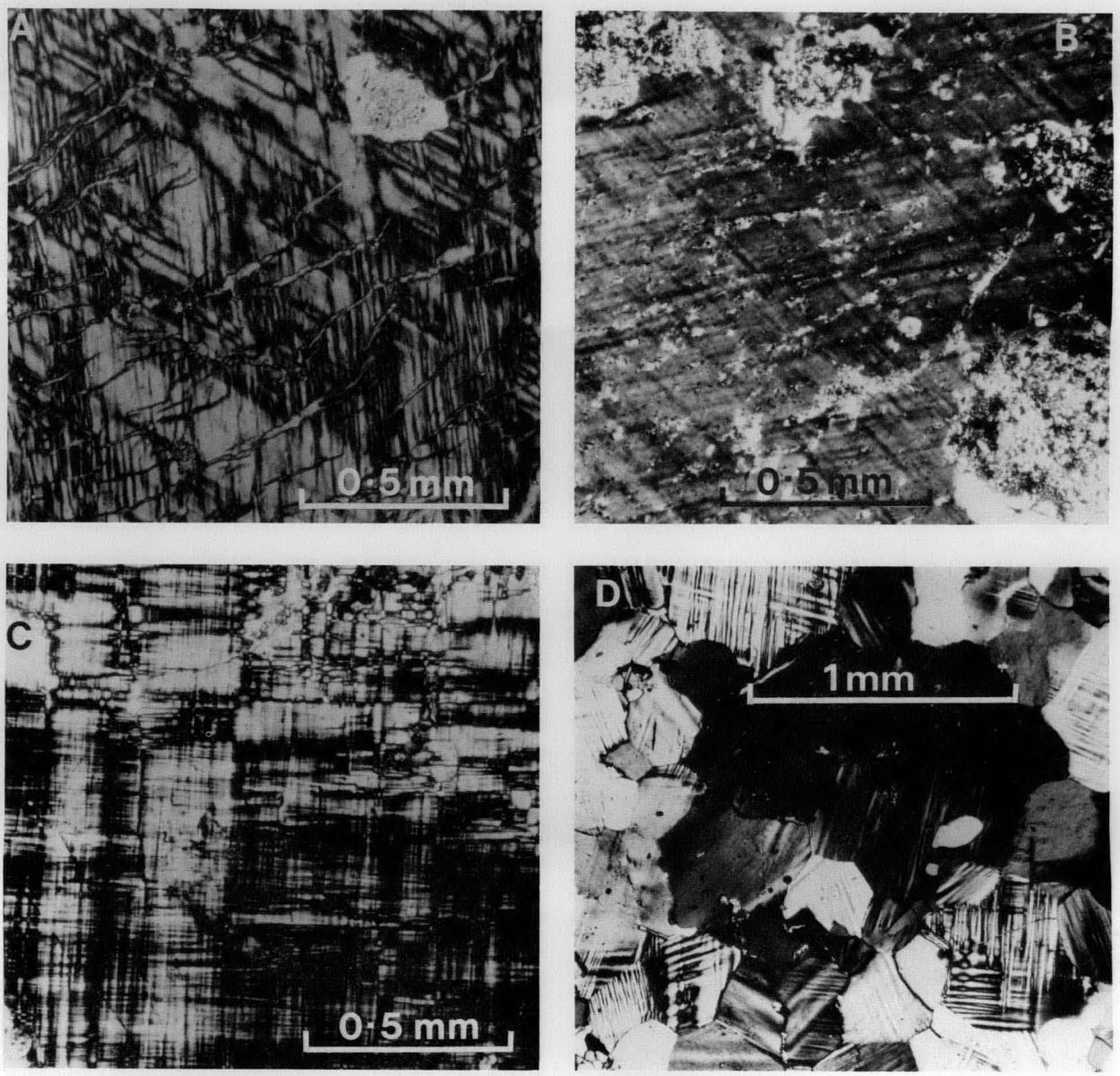

Figure 4. K-feldspars from the Kalkadoon Batholith:
A — coarse perthite intergrowths in K-feldspar from greenschist grade, sample 77534668; B — vein and patch perthite in K-feldspar, sample 78206042; C — cross-hatched microcline from amphibolite grade, sample 78206000; D — recrystallised microcline mosaic from amphibolite grade, sample 78206057.

Table 2. Representative biotite and amphibole analyses from the Kalkadoon and Ewen Batholiths.
Analyses done using the TPD energy-dispersive microprobe at the School of Earth Sciences, Australian National University, following the methods of Reed & Ware (1975) and Ware (1981).

	AMPHIBOLES				*BIOTITES*									
Pluton	*Ewen*		*Kalkadoon*		*Ewen*		*Kalkadoon*		*Kalkadoon*		*Kalkadoon*		*Kalkadoon*	
Type	*Batholith*		*Granodiorite*		*Batholith*		*Granodiorite*		*Granodiorite*		*Granodiorite*		*Granodiorite*	
Sample	*Igneous*		*Lower amphibolite*		*Igneous*		*Lower greenschist*		*Upper greenschist*		*Lower amphibolite*		*Upper amphibolite*	
Number	*78536117*		*78206045*		*78206117*		*77534668*		*78206142*		*78206045*		*78206081*	
SiO_2	44.53	45.23	38.86	37.89	35.30	35.41	34.77	34.89	34.93	34.74	34.07	35.41	34.76	34.43
TiO_2	.60	1.27	.44	.36	3.42	3.16	1.34	1.31	1.88	1.75	1.95	2.10	2.59	2.56
Al_2O_3	7.42	8.29	14.03	14.91	14.33	14.01	16.29	16.37	17.32	17.08	15.96	16.10	16.61	16.75
FeO	22.93	22.87	25.06	25.30	24.57	24.73	26.36	25.79	25.08	24.67	24.74	24.55	26.70	27.08
MnO	.66	.54	.26	.24	.16	.20	.20	.18	.23	.25	—	—	.23	.29
MgO	7.91	7.42	5.01	4.82	7.18	7.51	5.80	5.93	6.52	6.55	7.54	7.58	5.49	5.45
CaO	10.77	10.71	11.80	11.87	—	—	—	—	—	—	—	—	—	—
K_2O	88	1.04	2.07	2.15	9.39	9.60	9.71	9.70	9.54	9.20	9.49	9.73	9.90	9.70
Na_2O	1.42	1.59	1.30	1.47	—	—	—	—	—	.20	—	.18	—	.19
Cl	.09	.09	.84	.97	.07	—	.06	—	.10	.07	.47	.44	—	—
Total	97.21	97.06	99.69	100.00	94.41	94.61	94.52	94.16	95.60	94.54	94.23	96.08	96.29	96.44
	Cations per 23 0				Cations per 22 0									
Si	6.917	6.748	6.078	5.938	5.610	5.624	5.568	5.585	5.478	5.499	5.456	5.539	5.469	5.421
Al^{IV}	1.083	1.252	1.922	2.062	2.390	2.377	2.432	2.415	2.522	2.501	2.544	2.461	2.531	2.579
Al^{VI}	.276	.273	.664	.692	.294	.246	.642	.674	.680	.685	.489	.507	.449	.530
Ti	.070	.149	.052	.043	.408	.377	.161	.157	.221	.209	.234	.247	.307	.304
Fe	2.979	2.985	3.277	3.317	3.265	3.286	3.530	3.452	3.289	3.266	3.312	3.212	3.514	3.566
Mn	.087	.072	.034	.032	.021	.026	.027	.024	.031	.034	—	—	.031	.038
Mg	1.831	1.726	1.169	1.127	1.700	1.779	1.383	1.415	1.524	1.546	1.800	1.767	1.288	1.280
Ca	1.793	1.790	1.977	1.994	—	—	—	—	—	—	—	—	—	—
K	.175	.207	.413	.431	1.904	1.945	1.984	1.981	1.908	1.858	1.939	1.941	1.988	1.948
Na	.426	.480	.395	.447	—	—	—	—	—	.062	—	.054	—	.058
Cl	.025	.024	.224	.259	.020	—	.015	—	.027	.019	.128	.116	—	—
Total	15.660	15.707	16.205	16.340	15.611	15.660	15.742	15.703	15.680	15.679	15.882	15.843	15.677	15.723
Mg	38.1	36.6	26.3	25.4	34.2	35.1	28.2	29.1	31.7	32.1	35.2	35.5	26.8	26.4

oriented plates. Some large primary biotite shapes are still preserved in greenschist grade rocks, although, chemically, they have been altered and contain inclusions of ilmenite surrounded by sphene, and abundant pleochroic haloes. With increasing metamorphic grade, the biotites tend to become richer in Ti (Table 2) and contain only sphene inclusions with few haloes.

Hornblende (α = straw, β = green, γ = deep green-blue) has been recognised only in amphibolite grade rocks, and is magnesian hastingsite to hastingsite (Leake, 1978). These amphiboles have relatively high K_2O contents (> 2%) and up to 1% Cl (Table 2). Triple point junctions at grain boundaries (Fig. 5A) and poikiloblastic anhedral grainshapes (Fig. 5B) confirm that these amphiboles are metamorphic. Pseudomorphs of biotite and epidote after amphibole are common, particularly in greenschist grade rocks (Fig. 5D).

Scapolite occurs only in amphibolite grade rocks and is usually restricted to amphibole-bearing rocks that contain little or no calcite. It is common in the north of MARY KATHLEEN, PROSPECTOR, and the south of ALSACE. Compositionally, it is mizzonite (Shaw, 1960) with 52–60% meonite, and contains 1.0–1.8 per cent chlorine.

Sphene becomes coarser and more abundant with increasing metamorphic grade. Allanite, often replaced by alteration products, is present throughout all grades. Opaque minerals are sparsely distributed. Ilmenite occurs predominantly in greenschist grade rocks and is usually surrounded by sphene, whilst magnetite is present in small amounts, mainly in lower greenschist or upper amphibolite grade rocks. Calcite, epidote, and chlorite decrease in abundance with increasing metamorphic grade, but also occur as retrograde minerals in some amphibolite grade rocks. Coarse, secondary muscovite plates are restricted to upper greenschist or amphibolite grade rocks.

Ewen Batholith

Igneous minerals and textures are commonly preserved in the Ewen Batholith, in contrast to the Kalkadoon Batholith. The granites of the batholith are mostly medium grained and, in places, porphyritic with phenocrysts of K-feldspar and rounded quartz grains. Compositionally, they also range from tonalites, through granodiorite, to monzogranite and syenogranite.

Quartz and K-feldspar show some recrystallisation. Much of the plagioclase is cloudy. Where fresh, plagioclase ranges from An_{40} (core) to An_5 (rim). Biotite (α = straw, $\beta = \gamma$ = red brown) forms coarse plates containing abundant pleochroic haloes and minute opaque inclusions, and is higher in TiO_2 content (> 3%) than the metamorphosed biotites of the Kalkadoon Batholith (Table 2). Igneous amphibole (α = straw, β = bluish green, γ = green brown) is common in the more mafic phases, and is optically and chemically distinct from the deep green-blue metamorphic amphibole of the Kalkadoon Batholith (Fig. 6). Compositionally, it is edenite (Leake, 1978) and contains more MgO and less K_2O and Cl (Table 2) than amphiboles of the Kalkadoon Batholith. Some amphiboles have cores of colourless clinopyroxene, suggesting that the edenites were formed by reaction between clinopyroxene and melt.

The significant differences between the igneous assemblages of the Ewen Batholith and the metamorphic mineralogy of the Kalkadoon Batholith are the composition and texture of the K-feldspars, biotites, and amphiboles, and the presence of high-Ti biotite + minor magnetite in the former, in contrast to low-Ti biotite + sphene in the latter.

Geochronology

Kalkadoon Batholith

Page (1978) reviewed earlier geochronological results, reported new data from the Kalkadoon Granodiorite, and demonstrated that the young apparent Rb-Sr isochron ages do not bear any relation to the time of the primary magmatic crystallisation event. The metamorphic disturbance that caused these aberrations was estimated to have a maximum age of 1640 m.y.

The U-Pb zircon age for the Kalkadoon Granodiorite of 1862 $\pm^{27}_{21}$ m.y. combined with the U-Pb age for the Leichhardt suite of 1865 ± 3 (Page, 1978) suggests the two units are

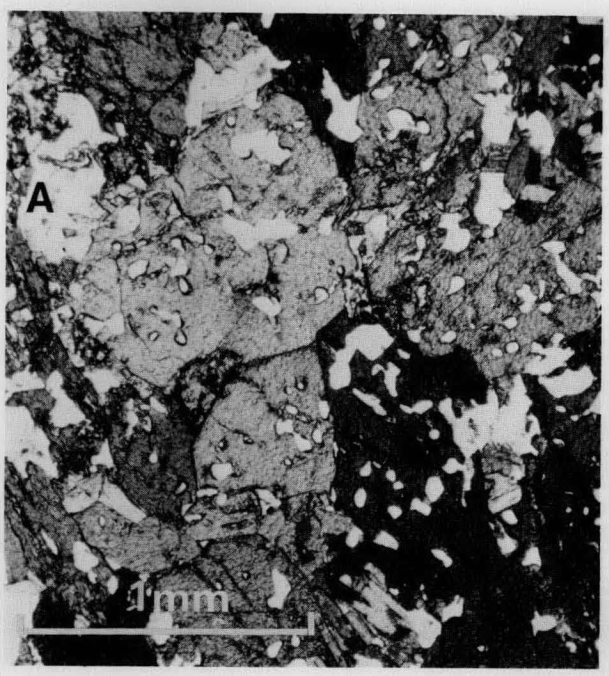

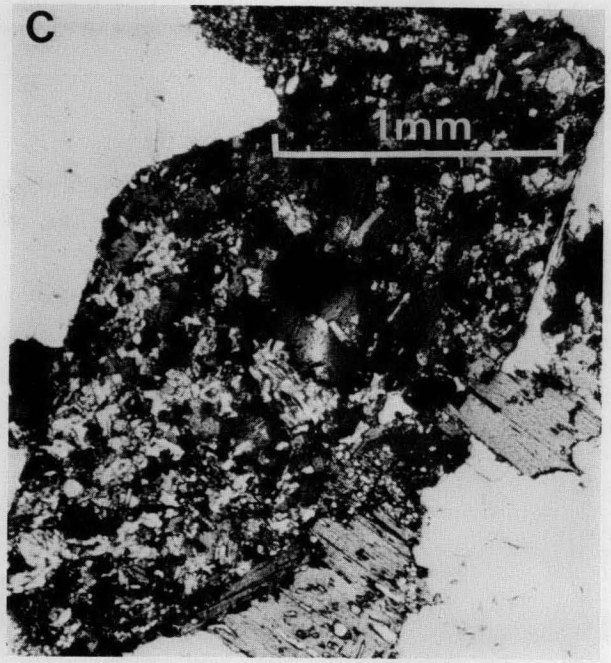

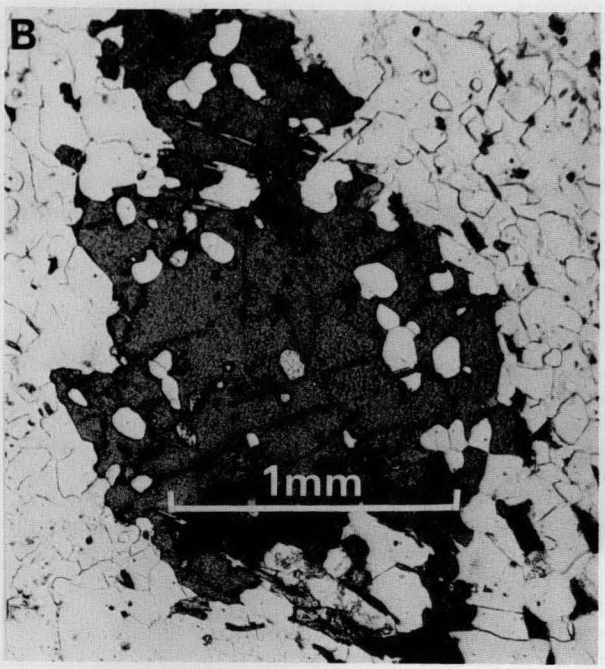

Figure 5. Amphiboles from the Kalkadoon Batholith:
A — anhedral poikiloblastic green-blue amphiboles (hastingsites) with triple point junctions from amphibolite grade, sample 78206042; B — anhedral poikiloblastic green-blue amphibole from amphibolite grade, sample 78206057; C — amphibole replaced by biotite and epidote, sample 79205309.

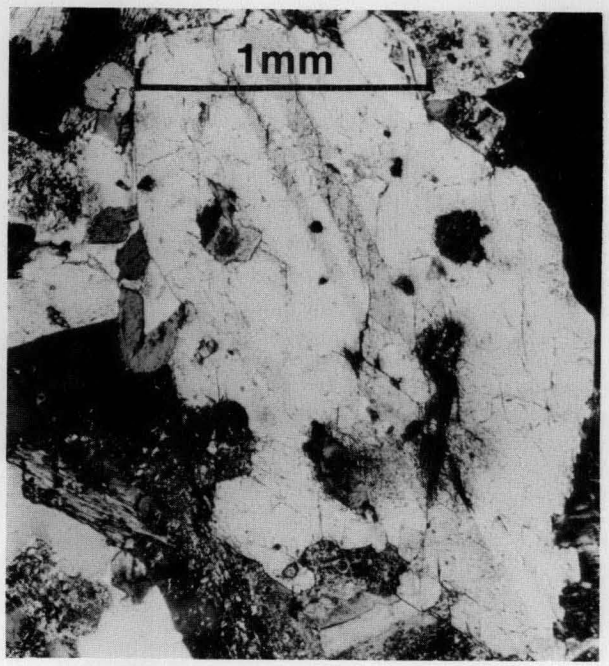

Figure 6. Igneous amphibole from Ewen Batholith.

coeval. Although these zircons came from sites that have been metamorphosed, some to amphibolite grade, the U-Pb zircon systems are unaffected and provide precise, stratigraphically meaningful ages. An additional sample of Kalkadoon Granodiorite was selected from the southern part of the Mount Isa Inlier, about 150 km south of the other localities. This sample is a slightly xenolithic biotite granodiorite with megacrysts of K-feldspar. It contains abundant metamorphic biotite and pseudomorphs after hornblende (Fig. 5C), and has been metamorphosed to at least upper greenschist grade. Three kilometres west of the sample site, the Kalkadoon Granodiorite is unconformably overlain by basal units of the Haslingden Group. The age of this group must be younger than $1790 \pm {}^{10}_{8}$ m.y., the age of the Bottletree Formation, which the Haslingden Group conformably overlies (Page, in press; Bultitude & others, 1982).

U-Pb data. The new U-Pb data (Table 3) are based on five sized and magnetically split zircon fractions. These are a well-formed, almost colourless population with many translucent cavities and inclusions, and sparse opaque inclusions. Many grains exhibit euhedral internal zoning.

In Figure 7, U-Pb data for the five zircon fractions are plotted on the concordia diagram (Wetherill, 1956). The fractions are variably discordant with $^{207}Pb/^{206}Pb$ ages ranging from 1817 m.y. to 1834 m.y. Uranium concentrations of 620–720 ppm are similar to or somewhat higher than those reported by Page (1978) for the northern Kalkadoon Granodiorite zircons. The

amount of common Pb is, however, much higher than in the latter zircons, ranging from 9 to 14 ppm.

Projection of this discordant pattern toward the concordia curve gives a regression result that is substantially a model 1 fit (mean square of weighted deviates, M.S.W.D. = 3.1, not significantly greater than unity at the 5% level), and an intersection age of 1856 $\pm \frac{11}{9}$ m.y. The zircon morphology and good fit of the U-Pb data strongly suggest that the interpreted isotope relations are recording the primary crystallisation age of this granite.

This result and the lower concordia intersection age of 350 ± 85 m.y., are essentially the same as those for the northern part of the Kalkadoon Granodiorite (Page, 1978). An 1856 $\pm \frac{11}{9}$ m.y. granite crystallisation age is stratigraphically and geochronologically consistent with earlier-mentioned constraints derived from the younger felsic volcanic sequences.

Ewen Batholith

An apparent paradox in early geochronological data from the Mount Isa Inlier concerned the relatively old biotite ages measured on granite from the Ewen Batholith. K-Ar biotite ages from most other granitic rocks of the Mount Isa Inlier gave reasonably consistent cooling ages (quite unrelated to emplacement ages) of 1400–1450 m.y. However, biotite K-Ar measurements of two samples from the northern part of the Ewen Batholith gave a minimum age of about 1774 m.y. (Richards & others, 1963). This result was important, for it gave some constraint on the age of the Eastern Creek Volcanics, which unconformably overlie this part of the Ewen Batholith. Later Rb-Sr total-rock and biotite measurements (McDougall & others, 1965; Arriens & others, 1966) more or less confirmed this minimum age (Table 4), even though some isotopic disturbance was evident in both the feldspar and whole-rock systems.

The original GA 584 locality of Richards & others (1963) near Gunpowder Creek (southern MYALLY) was resampled for this study (sample 79205303), for U-Pb zircon work, and further Rb-Sr total-rock and biotite work was undertaken on samples from two sites north-east of Rocky Glen on southern ALSACE.

U-Pb zircon data. Four zircon fractions from the locality on MYALLY have been analysed (Table 3). The zircons are euhedral, colourless to pale brown and contain small translucent and some opaque inclusions. Morphologically, they are like zircon populations observed in the Kalkadoon Granodiorite, but they differ in their U and Pb isotopic characteristics. The U concentration is about half that in zircons from the Kalkadoon Granodiorite, and the very high initial common Pb gives rise to large uncertainties in the plotted data (Fig. 7), which are all displaced to the left of the Kalkadoon Granodiorite zircon data, but do not define any clear discordia array. The $^{207}Pb/^{206}Pb$ ages fall in the range 1800–1816 m.y., and this is the best minimum age obtainable from the present data. The consistent displacement of the Ewen data with respect to the Kalkadoon data suggests that the Ewen zircon isotopic systems were initiated between about 1820 m.y. and 1860 m.y.

Rb-Sr data. A model age for the original total-rock sample of Richards & others (1963) is 1766 m.y. (McDougall & others, 1965). The sample is quite enriched in radiogenic Sr, yet is anomalously young, for new analyses of biotite separated from GA.584 give ages close to 1800 m.y., in good agreement with biotite ages from 79205303 and GA.585 (Table 4) and a reliable minimum age for the emplacement of the granite.

Rb-Sr data (Table 4, Fig. 8) from granites in the south of the Ewen Batholith, in ALSACE, in part show a similar isotopic disturbance of the total-rock and biotite systems, giving apparent ages of between 1595 m.y. (74-161A biotite) and 2000 m.y. (74-161A, total rock). These ages are not geologically interpretable, as they are merely artefacts of partly updated isotopic systems.

The data from one of the ALSACE sites (74-162) do, however, define a meaningful isochron when one of the apparently 2000 m.y. old samples, 74-162A, is excluded. The resultant model 3 fit (M.S.W.D. = 9.4) gives an age of 1840 ± 50 m.y., with an initial $^{87}Sr/^{86}Sr$ for the system of 0.704 ± 0.002 (Fig. 8). This result is consistent with the minimum ages interpreted from the Rb-Sr biotite and U-Pb zircon data, and remains our best estimate for the crystallisation age of this part of the Ewen Batholith. The biotite ages from rocks of the Ewen Batholith are only some 4–5 per cent younger than the probable emplacement age of the system, whereas in the Kalkadoon-Leichhardt block and elsewhere in the south of the Mount Isa Inlier, enhanced and prolonged metamorphic disturbances have resulted in the regionally significant biotite ages of about 1400 m.y., some 20 per cent younger than the emplacement age.

The 1840 ± 50 m.y. Rb-Sr age accords well with the 1852 ± 7 m.y. zircon age of felsic volcanic rocks in the Leichhardt suite, which are intruded by the Ewen Batholith (Page, in press). The similarity of these crystallisation ages makes it likely that this volcanic-plutonic pair mirrors the same petrogenetic relation as the volcanics of the Leichhardt suite and their intrusive equivalent, the Kalkadoon Batholith. It is also likely that the felsic magmas of the Ewen and Kalkadoon-Leichhardt blocks could be part of the same magmatic suite.

Table 3. U-Pb analytical data for zircons from the Kalkadoon and Ewen Batholiths.
See appendix for analytical methods.

Size in microns, Magnetic susceptibility	*Weight (mg)*	*Concentration (ppm)**			$^{206}Pb/^{204}Pb$ *(measured)*	**Radiogenic ratios (age)*		
		Radiogenic Pb	*Common Pb*	*U*		$^{207}Pb/^{206}Pb$	$^{206}Pb/^{238}U$	$^{207}Pb/^{235}U$
Kalkadoon Granite (7920.5309)								
–215 NM1	2.07	190.9	11.4	647.2	905	0.11108 (1817)	0.27653	4.2353
–150 NM1	2.23	195.7	9.2	618.1	1137	0.11211 (1834)	0.29619	4.5786
–150 M0	3.73	203.1	11.2	669.4	980	0.11110 (1817)	0.28468	4.3608
–75 NM0	2.06	204.7	9.9	646.7	1110	0.11185 (1830)	0.29444	4.5408
–45 NM2	1.59	216.5	13.8	719.5	822	0.11117 (1819)	0.27687	4.2437
Ewen Granite (7920.5303)								
–150 NM2	0.49	103.0	47.7	315.6	119.19	0.11102 (1816)	0.27560	4.2189
–75 NM2	0.64	114.9	43.6	352.1	145.7	0.11023 (1803)	0.28332	4.3059
–75 M2	1.46	121.1	69.2	349.2	99.13	0.11031 (1805)	0.28844	4.3869
–60 M2	0.56	133.4	83.8	399.8	91.31	0.11002 (1800)	0.27725	4.2057

* Radiogenic components corrected for Pb blank of 0.25 ng, of composition: $^{206}Pb/^{204}Pb$ = 17.97, $^{207}Pb/^{204}Pb$ = 15.55, $^{208}Pb/^{204}Pb$ = 37.71.
Common Pb corrections based on 1850 m.y. Pb from Cumming & Richards (1975).

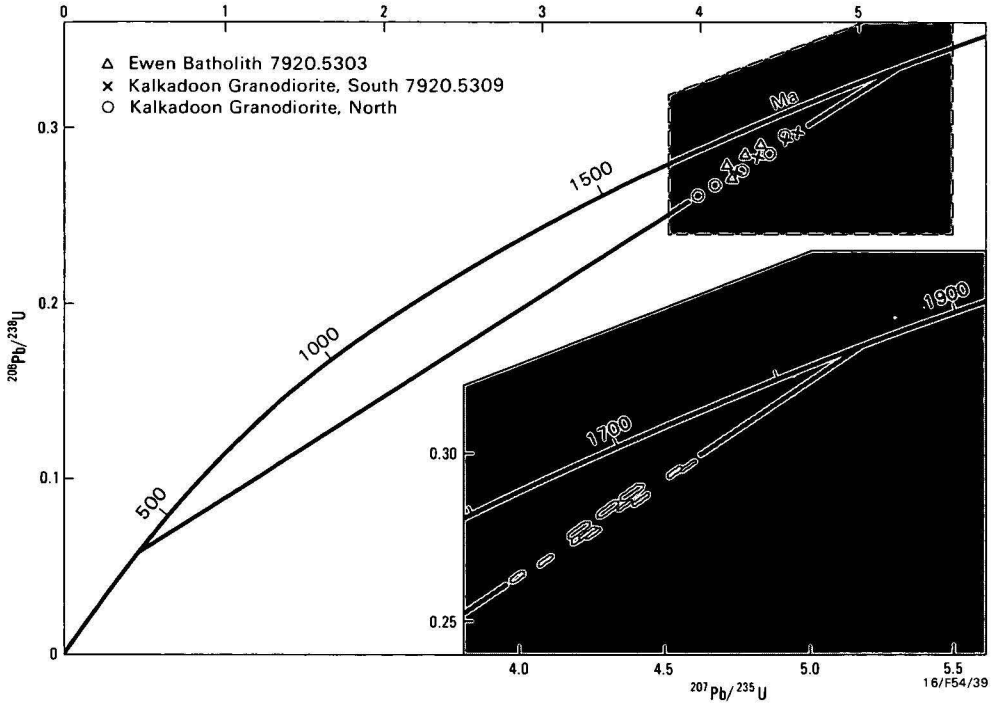

Figure 7: U-Pb zircon concordia for the Kalkadoon and Ewen Batholiths.

Table 4. Rb-Sr analytical data and ages for the Ewen Batholith.
See appendix for analytical methods.

Sample		*Rb ppm*	*Sr ppm*	$^{87}Rb/^{86}Sr$	$^{87}Sr/^{86}Sr$	*Age*[5] *(m.y.)*
74–161A	Granodiorite	127.2	436.3	0.844	0.72840	
74–161A	Biotite	396.1	7.55	229.4	5.9640	1595
74–161B	Leucogranite	256.1	131.9	5.683	0.84804	1763
74–162A	Granodiorite	127.9	381.4	0.970	0.73234	
		133.5	399.9	0.967	0.73223	
B	Leucogranite	301.5	147.8	5.981	0.86236	)
D	Granodiorite	142.8	333.1	1.242	0.73702	)
F	Granodiorite	144.6	270.6	1.549	0.74547	) 1840 ± 50
G	Granodiorite	231.3	224.4	2.998	0.78230	)
H	Granodiorite	117.5	452.2	0.751	0.72312	)
GA.584	Granite[1]	469	47.0	30.99	1.491	1766
GA.584	Biotite[2,3]	2429	20.4	2451.8	63.40	1778
GA.584	Biotite[4]	2324	19.9	2266.3	59.30	1798
		2357	19.9	2568.3	67.32	1803
7920.5303	Biotite	2363	20.31	2327.7	61.32	1810
		2381	20.33	2370.4	62.15	1802
GA.585	Biotite[3]	881.2	28.2	116.9	3.7330	1801

[1] McDougall & others, 1965
[2] Arriens & others, 1966
[3] cf. K-Ar ages of 1778 m.y. (GA.584) and 1774 m.y. (GA.585) — Richards & others, 1963
[4] New analyses of same original mineral separate.
[5] Model ages based on $(^{87}Sr/^{86}Sr)_i$ of 0.704.

Chemistry

Eighty-one rocks were selected for both major and trace element analysis: analyses of the One Tree, Woonigan, and Wills Creek Granites, and granites of the Ewen Batholith, are listed in Table 5, and average analyses of the Kalkadoon Granodiorite, in Table 6. Because of the extent of the Kalkadoon Granodiorite, four or five samples were taken from each of two or three discrete areas of granite in each 1:100 000 Sheet area. Two areas of massive granite were also sampled in the Kalkadoon Granodiorite (one in the south of MARY KATHLEEN and the other, west of Dobbyn in ALSACE) for comparison with the foliated granite types. The chemistry of the Ewen and Kalkadoon Batholiths is summarised on selected Harker variation diagrams (Fig. 9).

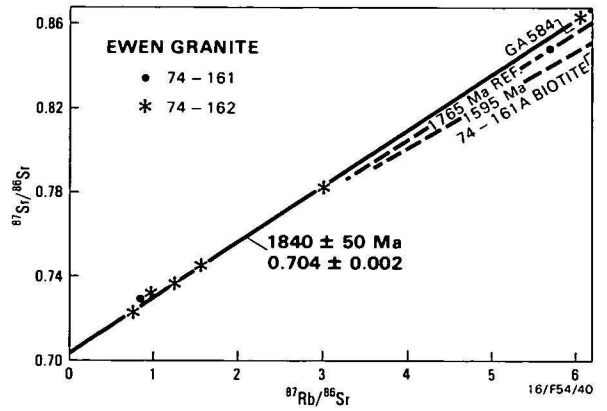

Figure 8. Rb-Sr isochron for the Ewen Batholith.

Conspicuous chemical features of both batholiths are:

(1) the complete progression from 60–77% with no compositional breaks;
(2) MgO, CaO, P_2O_5, and Ni show inverse linear trends that intersect the SiO_2 axis at 75–77%;
(3) K_2O is high (3–6%) and increases in proportion to the amount of modal feldspar. There is no chemical evidence of potassium metasomatism (cf. Derrick & others, 1977);
(4) the K/Rb ratio is constant, implying no fractional crystallisation (Collins & others, 1982);
(5) for most samples the molecular ratio of Al_2O_3/K_2O + Na_2O + CaO ranges between 0.9 and 1.1, and most samples have less than 1% normative corundum;
(6) particularly at lower silica values, most samples have less than 13 ppm Ni and 30 ppm Cr. From this it can be inferred that the source is also low in these elements and is probably relatively siliceous.

Kalkadoon Batholith

The concentrations of certain elements in the Kalkadoon Granodiorite differ from one area to another: for instance, one group in the centre of DAJARRA has relatively low TiO_2. The One Tree Granite, which differs from the Kalkadoon Granodiorite in being unconformably overlain by rocks of the Leichhardt suite rather than intruding them, is fairly distinctive in certain elements, having lower Sr and Al_2O_3 and higher total Fe and TiO_2, possibly indicating a more felsic source. The two analysed samples from the Wills Creek Granite (which has no minimum age control*) have high SiO_2 (74.2 and 75.5 wt %) and are tentatively correlated with granites of the Kalkadoon Batholith, as, at these high SiO_2 levels, distinction of granitic suites by trace elements is less precise. Nonetheless, the chemical differences between granites of the Kalkadoon Batholith are relatively insignificant when a comparison is made with other granites of the Mount Isa Inlier (Fig. 11).

The massive granite samples were chemically indistinguishable from the foliated phases. This result is similar to those of Ashley & Chenhall (1976) and Kerrick & others (1980), who, in comparing the chemistry of strongly deformed and massive granitic rocks, found only minor compositional changes.

Table 5. Chemical analyses of the One Tree, Wills Creek and Woonigan Granites and the granites from the Ewen Batholith.
See appendix for analytical methods. Locations listed in Wyborn (in preparation).

				KALKADOON BATHOLITH						*EWEN BATHOLITH*			
Pluton	*Wills Creek*		*Woonigan*			*One Tree Granite*				*Pluton on*		*Pluton on*	
Sample	*Granite*		*Granite*							*Myally*		*Alsace*	
Number	*79205311*	*78531778*	*77535112*	*78206120*	*78206121*	*78206122*	*78206123*	*79532553*	*79532542*	*78206051*	*78536153*	*78206116*	*78206117*
SiO_2	74.20	75.50	79.60	72.02	68.65	71.81	73.02	72.80	68.30	76.19	68.40	71.15	68.92
TiO_2	0.23	0.20	0.07	0.43	0.66	0.40	0.37	0.36	0.66	0.14	0.47	0.34	0.45
Al_2O_3	12.60	12.60	12.00	13.14	13.75	13.05	12.94	12.60	13.70	12.34	14.70	13.95	14.17
Fe_2O_3	0.51	0.64	0.06	0.52	1.08	0.69	0.65	1.11	0.76	0.28	1.45	0.42	0.69
FeO	1.30	0.80	0.19	3.03	4.15	2.62	2.44	2.01	4.10	1.05	1.84	2.33	2.90
MnO	0.02	0.01	<0.01	0.06	0.08	0.04	0.04	0.04	0.05	0.05	0.05	0.05	0.06
MgO	0.57	0.86	0.05	0.70	1.16	0.58	0.76	0.53	1.08	0.18	1.44	0.82	1.08
CaO	0.38	0.33	0.14	1.58	2.60	1.66	1.01	1.54	2.60	0.82	2.35	2.06	2.57
Na_2O	3.05	2.76	6.90	2.32	2.00	2.54	2.14	2.50	2.50	3.00	2.29	2.62	2.50
K_2O	5.85	4.77	0.44	5.00	4.10	5.07	5.25	5.27	4.65	4.96	4.88	4.77	4.66
P_2O_5	0.05	0.08	0.01	0.07	0.13	0.06	0.08	0.07	0.14	0.02	0.15	0.07	0.09
H_2O+	0.66	0.64	0.30	0.83	1.12	1.00	0.87	0.69	0.93	0.66	1.37	0.94	1.19
H_2O-	0.20	0.11	0.09	<0.01	0.01	0.02	<0.01	0.14	0.16	0.07	0.19	0.02	0.01
CO_2	0.01	0.05	0.10	0.08	0.11	0.06	0.05	<0.05	0.07	0.06	0.05	0.05	0.04
Rest	0.17	0.10	0.07	0.21	0.21	0.18	0.19	0.19	0.20	0.15	0.23	0.19	0.32
Total	99.79	99.40	100.02	99.99	99.81	99.78	99.81	99.85	99.90	99.97	99.86	99.78	99.65
Ba	660	203	54	725	606	724	611	697	680	148	772	546	812
Li	—	3	1	12	13	43	13	8	—	61	9	17	17
Rb	210	194	19	240	196	214	240	208	220	480	191	246	216
Sr	65	48	12	102	134	89	95	87	130	51	309	163	199
Pb	11	11	7	63	32	26	24	22	20	52	36	69	797
Th	26	40	28	27	23	31	33	24	22	46	25	25	30
U	4	8	4	6	5	5	4	5	4	19	5	5	6
Zr	260	116	124	216	209	20	191	181	280	110	171	147	188
Nb	10	10	10	9	11	9	11	8	13	16	10	9	10
Y	20	23	42	37	32	38	36	36	30	30	25	29	30
La	70	36	45	54	55	67	64	58	50	27	54	48	65
Ce	100	67	88	101	103	121	117	107	100	58	94	94	123
Nd	—	28	45	46	45	51	54	44	—	27	39	42	52
Sc	—	2	<2	6	11	4	4	3	—	13	8	5	7
V	20	11	<2	23	54	2	18	18	60	3	50	29	41
Cr	—	9	4	10	24	21	9	11	—	6	47	15	21
Co	—	—	<5	8	14	8	8	5	—	2	—	8	10
Ni	—	2	1	4	11	8	4	4	—	2	19	5	7
Cu	10	6	21	19	23	5	9	13	10	3	13	6	9
Zn	28	8	6	49	87	15	25	38	60	29	48	53	52
Sn	2	8	4	8	4	5	6	4	2	13	2	5	10
Ga	—	13	15	17	16	16	16	15	—	17	14	14	18
As	—	<1	1	<1	1	1	1	1	—	<1	<1	<1	<1

Table 6. Average chemical analyses of the Kalkadoon Granodiorite.
See appendix for analytical methods. Full analyses and locations listed in Wyborn (in preparation).

Rock type	*tonalite*		*granodiorite*		*monzogranite*		*syenogranite*	
No. of samples	*19*		*30*		*15*		*4*	
	$\bar{x}$	*S.D.*	$\bar{x}$	*S.D.*	$\bar{x}$	*S.D.*	$\bar{x}$	*S.D.*
SiO_2	63.87	3.17	69.95	2.72	73.27	1.59	75.62	0.59
TiO_2	0.66	0.20	0.44	0.14	0.21	0.08	0.11	0.05
Al_2O_3	16.25	1.00	15.27	1.10	13.63	0.66	12.60	0.03
Fe_2O_3	0.97	0.44	0.74	0.29	0.42	0.22	0.30	0.11
FeO	4.06	0.96	2.73	0.84	1.41	0.48	0.99	0.14
MnO	0.07	0.02	0.05	0.01	0.03	0.01	0.03	0.01
MgO	1.50	0.71	0.93	0.38	0.38	0.19	0.32	0.18
CaO	4.12	1.12	3.01	0.94	1.67	0.45	1.03	0.29
Na_2O	2.93	0.80	2.84	0.32	2.69	0.39	2.64	0.44
K_2O	3.35	0.78	4.31	0.58	5.07	0.70	5.39	0.69
P_2O_5	0.17	0.08	0.11	0.14	0.06	0.04	0.03	0.03
Ba	956	436	888	287	648	451	261	80
Li	13	5	11	7	14	14	9	10
Rb	143	36	174	32	227	64	221	50
Sr	305	129	262	103	159	73	83	26
Pb	28	16	21	6	33	10	44	18
Th	17	4	21	6	31	11	32	16
U	3	2	3	3	4	2	7	3
Zr	257	81	213	59	143	29	105	26
Nb	12	4	11	3	9	4	8	2
Y	29	7	24	8	24	10	17	10
La	66	23	63	20	57	19	38	20
Ce	120	41	112	33	104	33	76	35
Nd	53	13	49	14	43	10	34	16
Sc	9	3	6	4	3	4	5	7
V	55	21	34	16	12	8	4	3
Cr	24	12	17	15	8	6	7	3
Co	12	3	8	4	4	2	3	—
Ni	7	5	5	4	3	2	2	1
Cu	15	8	11	6	6	3	5	3
Zn	56	12	45	17	28	7	29	2
Sn	4	4	4	5	6	4	4	5
Ga	18	2	17	2	15	2	14	1
As	2	3	2	2	1	3	1	1

Ewen Batholith

The four analysed samples of the Ewen Batholith (Table 5) are chemically similar to the granites of the Kalkadoon Batholith with the exception of the fluorite-bearing sample (78206051), which has 76.19 per cent SiO_2 and relatively higher Rb, Th, and U, and lower Sr contents.

Comparison of granites of the Ewen and Kalkadoon Batholiths with rocks of the Leichhardt suite

The similarity in the chemistry (Fig. 10) and age of the granites of the Ewen and Kalkadoon Batholiths and volcanic rocks of the Leichhardt suite suggests strongly that they are comagmatic, and implies that the granites were emplaced at fairly shallow, probably subvolcanic levels.

Both the granites and volcanics would have been produced by the same partial melting event from a fairly uniform source region. However, slight recognisable differences in the composition of the granites, which cannot be produced by mineral fractionation, imply that there are minor regional variations in the composition of the source region. The granites of the Kalkadoon and Ewen Batholiths, therefore, do not form a 'suite' in the strict sense (Chappell, 1979), and for rocks produced by this large melting event at approximately 1840–1870 m.y., it is proposed to use the term 'Kalkadoon–Ewen–Leichhardt association' (cf. Wyborn & others, 1981). In view of their similarity in composition, the rocks of the One Tree Granite and the Wills Creek Granite are tentatively regarded as being part of the Kalkadoon–Ewen–Leichhardt association, even though there are petrographic and stratigraphic differences, which may or may not be significant.

Comparison with other granites of the Mount Isa Inlier

Compared with other major granitic intrusions of the Mount Isa Inlier (Sybella and Wonga Batholiths and the Naraku Granite), rocks of the Kalkadoon–Ewen–Leichhardt association, particularly at lower silica values, have higher Sr and Al_2O_3 and lower TiO_2, Zr, Nb, and Th (Fig. 10). These parameters appear to be useful for distinguishing the older granites of the Mount Isa Inlier. The only other felsic igneous rocks in the Mount Isa Inlier known to be of similar composition are part of the Big Toby Granite, the Yeldham Granite (both known to be approximately 1800 m.y.; Page, unpublished data), and two intrusive samples of the Plum Mountain Gneiss (Bultitude & Wyborn, 1982).

Discussion

Metamorphism and deformation

All rocks in the Kalkadoon–Ewen–Leichhardt association have been affected to various degrees by regional metamorphism. In the Ewen Batholith this is least in the north, whilst further south the degree of recrystallisation increases. In the Kalkadoon Batholith, metamorphism is generally more intense, and amphibolite and greenschist grades alternate in both a north–south and an east–west direction. The metamorphism is thought to be younger than 1640 m.y. (Page, 1978) and probably coincided with regional metamorphism in the southeastern part of the Inlier and near Mary Kathleen, which has been estimated to have resulted from pressures of 3–4 kb and temperatures of up to 660°C (Jaques & others, 1982; Cruikshank & others, 1980).

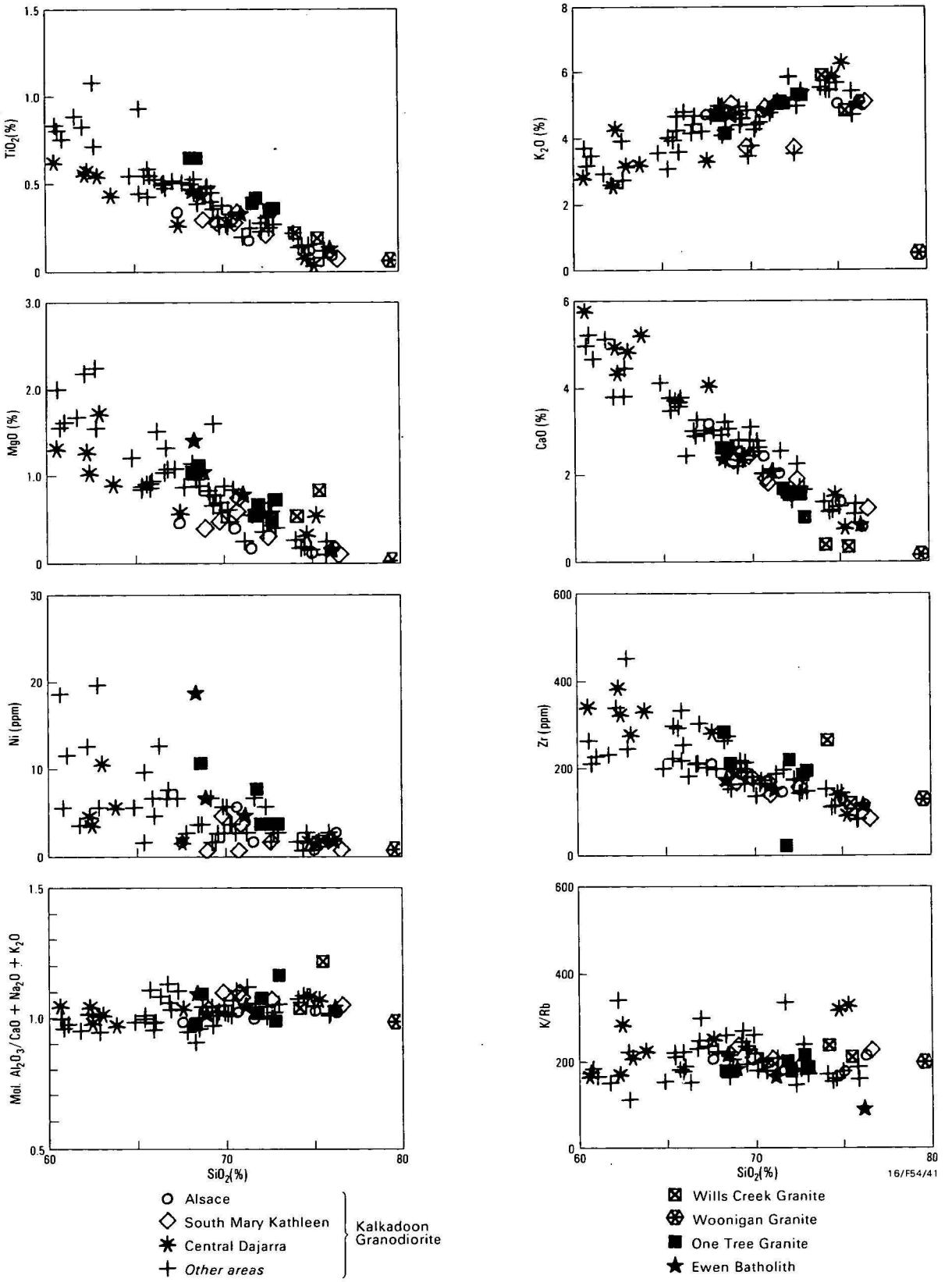

Figure 9. Representative Harker variation diagrams for the Kalkadoon and Ewen Batholiths.

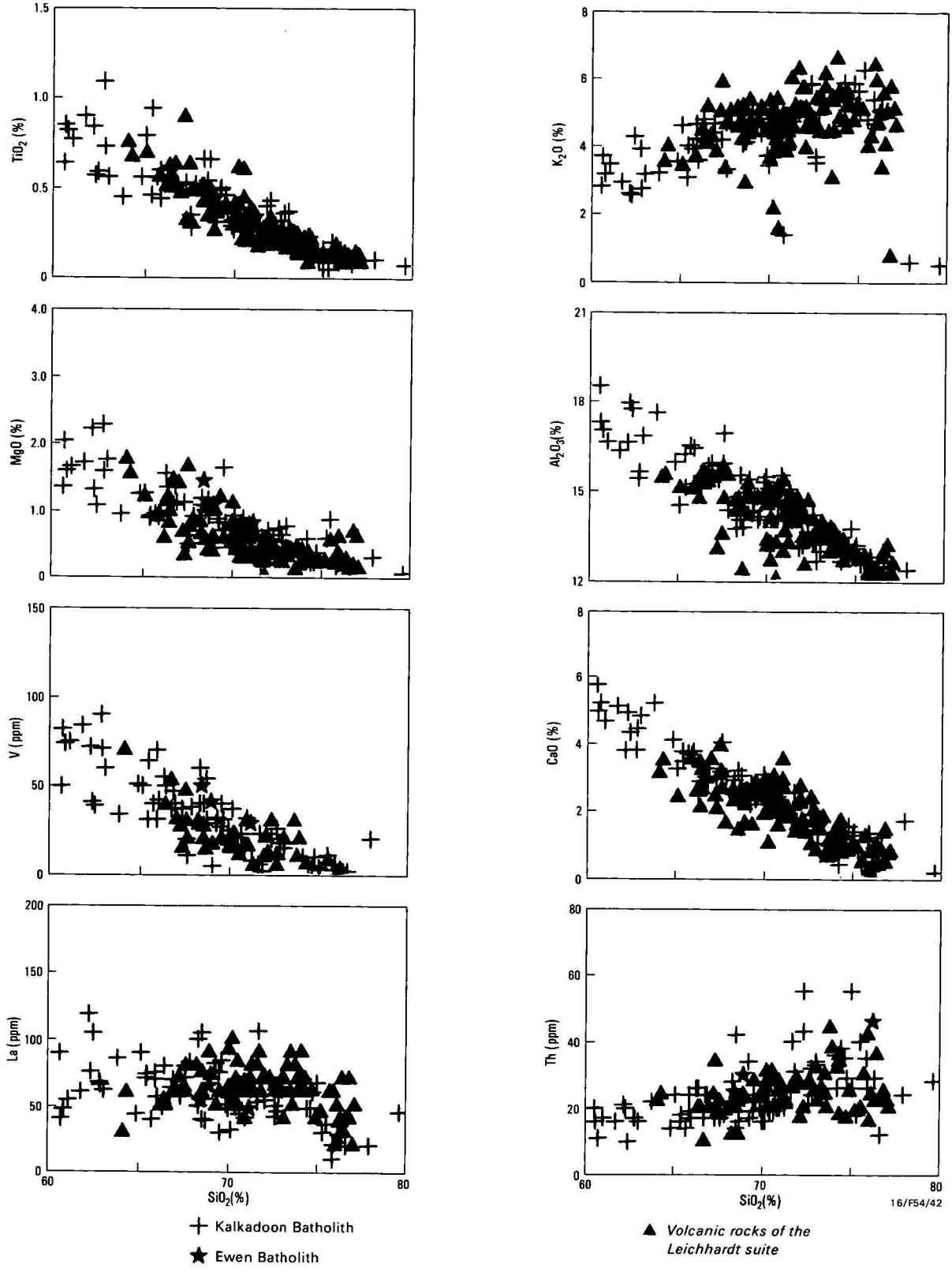

Figure 10. Comparison between the Kalkadoon and Ewen Batholiths and rocks of the Leichhardt suite (data for the Leichhardt suite is listed in Wyborn, in preparation).

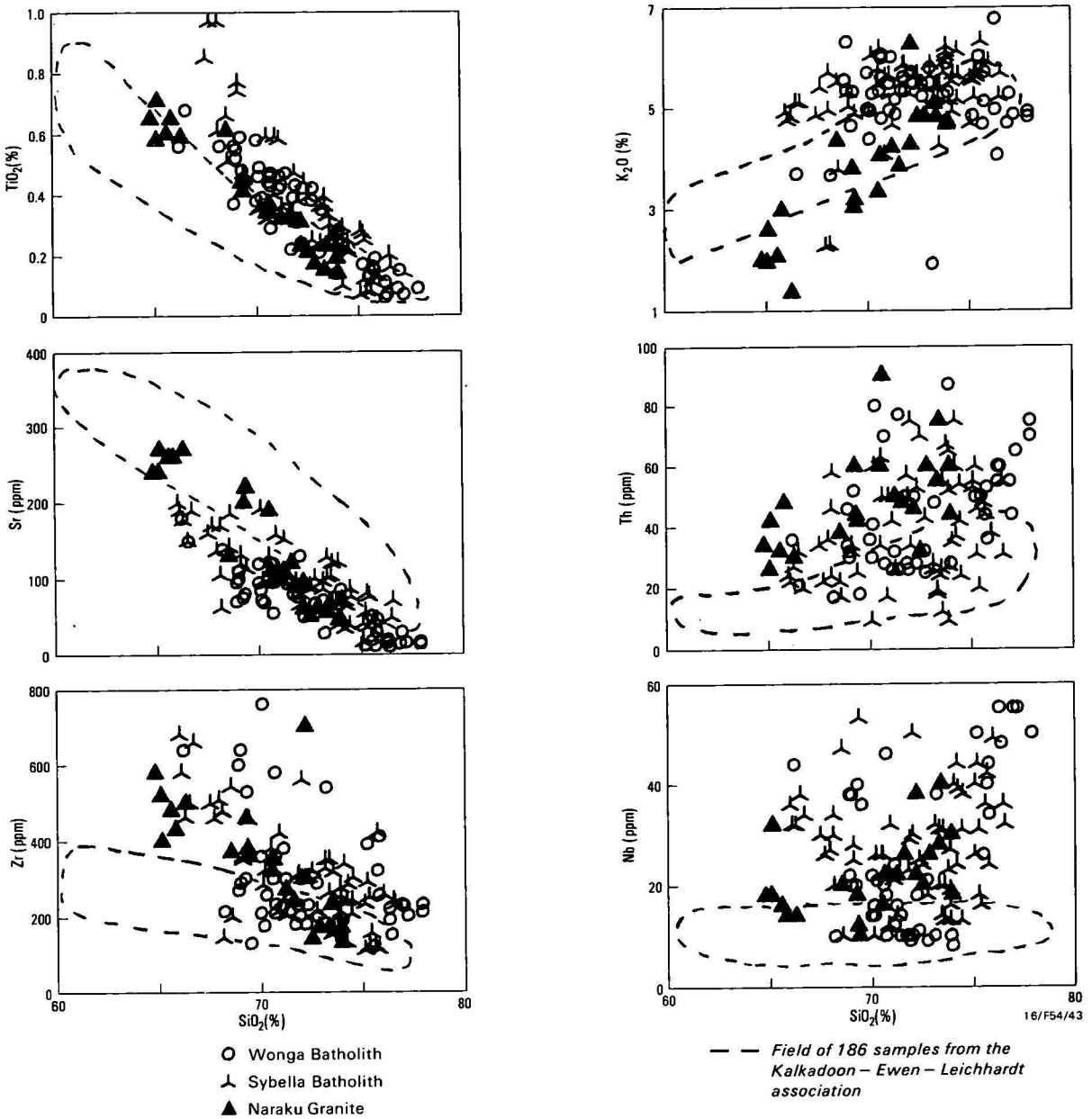

Figure 11. Comparison between granitic rocks of Mount Isa.

The deformation that accompanied the metamorphism, was mostly very weak in the Ewen Batholith, whilst in the Kalkadoon Batholith its effect was variable. However, as the age of the metamorphism and deformation is now known to be significantly younger than the age of emplacement, it is clear that degree of deformation is unrelated to age.

Geochronology

U-Pb determinations on zircons and some Rb-Sr total-rock data suggest that, following a significant and extensive partial melting event in the lower crust in the Mount Isa Inlier at about 1840–1870 m.y., there was extrusion of abundant felsic volcanics and intrusion of comagmatic granites. The apparent 20 m.y. age difference in the emplacement ages of the Kalkadoon-Leichhardt and Ewen blocks suggests that intrusion of the melts was slightly later in the latter.

Later regional metamorphism had no effect on the U-Pb zircon ages, but severely modified most K-Ar and Rb-Sr ages and raised the apparent initial $^{87}Sr/^{86}Sr$ ratios (Page, 1978). The Sr isotopic resetting evident in the Kalkadoon Granodiorite data (Page, 1978) allows extrapolation of an approximate magmatic initial $^{87}Sr/^{86}Sr$ of 0.704 ± 0.002 at 1870 m.y. This is in accord with the indicated $^{87}Sr/^{86}Sr$ of 0.704 ± 0.002 at 1840 m.y. found in the Ewen Batholith. We believe that the high and variable apparent initial $^{87}Sr/^{86}Sr$ ratios of the Mount Isa melts are the result of later regional metamorphism, as stated by Page (1978), and not derivation from old sialic crust, as suggested by Glikson (1980). We think that the initial $^{87}Sr/^{86}Sr$ ratio was about 0.704 (only slightly higher than the mantle growth curve) and that this and the high Rb/Sr of the melts implies that their crustal residence time was short and that there was no old sialic component.

Chemistry

The uniform age of rocks of the Kalkadoon–Ewen–Leichhardt association is mirrored also in their compositional similarity over a large area (at least 5000 km^2). From the occurrence of amphibole in the granites and the presence of normative

diopside or less than one per cent normative corundum, the rocks of the association can be classed as I-type granites (Chappell & White, 1974).

Relative to Palaeozoic I-type granites of the Lachlan Fold Belt (White & others, 1976; Hine & others, 1978; Griffin & others, 1978) and Mesozoic and Cenozoic I-type granites of North and South America (Bateman & Chappell, 1979; Perfit & others, 1980; Smith & others, 1979), the rocks of the Kalkadoon–Ewen–Leichhardt association are enriched in K_2O, Rb, Nb, Th, U, La, Ce, and Pb, and depleted in CaO, MgO, Ni, and Cr, implying that the source region for the Kalkadoon–Ewen–Leichhardt association was fractionated.

Composition of the source region for the Kalkadoon–Ewen–Leichhardt association

The relatively uniform composition and large areal extent of this association imply that the source region must also be uniform and of even larger extent than that exposed at the surface. The low MgO, Ni, and Cr values argue for the source being fractionated and unlikely to involve much basaltic material. Also, the high Na_2O content, the presence of hornblende and relict clinopyroxene in the unmetamorphosed samples, the low initial $^{87}Sr/^{86}Sr$ ratio, and the absence of zircon inheritance features argue against a pelitic or clastic sedimentary source. Further, it is unlikely that the large volume of silicic melt could be produced directly from the mantle. Our estimated initial $^{87}Sr/^{86}Sr$ ratio of 0.704 suggests that the source resided in the crust for at least a short time, and we believe it was lower crustal, of intermediate igneous composition, and formed by accretion of igneous material to the base of the crust during a significant mantle fractionation event.

It is possible to constrain the SiO_2 content of the source region. Chappell (1978) interpreted linear variation lines of granites, such as those from the Kalkadoon and Ewen Batholiths, as mixing lines between a melt end-member and refractory source residue, 'restite'. Using this 'restite' model, Compston & Chappell (1979) were able to calculate the composition and age of the source regions. Although granites that have formed by fractional crystallisation can have linear variation diagrams (Whalen & others, 1982), these Mount Isa granites are not likely to have formed in this way. The K/Rb ratios do not decrease towards high silica levels, and, in addition, the Mount Isa granites are enriched in the incompatible elements throughout the 60–76 per cent SiO_2. range; that is, they are not concentrated by fractional crystallisation at higher silica levels. This suggests that the source region for the Kalkadoon–Ewen–Leichhardt association was also enriched in these elements.

If Compston & Chappell's (1979) model is used for the Mount Isa association, the average melt composition has 76 per cent SiO_2 and the 'model restite', which is defined as when normative quartz disappears as the variation lines of the major elements are extrapolated towards lower SiO_2, has 47 per cent SiO_2. The source composition should, therefore, lie between these two extreme values.

Compston & Chappell (1979) argued that the amount of material that can melt in a source region to produce large granite bodies must lie between 15 and 60 per cent, which is equivalent to a source composition for the Kalkadoon–Ewen–Leichhardt association of 51–66 per cent SiO_2. The fact that the volume of the melt itself is so large would make the source more likely to be at least 60 per cent SiO_2, equivalent to 45 per cent melting. Anything lower would mean an immense source from which only a small fraction of material has been extracted. However, the source composition is not likely to be much higher than 65 per cent SiO_2 as this would be too felsic to produce the more mafic end members of the association.

If the source was at least 60 per cent SiO_2, i.e. fractionated, this could explain the enrichment in elements such as K_2O, Rb, La, Ce, and Th, and depletion in CaO, MgO, Ni, and Cr. If 45 per cent (or even only 15 per cent) of the source material was melted, this melt fraction would contain most if not all of the available minimum melt component. The removal of this would irreversibly change the composition of the source region, making it impossible to produce a melt of a similar composition to the first fraction in the same area during any later melting event. This hypothesis is supported by the fact that younger melts within the area of the Kalkadoon–Ewen–Leichhardt association, such as the Bottletree and Argylla Formations, are of radically different compositions, having much higher concentrations of Zr, Nb, Y, TiO_2 and total Fe, and relatively lower Al_2O_3 (Wilson, 1978; Bultitude & Wyborn, 1982).

Age of the source region

The low initial $^{87}Sr/^{86}Sr$ ratios and the absence of inheritance features in the U-Pb zircon data indicate that the age of the source cannot be much older than the age of emplacement of the melt. Based on the interpolated Rb and Sr composition at various silica values, calculations of the approximate crustal residence time for the source can be made. From the measured emplacement age of 1840 ± 50 m.y. and initial $^{87}Sr/^{86}Sr$ (0.704 ± 0.002) of the Ewen Granite, and the Rb and Sr values calculated between the most probable SiO_2. limits of 55–60 per cent, the crustal residence time for such a source would be between 100 m.y. and 230 m.y., depending on which mantle evolution model (chondritic bulk earth or depleted mantle) is adopted. Even if a rather mafic source (50% SiO_2) with a lower Rb/Sr ratio is considered, its residence time would be no more than 320 m.y. This implies that the source of the felsic magmas was no older than early Proterozoic. We consider, therefore, that a significant proportion of the continental crust beneath the Mount Isa Inlier formed by differentiation from the mantle between 1900 and 2100 m.y. ago. We believe this mantle extraction event may be recognisable in wider areas of northern Australia, as granites of similar composition, age, and low $^{87}Sr/^{86}Sr$ initial ratios are present in other Proterozoic terrains of northern Australia (Fig. 1). These include the Nimbuwah Complex of the Pine Creek Inlier (Page & others, 1980; Ferguson & others, 1980), and the Nicholson Granite Complex of the Murphy Inlier (Sweet & others, 1981a, 1981b), and, possibly, the Bow River Granite of the Halls Creek Inlier (Page, 1976). A widespread mantle event of 1800 m.y. is also evident from initial $^{143}Nd/^{144}Nd$ measurements in Proterozoic granite basement of Colorado (De Paolo, 1981).

Conclusions

U-Pb zircon data and selected Rb-Sr total-rock data show that, during the period 1840–1870 m.y., granites of the Kalkadoon and Ewen Batholith and volcanics of the Leichhardt suite were emplaced in the Mount Isa Inlier. Rocks of this association are chemically and isotopically very uniform over an area of at least 5000 km^2. The source region for these melts was not much older and formed by differentiation from the mantle approximately 1900–2100 m.y. ago. This source was relatively fractionated, enriched in K_2O, Rb, Th, U, La, Ce, Zr, and Nb, and depleted in CaO, MgO, Ni, and Cr. Similar sources were probably present in other areas of Proterozoic crustal formation in Northern Australia.

Regional metamorphism and deformation, which have a maximum age of 1640 m.y., caused significant textural changes, especially in the Kalkadoon Batholith, and reset the K-Ar and Rb-Sr ages, making them 4–5 per cent younger in the Ewen Batholith and up to 20 per cent younger in the Kalkadoon Batholith.

Acknowledgements

We gratefully acknowledge useful discussions with D. Wyborn, D.H. Blake, R.J. Bultitude, and M.T. McCulloch. J. Pyke analysed the trace elements in the BMR laboratories, and T.K. Zapasnik, D.B. Guy, and M.J. Bower gave significant contributions to the isotopic analyses. M. Owen wrote the computer programs used in assessing and plotting the geochemical data and calculating the areas covered by the various plutons.

* Note added in proof: A $^{207}Pb/^{206}Pb$ age just obtained for a zircon fraction from the Wills Creek Granite indicates a minimum age of 1830 m.y., closely akin to the minimum ages of zircon fractions from the Kalkadoon Granodiorite.

References

Arriens, P.A., Brooks, C., Bofinger, V.M., & Compston, W., 1966 — The discordance of mineral ages in granitic rocks resulting from the redistribution of rubidium and strontium. *Journal of Geophysical Research*, 71, 4981–4994.

Ashley, P.M., & Chenhall, B.E., 1976 — Mylonitic rocks in the Young Granodiorite, southern New South Wales. *Journal and Proceedings, Royal Society of New South Wales*, 109, 25–33.

Bateman, P.C., & Chappell, B.W., 1979 — Crystallisation, fractionation, and solidification of the Tuolumne Intrusive Series, Yosemite National Park, California. *Geological Society of America Bulletin*, Part 1, 90, 465–482.

Blake, D.H., Bultitude, R.J., & Donchak, P.J.T., 1981 — Definitions of newly named and revised Precambrian stratigraphic and intrusive rock units in the Duchess and Urandangi 1:250 000 sheet areas, Mount Isa Inlier, northwestern Queensland. *Bureau of Mineral Resources, Australia, Report* 233; *BMR Microform* MF164.

Blake, D.H., Bultitude, R.J., & Donchak, P.J.T., 1982 — Dajarra, Queensland. *Bureau of Mineral Resources, Australia, 1:100 000 Geological Map Commentary.*

Bultitude, R.J., & Wyborn, L.A.I., 1982 — Distribution and geochemistry of volcanic rocks in the Duchess-Urandangi region, Queensland. *BMR Journal of Australian Geology & Geophysics*, 7, 99–112.

Bultitude, R.J., Blake, D.H., Donchak, P.J.T., & Mock, C.M., 1982 — Duchess Region, Queensland. *Bureau of Mineral Resources, Australia, 1:100 000 Geological Map Commentary.*

Carter, E.K., Brooks, J.H., & Walker, K.R., 1961 — The Precambrian mineral belt of northwestern Queensland. *Bureau of Mineral Resources, Australia, Bulletin* 51.

Chappell, B.W., 1978 — Granitoids from the Moonbi district, New England Batholith, eastern Australia. *Journal of the Geological Society of Australia*, 25, 267–283.

Chappell, B.W., 1979 — Granites as images of their source rocks. *Geological Society of America, 92nd Annual Meeting, Abstracts with Programs*, 11(7), 400.

Chappell, B.W., & White, A.J.R., 1974 — Two contrasting granite types. *Pacific Geology*, 8, 173–174.

Collins, W.J., Beams, S.D., White, A.J.R., & Chappell, B.W., 1982 — Nature and origin of A-type granites with particular reference to southeastern Australia. *Contributions to Mineralogy and Petrology*, 80, 189–200.

Compston, W., & Chappell, B.W., 1979 — Sr-isotope evolution of granitoid source rocks. *In* McElhinny, M.W. (editor), The Earth, its origin, structure and evolution. *Academic Press, London*, 377–426.

Cruikshank, B.I., Ferguson, J., & Derrick, G.M., 1980 — The association of uranium and skarn development in the Mary Kathleen area, Queensland. *In* Ferguson, J., & Goleby, A.B. (editors), Uranium in the Pine Creek Geosyncline. *International Atomic Energy Agency, Vienna*, 693–706.

Cumming, G.L., & Richards, J.R., 1975 — Ore lead isotope ratios in a continuously changing earth. *Earth and Planetary Science Letters*, 28, 155–171.

Day, H.W., & Brown, V.M., 1980 — Evolution of perthite composition and microstructure during progressive metamorphism of hypersolvus granite, Rhode Island, USA. *Contributions to Mineralogy and Petrology*, 72, 353–365.

De Paolo, D.J., 1981 — Neodymium isotopes in the Colorado Front Range and crust-mantle evolution in the Proterozoic. *Nature*, 291, 193–196.

Derrick, G.M., & Wilson, I.H., 1982 — Geology of the Alsace 1:100 000 Sheet area (6858), Queensland. *Bureau of Mineral Resources, Australia, Record* 1982/6 (unpublished).

Derrick, G.M., Wilson, I.H., Hill, R.M., Glikson, A.Y., & Mitchell, J.E., 1977 — Geology of the Mary Kathleen 1:100 000 Sheet area, northwest Queensland. *Bureau of Mineral Resources, Australia, Bulletin* 193.

Derrick, G.M., Wilson, I.H., & Sweet, I.P., 1980 — Quilalar and Surprise Creek Formations — new Proterozoic units from the Mount Isa Inlier: their regional sedimentology and application to regional correlations. *BMR Journal of Australian Geology & Geophysics*, 5, 215–223.

Ferguson, J., Chappell, B.W., & Goleby, A.B., 1980 — Granitoids in the Pine Creek Geosyncline. *In* Ferguson, J., & Goleby, A.B. (editors), Uranium in the Pine Creek Geosyncline. *International Atomic Energy Agency, Vienna*, 73–90.

Glikson, A.Y., 1980 — Precambrian sima-sial relations: evidence for earth expansion. *Tectonophysics*, 63, 193–234.

Griffin, T.J., White, A.J.R., & Chappell, B.W., 1978 — The Moruya Batholith and geochemical contrasts between the Moruya and Jindabyne suites. *Journal of the Geological Society of Australia*, 25, 235–247.

Hine, R., Williams, I.S., Chappell, B.W., & White, A.J.R., 1978 — Contrasts between I- and S-type granitoids of the Kosciusko Batholith. *Journal of the Geological Society of Australia*, 25, 219–234.

Jaques, A.L., Blake, D.H., & Donchak, P.J.T., 1982 — Regional metamorphism in the Selwyn Range area, northwestern Queensland. *BMR Journal of Australian Geology & Geophysics*, 7, 181–196.

Joplin, G.A., & Walker, K.R., 1961 — The Precambrian Granites of north-western Queensland. *Proceedings of the Royal Society of Queensland*, 72, 21–57.

Kerrich, R., Allison, I., Barnet, R.L., Moss, S., & Starkey, J., 1980 — Microstructural and chemical transformations accompanying deformation of granite in a shear zone at Mieville, Switzerland, with implications for stress corrosion cracking and superplastic flow. *Contributions to Mineralogy and Petrology*, 73, 221–242.

Krogh, T.E., 1973 — A low-contamination method for hydrothermal decomposition of zircon and extraction of U and Pb for isotopic age determination. *Geochimica et Cosmochimica Acta*, 37, 485–494.

Leake, B.E., 1978 — Nomenclature of amphiboles. *Canadian Mineralogist*, 16, 501–520.

Ludwig, K.R., 1980 — Calculation of uncertainties of U-Pb isotope data. *Earth and Planetary Science Letters*, 46, 212–220.

McDougall, I., Dunn, P.R., Compston, W., Webb, A.W., Richards, J.R., & Bofinger, V.M., 1965 — Isotopic age determinations on Precambrian rocks of the Carpentarian region, Northern Territory, Australia. *Journal of the Geological Society of Australia*, 12, 67–90.

McIntyre, G.A., Brooks, C., Compston, W., & Turek, A., 1966 — The statistical assessment of Rb-Sr isochrons. *Journal of Geophysical Research*, 71, 5459–5468.

Page, R.W., 1976 — Reinterpretation of isotopic ages from the Halls Creek Mobile Zone, northwestern Australia. *BMR Journal of Australian Geology & Geophysics*, 1, 79–81.

Page, R.W., 1978 — Response of U-Pb zircon and Rb-Sr total-rock and mineral systems to low-grade regional metamorphism in Proterozoic igneous rocks, Mount Isa, Australia. *Journal of the Geological Society of Australia*, 25, 141–164.

Page, R.W., in press — Timing of superposed volcanism in the Proterozoic Mount Isa Inlier, Australia.

Page, R.W., Compston, W., & Needham, R.S., 1980 — Geochronology and evolution of the late-Archean basement and Proterozoic rocks in the Alligator River Uranium Field, Northern Territory, Australia. *In* Ferguson, J., & Goleby, A.B. (editors), Uranium in the Pine Creek Geosyncline. *International Atomic Energy Agency, Vienna*, 39–68.

Perfit, M.R., Brueckner, H., Lawrence, J.R., & Kay, R.W., 1980 — Trace element and isotopic variations in a zoned pluton and associated volcanic rocks, Unalaska Island, Alaska: A model for fractionation in the Aleutian calcalkaline suite. *Contributions to Mineralogy and Petrology*, 73, 69–87.

Plumb, K.A., & Derrick, G.M., 1975 — Geology of the Proterozoic rocks of the Kimberley to Mount Isa region. *In* Knight, C.L. (editor), Economic geology of Australia and Papua New Guinea. Volume 1–Metals. *Australasian Institute of Mining and Metallurgy Monograph* 5, 217–252.

Plumb, K.A., Derrick, G.M., & Wilson, I.H., 1980 — Precambrian geology of the McArthur River-Mount Isa region, northern Australia. *In* Henderson, R.A., & Stephenson, P.J. (editors), The geology and geophysics of northeastern Australia. *Geological Society of Australia, Queensland Division, Brisbane*, 71–88.

Reed, S.J.B., & Ware, N.G., 1975 — Quantitative electron microprobe analysis of silicates using energy-dispersive X-ray spectrometry. *Journal of Petrology*, 16, 499–515.

Richards, J.R., Cooper, J.A., & Webb, A.W., 1963 — Potassium-argon ages on micas from the Precambrian region of northwestern Queensland. *Journal of the Geological Society of Australia*, 10, 299–312.

Shaw, D.M., 1960 — The geochemistry of scapolite, Part 1. Previous work and general mineralogy. *Journal of Petrology*, 1, 218–260.

Smith, T.E., Riddle, C., & Jackson, T.A., 1979 — Chemical variation within the Coast Plutonic Complex of British Columbia between latitude 53° and 55°N. *Geological Society of America Bulletin*, Part 1, 90, 346–356.

Steiger, R.H., & Jager, E., 1977 — Subcommission on geochronology: convention on the use of decay constants in geo- and cosmochronology. *Earth and Planetary Science Letters*, 36, 359–362.

Streckeisen, A.L., 1973 — Plutonic rocks. Classification and nomenclature recommended by the IUGS Subcommission on the systematics of igneous rocks. *Geotimes*, 18(10), 26–30.

Sweet, I.P., Mock, C.M., & Mitchell, J.E., 1981a — Seigal, Northern Territory and Hedleys Creek, Queensland. *Bureau of Mineral Resources, Australia 1:100 000 Geological Map Commentary.*

Sweet, I.P., Mock, C.M., & Mitchell, J.E., 1981b — Chemical analyses of igneous rocks from the Seigal and Hedleys Creek 1:100 000 Sheet areas, Northern Territory and Queensland. *Bureau of Mineral Resources, Australia, Report* 226; *BMR Microform* MF151.

Ware, N.G., 1981 — Computer programs and calibration with the PIBS technique for quantitative electron probe analysis using a lithium-drifted silicon detector. *Computers & Geoscience*, 7, 167–184.

Wetherill, G.W., 1956 — Discordant uranium-lead ages, 1. *Transactions of the American Geophysical Union*, 37, 320–326.

Whalen, J.B., Britten, R.M., & McDougall, I., 1982 — Geochronological and geochemistry of the Freida River Prospect Area, Papua New Guinea. *Economic Geology*, 77, 592–616.

White, A.J.R., Chappell, B.W., & Williams, I.S., 1976 — Berridale, New South Wales, 1:100 000 Geological Sheet. *Geological Survey of New South Wales, Sydney.*

Wilson, I.H., 1978 — Volcanism on a Proterozoic continental margin in northwestern Queensland. *Precambrian Research*, 7, 205–235.

Wilson, I.H., & Grimes, K.G., in press — Myally, Queensland. *Bureau of Mineral Resources, Australian 1:100 000 Geological Map Commentary.*

Wyborn, D., Chappell, B.W., & Johnston, R.M., 1981 — Three S-type volcanic suites from the Lachlan Fold Belt, southeast Australia. *Journal of Geophysical Research*, 86(B11), 10335–10348.

Wyborn, L.A.I., in preparation — Geochemical analyses of the Mount Isa Region. *Bureau of Mineral Resources, Australia, Report.*

York, D., 1969 — Least-squares fitting of a straight line with correlated errors. *Earth and Planetary Science Letters*, 5, 320–324.

Appendix 1. Analytical techniques

Geochronology

The Rb-Sr total-rock approach for the two Ewen Granite sites was based on clustered sampling, whereby different samples (shown by same number with different alphabetical suffixes) with a dispersion in Rb/Sr were collected from an area about 50 m across. Rb, Sr, and $^{87}Sr/^{86}Sr$ were measured by isotope dilution procedures, employing a mixed $^{85}Rb/^{84}Sr$ spike. The Rb-Sr isochron regression was carried out using McIntyre & others' (1966) program with coefficients of variation for x and y of 0.50 per cent and 0.015 per cent, respectively. Errors quoted for the Rb-Sr isochron results are at the 95 per cent confidence level.

The zircon separation, dissolution, anion-exchange chemistry, and mass spectrometry followed the techniques of Krogh (1973). Measurements were made on a 30-cm radius, 60°-sector Nuclide Analysis Associates machine. Blank levels and compositions are referred to in Table 3. A modified York (1969) program was used to statistically regress the U-Pb data, and the resultant uncertainties are quoted at the 2-sigma level, using estimated 2-sigma error assignments of 0.7 per cent for U/Pb ratios, 0.2 per cent for $^{207}Pb/^{206}Pb$ ratios, and a correlation coefficient of 0.96 derived from the treatment of Ludwig (1980). All ages referred to in this paper have been calculated using decay constants recommended in Steiger & Jager (1977).

Geochemistry

All major elements were analysed by x-ray fluorescence (XRF) at the Australian Mineral Development Laboratories (AMDEL). Most trace element analyses were carried out by the BMR laboratories, the remainder by AMDEL. Li, Co, Cr, Cu, Zn, and Ni were determined by atomic absorption spectrometry, the remaining trace elements by XRF, and H_2O^+, H_2O^- and CO_2 by gravimetric techniques.

Appendix 2. Kalkadoon Granodiorite (variation of published name/redefinition of Kalkadoon Granite by Carter & others, 1961)

Proposer. L.A.I. Wyborn

Definition approved. 15 February 1983

Derivation of name. Kalkadoon Copper Mine, ALSACE 1:100 000 Sheet area, grid reference 862092 (Carter & others, 1961)

Distribution. Extends in a narrow north trending belt, up to 15 km wide, for 200 km between Dobbyn and Dajarra on the ALSACE, PROSPECTOR, MARY KATHLEEN, DUCHESS, and DAJARRA 1:100 000 Sheet areas. Total outcrop area is 1280 km^2.

Type area. No type area nominated by Carter & others (1961). A lectostratotype has been designated on DAJARRA, at grid reference 542772, 0.5 km west of Dajarra–Boulia road, 25 km SSE of Dajarra. This locality is the U-Pb zircon age determination site, 79205309. 1 km to the east, the granodiorite intrudes undivided Tewinga Group, whilst 3 km west of the site, the granodiorite is unconformably overlain by Haslingden Group (Blake & others, 1982). The dominant rock type at the lectostratotype is a porphyritic granodiorite containing some mafic xenoliths. The locality is cut by dolerite dykes and aplite veins.

Lithology. The Kalkadoon Granodiorite is medium to coarse-grained and ranges from a K-feldspar-free tonalite, through granodiorite to monzogranite (IUGS nomenclature, Streckeisen, 1973) with granodiorite being the most abundant. Tonalites are even-grained, with K-feldspar forming sparse phenocrysts up to 1 cm long in the more felsic varieties. The more mafic granodiorites are strongly porphyritic, and contain K-feldspar phenocrysts up to 5 cm long. The phenocrysts decrease in abundance from the granodiorite into the monzogranite as the rocks become more even-grained. Most of the Kalkadoon Granodiorite has been regionally metamorphosed and primary igneous textures are rarely preserved.

Relationships. The Kalkadoon Granodiorite intrudes rocks of the Leichhardt Volcanics, Leichhardt Metamorphics, and undivided Tewinga Group. It is intruded by dolerite, Wills Creek Granite, Woonigan Granite and granophyre. It is unconformably overlain by rocks of the Bottletree Formation, Haslingden Group, and Quilalar and Surprise Creek Formations in the west (Bultitude & others, 1982; Blake & others, 1982; Derrick & others, 1980) and the Magna Lynn Metabasalt, Argylla Formation, and Mary Kathleen Group in the east (Plumb & others, 1980).

Age. Early Proterozoic. A U-Pb zircon age determination of 1856 $\pm$ ^{11} m.y. was obtained on a sample from the lectostratotype (Page & Wyborn, 1983). This is in agreement with a zircon age of 1862 $\pm$ ^{27} m.y. from samples on MARY KATHLEEN 1:100 000 Sheet area. All Rb-Sr age determinations are reset (Page, 1978).

Synonomy. Previously mapped as part of the Kalkadoon Granite (Carter & others, 1961).

Remarks. The original definition of Carter & others (1961) for the Kalkadoon Granite was essentially referring to a 'geographical entity' in which the granite was 'composite, containing rocks of different ages and compositions' (Carter & others, 1961, p. 143). Essentially, their definition was that of a granite batholith, i.e., a structural term. However, Carter & others (1961) and Joplin & Walker (1961) noted that the dominant phase within the Kalkadoon Granite was a granodiorite, intrusive into the Leichhardt Metamorphics. The name change proposed here, restricts the name Kalkadoon Granodiorite to a particular intrusive phase (aged between 1850 and 1870 m.y.) in which the dominant rock type is granodiorite. Although Derrick & others (1977) recorded a dominance of syenogranite, this result is at variance with the work of Carter & others (1961), Joplin & Walker (1961) and Wyborn & Page (1983). In the last study, rock nomenclature was based on accurate point counts made on 15 x 10 cm stained rock slabs, which, in view of the medium to coarse grain size and sometimes porphyritic rock types, would be more accurate than the estimated modal analyses on 5 x 2 cm thin sections used by Derrick & others (1977). The name Kalkadoon Granite of Carter & others (1961) is essentially synonomous with the structural term, Kalkadoon Batholith of Wyborn & Page (1983). Kalkadoon Batholith now encompases the proposed Kalkadoon Granodiorite and the One Tree, Woonigan, and Wills Creek Granites of Blake & others (1981).

References

Blake, D.H., Bultitude, R.J., & Donchak, P.J.T., 1981 — Definitions of newly named and revised Precambrian stratigraphic and intrusive rock units in the Duchess and Urandangi 1:250 000 Sheet areas, Mount Isa Inlier, northwestern Queensland. *Bureau of Mineral Resources, Australia, Report* 233; *BMR Microform* MF164.

Blake, D.H., Bultitude, R.J., & Donchak, P.J.T., 1982 — Dajarra, Queensland. *Bureau of Mineral Resources, Australia, 1:100 000 Geological Map Commentary.*

Bultitude, R.J., Blake, D.H., Donchak, P.J.T., & Mock, C.M., 1982 — Duchess Region Queensland. *Bureau of Mineral Resources, Australia, 1:100 000 Geological Map Commentary.*

Carter, E.K., Brooks, J.H., & Walker, R.R. 1961 — The Precambrian mineral belt of north-western Queensland. *Bureau of Mineral Resources, Australia, Bulletin* 51.

Derrick, G.M., Wilson, I.H., Hill, R.M., Glikson, A.Y., & Mitchell, J.E., 1977 — Geology of the Mary Kathleen 1:100 000 Sheet Area, northwest Queensland. *Bureau of Mineral Resources, Australia, Bulletin* 193.

Derrick, G.M., Wilson, I.H., & Sweet, I.P., 1980 — Quilalar and Surprise Creek Formations — new Proterozoic units from the Mount Isa Inlier: their regional sedimentology and application to regional correlations. *BMR Journal of Australian Geology & Geophysics*, 5, 215–223.

Joplin, G.A., & Walker, K.R., 1961 — The Precambrian granites of northwestern Queensland. *Proceedings of the Royal Society of Queensland*, 72, 21–57.

Page, R.W., 1978 — Response of U-Pb zircon and Rb-Sr total-rock and mineral systems to low-grade regional metamorphism in Proterozoic igneous rocks, Mount Isa, Australia. *Journal of the Geological Society of Australia*, 25, 141–164.

Plumb, K.A., Derrick, G.M., & Wilson, I.H., 1980 — Precambrian geology of the McArthur River–Mount Isa region, northern Australia. *In* Henderson, R.A., & Stephenson, P.J. (editors), The geology and geophysics of northeastern Australia. *Geological Society of Australia, Queensland Division, Brisbane*, 71–88.

Streckeisen, A.L., 1973 — Plutonic rocks. Classification and nomenclature recommended by the IUGS Subcommission on the systematics of igneous rocks. *Geotimes*, 18 (10), 26–30.

Wyborn, L.A.I., & Page, R.W., 1983 — The Proterozoic Kalkadoon and Ewen Batholiths, Mount Isa Inlier, Queensland: source, chemistry, age, and metamorphism. *BMR Journal of Australian Geology & Geophysics*, 8, this paper.

BMR Journal of Australian Geology & Geophysics, 8, 71-81

A NEW ANTIARCHAN FISH (PLACODERMI) FROM THE LATE DEVONIAN OF SOUTHEASTERN AUSTRALIA

G.C. Young

A new asterolepidoid antiarch is described from sediments of probable Late Devonian (Frasnian) age in the Boyd Volcanic Complex, on the south coast of New South Wales. It occurs as a rare element in an assumed freshwater assemblage with abundant *Bothriolepis* and *Phyllolepis*, and less common rhipidistian, acanthodian, and possible onychodontid remains. *Pambulaspis cobandrahensis* gen. et sp. nov. resembles *Remigolepis* in possessing separate posterior dorsolateral and lateral plates and a prominent postorbital crista, and resembles *Asterolepis* in having an elongate postorbital process and prominent subobstantic area, and lacking the posterior oblique pit-line groove in the adult. It differs from both in that the posterior dorsolateral completely overlaps the anterior median dorsal, and the lateral line canal crosses the posterior lateral plate instead of the posterior dorsolateral. The preorbital region of the skull, certain plates of the trunk, and the basic structure of the pectoral fin are not known. It is suggested that *Pambulaspis* is closely related to *Asterolepis* and *Remigolepis*, and may be a sister taxon to the latter. The most recent common ancestor of these genera must have been Eifelian or older.

Introduction

Diverse faunas of Devonian fishes were discovered in the Eden–Pambula area of southeastern New South Wales during detailed mapped of the area in 1978. The mapping was undertaken to investigate the relation between intrusive and extrusive igneous rocks and associated sediments of Mid-Late Devonian age, which are widespread in the region. A preliminary study of a small collection of fish material from eight new localities (Young, *in* Fergusson & others, 1979) indicated that four assemblages were probably represented, ranging in age possibly from the latest Middle Devonian (Givetian) through to the end of the Late Devonian (Famennian). The fact that the fishes occur stratigraphically above and below a marine formation with an invertebrate fauna of Frasnian age and that granites intruding the sequence have been dated isotopically suggested that more detailed study of the fishes might provide information of biostratigraphic significance. Accordingly, the area was revisited in 1979 and much new material was collected from the original and some additional localities. Elasmobranchs in this new collection from Bunga Head, north of Pambula, have recently been described (Young, 1982).

In this paper, a new antiarch belonging to the suborder Asterolepidoidei is reported from sediments of probable Frasnian age. The occurrence is of interest in filling out the record of this major subgroup of antiarchs in Australian rocks, a group that, until fairly recently, appeared to be poorly represented. Previous assignments include Hills' (1936, 1958) determination of an antiarch plate from Gilberton in Queensland as belonging to *Asterolepis*, although this specimen is not diagnostic and may belong instead to the much more common form, *Bothriolepis*. Other material from Western Australia (*see* Young, 1974, p. 252) can, however, be referred with confidence to the suborder, but the material is insufficient to determine conclusively whether it belongs to *Asterolepis* or *Remigolepis*. The latter genus, first described by Stensiö (1931) from near the top of the Devonian vertebrate succession in east Greenland, has been known to occur in Australia since Hills (1932) reported plates of a new species from the Upper Devonian Hervey Group (Connolly, 1965), north of Parkes in central western New South Wales. *Remigolepis* has since been reported (but not described) from other localities in southeastern Australia (Tomlinson, 1968; Young, 1974; Ritchie, 1975; Campbell & Bell, 1977), and it also occurs abundantly in the youngest known vertebrate horizon in the Eden–Pambula area (the Worange Point Formation; *see* Fergusson & others, 1979). These occurrences have generally been regarded as Late Devonian in age, by comparison with the European occurrences of *Remigolepis*, considered to be latest Late Devonian (Famennian) or even Early Carboniferous (e.g. Westoll, 1951, 1979; Jarvik, 1961; Andrews, 1978). However, the possibility of an earlier age for *Remigolepis* in Australia has not been discounted (Tomlinson, 1968; Young, 1974).

In Europe, the suborder Asterolepidoidei is also well represented in Middle Devonian deposits, but equivalent occurrences were unknown in Australia until fairly recently. Young & Gorter (1981) described a new form *Sherbonaspis hillsi* from a Middle Devonian fauna near Wee Jasper, New South Wales, and reported similar remains from the Broken River area of Queensland. The earliest known asterolepidoid occurrence in Australian rocks, and one of the earliest yet recorded, is from the Early Devonian of the Georgina Basin, central Australia (Young, in preparation). The new member of this group, described below as *Pambulaspis cobandrahensis* gen. et sp. nov., fills a gap between the Middle Devonian occurrences in New South Wales and Queensland and the Late Devonian *Remigolepis* occurrences of southeastern Australia.

Dermal bone terminology and antiarch classification used here generally follow those of Miles (1968). Measurement of dermal bones is in accordance with the system of Karatajute-Talimaa (1963). All described and figured specimens are deposited in the Commonwealth Palaeontological Collection (prefix CPC), housed in the Bureau of Mineral Resources, Canberra.

Stratigraphy

In a revision of previous stratigraphic schemes, based on more detailed mapping, Fergusson & others (1979) proposed a new stratigraphic unit, the Boyd Volcanic Complex, for the interbedded volcanic and sedimentary rocks of the Eden–Pambula area (Fig. 1). Of the nine facies identified within this complex, two contain fish faunas (Fig. 2). The age relation between these is uncertain; similar plants have been reported from both facies, but the fish faunas have few elements in common, and the Facies 2 fauna may be slightly older. The Boyd Volcanic Complex is overlain by sediments of the Merimbula Group, at some locations without apparent discordance, but elsewhere with a high angular unconformity. However, the fault movements that caused the unconformity were probably contemporaneous with deposition of the Boyd Volcanic Complex (Fergusson & others, 1979, p. 97). Three formations are recognised in the Merimbula Group (Fig. 2): the Bellbird Creek Formation contains a marine invertebrate fauna, including Frasnian brachiopods (Talent, 1969), and the overlying Worange Point Formation and underlying Twofold Bay Formation contain Late Devonian fish faunas. In the southern part of the area the Gabo Island Granite intrudes other facies of the Boyd Volcanic Complex, and is also overlain by

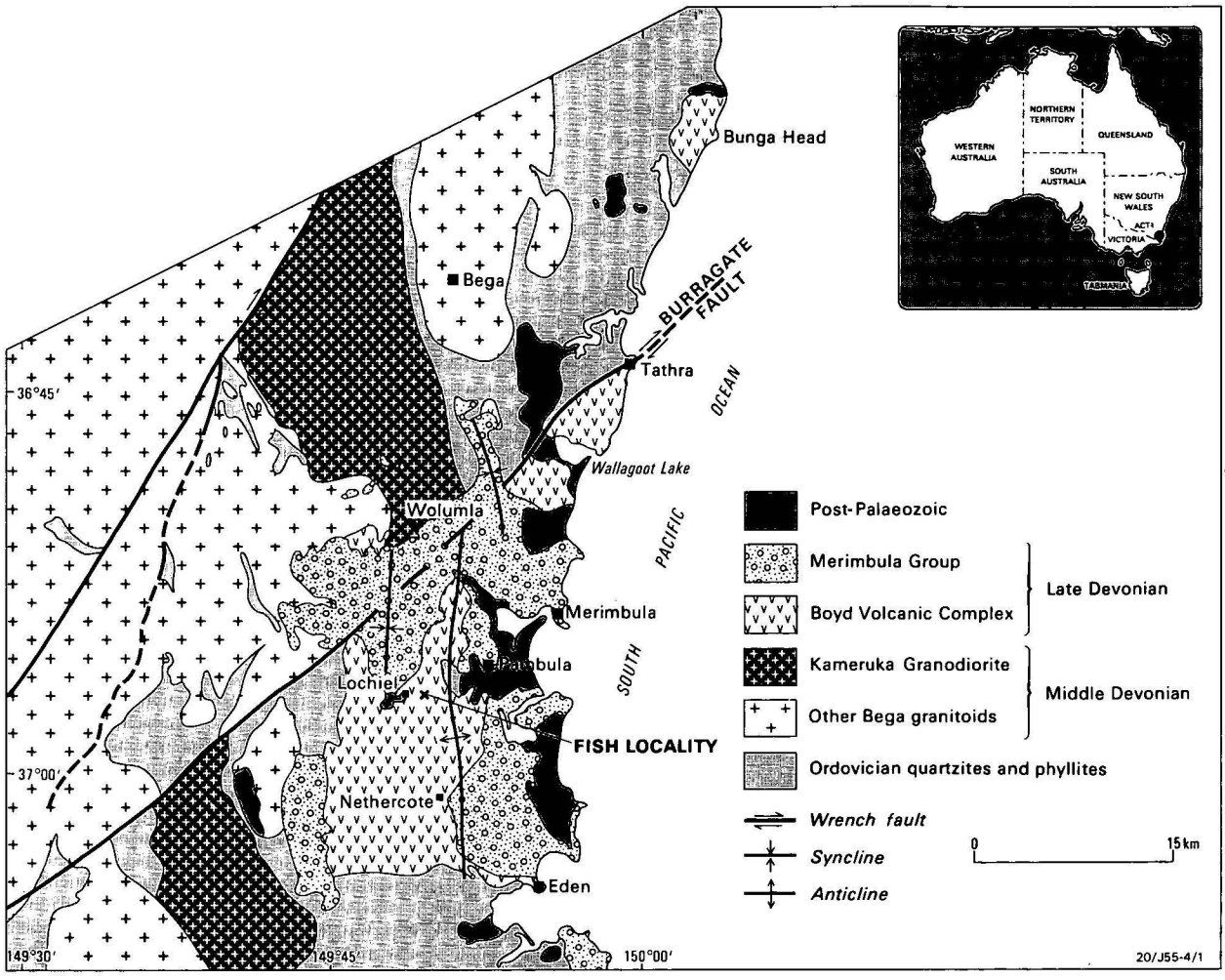

Figure 1. Regional geology of the Eden–Pambula District, south-eastern New South Wales (after Fergusson & others, 1979).

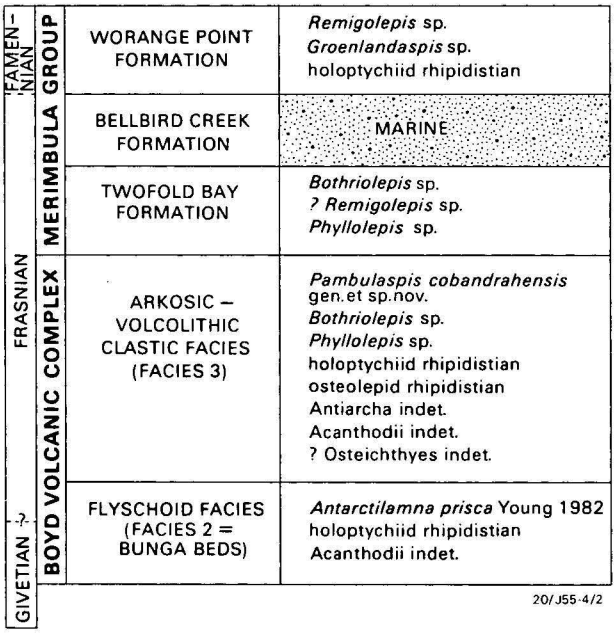

Figure 2. Summary of the stratigraphy and vertebrate faunas in the Middle (?) and Late Devonian rocks of the Eden-Pambula district.

sediments of the Merimbula Group. An isotopic age of 363 ± 12 m.y. for this intrusion (Fergusson & others, 1979) is not inconsistent with Ziegler's (1978, fig. 1) estimate of about 370 m.y. for the Givetian/Frasnian boundary.

The specimens described below come from Facies 3 of the Boyd Volcanic Complex, from the same locality (GR 7510E 59081N, Pambula 1:25 000 Sheet) that previously yielded *Bothriolepis* plates, remains of a smaller antiarch and a possible osteichthyan, and striated and tuberculate acanthodian spines (Fergusson & others, 1979, p. 103). The considerable quantity of new material from here, collected in 1979, has yielded much additional *Bothriolepis* material, abundant *Phyllolepis*, other indeterminate antiarch remains, acanthodian spines, osteolepid and holoptychiid rhipidistian remains, and other ornamented bones, referred to previously as osteichthyan (Fergusson & others, 1979), but which may be acanthodian (J. Long, Monash University, personal communication, 1982).

Current knowledge of the faunal content of vertebrate assemblages in the Eden–Pambula and Bunga Head regions is summarised in Figure 2. Only eight specimens of *Pambulaspis* have been identified in a collection of over 180 specimens, and it was a relatively rare element in the fish fauna.

Systematic palaeontology

Subclass Placodermi

Order Antiarcha

Suborder Asterolepidoidei Miles 1968

Definition. *See* Young & Gorter (1981, p. 100)

Genus *Pambulaspis* nov.

Pambulaspis cobandrahensis sp. nov.

Name. After the town of Pambula, and the Greek *aspis* (a shield). The fossil locality is on the property 'Cobandrah', about 5 km west of Pambula.

Holotype. CPC 22559, an incomplete skull-roof in part and counterpart.

Other material. Three anterior median dorsal plates (CPC 22560–22562), associated posterior dorsolateral and incomplete posterior lateral and posterior ventrolateral plates (CPC 22563), an isolated posterior lateral (CPC 22564), and a lateral marginal plate from the pectoral fin, (CPC 22565). An associated incomplete posterior ventrolateral and probable median ventral plate (CPC 22566) are tentatively referred to the species.

Locality. Grid reference 7510E 5908IN on the Pambula 1:25 000 Sheet, about 5 km west of Pambula, on the south coast of New South Wales, Australia.

Horizon and age. Facies 3 of the Boyd Volcanic Complex (Fergusson & others, 1979), probably Frasnian in age (early Late Devonian).

Diagnosis. An asterolepidoid antiarch of medium size, with trunk armour attaining a mid-dorsal length of about 130 mm. Skull-roof with convex posterior and narrow rostral margins, a relatively large orbital fenestra, and well-developed subobstantic and obtected nuchal areas. Breadth/length index of nuchal plate about 150. Lateral plate long and narrow. Endocranial postorbital process extending as far forward as the maximum width of the orbital fenestra. Postorbital crista strongly formed, and a prominent ventral process developed inside the anterior margin of the post-pineal plate. Anterior median dorsal plate with a breadth/length index ranging from 80 in small specimens to 55 in large, the anterior division of the plate slightly longer than the posterior, and a low median crest sometimes developed. Posterior dorsolateral plate with a breadth/length index of about 45, and posterior lateral plate slightly less than three times as long as deep. Ornament of tubercles normally coalesced into anastomosing ridges.

Remarks. In erecting the genus *Remigolepis*, Stensiö (1931) noted the following features by which it could be distinguished from *Asterolepis* Eichwald: the absence of a distal joint in the pectoral fin, the presence of separate posterior lateral and posterior dorsolateral plates instead of a single mixilateral, the overlap relations between the anterior median dorsal and posterior dorsolateral plates — with a prominent dorsal process on the latter — and the absence of median grooves, ridges, processes, tuberosities, or pits on the visceral surface of the anterior and posterior median dorsal plates. In other respects *Asterolepis* and *Remigolepis* exhibit a general similarity, and there are said to be fairly detailed resemblances in the preorbital region of the skull (Stensiö, 1931, pp. 31–34). Apart from Stensiö, most authors since Gross (1965) have accordingly regarded the two genera as closely related, on the assumption that the absence of the distal joint in the pectoral fin in *Remigolepis* is secondary. Unfortunately, the new material described here is insufficient to establish the presence or absence of a distal joint in the pectoral fin, and, otherwise, this new species exhibits characters previously regarded as typical of either *Asterolepis*, or *Remigolepis* together with several peculiarities of its own.

Points of resemblance with *Asterolepis* are the more elongate postorbital processes of the endocranium, the absence in the adult of posterior oblique pit-line grooves on the anterior median dorsal plate, the bilobed form of the paranuchal trochlea, the configuration of the posterolateral region of the skull, with well-developed subobstantic areas, and the grooves on the anterior median dorsal plate crossing the contact faces for the anterior dorsolaterals. However, information on the last three characters is not available for *Remigolepis*, and in the new Chinese species *R. zhongningensis*, the posterior oblique pit-line groove is said also to be weakly developed or absent (Pan & others, 1980), even though this groove is prominent in Greenland species of the genus.

In common with *Remigolepis* the new form described here has a strong postorbital crista and associated ventral process on the postpineal plate of the skull, and retains separately ossified posterior dorsolateral and lateral plates. In addition, openings for the endolymphatic ducts are not visible externally, although in *Remigolepis* this feature is poorly known. Other antiarchs and euarthrodires have separate posterior dorsolateral and lateral plates, which is, therefore, probably a primitive feature, and the same may apply to the postorbital crista, which is also well developed in *Yunnanolepis* (e.g. Liu, 1963). Neither character can, therefore, be used to proposed close affinity between *Remigolepis* and this new form. However, the pronounced rounded thickening on the visceral surface of the postpineal is a feature apparently absent in *Asterolepis* (e.g. Stensiö, 1931, fig. 12; Karatajute-Talimaa, 1963), but clearly developed in one well-preserved skull of *Remigolepis* (Stensiö, 1948, fig. 16).

Finally, the new form differs from both *Asterolepis* and *Remigolepis* in that the posterior dorsolateral overlaps the anterior median dorsal over the length of their common suture, and the main lateral line groove on the flank crosses the posterior lateral rather than the posterior dorsolateral. The former condition is seen in several other asterolepidoids (e.g. *Pterichthyodes, Gerdalepis, Sherbonaspis)*, but these are all forms with a short, high trunk-armour. The presence of the main lateral line groove on a discrete posterior lateral plate is, however, unique to this form, which I therefore propose as a new genus and species of asterolepidoid antiarch, possibly closely allied with *Remigolepis*.

Description. Of the skull-roof, only the postorbital region is known, although an impression of part of the anterior margin of the orbital fenestra is preserved. There is no information on the form of the rostral, pineal, and sclerotic plates. On the right side, the paranuchal and postmarginal plates have been broken away, and the specimen has been subject to some distortion. An attempted restoration is shown in Figure 3B & 3D. The posterior margin is gently convex, and the skull was apparently somewhat narrower anteriorly than in the postorbital region. In general shape it thus resembles particularly the skull of *Asterolepis* sp. figured by Murphy & others (1976) from the Late Devonian of Central Nevada. In other species of *Asterolepis* the rostral margin also tends to be narrower than the posterior margin, but the difference may be less pronounced (e.g. Karatajute-Talimaa, 1963). The skull-roof outline in *Remigolepis* is less well known (e.g. Stensiö, 1931), but published figures suggest that the orbital fenestra was relatively smaller than in *Pambulaspis*. Although the orbital fenestra is (*f. orb*) incompletely preserved, it is also clear that it was larger than the suborbital fenestra in *Pambulaspis*. This is a character that distinguishes both *Asterolepis* and *Remigolepis* from *Bothriolepis* (Stensiö, 1948, p. 48).

The unornamented obtected nuchal area (*nm*, Fig. 3B) is broadly developed, especially in the region of the nuchal plate.

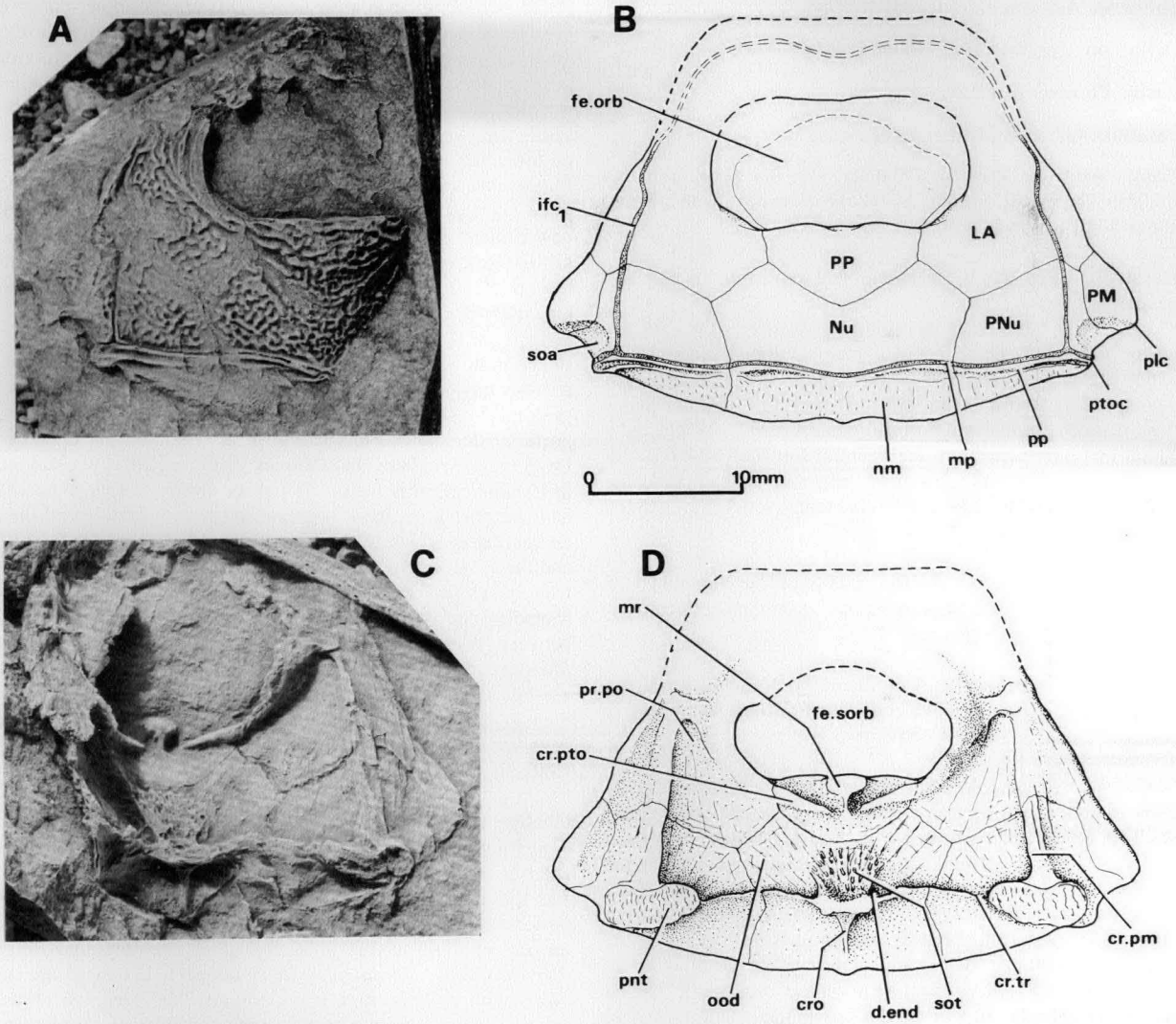

Figure 3. ***Pambulaspis cobandrahensis*** **gen. et sp.nov.**
The holotype, CPC 22559, an incomplete skull roof in dorsal (A) and ventral (C) views. B, D, restorations of the skull in dorsal and ventral views, based on the holotype. *cro*, median occipital crista; *cr.pm, cr.pto*, paramarginal and postorbital cristae; *cr.tr*, transverse nuchal crista; *d.end*, endolymphatic duct opening; *fe.orb*, orbital fenestra; *fe.sorb*, suborbital fenestra; ifc_1, infraorbital sensory groove; *LA*, lateral plate; *mp*, middle pit-line; *mr*, median thickening beneath postpineal plate; *nm*, obtected nuchal area; *Nu*, nuchal plate; *ood*, otico-occipital depression; *plc*, preobstantic corner; PM, postmarginal plate; *PNu*, paranuchal plate; *pnt*, paranuchal trochlea; *PP*, postpineal plate; *pp*, posterior pit-line; *pr.po*, postorbital process; *pt.oc*, postobstantic corner; *soa*, subobstantic area; *sot*, supraotic thickening.

It is noteworthy that in many species of *Asterolepis* this area is densely covered with ornament (e.g. Pan, 1964; Murphy & others 1976; Lyarskaya, 1981). Two transverse grooves cross the paranuchal and nuchal plates. The posterior one (*pp*) is distinct and continuous laterally, but less clearly defined on the nuchal plate. It lies along the anterior edge of the obtected nuchal area. The anterior groove (*mp*) lies at the posterior margin of the ornamented region of the skull, and passes laterally off the skull-roof in front of the postobstantic corner (*ptoc*). Following Stensiö's (1931) interpretation of similar grooves in *Asterolepis*, these are termed the middle and posterior pit-lines. The external openings of the endolymphatic ducts could not be discerned on the specimen. Only the posterior part of the infraorbital sensory groove is preserved (ifc_1). A noteworthy feature of the skull is the small but distinct subobstantic area (*soa*), which is similarly developed to this area in other asterolepidoids (e.g. Hemmings, 1978, fig. 1). The subobstantic area is not preserved in previously described *Remigolepis* material.

As restored, the nuchal plate has a breadth/length index estimated at 150, which is comparable to that in *Remigolepis zhongningensis* (*see* Pan & others, 1980), but broader than in some *Remigolepis* species from Greenland (e.g. *R. acuta, R. cristata*; see Stensiö, 1931). In another Greenland species (*R. kochi*) the nuchal is broader, and similar variation is seen in species of *Asterolepis* (e.g. Stensiö & Save-Söderbergh, 1938), although many species have comparable values to that reported here (e.g. *A. radiata, A. sinensis*; *see* Karatajute-Talimaa, 1963; P'an, 1964). The paranuchal and postpineal plates are similarly developed to other species in both genera. The posterolateral corner (*plc*) is not clearly preserved, but the postmarginal plate was probably less elongate than in *Asterolepis* or *Pterichthyodes* (e.g. Nilsson, 1941; Karatajute-Talimaa, 1963; Hemmings, 1978; Lyarskaya, 1981). This bone is poorly known in *Remigolepis* (Stensiö, 1931). Enough of the lateral plate is preserved to indicate its narrow form, as in some Greenland species of *Remigolepis* (Stensiö, 1931, pl. 4, fig. 2), although, in others, this plate was considerably broader (Stensiö, 1948, fig. 16; Pan & others, 1980). The lateral plate is also elongate in *Asterolepis*.

Structures on the visceral surface of the skull-roof are well displayed on the counterpart of the holotype (Fig. 3C, D). The

transverse nuchal crista (*cr.tr*) is strong, with a roughened elevation laterally (*pnt*), which in its bilobed form is reminiscent of the paranuchal trochlea in *Asterolepis ornata* (Karatajute-Talimaa, 1963, fig. 26). The median occipital crista (*cro*) is prominent, and the supraotic thickening (*sot*) forms an elevated area of cancellous texture in the centre of the nuchal plate. The internal endolymphatic duct openings occupy deep depressions lateral to the junction of this thickening with the transverse nuchal crista. Other prominent structures are the paramarginal and post-orbital cristae (*cr.pm, cr.pto*), which delineate the otico-occipital depression (*ood*). As previously reported for *Remigolepis* (Stensiö, 1931), this depression in *Pambulaspis* is much broader and deeper than in *Bothriolepis*. However, in *Pambulaspis* the anterolateral corner of the depression (*pr.po*), which housed the dorsal face of the endocranial postorbital process, extends farther forward than previously reported for *Remigolepis* (Stensiö, 1948, fig. 16). A more elongate postorbital process is also seen in *Asterolepis* (Stensiö, 1931; Karatajute-Talimaa, 1963). The postorbital crista is strongly developed on the visceral surface of the postpineal plate, which at its anterior margin bears a conspicuous thickening. Both features are typical of *Remigolepis* (Stensiö, 1948, fig. 16); in *Asterolepis* they are only slightly developed (Stensiö, 1931, fig. 12; Karatajute-Talimaa, 1963, pl. 8).

The trunk-shield of *Pambulaspis cobandrahensis* is represented by a small number of disarticulated plates. The three examples of the anterior median dorsal plate (Figs. 4, 5) differ considerably in size, and show some variation in morphology and proportions, which may be ontogenetic features. On available evidence the breadth/length index decreases considerably with size (Table 1), although the opposite trend has been recorded in *Bothriolepis* (Stensiö, 1948, p. 287), and in *Asterolepis* no such variation is evident (*see* Karatajute-Talimaa, 1963, p. 160). In the two smaller examples of this bone there is a low median crest developed behind the tergal angle. In the largest specimen, however, this crest is reduced to a prominent median dorsal ridge (Fig. 4A). A third feature possibly related to growth is the development of sensory grooves on the plate. In the smallest specimen the posterior and anterior oblique abdominal pit-line grooves are clearly seen (dlg_1, dlg_2, Fig. 4A), although the anterior one is manifested as a ridge rather than a groove. In the larger specimens these grooves are inconspicuous or absent. In *Bothriolepis* the strong development of the anterior pit-line groove is a juvenile character (Stensiö, 1948, p. 185), and the same can be assumed here. The poor development of the posterior oblique pit-line groove in the larger plates is in contrast to the situation in the Greenland species of *Remigolepis*, in which they are well developed (Stensiö, 1931). However, these grooves are also absent or poorly developed in the Chinese species *Remigolepis zhongningensis* (Pan & others, 1980). Both grooves are normally absent in *Asterolepis*, although there are exceptions (e.g. Karatajute-Talimaa, 1963, pl. 1, fig. 13; Lyarskaya, 1981, pl. 1, fig. 2).

In all three examples of this plate the anterior division is slightly longer than the posterior, the anterior and posterior margins are of similar length, and the tergal angle lies in the anterior half, but not the anterior third, of the plate. The broad anterior margin and the tendency to develop a low median dorsal crest are resemblances to the Greenland species *Remigolepis cristata* (Stensiö, 1931). The overlap area for the posterior dorsolateral plate (*oa. PDL*) is clearly developed in each specimen, but, in contrast to the situation in *Remigolepis*, it extends along the posterolateral margin almost to the lateral corner. This condition is typical of *Bothriolepis*, and amongst other asterolepidoids is seen in *Pterichthyodes* and *Sherbonaspis* (Hemmings, 1978; Young & Gorter, 1981). The remigolepid condition typical of species of *Remigolepis* occurs also in *Byssacanthus* and *Stegolepis*, and occasionally in *Sherbonaspis* and *Bothriolepis* (e.g. Miles, 1968). In *Asterolepis* the anterior median dorsal completely overlaps the posterior dorsolateral, whereas some of the Chinese yunnanolepids also have the remigolepid overlap arrangement (Zhang, 1978). The taxonomic significance of this character at the suprageneric level is obscure, but at least in *Remigolepis* it is consistently developed in all known species.

Other features of the anterior median dorsal in *Pambulaspis* include the slight postnuchal notch (*npn*) and external postlevator process (*pr.pl*; this feature is absent in CPC 22562), and on the visceral surface a distinct supranuchal area (*sna*) and postlevator thickening (*alr*). Beneath the external postlevator process on the visceral surface is a groove (*f*) on the contact face for the anterior dorsolateral plate, similar to that observed in the Baltic species *Asterolepis estonica* (Gross, 1940, p. 34; Karatajute-Talimaa, 1963, fig. 14). The presence or absence of this feature in the Greenland *Remigolepis* has not been determined (Stensiö, 1931).

The posterior dorsolateral plate is represented by one incomplete specimen from the right side, closely associated with incomplete right posterior lateral and posterior ventrolateral plates. These are assumed to come from the same individual. Total preserved length of the posterior dorsolateral is 60 mm. The relatively smaller anterior median dorsal plate from the same block (CPC 22561) is assumed to belong to a different individual. As restored (Fig. 7A), the posterior dorsolateral is fairly elongate, but proportions of this plate are known to vary considerably in species of *Remigolepis* (Stensiö, 1931, pp. 186, 191), so inclusion of this character in the diagnosis is only tentative. Some irregularities in the plate margins are due to oblique distortion, as evidenced by slight crenulations of the ornamented surface of the plate (Fig. 6A). These have been rectified in the reconstruction. Only one overlap area is well preserved on the specimen (*oa.PL*, Fig. 7A), but overlap areas for the posterior median dorsal and anterior dorsolateral plates have been restored after the condition in other asterolepidoid antiarchs. The small section of the overlap area for the anterior dorsolateral, as preserved near the anterodorsal corner (*adc*), has a plate margin that suggests it abutted against the contiguous plate without overlap. However, such a condition is not known in other forms, and further specimens are required to clarify this point of structure. Near its posterior end the ventral overlap area for the posterior lateral has a distinct notch (*vn*, Fig. 7A), as in *Remigolepis* (Stensiö, 1931, fig. 85). The contact face on the posterior lateral is correspondingly developed. A notable feature of the plate is the apparent absence of the sensory canals and pit-line grooves normally situated on the posterior dorsolateral in other placoderms. As described below, the lateral line groove is situated on the posterior lateral plate in *Pambulaspis*.

The external surface of the plate is gently arched dorsoventrally, without a clearly developed dorsolateral ridge or keel. The visceral surface is poorly preserved, the only significant feature being an impression of the crista transversalis interna posterior, which extends dorsally from the region of the ventral notch. The posterior margin of the plate is not well shown, but was, presumably, short.

The posterior lateral plate associated with the specimen just described is too fragmented to show details of structure, but in another specimen (CPC 22564) the morphology of this plate is well displayed, although again it is incomplete posteriorly (Figs. 6C, 6D, 7B, 7C). Total preserved length of this example is 52 mm. It comes from the right side, as indicated by the

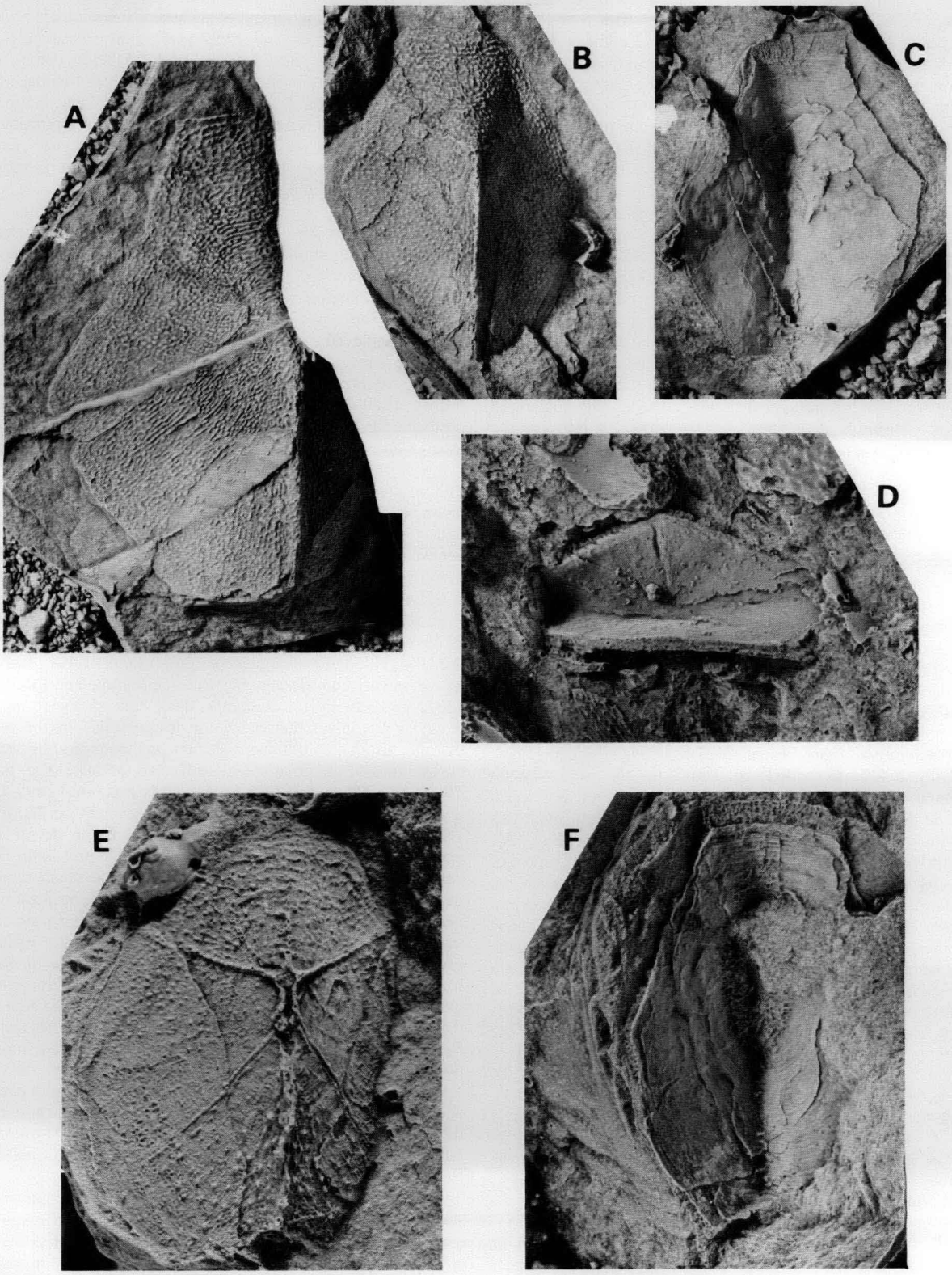

Figure 4. ***Pambulaspis cobandrahensis*** **gen. et sp.nov.**
A, anterior median dorsal plate in dorsal view, CPC 22562 (x1); B, C, anterior median dorsal in dorsal and ventral views, CPC 22561 (x 1.5); D, lateral marginal plate from the pectoral fin, CPC 22565 (x 3); E, F, anterior median dorsal in dorsal and ventral views, CPC 22560 (x 3).

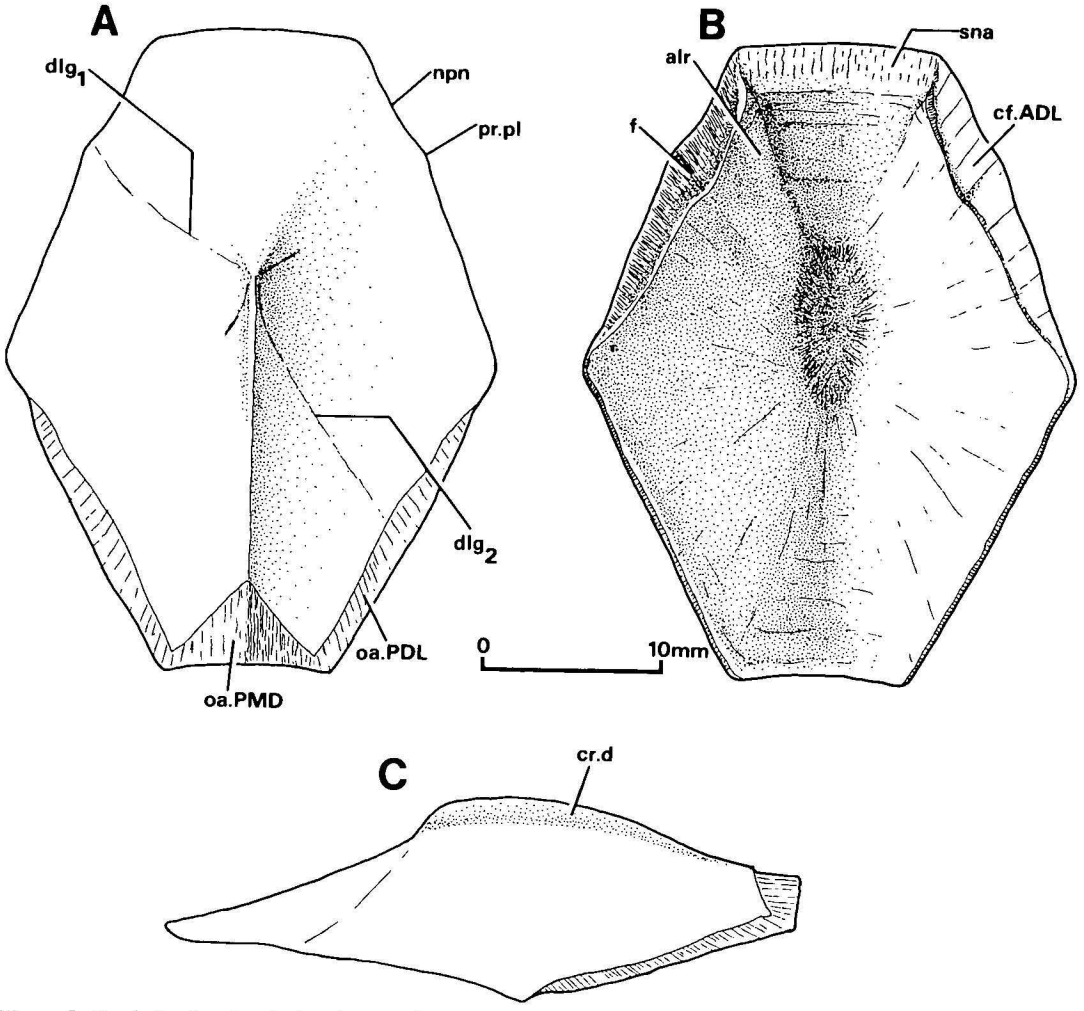

Figure 5. *Pambulaspis cobandrahensis* gen. et sp. nov.
Reconstruction of the anterior median dorsal plate in dorsal (A), ventral (B), and left lateral (C) views. After CPC 22560, 22561. *alr*, postlevator thickening; *cf.ADL*, contact face for anterior dorsolateral; *cr.d*, median dorsal crest; dlg_1,dlg_2, anterior and posterior oblique abdominal pit-line grooves; *f*, groove crossing contact face for anterior dorsolateral; *npn*, postnuchal notch; *oa.PDL*, *oa.PMD*, overlap areas for posterior dorsolateral and posterior median dorsal plates; *pr.pl*, postlevator process; *sna*, supranuchal area.

ventral overlap area for the posterior ventrolateral, and the dorsal contact face for the posterior dorsolateral (*oa.PVL*, *cf.PDL*, Figs. 7B, 7C). This overlap relation to the posterior dorsolateral and ventrolateral plates is also seen in some other antiarchs with a separate posterior lateral (e.g. Malinovskaya, 1973, fig. 3; Zhang, 1978, fig. 1), and in euarthrodires (e.g. Denison, 1958, fig. 111). It is likely, therefore, that this is the primitive relation between these plates in both groups. Other narrow overlap areas are developed anteriorly for the anterior dorsolateral and ventrolateral plates (*oa.ADL*, *oa.AVL*). The plate is slightly angled dorsoventrally about a line running from the presumed position of the dorsal angle (*d*) to the anterior margin, just ventral to the anterior corner (*arc*). However, no distinct keel or ridge is developed. On the visceral surface the dorsolateral and ventrolateral laminae of the plate are separated by a shallow depression, with an adjacent short ridge (*ri*. Fig. 7C) near the anterior margin.

Along the length of the preserved dorsal margin of this plate is a clearly defined sensory groove for the main lateral line canal (*lc*, Figs. 6C, 7B). In some other antiarchs (e.g. *Gerdalepis*, *Stegolepis*, *Sherbonaspis*) showing incipient fusion of the posterior dorsolateral and lateral plates to form a mixilateral, the sensory groove and the bone suture appear coincident (Gross, 1965; Malinovskaya, 1973; Young & Gorter, 1981). On the other hand, in the *Remigolepis* material described by Stensiö (1931) the sensory groove lies adjacent to the ventral margin of the posterior dorsolateral, thus retaining its primitive position. As noted above, sensory grooves are apparently completely absent from the posterior dorsolateral, and *Pambulaspis cobandrahensis* is, therefore, the only antiarch clearly showing displacement of the lateral line onto a separately ossified posterior lateral plate.

On the visceral surface of the plate (Fig. 7C) the contact face for the posterior dorsolateral is not clearly delineated, except posteriorly, where it is expanded to occupy the notch described above on the ventral margin of the posterior dorsolateral.

Little is known of the remaining plates of the trunk-shield in *Pambulaspis*. The posterior ventrolateral associated with the posterior dorsolateral described above is represented only by the anterior parts of its ventral and lateral laminae, which show no significant features. The second fragmentary posterior ventrolateral (CPC 22566) is only tentatively referred to this

Table 1. Measurements (in millimetres) and indices for three anterior median dorsal plates of *Pambulaspis cobandrahensis* gen. et sp. nov.

	CPC 22560	*CPC 22561*	*CPC 22562*
total length	18.8	36	80
total breadth	15	27	44
length of anterior division	10	18.5	43
length of anterior margin	7	10.5	37
breadth/length index	80	75	55

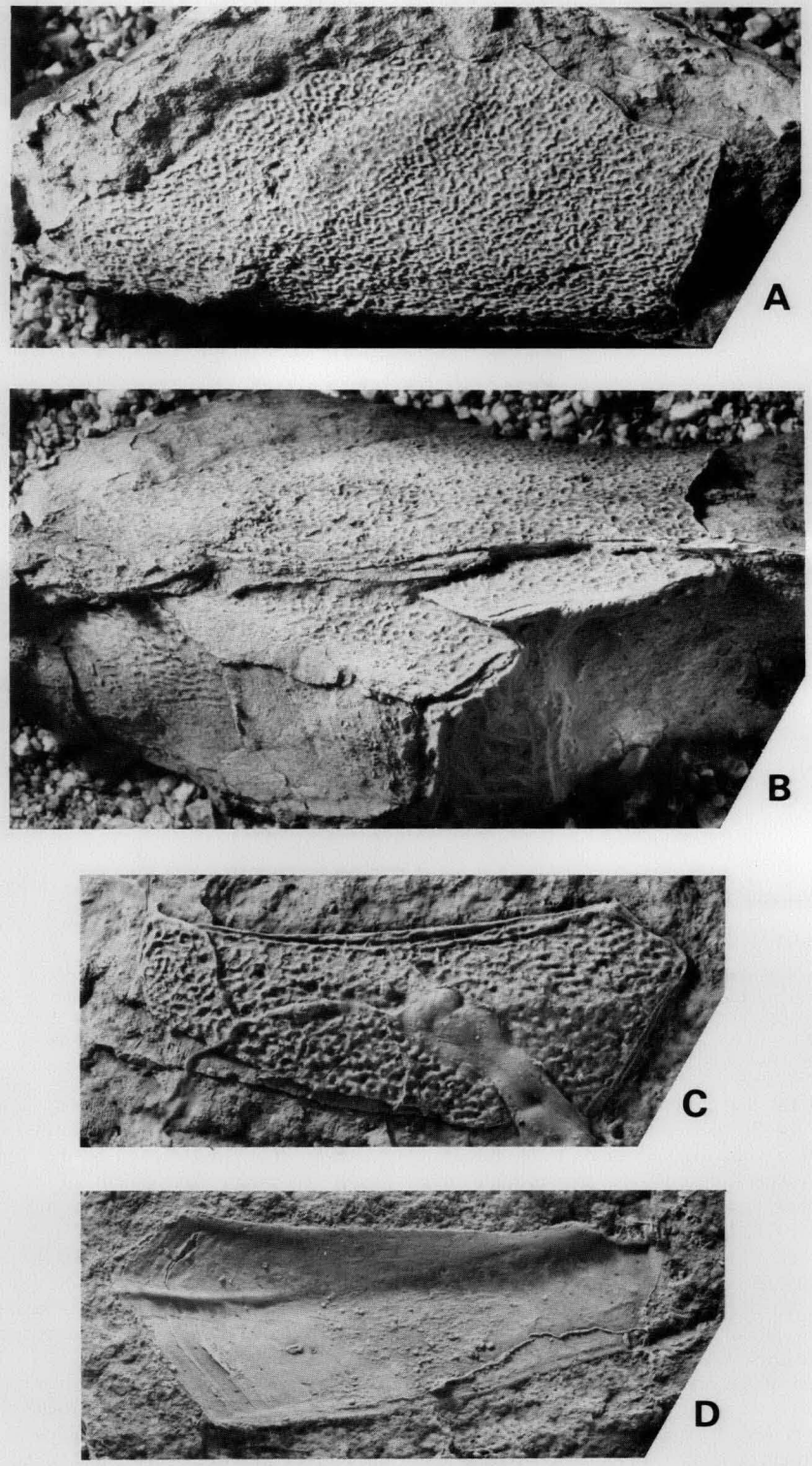

Figure 6. ***Pambulaspis cobandrahensis*** **gen. et sp. nov.**
A, right posterior dorsolateral plate, CPC 22563 (x 1.5). B, the same plate in ventral view, showing the overlap area for the posterior lateral plate, and part of this plate and the posterior ventrolateral (x 1.5). C, D, right posterior lateral plate in lateral and mesial views, CPC 22564 (x 1.5).

species on the basis of ornament (coarser than in the associated *Bothriolepis* material). The posterior margin of the lateral lamina, as preserved in this specimen, is normal to the ventrolateral ridge. The dorsal corner of the lateral lamina, and mesial and anterior margins of the ventral lamina are missing. Associated is another plate fragment, tentatively identified as a median ventral plate. The posterior median dorsal, anterior dorsolateral, anterior ventrolateral, and semilunar plates are unknown.

The pectoral fin is represented by a single disarticulated plate (Fig. 4D), probably the lateral marginal plate from a proximal pectoral fin segment. In its short, broad proportions, this plate is more reminiscent of *Pterichthyodes* than *Asterolepis* (e.g. Hemmings, 1978). However, it is also possible that the plate is one of a lateral marginal series, as occurs in *Remigolepis* (e.g. Stensiö, 1931, fig. 88). Thus, the important question of whether the pectoral fin had a distal joint cannot be answered on available evidence.

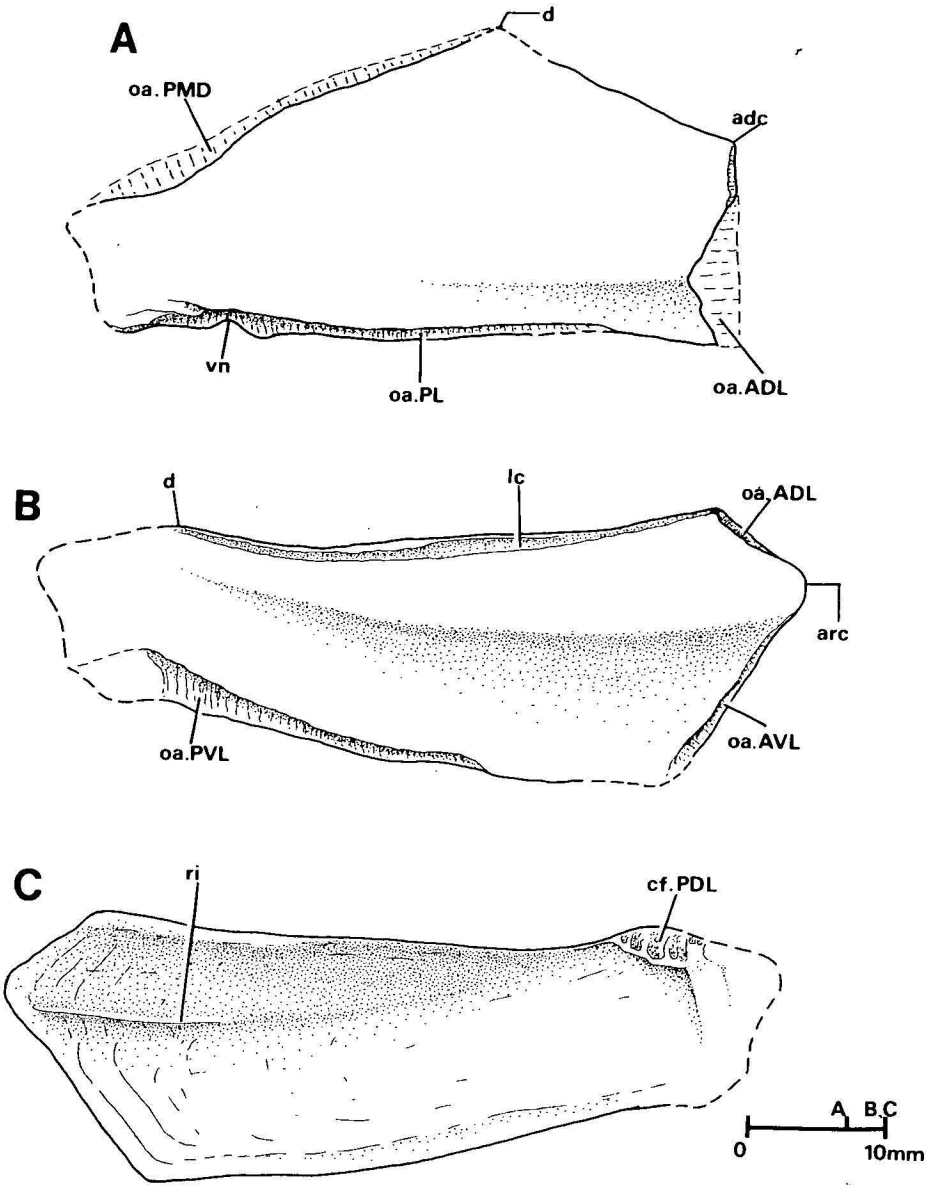

Figure 7. ***Pambulaspis cobandrahensis*** **gen. et sp. nov.**
A, reconstruction of posterior dorsolateral plate in lateral view, after CPC 22563. B, C, reconstruction of posterior lateral plate in lateral and mesial views, after CPC 22564. *adc*, anterodorsal corner; *arc*, anterior corner; *cf.PDL*, contact face for posterior dorsolateral; *d*, dorsal corner; *lc*, lateral line sensory groove; *oa.ADL*, *oa.AVL*, overlap areas for anterior dorsolateral and ventrolateral plates; *oa.PL*, *oa.PMD*, *oa.PVL*, overlap areas for posterior lateral, posterior median dorsal, and posterior ventrolateral plates; *ri*, ridge; *vn*, ventral notch.

The dermal ornament of *Pambulaspis cobandrahensis* typically forms short anastomosing ridges (Figs. 2, 4, 6). Similar ornament is seen in some species of *Asterolepis* (e.g. Pan, 1964), although, in others, the ornament tends to be coarser and more tuberculate (e.g. Wells, 1964; Murphy & others, 1976). The same applies to the various species of *Remigolepis*, described by Stensiö (1931). In one small plate of *Pambulaspis*, fine widely spaced tubercles are developed (Fig. 4E), and this is possibly a juvenile feature. In CPC 22562, a slight tendency to alignment of ridges is evident (Fig. 4A). The dermal ornament of *Pambulaspis* is generally readily distinguishable from the more delicate ornament of the associated *Bothriolepis* material.

Discussion

The antiarchs were one of the most successful and widespread groups of placoderm fishes, and have been recorded from Middle and Upper Devonian rocks in most regions of the world. An analysis of their distribution in space and time during the Devonian Period poses many problems of biostratigraphic and biogeographic importance (e.g. Young, 1981; Janvier & Pan, in press). In the European vertebrate succession, asterolepidoid antiarchs were predominant during the Middle Devonian (e.g. Young, 1974), but were apparently largely replaced in the Late Devonian by *Bothriolepis*. However, one asterolepidoid, *Remigolepis*, persisted in the Late Devonian of east Greenland and southeastern Australia, and has recently been reported also from Scotland (Andrews, 1978) and China (Pan & others, 1980). Another, *Asterolepis*, is now definitely known to range through to the late Frasnian in the Baltic succession (e.g. Lyarskaya, 1981), and it occurs in rocks of similar age in the United States (Wells, 1964; Murphy & others 1976; Gregory & others, 1977) and Iran (Janvier, 1979). However, the Chinese species *A. sinensis* P'an, 1964, is apparently of latest Devonian age (Pan, 1981).

As noted above, it has been suggested, on the basis of similarity in overall structure, that *Remigolepis* and *Asterolepis* are closely related, the former being derived from the latter (or

a close relative) by loss of the distal joint in the pectoral fin. One of the difficulties with this idea is that *Remigolepis* is more primitive than all known species of *Asterolepis*, in retaining separate posterior dorsolateral and lateral plates. The picture is further complicated by the fact that some Early Devonian antiarchs from Yunnan, China, also had an unjointed fin, said by Zhang (1978) to be similar in structure to that of *Remigolepis*. The detailed arrangement of plates in the yunnanolepid pectoral fin is not known, and there is no evidence on whether a ventral central series of plates was present, as in antiarchs generally, or whether this series was absent, as in *Remigolepis* (Stensiö, 1931). It has been argued, however, (Young & Gorter, 1981, p. 100) that acceptance of similarities in the preorbital region of the skull as shared specialisations of *Asterolepis* and *Remigolepis* implies that the unjointed pectoral fin in *Remigolepis* is a secondary condition. The new form, *Pambulaspis*, described here may be accommodated within this hypothesis as an assumed close relative of the most recent common ancestor of *Asterolepis* and *Remigolepis*. There is also some slight evidence (similar development of the visceral surface of the postpineal plate) suggesting a closer relation between *Pambulaspis* and *Remigolepis* than either has with *Asterolepis*. This suggestion would be confirmed by the demonstration that the pectoral fin in *Pambulaspis* lacks a distal joint, but would not be refuted if *Pambulaspis* was shown to possess such a joint, this feature then being interpretable as a symplesiomorphy of *Asterolepis* and *Pambulaspis*. However, the demonstration that in *Pambulaspis* the rostral region and jaws were specialised in the same way as in *Asterolepis* and *Remigolepis* would be important evidence corroborating the suggested close relationship between these three genera. Further information on the morphology of *Pambulaspis* is required to resolve these issues.

Since *Asterolepis* first occurs as early as Eifelian in the Baltic sequence (e.g. Lyarskaya, 1981), the above hypothesis implies also that the *Pambulaspis–Remigolepis* lineage must have differentiated in the Eifelian or earlier. Biogeographic considerations in relation to a period during which these groups were isolated from each other (perhaps the duration of the Middle Devonian) will be considered in detail elsewhere.

Acknowledgements

I thank R.W. Brown for assistance in collecting and curating the material, and W. Peters for carrying out the preparation work and photographing the specimens. Professor K.S.W. Campbell kindly read and commented on the manuscript.

References

Andrews, S.M., 1978 — A possible occurrence of *Remigolepis* in the topmost Old Red Sandstone of Berwickshire. *Scottish Journal of Geology*, 14, 311–315.

Campbell, K.S.W., & Bell, M.W., 1977 — A primitive amphibian from the Late Devonian of New South Wales. *Alcheringa*, 1, 369–381.

Conolly, J.R., 1965 — The stratigraphy of the Hervey Group in central New South Wales. *Journal and Proceedings of the Royal Society of New South Wales*, 98, 37–84.

Denison, R.H., 1958 — Early Devonian fishes from Utah. 3. Arthrodira. *Fieldiana: Geology*, 11, 461–551.

Fergusson, C.L., Cas, R.A.F., Collins, W.J., Craig, G.Y., Crook, K.A.W., Powell, C.McA, Scott, P.A., & Young, G.C., 1979 — The Late Devonian Boyd Volcanic Complex, Eden, N.S.W. *Journal of the Geological Society of Australia*, 26, 87–105.

Gross, W., 1940 — Acanthodier und Placodermen aus *Heterostius*-Schichten Estlands und Lettlands. *Annales Societatis rebus naturae Investigandis in universitate Tartuensi constituae*, 46, 1–88.

Gross, W., 1965 — Über die Placodermen-Gattungen *Asterolepis* und *Tiaraspis* aus dem Devon Belgiens und einen fraglichen *Tiaraspis*-Rest aus dem Devon Spitzbergens. *Institut royal des Sciences naturelles de Belgique, Bulletin* 41, 1–19.

Gregory, J.T., Morgan, T.G., & Reed, J.W., 1977 — Devonian fishes in central Nevada. *In* Murphy, M.A., Berry, W.B.N., & Sandberg, C.A. (editors). Western North America: Devonian. *University of California Riverside campus Museum contribution*, 4, 112–120.

Hemmings, S.K., 1978 — The Old Red Sandstone antiarchs of Scotland: *Pterichthyodes* and *Microbrachius*. *Palaeontological Society (Monograph)*, 131, 1–64.

Hills, E.S., 1936 — Records and descriptions of some Australian Devonian fishes. *Proceedings of the Royal Society of Victoria*, 48(N.S.), 161–171.

Hills, E.S., 1958 — A brief review of Australian fossil vertebrates. *In* Westoll, T.S. (editor). Studies on fossil vertebrates. *Athlone Press, London*.

Janvier, P., 1970 — Les vertébres Dévoniens de l'Iran central. 3: Antiarches. *Geobios*, 12, 605–608.

Janvier, P., & Pan, J., in press — *Hyrcanaspis bliecki* n.g., n.sp., a new primitive euantiarch (Antiarcha, Placodermi) from the Eifelian of Northeastern Iran, with a discussion on antiarch phylogeny.

Jarvik, E., 1961 — Devonian vertebrates. *In* Raasch, G.O. (editor). Geology of the Arctic. *University of Toronto Press*. 197–204.

Karatajute-Talimaa, V.N., 1963 — Genus *Asterolepis* from the Devonian of the Russian Platform. *In* Grigelis, A., & Karatajute-Talimaa, V. (editors). The data of geology of the Lithuania. *Geological and Geographical Institute of the Academy of Sciences of the Lithuanian SSR, Vilnius*. 65–223 (in Russian with English summary).

Liu, Y-H., 1963 — On the Antiarchi from Chutsing, Yunnan. *Vertebrata PalAsiatica*, 7, 39–46.

Lyarskaya, L., 1981 — Baltic Devonian Placodermi. Asterolepididae. *Zinatne, Riga* (in Russian with English abstract).

Malinovskaya, S.P., 1973 — *Stegolepis* (Antiarchi, Placodermi), a new Middle Devonian genus from Central Kazakhstan. *Paleontological Journal*, 7, 189–199.

Miles, R.S., 1968 — The Old Red Sandstone antiarchs of Scotland. Family Bothriolepididae. *Palaeontographical Society (Monograph)*, 122, 1–130.

Murphy, M.A., Morgan, T.G., & Dineley, D.L., 1976 — *Astrolepis* sp. from the Upper Devonian of central Nevada. *Journal of Paleontology*, 50, 467–471.

Nilsson, T., 1941 — The Downtonian and Devonian vertebrates of Spitsbergen. 7. Order Antiarchi. *Skrifter om Svalbard og Ishavet*, 82, 1–54.

P'an Kiang, 1964 — Some Devonian and Carboniferous fishes from South China. *Acta palaeontologica Sinica*, 12, 139–183 (in Chinese and English).

Pan Jiang, 1981 — Devonian antiarch biostratigraphy of China. *Geological Magazine*, 118, 69–75.

Pan Jiang, Wang Shitao, Liu Shiyu, Gu Qichang, & Jia Hang, 1980 — Discovery of Devonian *Bothriolepis* and *Remigolepis* in Ningxia. *Acta Geologica Sinica*, 3, 176–185 (in Chinese with English abstract).

Ritchie, A., 1975 — *Groenlandaspis* in Antarctica, Australia and Europe. *Nature*, 254, 569–573.

Stensiö, E.A., 1931 — Upper Devonian vertebrates from East Greenland, collected by the Danish Greenland Expedition in 1929 and 1930. *Meddelelser om Gronland* 86, 1–212.

Stensiö, E.A., 1948 — On the Placodermi of the Upper Devonian of East Greenland. 2. Antiarchi: subfamily Bothriolepinae. With an attempt at a revision of the previously described species of that family. *Meddelelser om Gronland*, 139 (*Palaeozoologica Groenlandica*, 2), 1–622.

Stensiö, E.A., & Säve-Söderbergh, G., 1938 — Middle Devonian vertebrates from Canning Land and Wegener Peninsula (east Greenland). Part 1, Placodermi, ichthyodorulithes. *Meddelelser om Gronland*, 96, 1-38.

Talent, J., 1969 — The geology of east Gippsland. *Proceedings of the Royal Society of Victoria*, 82, 37–60.

Tomlinson, J.G., 1968 — A new record of *Bothriolepis* in the Northern Territory of Australia. *Bureau of Mineral Resources, Australia, Bulletin* 80, 191–224.

Wells, J.W., 1964 — The antiarch *Asterolepis* in the Upper Devonian of New York. *Journal of Paleontology*, 38, 492–495.

Westoll, T.S., 1951 — The vertebrate-bearing strata of Scotland. *International Geological Congress, 1948*, 18(2), 5–20.

Westoll, T.S., 1979 — Devonian fish biostratigraphy. *In* House, M.R., Scrutton, C.T., & Bassett, M.G. (editors). The Devonian System. *Special Papers in Palaeontology*, 23, 341–353.

Young, G.C., 1974 — Stratigraphic occurrence of some placoderm fishes in the Middle and Late Devonian. *Newsletters on Stratigraphy*, 3, 243–261.

Young, G.C., 1981 — Biogeography of Devonian vertebrates. *Alcheringa*, 5, 225–243.

Young, G.C., 1982 — Devonian sharks from southeastern Australia and Antarctica. *Palaeontology*, 25, 817–843.

Young, G.C., in preparation — An asterolepidoid antiarch (placoderm fish) from the Early Devonian of the Georgina Basin, central Australia. *Alcheringa*.

Young, G.C., & Gorter, J.D., 1981 — A new fish fauna of Middle Devonian age from the Taemas/Wee Jasper region of New South Wales. *Bureau of Mineral Resources, Australia, Bulletin*, 209, 83-147.

Zhang Guorui, 1978 — The antiarchs from the Early Devonian of Yunnan. *Vertebrata PalAsiatica*, 16, 147–186 (in Chinese with English summary).

Ziegler, W., 1978 — Devonian. *In* Cohee, G.V., Glaessner, M.F., & Hedberg, H.D. (editors), Contributions to the geological time scale. *American Association of Petroleum Geologists, Studies in Geology*, 6, 337-339.

BMR Journal of Australian Geology & Geophysics, 8, 83-87

DESERT VARNISH COATINGS AND MICROCOLONIAL FUNGI ON ROCKS OF THE GIBSON AND GREAT VICTORIA DESERTS, AUSTRALIA

J.T. Staley[1], M.J. Jackson[2], F.E. Palmer[1], J.B. Adams[3], D.J. Borns[3,4], B. Curtiss[3], & S. Taylor-George[3]

Desert varnish coatings rich in manganese are reported, to the authors' knowledge, for the first time on desert rocks from Australia. Varnish was found on chert, dolomite, sandstone, siltstone, and conglomerate rocks in stony pavements of the Gibson Desert and the Great Victoria Desert of Western Australia and South Australia. The widespread occurrence of desert pavements in Australia suggests that desert varnish, also, may be widespread. Fungi that form microcolonies have been found on rocks with desert varnish. Manganese was found in higher concentrations inside some of the microcolonies than in the surrounding substrate, suggesting that microcolonial fungi are involved in the formation of desert rock varnish in these areas.

Introduction

According to Potter & Rossman (1977, 1979), there are two types of desert varnish, a coating found on rocks from desert regions. The most common type is reddish orange in appearance and contains iron oxides mixed with clay minerals. Darker coatings that contain, in addition, high concentrations of manganese oxides have a more limited distribution. Manganese-rich desert varnishes have been reported to occur in many of the desert regions of the world, including the Negev and Sinai deserts of the Middle East (Humboldt, 1793; Krumbein & Jens, 1981), the Mojave Desert (Laudermilk, 1931; Engel & Sharp, 1958) and the Sonoran Desert of the southwestern United States (Perry & Adams, 1978) and northwestern Mexico (Hayden, 1976), the Gobi Desert of China, and the Sahara Desert of northern Africa (Lucas, 1905). Recently, manganese-deficient desert varnish has been reported in Antarctica, (Glasby & others, 1981).

In this paper the occurrence of manganese-rich desert varnish in the Gibson and Great Victoria deserts of Western Australia and South Australia is documented. In addition, evidence is submitted that implicates microcolonial fungi in the formation of some of these varnish coatings.

Method of study

The samples were collected in 1971 and 1972 during regional geological mapping of the Gibson and Great Victoria Deserts (Fig. 1) by the Bureau of Mineral Resources and Geological Survey of Western Australia, jointly (Jackson & van de Graaff, 1981; Jackson & Muir, 1981). Over 1500 samples were collected, but, at the completion of the program, the collection was reduced to about 300 samples, which were retained as a set representative of bedrock lithology and surface weathering textures. The collection was re-examined in 1980, when this study of desert varnish in Australia was initiated. About 50 of the specimens showed various forms of case-hardening, ferruginous or siliceous skins, or manganiferous surfaces. Twenty were selected for study, being chosen to cover a range of bedrock ages (mid-Proterozoic to Tertiary), rock types (volcanic, sedimentary), and types of varnish (thin brown coatings to thicker black shiny surfaces).

[1]Department of Microbiology and Immunology, and [3]Department of Geological Sciences, University of Washington, Seattle, U.S.A.; [2]Bureau of Mineral Resources, Geology and Geophysics, Canberra; [4]Present address: Sandia National Laboratories, Albuquerque, New Mexico, U.S.A. 87185

Chips from the rocks were mounted on scanning electron microscope (SEM) stubs with low resistance contact cement. Critical-point drying was found not to be necessary for the preservation of biological structures on these specimens. The samples were then sputter-coated with palladium and examined in a Cambridge S4-10 SEM equipped with an energy dispersive X-ray analyser (EDAX).

Portions of coating were scraped from the rock surface, placed on solidified water agar (1.5%) in petri dishes, and tested for manganese, using the benzidine reaction (Feigl, 1958). Positive reactions for manganese were recorded when blue, indicative of Mn IV, diffused into the agar from the scrapings. The presence of manganese was independently confirmed in many samples by SEM-EDAX analyses.

Small black, globular structures found on the rocks resemble microcolonial fungi that have been recently reported from rocks in other desert regions (Staley & others, 1982). Individual structures, which are generally less than 100 μm in diameter, were picked from some of the specimens, using 40-mm, 26 gauge inoculating needles under a dissecting microscope at 30x or 60x magnification. These were fixed with osmium tetroxide in 0.1 M cacodylate buffer (pH 7.0), dehydrated in acetone, and embedded in an Epon 812-815 mixture. Thin sections were cut with a Zeiss Ultramicrotome, stained with lead citrate, and examined at 60 kV in a Jeol JEM 100 B transmission electron microscope (Staley & others, 1982).

Results

The chemical and SEM-EDAX analyses indicate that many of the dark coatings contain manganese (Table 1) as well as iron and other elements indicative of varnish. Proterozoic rocks from near the margins of the sampled area have the best-developed desert varnish. All five samples from the mid-Proterozoic Bangemall Basin, on the northwest margin of the area, contained desert varnish. These included chertified carbonates from the Skates Hills Formation, feldspathic sandstone from the Durba Sandstone, and a dolerite sample from a sill intruding the sequence. Proterozoic conglomerate, sandstone, and siltstone from the Townsend Quartzite and Punkerri Beds of the Officer Basin sequence in the eastern part of the area also had good desert varnish coatings, as did a sample of Proterozoic brecciated chert from the rimrocks of a salt diapir at Woolnough Hills in the far north of the region.

In contrast to the Proterozoic samples, the Phanerozoic samples collected showed less impressive development of desert

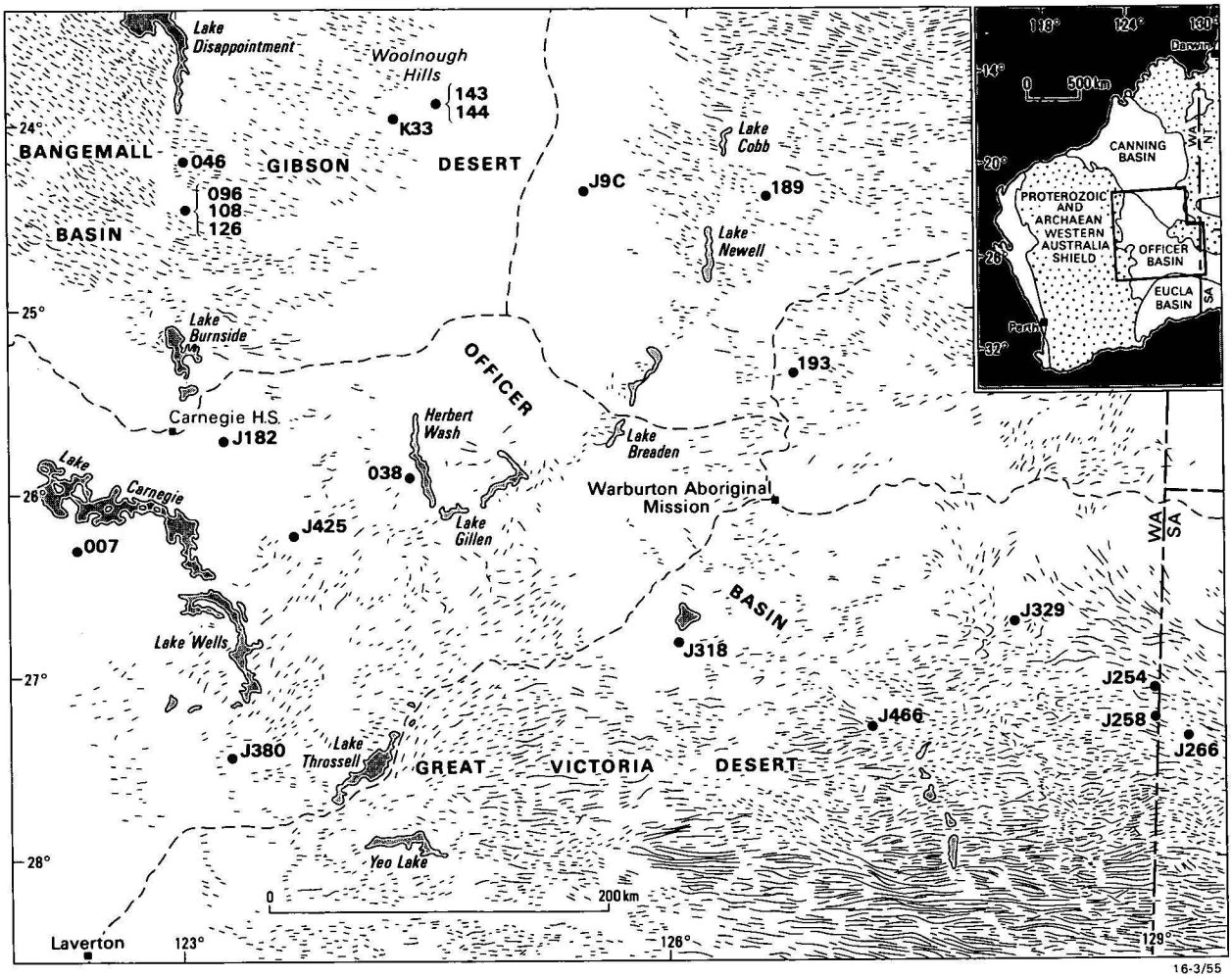

Figure 1. Map showing location of Gibson and Great Victoria Deserts in which rock specimens (identified by number) were collected.

varnish (Table 1). A manganese-enriched coating from a basalt sample was collected from the Early Cambrian Table Hill Volcanics of the Great Victoria Desert, but only two of the six specimens from the Permian Paterson Formation had significant amounts of manganese.

The appearance of the varnish on these Australian rocks is quite distinctive. The black areas that are manganese-rich appear most commonly as patches over the surface of the rock; in some places these overlap to form a confluent black area (Fig. 2). The patches are generally round and range in diameter from less than 1 mm to several mm. The appearance is almost as if black paint were spattered over the surface by the flicking of a brush. The varnish coatings appear to overlie an almost uniform coating of hematite.

Lichens were found only rarely on the varnished specimens examined and algal growth was uncommon. However, we frequently observed microscopic black, globular structures (10–100 μm across), which resemble the microcolonial fungi recently reported to occur on desert rock surfaces (Staley & others, 1981). To test whether or not these were indeed microorganisms, they were picked from the rock, embedded in Epon resins, and sectioned for observation with the transmission electron microscope. Their ultrastructural appearance is identical to that of the known microcolonial fungi. The most distinctive feature is the concentric body that is uniquely associated with certain fungi (Griffiths & Greenwood, 1972; Samuelson & Bezerra, 1977). Also, we have cultivated fungi from the microcolonial structures on rocks collected in August 1981 from the same area. The discovery of microcolonial fungi associated with desert varnish in these Australian rocks is consistent with the finding of microcolonial fungi and desert varnish in the southwestern United States, the Sahara Desert in Egypt, and the Gobi Desert in China.

Evidence that microcolonial fungi on the surface of these Australian rocks are involved in manganese accumulation and, hence, desert varnish formation has been obtained from SEM-EDAX analyses. Five rocks were carefully examined (Table 2). In all cases we examined rocks that contained both varnish patches and fungal microcolonies, but for these studies we confined the SEM-EDAX analyses to areas on the rock that were away from a macroscopic patch of varnish (for example, the circled area in Figure 2). We then compared the concentration of manganese within the microcolony with that outside the microcolony (Table 2; Fig. 3). Manganese is present in the microcolony, but was not detected in the areas immediately next to it. Not all microcolonies away from macroscopic patches of varnish contain manganese, and it is not known whether this is due to variations in species composition, physiological state, or some other factor. Microcolonial fungi were also found within the macroscopic patches of varnish.

Discussion

Although siliceous skins on Australian silcretes have received some study (Hutton & others, 1972, Milnes & Hutton, 1974),

Table 1. Manganese analyses and description of rock specimens with black coating obtained from the Gibson and Great Victoria Deserts.

BMR registration number	*Field collection number*	*Stratigraphy*		*Rock type*	*Manganese analysis**	
		Formal Name	*Age*		*SEM-EDAX*	*Chemical*
71880007	None	Unnamed	Middle Proterozoic	Dolerite	+	+
72880038	J111	Table Hill Volcanics	Lower Cambrian	Porous fine-grained sandstone	N.A.	+
72880046	None	Durba Sandstone	Middle Proterozoic	Pink feldspathic sandstone	N.A.	+
72880096	J134	Skates Hill Formation	Proterozoic	Chertified stromatolitic carbonate	+	+
72880108	K73	Skates Hill Formation	Proterozoic	Vuggy chertified sandy carbonate	N.A.	+
72880126	J132	Skates Hill Formation	Proterozoic	Chertified silty carbonate	+	+
72880143	J28	Woolnough Beds	Proterozoic	Dolomite/chert breccia	N.A.	+
72880144	J30	Madley Beds	Proterozoic	Chalcedonic ferruginous silt	—	—
72880189	J123	Paterson Formation	Lower Permian	Intensely ferruginised sandstone	N.A.	—
72880193	J52	Paterson Formation	Lower Permian	Intensely ferruginised sandstone	N.A.	—
None	J9c	Samuel Formation	Lower Cretaceous	Silicified fine sandstone	N.A.	—
None	J182	Paterson Formation	Lower Permian	Silicified burrowed clayey fine sandstone	+	+
None	J254	Townsend Quartzite	Proterozoic	Ferruginous conglomerate	+	+
None	J258	Punkerri Beds	Proterozoic	Coarse silicified sandstone	+	+
None	J266	Punkerri Beds	Proterozoic	Silicified sandstone and siltstone	+	+
None	J329	Table Hill Volcanics	Lower Cambrian	Purple basalt	N.A.	+
None	J380	'Silcrete'	Tertiary	Silicified angular quartz wacke	+	+
None	J425	Paterson Formation	Lower Permian	Silicified coarse sandstone with siltstone clast	N.A.	+
None	J466	Lennis Sandstone	Cambrian	Fine-grained silicified sandstone	N.A.	—

* + manganese detected.
— manganese not detected by the method used.
N.A. Not analysed.

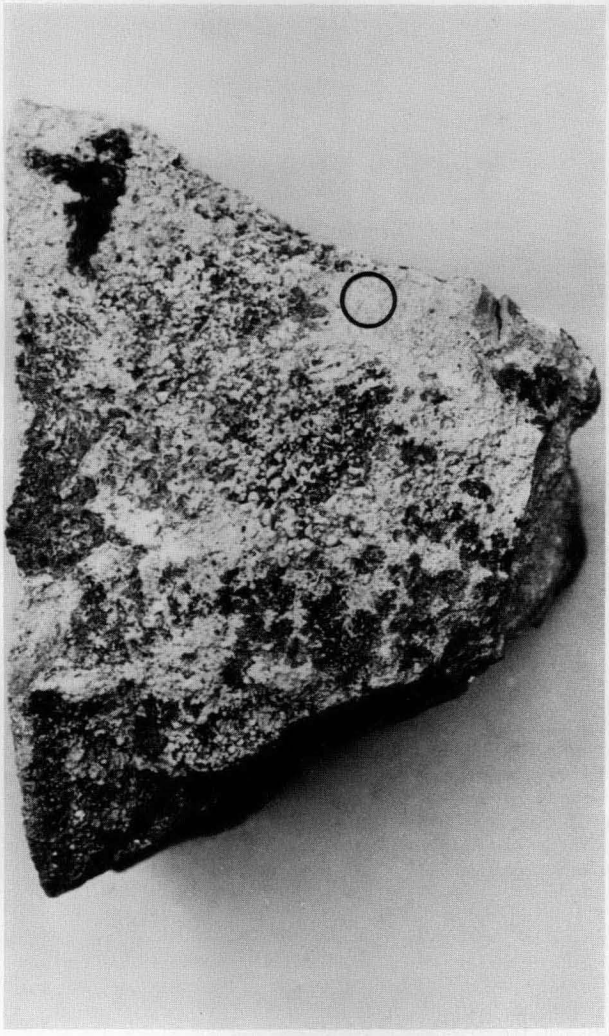

Figure 2. Photograph of a typical rock specimen (J266).
The desert varnish appears as black patches, which are progressively smaller away from larger patches. Some areas appear to be devoid of varnish (e.g., the circle outlined). Microcolonial fungi occur in such areas and some are enriched in manganese relative to their immediate surroundings. Sample is about 10 cms across.

to our knowledge, manganiferous desert varnish has not been previously reported in Australia. However, Francis (1920) described black, manganese-rich coatings found on rocks in stream beds in Queensland rain forests. Also, archaeologists have described aboriginal tools with dark coatings that have been regarded as desert varnish (C. Elvidge, personal communication). The widespread stony pavement characteristic of many Australian desert areas indicates that desert varnish coatings are also likely to be widespread.

In the southwestern United States and in Egypt, desert varnish is associated with a variety of lithologies that, through mechanical weathering, produce the most stable surfaces. In Australia, the desert varnish coatings studied also occur on a variety of rock types, including dolomite, sandstone, siltstone, conglomerate, and chert. The older Proterozoic samples have much better developed desert varnishes than their younger Permian and Tertiary counterparts. The most obvious logical explanation for this is that the Proterozoic rocks are more indurated and resistant to erosion, and have, therefore, formed more stable, longer-lived physiographic features upon which the varnish has developed. The Permian and younger rocks are generally deeply weathered and kaolinised and much more easily eroded.

Although our evidence does not prove that microcolonial fungi are responsible for desert varnish in these Australian samples, it is consistent with the results of other recent investigations that have implicated microorganisms in the formation of rock

Table 2. Relative manganese content within and outside microcolonies in areas away from macroscopic varnish patches.

Rock specimen	*Within microcolony*	*Outside microcolony*		
		Area 1	*Area 2*	*Area 3*
J266*	0.09	0.02	0.02	0.02
J380	0.12	0.01	0.02	0.01
J254	0.07	0.02	0.02	0.01
J182	0.11	0.02	N.A.	N.A.
J258	0.42	0.02	N.A.	N.A.

Relative concentrations of manganese as determined by SEM-EDAX. Counts were normalised by bringing the silicon count accumulations to 1.0 in each case.
N.A. Not analysed.
* Shown in Figure 3.

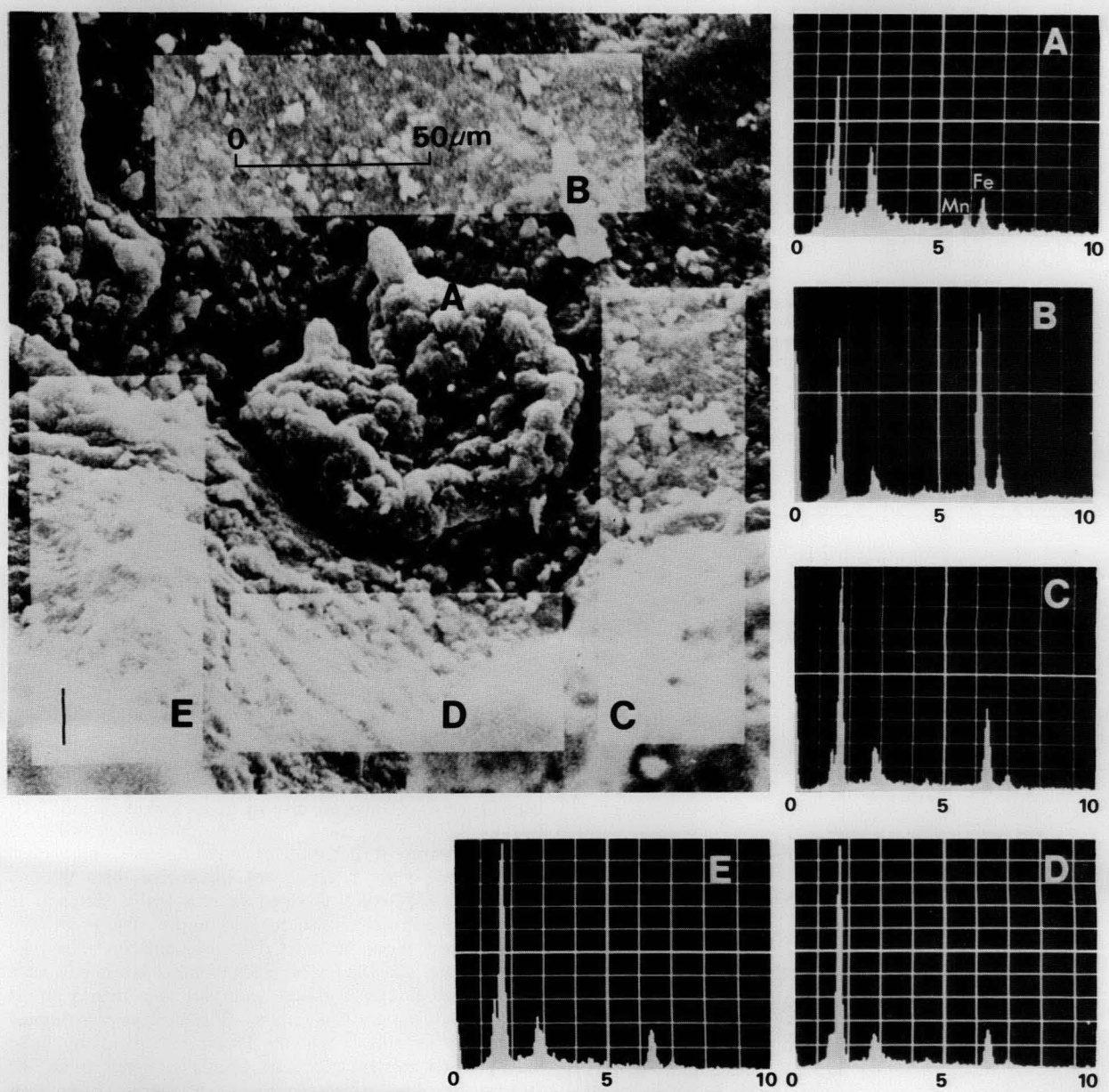

Figure 3. A scanning electron micrograph showing a microcolonial fungus from rock J266.
EDAX analyses were performed on the microcolony and the adjoining areas. The Kα and Kß peaks for manganese are located at 5.89 and 6.49, respectively. For iron the Kα peak is 6.40 and the Kß peak is 7.06. Note that manganese is concentrated within the microcolony.

varnishes (Perry & Adams, 1978; Krumbein & Jens, 1981; Dorn & Oberlander, 1981a,b). The major piece of evidence in support of a biological origin for the Australian desert varnish is the discovery of isolated fungal microcolonies where manganese is found within but not outside the microcolony, implying that some of the fungi act as sites for the start of varnish formation. An alternative explanation is that the microcolonial fungi are simply settling and growing in areas where manganese is rich on the rock surfaces. Also, it is possible that bacteria could be associated with the microcolonial fungi and be responsible for the manganese deposition. These possibilities will be investigated in future studies in which we plan to cultivate organisms from freshly collected rocks and determine their capabilities in pure culture.

References

Dorn, R.I. & Oberlander, T.N., 1981a — Microbial origin of desert varnish. *Science*, 213, 1245–1247.

Dorn, R.I. & Oberlander, T.M., 1981b — Rock varnish origin, characteristics and usage. *Zeitschrift Geomorphologie* N.F. 25(4), 420–436.

Engel, C.G. & Sharp, R.P., 1958 — Chemical data on desert varnish. *Bulletin of the Geological Society of America* 69, 487–518.

Francis, W.D., 1920 — The origin of black coatings of iron and manganese oxides on rocks. *Proceedings of the Royal Society of Queensland*, 32, 110–116.

Glasby, G.P., McPherson, J.G., Kohn, B.P., Johnston, J.H., Keys, J.R., Freeman,A.G., & Tricker, M.J., 1981 — Desert varnish in Southern Victoria Land, Antarctica. *New Zealand Journal of Geology and Geophysics*, 24, 389–397.

Griffiths, H.B. & Greenwood, A.D., 1972 — The concentric bodies of lichenized fungi. *Archives of Microbiology*, 87, 285–302.

Hayden, J.D., 1976 — Pre-altithermal archaeology in the Sierra Pinacate, Sonora Mexico. *American Antiquity*, 41, 274–289.

Humboldt, A. von, 1793 — Florae Fribergensis specimen plantas cryptogamicas praesertim subterraneas exhibens. Edidit Accedunt Aphorismi en doctrina physiologiae & chemicae plantarum, Berolini, Rottmann, I-XIV.

Hutton, J.T., Twidale, C.R., Milnes, A.R., & Rosser, H., 1972 — Composition and genesis of silcretes and silcrete skins from the Beda Valley, southern Arcoona Plateau, South Australia. *Journal of the Geological Society of Australia*, 19(1), 31–39.

Jackson, M.J. & van de Graaff, W.J.E., 1981 — Geology of the Officer Basin. *Bureau of Mineral Resources, Australia, Bulletin* 206.

Jackson, M.J. & Muir, M.D., 1981 — The Babbagoola Beds, Officer Basin, Western Australia: correlations, micropalaeontology and implications for petroleum prospectivity. *BMR Journal of Australian Geology & Geophysics*, 6, 81–93.

Krumbein, W.E., & Jens, K., 1981 — Biogenic rock varnishes of the Negev Desert (Israel) an ecological study of iron and manganese transformation by Cyanobacteria and fungi. *Oecologia*, 50, 25–38.

Laudermilk, J.D., 1931 — On the origin of desert varnish. *American Journal of Science*, 21, 51–66.

Lucas, A., 1905 — The blackened rocks of the Nile cataracts and of the Egyptian deserts. *Egypt Geological Survey, Report*, 55 pp.

Milnes, A.R., & Hutton, J.T., 1974 — The nature of microcryptocrystalline titania in 'silcrete' skins from the Beda Hill area of South Australia. *Search*, 5(4), 153–154.

Perry, R.S., & Adams, J.B., 1978 — Desert varnish: evidence for cyclic deposition of manganese. *Nature*, 276, 489–491.

Potter, R.M., & Rossman, G.R., 1977 — Desert varnish: the importance of clay minerals. *Science*, 196, 1446-1448.

Potter, R.M., & Rossman, G.R., 1979 — The manganese-and iron-oxide mineralogy of desert varnish. *Chemical Geology*, 25, 79-94.

Samuelson, D.A., & Bezerra, J., 1977 — Concentric bodies in two species of the Loculoascomycetes. *Canadian Journal of Microbiology*, 23, 1485-1488.

Staley, J.T., Palmer, F.E., & Adams, J.B., 1982 — Microcolonial fungi: common inhabitants of desert rocks? *Science*, 215, 1093–1095.

BMR Journal of Australian Geology & Geophysics, 8, 89-91

AN INSTRUMENT FOR SIMULTANEOUS MEASUREMENT OF Eh AND pH IN BOREHOLES

K.J. Seers

An instrument is described that measures Eh and pH simultaneously in boreholes. The temperature of the borehole fluid and its self-potential with respect to an up-hole mud probe can also be measured. Operation should be possible in water depths to 100 m. By connecting the pH electrode system in a feedback circuit, electrometer amplifier performance is obtained from a cheaper, lower quality amplifier. Signal subtraction operations allow the same reference electrode to be used simultaneously for all measurements. Sources of error are reduced by careful guarding of the high-resistance input circuits and by using isolation amplifiers to prevent ground leakage currents. A number of future development possibilities are indicated.

Introduction

A prototype field instrument, the KEP–1 Eh–pH probe, has been developed by BMR for simultaneous in situ measurements of pH, Eh (oxidation-reduction potential), temperature, and SP (self-potential) in boreholes. Applications are in groundwater studies related to weathering, orebody formation, waste disposal, etc.

Unlike instruments previously reported in the literature (Back & Barnes, 1961; Bolviken & others, 1972; Mann, 1974), the KEP–1 uses industrial-type electrodes capable of withstanding pressures of 1034 kPa (150 psig) and so does not require a pressure-compensating mechanism for operation down to a water depth of 100 m. Furthermore, the circuitry developed for the KEP–1 ensures no observable interactions between simultaneous pH, Eh, and SP measurements, even though the common reference electrode is in the feedback circuit of the amplifier that measures pH. The ability to log all variables simultaneously simplifies field operations and guarantees accurate measurement correlation.

Measurement of pH

In conventional pH measurements the high resistance glass electrode connects to an electrometer amplifier and the reference electrode connects to signal ground. An electrometer amplifier is necessary because of its high input resistance ($> 10^{13}$ ohm), which prevents the flow of current through the glass electrode; also the input bias current required by an electrometer amplifier is very low (typically $< 10^{-14}$ amp), which ensures that electrode polarisation is negligible and solution potentials are unaffected. Such amplifiers are usually of hybrid rather than monolithic construction and so are more bulky and difficult to package in a slim probe; they are also expensive to replace if the probe is damaged or abandoned.

Figure 1 shows how a relatively cheap FET-input monolithic amplifier (Analog Devices AD545JH) is used in the KEP–1.

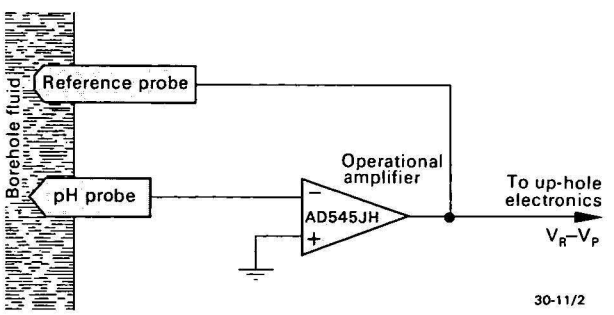

Figure 1. pH measurement

The amplifier is connected in a unity-gain inverting circuit, with the cell comprising the reference and pH electrodes forming the feedback path. This amplifier's open loop input resistance (10^{13}ohm) is thus effectively multiplied by its open loop gain (2×10^4) to give an effective input resistance of 2×10^{17} ohm. Bias current is less than 2 pA at 25°C, doubling for every 10°C increase; this is comparable with input currents specified in commercial pH meters. The glass electrode (Leeds & Northrup 117839) has a sensitivity of −59.16 mV per pH unit, and the maximum error caused by bias current flowing in the 77 Megohm electrode circuit is, therefore, 0.0026 pH unit at 25°C. The reference electrode (Leeds & Northrup 117481) is a diffusion type with saturated KCl gel electrolyte and Ag-AgCl internal element.

In Figure 1, if the half-cell potentials developed on the pH and reference electrodes are V_P and V_R, respectively, the amplified output is V_R–V_P. because V_R–V_P is zero at a nominal pH of 7, the KEP–1 system adds in a fixed voltage so that the analogue pH output range of 0–11 volts corresponds to 0–11 pH.

Gain and offset in the pH-measuring circuits are adjusted by front panel 'slope-correction' and 'standardise' controls that enable calibration with two buffer solutions of known pH. For recording small variations, an 11-position offset switch is provided to back off integral numbers of pH units, and a x10 gain switch increases the sensitivity for the residual fraction. Resolution is 0.001 pH unit; whether this is significant depends only on the repeatability of the electrode system, which is still under evaluation.

The initial plan was to compensate for the temperature coefficient of the glass electrode with a temperature-dependent resistance in the form of an automatic temperature compensation (ATC) probe (Leeds & Northrup 152137). However, in

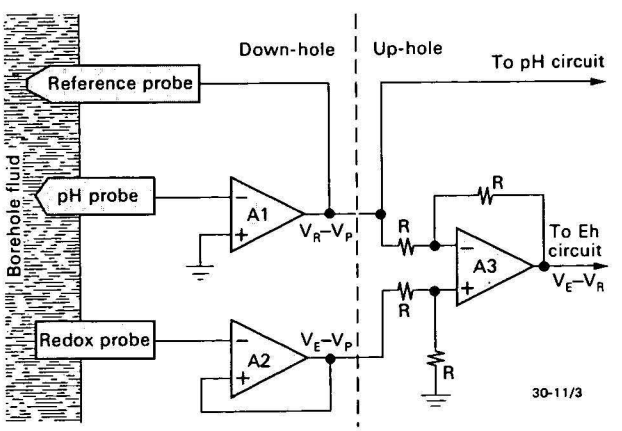

Figure 2. Eh measurement

the prototype, the ATC probe is used to measure temperature directly and the data are subsequently corrected for the glass electrode characteristic. The temperature of the borehole fluid can be measured to within 0.1°C, by passing a constant current through the ATC probe and measuring the voltage developed. An improved design is planned to include both temperature measurement and automatic compensation.

Measurement of Eh

A gold-tipped platinum redox electrode (Leeds & Northrup 117419) forms the measurement cell with the reference electrode used for pH measurement. The redox electrode connects to an amplifier of the type used for pH measurement; low bias current and high input resistance again ensure low errors. Figure 2 shows the analogue subtraction method used to obtain Eh.

If V_P is the half-cell potential across the glass electrode, the fluid may be considered to be at a potential of $-V_P$ with respect to signal ground. Thus, if the redox electrode half-cell potential is V_E, the output of amplifier A2 is V_E-V_P. The output of amplifier A1, V_R-V_P, is subtracted from this by amplifier A3 to give V_E-V_R, the potential that would be developed across the cell formed by the redox and reference electrodes alone.

This subtraction would be unnecessary if the connections to the pH and reference electrodes were reversed: the output of A2 would be V_E-V_R. directly. However, when tried, this configuration produced scatter in both Eh and pH readings. The cause of this has not been definitely established; it is likely that spurious solution potentials cause currents to flow in the high resistance glass electrode via the amplifier's low output resistance. Such currents would be negligible with the glass electrode connected to the high resistance input of the amplifier.

The instrument multiplies V_E-V_R by ten to give an analogue output of 1 volt per 100 millivolts Eh. Resolution is better than 1 mV Eh, but whether this is meaningful again depends on electrode constancy. The potential of the reference electrode (0.1985 V at 25°C) must be added to obtain the Eh value.

SP measurement

In principle, there is no limit to the number of electrodes that can be referred simultaneously to the one reference electrode, using the subtraction scheme outlined above. The only constraint is that any current drawn from the fluid by an electrode or its associated amplifier must be low enough to avoid errors in the potentials measured by the other electrodes. SP is, therefore, measured in the same way as Eh.

The SP electrode is a mud probe in the ground near the top of the borehole. A circuit similar to that in Figure 2 gives the potential developed between the probe and the down-hole reference. Output range and scale factor are as for Eh.

Ground isolation

It has been shown that the borehole fluid must be considered to be at a potential of $-V_P$ with respect to signal ground. This sets a stringent requirement for no ohmic connection between signal ground and the fluid, i.e., between signal ground and the actual ground — a requirement not easily met in field situations, where the recording system or its power supply can readily develop leakage paths to ground. Leakage of only 0.5 μA flowing in the reference electrode could produce an error of O.1 pH; an ohmic path of 10^8 ohm resistance between signal ground and the borehole fluid would almost halve the pH indication.

To avoid problems of this nature, all signals from the down-hole probe and the SP mud probe are passed through isolation amplifiers with carefully guarded inputs in the up-hole electronics unit. These amplifiers also provide isolated power supplies for the down-hole electrodes. Each amplifier (Analogue Devices 284J) has a minimum isolation resistance of 5×10^{10} ohm.

Because the probe cable is immersed in the fluid, its insulation must be of very high quality, electrically and mechanically. Long-term cable reliability has still to be investigated.

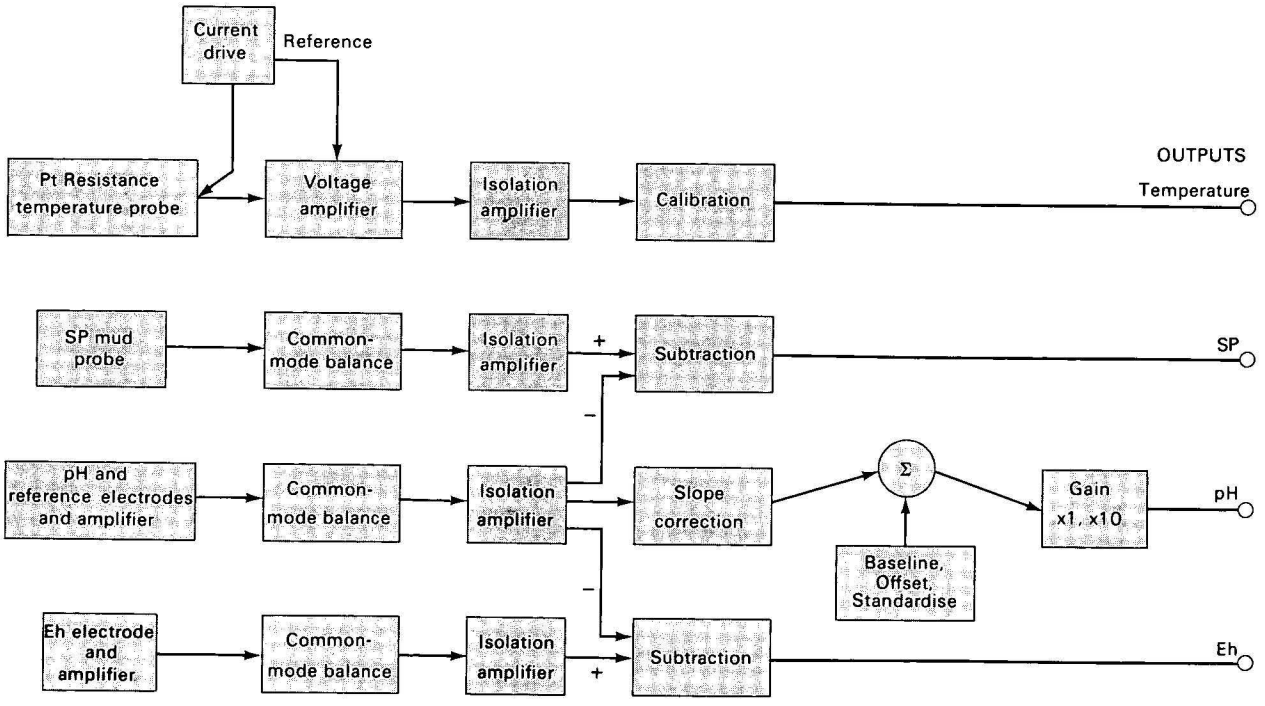

Figure 3. Simplified block diagram.

30-11/4

To guard against the possibility of errors caused by common-mode voltages induced in the long probe cable, common-mode balancing circuits are included at the input side of the isolation amplifiers.

Figure 3 is a simplified block diagram of the complete instrument.

Physical configuration

Figure 4 is a photograph of the down-hole probe and up-hole electronics unit. The down-hole probe contains the pH, redox, and reference electrodes and the ATC probe. These are mounted with 0-ring seals in a polycarbonate cylinder, designed to allow rapid displacement of entrapped air by the borehole fluid and to ensure free fluid flow around the electrodes. Amplifiers A1 and A2 (Fig. 2) are mounted in the upper part of the probe on a copper disc that forms part of the input guard. Probe length is 40 cm and its diameter is 6 cm. This is larger than necessary, because the original design included a pressure-compensating piston system as described by Mann (1974). This is not now considered necessary for water depths to 100 m.

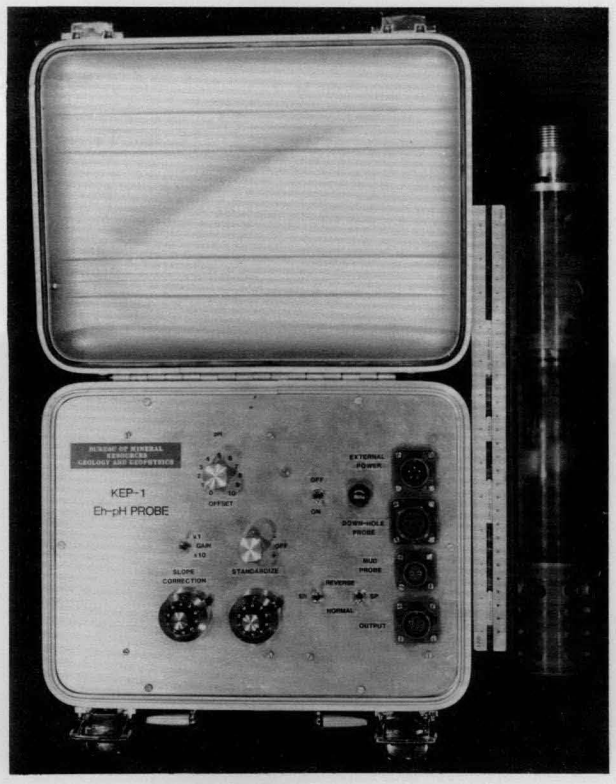

Figure 4. KEP–1 Eh-pH probe

The up-hole electronics are housed in an aluminium instrument case of approximate dimensions 30 cm x 23 cm x 13 cm. Simultaneous outputs of pH, Eh, SP, and temperature are provided for separate meters or chart recorders. The system operates from 12V d.c. and draws approximately 0.34 A. The probe is connected by six-core well-logging cable and a standard well-logging connector.

Proposed developments

The prototype has operated successfully in laboratory tests and in a bore-hole where depth has been limited to 45 m so far. After further testing and evaluation, the following improvements may be incorporated: automatic temperature compensation for the glass electrode, pressure and conductivity measurements, digitising and multiplexing all down-hole signals onto a single core, digital readout and, possibly, digital recording, reduction of probe dimensions.

Acknowledgements

The KEP–1 was designed for BMR's Engineering Geology Section. The author is grateful to R. Evans of that section for his assistance and clarification of many questions in the field of electro-chemistry. Thanks are also expressed to G. Black who constructed and tested the electronics and to G. Thom and A. Kores for designing and constructing the probe.

References

Back, W., & Barnes, I., 1961 — Equipment for field measurement of electrochemical potentials. *United States Geological Survey Professional Paper* 424-C, C366–C368.

Bolviken, B., Logn, O., Breen, A., & Uddu, O., 1972 — Instrument for in situ measurements of Eh, pH and self-potentials in diamond drill holes. *Geochemical Exploration 1972, (London), The Institution of Mining and Metallurgy*, 415–420.

Mann, A., 1974 — Down-hole Eh–pH and water sampler. *CSIRO Minerals Research Laboratories, Report* No. FP 5.

BMR Journal of Australian Geology & Geophysics, 8, 93-96

OCCURRENCES OF BORON-BEARING KORNERUPINE IN THE WESTERN HARTS RANGE AND NEAR MOUNT BALDWIN, ARUNTA BLOCK, CENTRAL AUSTRALIA

R.G. Warren & D.H. McColl*

Boron-bearing kornerupine occurs in phlogopite-albite gneisses of the Arunta Block, southwest of Mount Baldwin and in the western Harts Range. At the second locality, idioblastic sapphirine occurs with the kornerupine, and excellent crystals of both minerals have been collected. Most of the larger kornerupine crystals from the Mount Baldwin locality are, in fact, pseudomorphs of fine-grained phyllosilicates after kornerupine.

Introduction

Six separate occurrences of kornerupine, a rare aluminosilicate of magnesium and iron are known in the Arunta Block, central Australia (Fig. 1, Table 1). This note discusses the two most recently discovered localities, one near Mount Baldwin and the other in the western Harts Range.

During a rapid reconnaissance in 1976, large dark green prismatic crystals were found weathering out of a light-coloured quartzofeldspathic gneiss about 6 km southwest of Mount Baldwin. Investigations have shown that the majority of these crystals have been completely replaced by felted fine-grained minerals; but rare unaltered crystals, generally the more slender elongate forms, still consist partly or wholly of pale green kornerupine.

Large crystals and fragments of kornerupine were collected from float near a sapphirine-bearing outcrop in the western Harts Range in 1977, and later, this locality yielded well-formed crystals of both minerals, either weathered free or in a gneissic matrix of albite (Ab_{92-94}) and phlogopite (Figs. 2 & 3).

Mount Baldwin locality (Fig. 4)

The kornerupine-bearing rocks occur in a low hill rising out of a sand-covered plain. Strongly deformed, mylonitic rock crops out about 100 m to the southwest, and unrelated garnet-sillimanite gneiss of the Harts Range Group crops out about 0.5

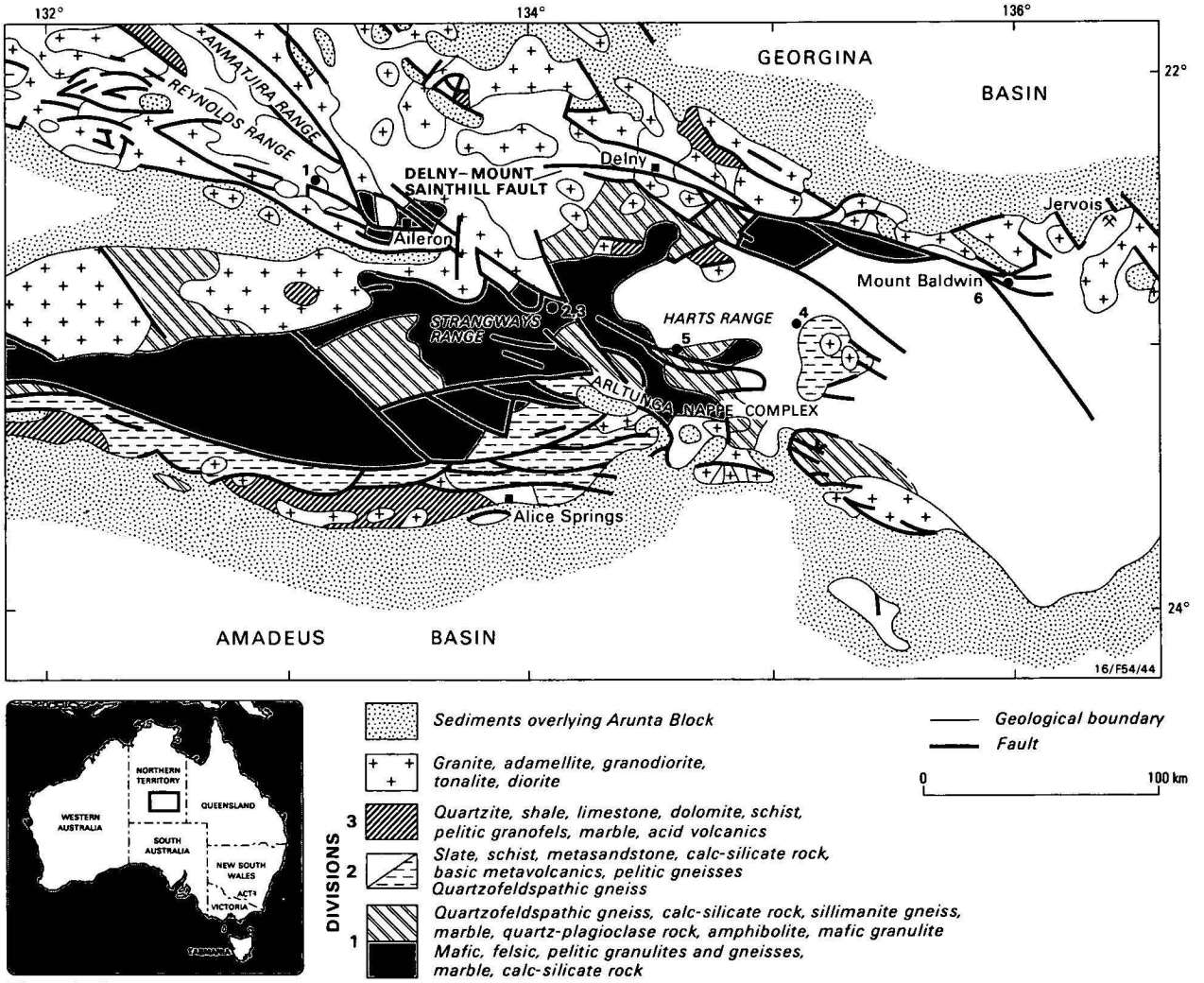

Figure 1. Generalised geology and kornerupine localities, Arunta Block.

*Present address: Australian Mineral Development Laboratories, P.O. Box 114, Eastwood, South Australia 5063.

Table 1. Kornerupine occurrences in the Arunta Block

Occurrence	*Unit*	*Associated minerals*	*Reference*
1. Reynolds Range	Pine Hill Formation	Quartz, sillimanite, cordierite, orthopyroxene, biotite	Stewart & others, 1977
2. SW of Mud Tank	Strangways Metamorphic Complex.	Orthopyroxene, cordierite, potassium feldspar	Woodford & Wilson, 1976
3. SW of Mud Tank	Strangways Metamorphic Complex.	Orthopyroxene, silimanite, plagioclase, quartz	Wilson, 1978
4. Eastern Harts Range	Harts Range Group.		Dobos, 1978
5. Western Harts Range	Strangways Metamorphic Complex	Albite, biotite, sapphirine	This note
6. WSW of Mount Baldwin	unknown	Albite, quartz, biotite	This note

Figure 2. Large crystals of kornerupine from the western Harts Range.

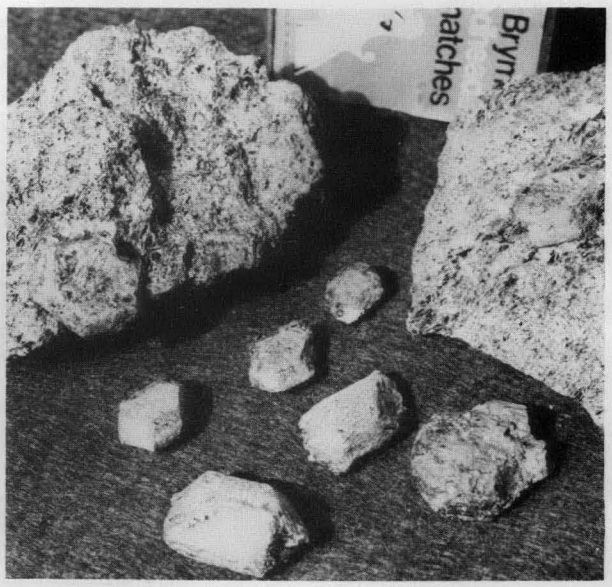

Figure 3. Sapphirine crystals in albite-phlogopite gneiss, western Harts Range.

km to the south. From the field observations and interpretation of lineaments, it is believed a spur of the Delny–Mount Sainthill Fault (Warren, 1978) passes close to the southern edge of the hill. The severe deformation and retrogressive metamorphism evident in thin sections of specimens from the kornerupine-bearing outcrops also indicate the proximity of a major fault.

The light-coloured quartzofeldspathic gneiss containing the kornerupine is well layered with a near north–south strike and steep to vertical dip. The amount of kornerupine varies from layer to layer: outcrops on the eastern edge of the hill are barren. Calc-silicate rocks crop out on the western edge of the hill.

Although the occurrence of kornerupine is in itself indicative of moderate to high temperatures (Werding & Schreyer, 1977, 1978), the assemblages at this locality are not exclusively diagnostic of either upper amphibolite or granulite facies. Exsolved rutile in biotite is common, suggesting re-equilibration of high-temperature assemblages has occurred. Rims of amphibole on clinopyroxene and epidote (probably iron epidote) in calcsilicate rock (BMR registered number 80096589A) are regarded as the products of later hydration.

Several specimens were collected (76096060, 80096589A–F) and microprobe analyses (Table 2) have been made of the minerals in one (76096060). In this, the original assemblage appears to have been rutile-quartz-kornerupine-albite, and retrogression has converted some of the kornerupine to tourmaline and phyllosilicates.

The phyllosilicates are too fine to be resolved optically, but appear to include either muscovite or phengite. Identification by XRD was also unsatisfactory, though chlorite is probably present too (D.G. Barnes, unpublished BMR Laboratory report). Other specimens contain phlogopite and fine-grained aggregates of phyllosilicates similar to pinite after cordierite. The kornerupine is thought to be boron-bearing, because of the presence of tourmaline amongst the retrogressed assemblages.

Western Harts Range locality (Fig. 5)

The kornerupine-bearing outcrops at the western Harts Range locality are confined to a single layer in a well-layered sequence of quartzofeldspathic gneiss in the Strangways Metamorphic Complex (Division 1 of the Arunta Block), an estimated 200 m below the local base of the Cadney metamorphics. Where the sapphirine and kornerupine occur, the layer is about 10 m thick. It can be traced in one direction for about 50 m before it lenses out abruptly, and, in the other, it persists as a thin unit for about 300 m before disappearing beneath Recent sediments. The layered sequence, including the kornerupine-bearing layer, has been intruded by basic pods (now two-pyroxene mafic granulites). A major fault is situated about 300 m to the north, and minor shears pass close to the kornerupine-bearing outcrops.

The kornerupine occurs as very dark green, four-sided or eight-sided prisms up to 20 x 4 cm, generally surrounded by a white halo of albite. Almost all the crystals show slight surface alteration and have a coat of fine, white, magnesian phlogopite,

Table 2. Electron microprobe analyses of minerals in specimen 76096060, Mount Baldwin locality

	Albite		*Kornerupine*			*Tourmaline*		*Rutile*[1]
SiO_2	66.14	66.13	30.41	29.81	30.09	35.17	35.54	
TiO_2				0.13	0.30	1.98	1.53	96.08
Al_2O_3	21.66	21.38	40.05	39.94	39.58	30.01	31.55	0.50
V_2O_3					0.11	0.22		
FeO*			6.69	6.69	7.22	4.65	4.18	0.41
MgO			17.13	17.29	17.01	9.49	9.79	
CaO	1.62	1.75				0.99	0.55	0.16
Na_2O	10.86	10.69	0.20	0.17	0.33	2.56	2.89	
K_2O		0.06				0.06		
Total	100.27	100.00	94.48	94.03	94.63	85.13	86.04	97.15
Si	2.894	2.902	7.838	7.730	7.779	11.625	11.561	
Ti				0.026	0.058	0.491	0.374	0.990
Al	1.117	1.106	12.166	12.208	12.061	11.690	12.096	0.008
V						0.060		
Fe^{2+}			1.442	1.452	1.561	1.285	1.138	0.005
Mg			6.580	6.684	6.557	4.674	4.746	
Ca	0.076	0.082				0.349	0.191	0.002
Na	0.921	0.909	0.100	0.086	0.165	1.640	1.820	
K		0.003				0.025		
Total	5.008	5.002	28.128	28.184	28.204	31.839	31.926	1.006
Oxygens	8	8	42	42	42	49	49	2
Mg number			82.0	82.2	80.8	78.4	80.7	

1. Rutile also contains Nb_2O_5, Rare earths, V_2O_3, Cr_2O_3
* All iron calculated as FeO

Table 3. Electron microprobe analysis, sample 78912955A, Western Harts Range locality

	Albite	*Albite*	*Phlogopite*	*Kornerupine* 1	2	3	4	*Tourmaline*
SiO_2	66.08	66.43	37.36	29.99	29.62	30.09	29.94	36.63
TiO_2			1.54		0.15		0.14	0.83
Al_2O_3	21.47	21.41	17.03	40.10	40.25	40.26	40.29	32.92
FeO*			8.94	11.00	10.19	9.88	9.59	5.77
MgO			18.79	14.73	15.57	15.59	15.89	9.09
CaO	1.41	1.23						0.40
Na_2O	10.80	10.86		0.20	0.23	0.18	0.17	3.03
K_2O	0.24	0.09	10.43					
Total	100.00	100.02	94.08	96.02	96.01	95.99	96.02	88.67

1–4 are analyses from margin to core of a single grain of kornerupine, approximately 1 cm across
* All iron calculated as FeO

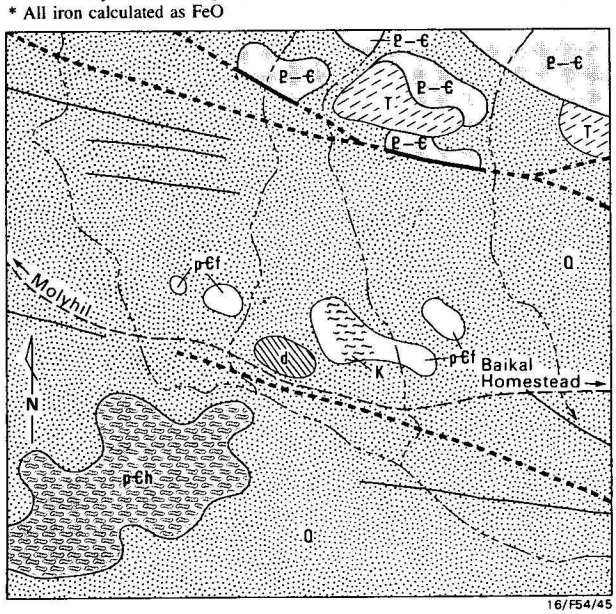

p€f *Light coloured quartzofeldspathic gneiss*
p€h *Garnet sillimanite gneiss (Harts Range Group)*
d *Deformed, mylonitic rocks*
P–€ *Georgina Basin sequence*
T *Deeply weathered rocks*
Q *Sand, red soil, fanglomerate*
K *Kornerupine–bearing layers*

Fault, where concealed, shown by short dashes
Lineament
Track
0 1 km

Figure 4. Geology of Mount Baldwin kornerupine locality (Fig. 1, No. 6).

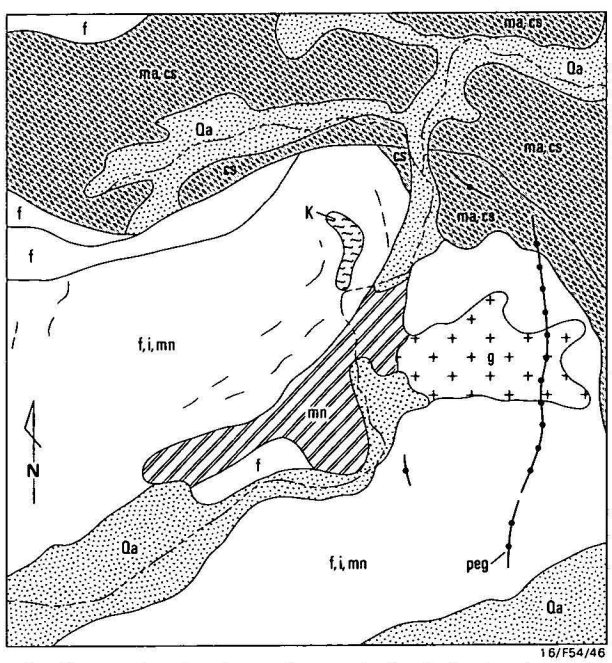

K *Kornerupine–bearing gneiss*
g *Meta-granodiorite*
peg *Pegmatite*
f *Quartzofeldspathic gneiss*
mn *Mafic granulite*
i *Cordierite–bearing gneiss*
cs *Calc-silicate rocks*
ma *Marble*
Qa *Soil, alluvium*
0 500 m

Figure 5. Geology of western Harts Range kornerupine locality (Fig. 1, No. 5).

Table 4. Chemical analyses of purified samples of single kornerupine crystals

	78912955C	*78912955D*	*78912762*
SiO_2	30.0	30.1	30.3
TiO_2	0.15	0.15	0.13
Al_2O_3	40.2	40.4	38.8
Fe_2O_3	5.34	4.89	6.86
FeO	3.53	4.08	4.24
MnO	0.03	0.03	0.03
MgO	14.4	15.4	14.9
CaO	0.01	0.01	0.01
Na_2O	0.10	0.10	0.09
K_2O	0.04	0.05	0.03
P_2O_5	0.10	0.06	0.08
H_2O^-	0.08	0.10	0.06
Corrected L.O.I*	1.11	1.29	1.47
B_2O_3	3.25	3.14	2.94
Total	98.34	99.80	99.94

* L.O.I. corrected for oxidation of ferrous to ferric iron.
Analyst — K.J. Henley (Australian Mineral Development Laboratories)

Table 5. Microprobe analyses 78912955E (Western Harts Range locality)

	Albite	*Sapphirine*	*Sapphirine*	*Phlogopite*	*Tourmaline**
SiO_2	66.49	12.83	12.86	38.19	35.78
TiO_2				2.10	0.69
Al_2O_3	21.30	59.65	60.03	15.94	32.91
FeO		10.68	10.06	7.92	4.92
MgO		16.69	16.50	20.01	9.01
CaO	1.38				0.46
Na_2O	10.75	0.15			2.79
K_2O	0.09			10.40	
Total	100.00	100.00	99.45	94.56	86.70

* Includes 0.14 weight per cent Cr_2O_3

which has also invaded transverse fractures, weakening many prisms along their length. Terminations are rare and poorly formed, but appear to be the dome (101). A crystal analysed in four steps from core to margin showed relative depletion of Mg at the margin (Table 3). Analyses of single crystals (Table 4) confirm that the kornerupine is boron-bearing. Werding & Shreyer (1978) pointed out that low boron activity favours kornerupine formation, and high activity favours tourmaline, which contains more boron, even at high temperatures.

The sapphirine crystals are mostly pseudo-hexagonal tabulae up to 2.0 x 0.5 cms, which are found aligned with the gneissic fabric of the matrix. Crystal margins are commonly altered to a fine intergrowth of corundum, tourmaline, and magnetite, and surround a deep blue-black vitreous core of sapphirine. The sapphirine is unusually iron-rich, and shows a trace of chromium (Table 5). In thin section, it is strongly pleochroic from deep cobalt-blue to pale yellow, has high dispersion, a small 2V (about 20°), and shows three oriented sets of fine platy inclusions (possibly magnetite or rutile).

The kornerupine and sapphirine are considered to be products of the granulite metamorphism, which occurred at high temperatures (as shown by the high TiO_2 in the phlogopite) and moderate to high pressures. Subsequent retrogression converted some kornerupine to coarse grained pseudomorphs of tourmaline and sillimanite and altered the margins of the sapphirine crystals.

Comparisons and correlations

The stratigraphic setting of the western Harts Range occurrence is clearly defined and very similar to that of the kornerupine locality southwest of Mud Tank described by Wilson (1978). The setting of the Mount Baldwin locality is uncertain. The nearest unit similar to the host rock is light-coloured quartzofeldspathic gneiss, rich in sodic plagioclase, in a predominantly calc-silicate sequence of Division 2, some 50 km to the west-northwest. These rocks lie north of the Delny–Mount Sainthill Fault, and their metamorphic grade is lower amphibolite. Harts Range Group units south of the fault are upper amphibolite grade, but, compositionally, they are metapelites and unlike the kornerupine-bearing rocks. For the present, it seems best to regard the kornerupine-bearing rocks and associated rocks at this locality as an isolated high-grade sliver pushed up between two parts of the Delny–Mount Sainthill Fault, and not to correlate them with either nearby high-grade rocks or chemically similar but distant units.

Both the occurrences described above are in albite-rich rocks, though in one case the rocks are silica-saturated and in the other, silica-undersaturated. The host rocks also resemble those of the Ianakafy (Malagasy) kornerupine occurrence (Megerlin, 1970), except that there the plagioclase is oligoclase, suggesting a slightly more calcareous host. The rocks in the three occurrences could be described as sodic, magnesian, and aluminous, with traces of boron, although, in other occurrences of kornerupine, the host rocks are chemically more diverse (e.g. 1, 2, and 3 in Table 1). Therefore, the occurrence of kornerupine is not confined to one chemically distinctive rock type, but it does depend on a high magnesium content in the host rock and an availability of boron.

Acknowledgements

Microprobe analyses were made at the Research School of Earth Sciences, Australian National University, using the data reduction program of Ware (1981).

References

Dobos, S.K., 1978 — Phase relationships, element distribution, and geochemistry of metamorphic rocks from the northeast Arunta Block. *Ph.D. Thesis Macquarie University, Sydney.*

Mergerlin, N., 1970 — Sur une roche à Kornerupine du sud de Ianakafy, (centre sud de Madagasca). *Comité national Malgache de Géologie Comptes rendus des Semains géologiques*, 1968–1969, 67–69.

Stewart, A.J., Warren, R.G., Langworthy, A.P. & Offe, L.A., 1977 — Arunta Block. *In* Geological Branch summary of activities 1976. *Bureau of Mineral Resources, Australia, Report* 196, 83–90.

Ware, N.G., 1981 — Computer programs and calibration with the PIBS technique for qualitative electron probe analysis using a lithium drifted silicon detector. *Computers and Geosciences*, 7, 167–184.

Warren, R.G., 1978 — Delny–Mount Sainthill fault system, eastern Arunta Block, central Australia. *BMR Journal of Australian Geology & Geophysics*, 3(1), 76–79.

Werding, G. & Schreyer, W., 1977 — Synthese von borhaltigen kornerupin und turmalin in system MgO–Al_2O_3–B_2O_3–SiO_2–H_2O. *Fortschritte der Mineralogie*, 55, Beihart 1, 152–154.

Werding, G. & Schreyer, W., 1978 — Synthesis and crystal chemistry of kornerupine in the system MgO–Al_2O_3–SiO_2–B_2O_3–H_2O *Contributions to Mineralogy and Petrology*, 67(3), 247–259.

Wilson, A.F., 1978 — Large crystals of kornerupine from a new locality in the granulites of the Strangways Range, central Australia. *Neues Jahrbuch fur Mineralogie Monatshefte*, 6, 249–56.

Woodford, P.J., & Wilson, A.F., 1976 — Kornerupine in metasomatic zones, Strangways Range, central Australia. *Mineralogical Magazine*, 40, 589–594.

BOOK REVIEW

Cooke-Ravian Volume of Volcanological Papers.

Edited by R. W. Johnson; *Geological Survey of Papua New Guinea, Memoir* 10, xvi + 265 pp, 1981. Price 22 PNG Kina.

In the early hours of 8 March 1979, Robin Cooke, Senior Government Volcanologist, and Elias Ravian, Volcano Observer, were killed by a volcanic explosion on Karkar Island, Papua New Guinea. They were occupying an observation camp on the rim of the main caldera, when an explosive eruption of the Bagiai cone, some 15 km away, overwhelmed them.

This volume of Volcanological Papers is a fitting memorial to their lives and works.

It was edited by R. W. Johnson, who not only compiled the papers, but also painstakingly extracted valuable material from Cooke's unpublished notes and photographs to form the basis of several of the contributions. All 25 papers are concerned with the volcanoes of Papua New Guinea, and most of them deal with the Bismarck Volcanic Arc, which extends along the north coasts of New Guinea and New Britain from Wewak to Rabaul. It is fitting that the core of the Memoir contains authoritative eruptive histories of the more important volcanoes in Papua New Guinea, because well-documented histories of active volcanoes are important if future eruptions are to be predicted. Thus, we are presented with the eruptive histories of the Kadovar, Bam, Manam, Karkar, Langila, Long, Pago, Ritter, Ulawan and Rabaul volcanoes, as well as those associated with Bougainville, Manus, and the M'Buke Islands, and the young volcanoes in eastern Papua.

The paper on Bam volcano, by Cooke & Johnson, sets the pattern for these histories. Starting with the early sightings of Bam by Schouten and Le Maire in 1616 and Tasman in 1643, we are led through to the late 1970s in an effort to recover the eruptions that took place during the last 350 years.

The four papers on the Karkar Island volcano contain accounts of the fatal 1979 eruption, an eruptive history of the last 9000 years, the lava fields in the minor caldera, and the tephra fallouts from recent eruptions. These papers provide fundamental data which will be invaluable in future studies of the Island.

Cooke's paper on the eruptive history of the volcano at Ritter Island deserves mention. In 1700, William Dampier (the first European known to have sighted it) described it as a 780-metre high, steep-sided, conical volcano. From that time until March 1888, it appears to have been in a state of almost continuous eruption. Then, on 13 March 1888, most of the Island suddenly disappeared into the sea and caused a major tsunami, which reached heights of 12–15 m above sea level on the western end of New Britain and devastated many coastal villages in the vicinity. Facsimiles of sketches of Ritter Island drawn in the eighteenth and nineteenth centuries and photographs of its recent appearance indicate the extent of the sudden change in the Island's shape on that fateful day in 1888.

Perhaps the greatest potential risk from volcanism in Papua New Guinea exists at Rabaul. Here, a town containing several thousand people is sited on the edge of an 8 × 14 km caldera which has been involved in eruptions several times in the last 4000 years. Walker & others describe some of the latest major eruptions.

The two largest occurred about 3500 years ago, when the main caldera was formed, and about 1400 years ago, when, it has been estimated, more than 11 km^3 of pumice and ash were generated. This later event was one to two orders of magnitude greater than any historical eruption, including the spectacular 1937 eruption of Tavurvur, which killed 507 people, and indicates the high risk of a devastating volcanic eruption at Rabaul.

In fact, the situation at Rabaul illustrates the paradox associated with active volcanoes, whereby they have the awesome power to cause death and destruction at the same time as they provide the necessary materials to create rich and fertile soil able to support large populations.

Overall, I found the Memoir well presented. The colour plates and line drawings are of high standard, but it is a pity that the reproduction of some of the black and white photographs is not of the same quality. Nevertheless, the publication makes a significant contribution to the study of Papua New Guinean volcanoes, and I am sure it will serve as an important reference work for many years to come.

David Denham

CORRECTION

D. J. Belford—Redescription of *Miogypsina neodispansa* (Jones & Chapman), Foraminiferida, Christmas Island, Indian Ocean.

Volume 7, number 4, 315–320.

The headings of Tables 1 and 2 were inadvertently transposed. They should read:
Table 1. Relation between width of test and number of lateral chamber layers.
Table 2. Statistical measurements on specimens of *M. neodispansa*

CONTENTS

R81/103(5) Cat. No. 83 0273 2